THE PHYSICS OF METALS AND METALLOGRAPHY

FIZIKA METALLOV I METALLOVEDENIE

VOLUME 4 No. 2 — 1957

CONTENTS

		PAGES
A Theory of Lattice-spin Relaxation in Paramagnetic Salts of Iron Group Elements with an Even Number of Electrons	V. I. AVVAKUMOV	1
Exciton Light Absorption Theory	S. V. VONSOVSKII, V. I. CHEREPANOV and V. S. GALISHEV	10
On the Fundamental Possibility of "Intrazonal" Mechanics of Light Absorption in Solid Materials	V. I. CHEREPANOV	15
The Possible Form of Surface of Constant Energy Electrons in a Periodic Lattice-field	G. E. ZILBERMAN and YA. AIZENBERG	18
Electron Emission Theory in Ferromagnetic Materials under the Action of an Electrostatic Field	A. Z. VEKSLER	23
Theory of Residual Electrical Resistance in Interstitial Type Alloys	A. A. SMIRNOV and I. A. STOYANOV	28
The Electrical and Magnetic Properties of the Intermetallic Compound CdSb	I. M. PILAT	31
Effect of Elastic Stresses and Mechanical Heat Treatment on the Magnetic Properties of Certain Hard Magnetic Materials	M. G. LUZHINSKAYA and YA. S. SHUR	36
Certain Magnetic Properties of Dispersion-hardening Fe—MO and Cu—Ni—Fe Alloys	V. I. IVANOVSKII	41
The Hall Effect and the Influence of a Magnetic Field on the Resistance of Magnetite	A. A. SAMOKHVALOV and I. G. FAKIDOV	44
Study of Coercivity of Cold-worked and Annealed Iron Alloys	G. M. FEDASH	50
Concerning Magnetic Effect on $I_s(t°)$ Curves in the Temperature Range 260–270° Drawn for Tempered and Annealed Specimens	B. A. APAEV	56
Texture of Iron Scale. X. Texture of Wustite Scale	V. I. ARKHAROV and M. I. SIMONOVA	65
The Occurrence of Internal Friction Peaks Associated with the Stress-induced Diffusion of Carbon in Alloy Steels having a Face-centred Cubic Lattice	KE T'ING-SUI and TSIEN CHIH-TSIANG	78
The Mechanism of Plastic Deformation and the Mechanical Properties of Aluminium —III. The Role of Plastic Deformation in the Formation of the Mechanical Properties of Aluminium	E. S. YAKOVLEVA	89
The Growth of Large Single Crystals of Zinc of Known Orientation	B. N. BUSHMANOV	92
Changes in the Properties and Structure of Nickel-base Solid Solutions	SH. SH. OBRAGIMOV and B. G. LIVSHITS	96
Volume Changes in the Carbide Phase During Annealing of Steel	N. N. LYULICHEVA	100
Recrystallization Texture in Low-carbon Steel after Cold Rolling	K. V. GRIGOROV and G. P. BLOKHIN	110

Printed in Great Britain by The Campfield Press, St. Albans

FIZIKA METALLOV I METALLOVEDENIE

Chief Editor:
S. V. VONSOVSKII

Deputy Chief Editor:
V. I. ARKHAROV

EDITORIAL BOARD:

A. F. IOFFE
S. T. KONOBEEVSKII
V. D. KUZNETSOV
G. V. KURDYUMOV
B. G. LAZAREV
V. A. PAVLOV
YU. B. RUMER
V. D. SADOVSKII
I. G. FAKIDOV
YA. S. SHUR

IMPORTANT EDITORIAL NOTICE

To assist readers, reprints of any article appearing in The Physics of Metals and Metallography can be obtained on application at a price of $2 (10s.) per reprint, to cover the overhead costs involved in production. The Reprint No. of each article (which appears on the foot of the first page of the article) must be quoted on every order. Orders should be accompanied by the correct remittance.

All orders of reprints of Russian articles should be addressed to The Administrative Secretary of The Pergamon Institute at either 122 East 55th Street, New York 22, or 4 and 5 Fitzroy Square, London W.1, whichever is more convenient.

VOL
4
195

VOLUME 4 No. 2 **CONTENTS**—*Continued* 1957

PAGE

The Effect of Intermediate Annealing on Cold-rolling and Recrystallization Texture
K. V. GRIGOROV and G. P. BLOKHIN 114

The Temperature Dependence of Internal Friction in Several Pure Metals
V. S. POSTNIKOV 118

Thermal Conductivity of Ordered Alloys in Stationary Thermal Equilibrium
G. E. ZOLOTUKHIN 124

The Redistribution of Carbon During the Transformation of Austenite in the Middle Temperature Range
L. I. KOGAN and P. I. ENTIN 131

Criticism

Limits of Utility of Repeated Measurements
R. I. YANUS 138

Letters to the Editor

The Problem of Magnetostriction in Hexagonal System Ferromagnetics
YU. B. KOSTYANITSYN 142

Magnetization of Objects with Alternating Current for Defectoscopy and Other Purposes
N. M. RODIGIN 144

The Magnetic Surface Effect when Flat Bodies are Magnetized in a Curved Field
YU. D. SYCHEV 146

The Measurement of Contact Angles of Iron Wetting Graphite Block
A. YA. KHRANOV and V. P. CHERNOBROVKIN 149

Internal Friction in Recrystallized Alloys of Aluminium and Magnesium
A. V. GRIN' 152

70th Birthday of V. D. KUZNETSOV—Editorial 153

VOL.
4
1957

VOL.
4
1957

A THEORY OF LATTICE-SPIN RELAXATION IN PARAMAGNETIC SALTS OF IRON GROUP ELEMENTS WITH AN EVEN NUMBER OF ELECTRONS *

V. I. AVVAKUMOV

(Received 20 October 1956)

A general formula has been derived for the times of lattice-spin relaxation of hydrated paramagnetic salts of iron group elements with an even number of electrons in the incomplete shell.

INTRODUCTION

Theoretical studies of the lattice-spin interaction in crystalline salts of elements of the first transitional group have referred hitherto only to salts of ions with an uneven number of electrons [1-3], because it is these ions which have been most thoroughly studied experimentally, especially by paramagnetic resonance. Lately, however, papers have been appearing which describe such experiments with slats of ions with even numbers of electrons [6,7].

A characteristic of these ions is that by virtue of Kramers' theorem [16], their spin degeneration can be fully related to crystal fields of sufficiently low symmetry and, as a result, the paramagnetic resonance can usually arise only at very high frequencies.

As the experimental technique of paramagnetic resonance is developed, interest in these ions will grow. Even so, very little theoretical work has as yet been done with salts of ions with even numbers of electrons and there is, in particular, a complete absence of a theoretical study of lattice-spin interaction in them.

The present work is making such a study for all the elements of the iron group, that is of ions which contain an even number of electrons in the incomplete $3d$-shell: Cr^{++}, $Mn^{+++}(3d^4\,{}^5D_0)$, Fe^{++} $(3d^6\,{}^5D_4)$, $V^{+++}(3d^2\,{}^3F_2)$, Ni^{++} $(3d^8\,{}^3F_4)$.

THE MECHANISM OF THE LATTICE-SPIN INTERACTION

The energy transfer in paramagnetic salts from the spins to the lattice vibrations and conversely, can be achieved by the modulation of the magnetic [1] or exchange [8] interactions between the paramagnetic ions by the lattice vibrations, or by the modulation of the crystal electric field acting on these ions [2,3]. This modulation makes an insignificant contribution to the relaxation, since the interactions depend to a great extent on the distance between the magnetic bodies, which in these cases are large. It is therefore assumed in this paper that the lattice-spin interaction mechanism is related to the modulation of the crystal electric fields by the lattice vibrations.

In aggreement with the hypothesis of Kronig and Van Vleck [3], which has been established for ions with an unequal number of electrons, it is assumed that the lattice-spin reaction is accomplished across the orbit owing to the presence of the orbital-spin bond.

The crystal field due to a magnetic ion is assumed to have a basic, cubic symmetry.

This is found frequently enough in hydrated salts. Since crystal fields of lower symmetry are always superposed on the cubic field in actual crystals, three cases of low-symmetry fields have been examined: a, tetragonal; b, trigonal, with the C_3 axis directed along the cube diagonal; c, orthorhombic.

The problem can be expressed as the Hamiltonian:

$$\mathbf{H} = \mathbf{H}_k + \mathbf{H}_n + \mathbf{H}_z + \mathbf{H}_{ss} + \mathbf{H}_{so} + \mathbf{H}_{ol} + \mathbf{H}_l, \quad (1)$$

where $\mathbf{H}_k$ is the energy of the ion in a crystal field of cubic symmetry; $\mathbf{H}_n$ is the ionic energy in a crystalline field of low symmetry; $\mathbf{H}_z$ the ionic energy in the outer constant magnetic field; (Zeeman energy); $\mathbf{H}_{ss}$ is the energy of the spin-spin interaction; $\mathbf{H}_{so}$ is the energy of the orbital spin interaction; $\mathbf{H}_{ol}$ is the energy of the orbit-lattice interaction; $\mathbf{H}_l$ is the lattice energy.

The terms in (1) which contain the spin variables are put into the form of a spin Hamiltonian [5],

* *Fiz. metal. metalloved.* 4, No. 2, 193-204, 1957 [Reprint Order No. POM 36].

$$W = H_z + H_{ss} + H_{so} =$$

$$= DS_z^2 + \beta(g_\perp H_x S_x + g_\perp H_y S_y + g_\parallel H_z S_z) \quad (2a)$$

for the field of axial symmetry, and

$$W = DS_z^2 + E(S_y^2 - S_x^2) +$$

$$+ \beta(g_\parallel H_x S_x + g_y H_y S_y + g_z H_z S_z) \quad (2b)$$

for the field of orthorhombic symmetry.

The calculations are made using the theory of disorder. The Starkie energy of the magnetic ion and the lattice energy, are taken as the undisordered and the orbital-spin and orbital-lattice interactions as the disordered.

The interaction of the magnetic particles with the lattice vibrations will differ in character at low and high temperatures. At a temperature T considerably lower than the Debye temperature θ, the lattice-spin interaction will be conditioned by direct processes, that is by processes in which the transition of the spin from one condition ($W\eta'$) to another ($W\eta''$) is accompanied by the appearance of a phonon with energy $h\omega = W\eta' - W\eta''$. At high temperatures ($T \sim \theta$), the process of combined dispersion of phonons will predominate in the lattice-spin interaction, these being processes during which the transition of spin from the state $W\eta'$ to the state $W\eta''$ will be accompanied by the absorption of one phonon (ω_i) and the emission of another (ω_j), so that

$$h\omega = h\omega_j - h\omega_i = W\eta' - W\eta''$$

Both these processes are discussed in this paper.

THE OPERATOR OF THE LATTICE-SPIN INTERACTION

The quantity which characterizes the lattice-spin interaction appears to be the time of the lattice-spin relaxation and, according to the theory of Kasimir and Du Pré [10], this is given by the formula

$$\tau = \frac{C_H}{\alpha}, \quad (3)$$

where C_H is the heat capacity of the spin system for a constant value of the intensity of the magnetic field H; α is the coefficient of thermal conductivity between the spin system and the lattice.

If T_s denotes the temperature of the spin system, T_l the temperature of the lattice and dQ/dt the rate of transfer of heat from the spin-system to the lattice then, neglecting the exchange interactions, we have:

$$C_H = \frac{b + CH^2}{T_s^2} \quad (4)$$

$$\alpha = \lim_{T_s \to T_l} \left[\frac{dQ}{dt} (T_s - T_l)^{-1} \right] =$$

$$= \frac{N}{2(2S+1)kT^2} \sum_{\eta'} \sum_{\eta''} A_{\eta'\eta''} (W_{\eta'} - W_{\eta''})^2. \quad (5)$$

In these formulae, b is the magnetic heat capacity constant, C the Curie constant, S the amount of spin, N the number of magnetic particles, $W\eta'$ and $W\eta''$ the energy of the spin levels η' and η'', $A\eta'\eta''$ the probability of transfer due to the lattice-spin interaction and is expressed by the following formulae: if the direct processes are responsible for the relaxation, by

$$A_{\eta_i'\eta_i''} = \frac{4\pi^2}{h^2}$$

$$\langle \rho_\omega |H'_{sl}(1, \eta', n_i;\ 1, \eta'', n_i + 1)|^2 \rangle_{cp}; \quad (6a)$$

but if the combined dispersion processes cause the lattice-spin interaction, by

$$A_{\eta'\eta''} = \frac{4\pi^2}{h^2} \int_c^{\frac{k\theta}{h}} \langle \rho_{\omega_i} \rho_{\omega_j} |H'_{sl}(1, \eta', n_i, n_j;$$

$$1, \eta'', n_i - 1, n_j + 1)|^2 \rangle_{cp} d\omega. \quad (6b)$$

In these formulae, ρ_ω is the spectral density of the phonons, θ the Debye temperature, H'_{sl} the matrix element of the lattice-spin interaction operator. The mean is taken of all directions of emission and of polarization, and of all quantum numbers of phonons. In the matrix elements H'_{sl} in (6a) and (6b), the first index determines the orbital condition of the ion, the second the state of spin, and the third and fourth (6b) the quantum state of the i th and j th lattice oscillors.

The operator of the lattice-spin interaction H'_{sl} must now be determined. As mentioned above, this interaction is achieved across the orbit, that is, it is the result of the orbital-spin interaction (H_{so}) from the one side, and the orbital-lattice interaction (H_{ol}) from the other. The formula given by the disorder theory is therefore [11]

$$H'_{sl}(i, i') = \sum_k{}' \frac{H_{so}(i, k) H_{ol}(ki')}{E_i - E_k} \qquad (7)$$

Integration is carried out for all the intermediate states required by the index K which is made up of the three indices which characterize respectively the orbital and spin states of the ion and the quantum state of the lattice.

The calculations also use the disorder formulae for H'_{sl}, when the transfer (of spin) is accomplished through two or three intermediate states.

The orbital-spin interaction operator is put into the form

$$H_{sl} = \lambda (LS)$$

There remains the orbital-lattice interaction operator H_{ol} to be determined before H'_{sl} can be found.

Let us consider the following model.

1. The magnetic ion is surrounded by six nearest neighbours (a XY_6 complex, where X represents the magnetic ion and Y the charges or electric dipoles) situated at equal distances from the magnetic ion, and having the same charge e, or dipole moment ν; the crystal field which they form with the magnetic ion has cubic symmetry.

2. The structural distortion of the complex XY_6 due to distant neighbours is not great, so we can take the equilibria of the state of XY as remaining unaltered. The inconsiderable structural distortion of the complex is equivalent to the formation of a weak crystal field of lower symmetry superposed on the cubic field around the magnetic ion.

Then in conformity with Van Vleck [13], the orbital-lattice interaction operator can be expressed by

$$H_{ol} = V_2 Q_2 + V_3 Q_3 + V_4 Q_4 + V_5 Q_5 + V_6 Q_6 + \\ + B (Q_p Q_r), \qquad (8)$$

where Q_K is the even (from reflexion by the centre of symmetry) normal vibration co-ordinate of the complex, presented as superposed on the normal lattice vibrations [3] by

$$Q_k = \sum_i a_{ki} q_i. \qquad (9)$$

$B (Q_p 1_r)$ includes the squared terms of Q.

In (9), q is the normal lattice vibration co-ordinate with matrix elements

$$q(n_i, n_i + 1) = \left[\frac{h(n_i + 1)}{4\pi^2 M \omega_i}\right]^{1/2}, \qquad (10)$$

where M is the total mass of the crystal, n_i is the quantum number of the lattice oscillator with frequency ω_i, and a_{ki} is the amplitude

The operators V_k in H_{ol} (8) have the following form (if they are the strong ones which connect the magnetic ion with its nearest neighbours, they will be isotropic),

$$V_2 = -\frac{18e\mu}{R^5} \sum (x_0^2 - y_0^2) - \\ - \frac{75}{4} \cdot \frac{e\mu}{R^7} \sum [x_0^4 - y_0^4 - 6z_0^2 (x_0^2 - y_0^2)],$$

$$V_3 = \frac{1}{\sqrt{3}} \left\{ - \frac{18e\mu}{R^5} \sum (x_0^2 + y_0^2 - 2z_0^2) \right. \\ - \frac{75}{4} \cdot \frac{e\mu}{R^7} \sum [x_0^4 + y_0^4 - 2z_0^4 - \\ \left. - 6x_0^2 (y_0^2 - z_0^2) - 6y_0^2 (x_0^2 - z_0^2)] \right| \qquad (11)$$

$$V_4 = \frac{24e\mu}{R^5} \sum x_0 y_0 + \\ + \frac{15e\mu}{R^7} \sum [(x_0^3 y_0 + x_0 y_0^3) - 6z_0^2 x_0 y_0]$$

$$V_5 = \frac{24e\mu}{R^5} x_0 z + \\ + \frac{15e\mu}{R^7} \sum [(x_0^3 z_0 + x_0 z_0^3) - 6y_0^2 x_0 z_0],$$

$$V_6 = \frac{24e\mu}{R^5} \sum y_0 z_0 + \\ + \frac{15e\mu}{R^7} \sum [(y_0^3 z_0 + y_0 z_0^3) - 6x_0^2 y_0 z_0].$$

Integration is carried out with respect to the co-ordinates of all the $3d$ electrons of the magnetic ion.

In computing the operators V_K we used the method of equivalent operators. Equivalent operators are known [5] for the co-ordinates of some of the operators entering into V_K; those remaining have to be calculated, viz:

$$\left.\begin{aligned}
\sum [x_0^4 - y_0^4 - 6z_0^2(x_0^2 - y_0^2)]\, MM' &= \frac{f}{2}[(L_x^2 - L_y^2)(L_x^2 + L_y^2 - 6L_z^2) + \\
&+ (L_x^2 + L_y^2 - 6L_z^2)(L_x^2 - L_y^2) + 10(L_x^2 - L_y^2)], \\
\sum [x_0^3 y_0 + x_0 y_0^3 - 6z_0^2 x_0 y_0]\, MM' &= \frac{f}{2}[(L_x L_y + L_y L_x)(L_x^2 + L_y^2 - 2L_z^2) + \\
&+ (L_x^2 + L_y^2 - 2L_z^2)(L_x L_y + L_y L_x) + 10(L_x L_y + L_y L_x)], \\
\sum [x_0^3 z_0 + x_0 z_0^3 - 6y_0^2 z_0 x_0]\, MM' &= \frac{f}{2}[(L_x L_z + L_z L_x)(L_x^2 + L_z^2 - 6L_y^2) + \\
&+ (L_x^2 + L_z^2 - 6L_y^2)(L_x L_z + L_z L_x) + 10(L_x L_z + L_z L_x)],
\end{aligned}\right\} \quad (12)$$

$$\left.\begin{aligned}
\sum [y_0^3 z_0 + y_0 z_0^3 - 6x_0^2 y_0 z_0]\, MM' &= \frac{f}{2}[(L_y L_z + L_z L_y)(L_z^2 + L_y^2 - 6L_x^2) + \\
&+ (L_z^2 + L_y^2 - 6L_x^2)(L_y L_z + L_z L_y) + 10(L_y L_z + L_z L_y)],
\end{aligned}\right\} \quad (13)$$

$$f = +\frac{3(2l+1-4S)[-7(l-2S)(l-2S+1)-3(l-1)(l+2)]\,\overline{r_0^4}}{(2l-3)(2l-1)(2l+3)(2l+5)(L-1)(2L-1)(2L-3)},$$

where L_x, L_y, L_z are the components of the orbital moment of the ion, l, L, S are the orbital moment of the electron and the orbital moment and spin of an atom respectively.

Finally, we reduce (5) for the coefficient of thermal conductivity α to a form convenient for computation. The matrix element of the operator H'_{sl} can be represented [15] as

$$H_{sl}(1, \eta_i', n_i, n_j;\ 1, \eta_i'', n_i + 1) = \\ = \sum H_k(1, \eta_i';\ 1, \eta_i'') Q_k(n_i, n_i + 1), \quad (14a)$$

if the direct processes are responsible for the lattice-spin interaction, and as

$$H_{sl}(1, \eta_i', n_i\, n_j;\ 1, \eta_i'', n_i - 1, n_j + 1) = \\ = \sum H_{km}(1, \eta_i';\ 1, \eta_i'') \cdot \\ \cdot Q_k(n_i, n_i - 1)\, Q_m(n_j, n_j + 1), \quad (14b)$$

if the lattice-spin reaction is due to the processes of combined phonon dispersion.

Since the normal co-ordinates are orthogonal and the i and j oscillators can be treated as independent variables, the expression for $A\eta'\eta''$ can be rewritten as

$$A_{\eta_i'\eta_i''} = \frac{4\pi^2}{h^2}\sum H_k(\eta_i', \eta_i'')^2 < \rho_\omega Q_k^2 >_{cp}, \quad (15a)$$

$$A_{\eta_i'\eta_i''} = \frac{4\pi^2}{h^2}\int_0^{\frac{k\theta}{h}} \sum H_{km}(\eta_i', \eta_i'')^2 < \rho_{\omega_i} Q_k^2 >_{cp} \\ < \rho_{\omega_j} Q_m^2 >_{cp} d\omega. \quad (15b)$$

Substituting (15a) and (15b) in (5), we obtain : for the direct processes

$$\alpha = \frac{NC_0}{2(2S+1)T}\sum \text{spur}\,[V_k W - W V_k]^2,$$

$$V = W H_k - H_k W,\ C_0 = \frac{16\pi^3 R^2}{15dh^4}\left(\frac{2}{v_l^5} + \frac{3}{v_t^5}\right) \quad (16a)$$

for the combined phonon dispersion processes

$$\alpha = \frac{NGI_n}{2(2S+1)kT^2}\sum \text{spur}\,[H_{km} W - W H_{km}]^2. \quad (16b)$$

where

$$G = \left[\frac{8\pi^3 R^2}{15d}\left(\frac{2}{v_l^5} + \frac{3}{v_t}\right)\right]^2$$

$$I_n = \int_0^{\frac{k\theta}{h}} \omega^n \frac{\exp\frac{h\omega}{kT}}{\left[\exp\left(\frac{h\omega}{kT}\right) - 1\right]^2} d\omega, \quad (17)$$

V_l, V_t, are the longitudinal and transverse components of the speed of sound, d the density of the crystal and R the equilibrium distance between the magnetic ion and a molecule of water.

Fe^{++} SALTS

Computations will be made in full only for Fe^{++} salts since those for the other ions are analogous.

In the crystal field of cubic symmetry, the ground state of the Fe^{++} ion, $3d^6 {}^5D_4$, is split into a doublet and triplet with the triplet lower (Fig. 1). The lower level is then divided by the field of lower

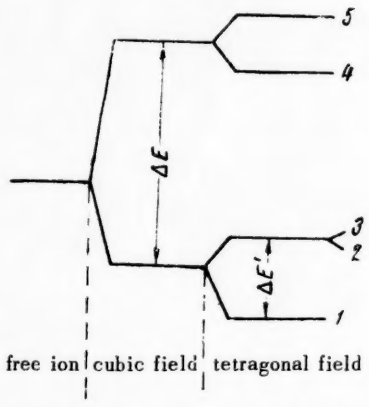

FIG. 1. Diagram of orbital levels of Fe^{++}. The numbers on the levels correspons to the first index of the matrix elements in (18).

symmetry which has already been mentioned as superposed on the cubic. The value of the cubic portion, $\Delta E \sim 10^4 cm^{-1}$, of the lower-symmetry portion, $\Delta E' \sim (10^2 - 10^3)$ cm^{-1} We shall neglect the effect of the excited cubic level when calculating the times of the lattice-spin relaxation: we shall also consider the value of $(\Delta E'/\Delta E) \approx (10^{-2} - 10^{-4})$ negligible in comparison with unity.

We shall assume that the splitting of the field of low symmetry is such that the orbital singlet as the lower state (Fig. 1).

Furthermore we require the following matrix elements:

$$H_{so}(1, \eta'; 2\tau_i'') = \lambda S_x(\tau_i', \eta''),$$

$$H_{so}(1, \tau_i'; 3, \eta'') = -i\lambda S_y(\tau_i'\eta''),$$

$$H_{so}(2, \eta'; 3, \eta'') = \lambda S_z(\eta', \eta''),$$

$$H_{ol}(2, n_i; 2, n_i + 1) =$$

$$= -a\left(\frac{1}{\sqrt{3}} Q_3 + Q_2\right)(n_i, n_i + 1),$$

$$H_{ol}(3\, n_i; 3, n_i + 1) =$$

$$= -a\left(\frac{1}{\sqrt{3}} Q_3 - Q_2\right)(n_i, n_i + 1), \quad (18)$$

$$H_{ol}(2, n_i; 1, n_i + 1) = 2ibQ_6(n_i n_i + 1),$$

$$H_{ol}(3, n_i; 2, n_i + 1) = 2ibQ_4(n_i, n_i + 1),$$

$$H_{ol}(3, n_i; 1, n_i + 1) = 2bQ_5(n_i, n_i + 1),$$

where λ is the orbital-spin bond constant, and the constants a and b are given by,

$$a = -\frac{4}{7}\left[\frac{9e\mu\overline{r_0^2}}{R^5} - \frac{25}{2}\cdot\frac{e\mu\overline{r_0^4}}{R^7}\right],$$

$$b = \frac{2}{7}\left[\frac{6e\mu\overline{r_0^2}}{R^5} - \frac{5e\mu\overline{r_0^4}}{R^7}\right];$$

r_0^2, r_0^4 are the mean square and the mean fourth power of the radius of the orbit of a $3d$ electron, e is the effective charge of the magnetic ion and μ is the dipole moment of a molecule of water.

(a) The direct processes

Let us first determine the approximation in which the matrix element H'_{sl} is greatest. Using the matrix elements from (18), for the case when there is a weak field of tetragonal symmetry, we obtain for the second approximation (7)

$$H_{sl}^{tetr} = 2i\lambda b\left[\frac{S_x Q_6}{-\Delta E' + W_{\tau_i'} - W_{\tau_i''}} - \frac{S_x Q_6}{-\Delta E' - \hbar\omega} - \right.$$

$$\left. - \frac{S_y Q_5}{-\Delta E' + W_{\eta_i'} - W_{\tau_i''}} + \frac{S_y Q_5}{-\Delta E' - \hbar\omega}\right]. \quad (19)$$

Substituting $\hbar\omega = W_{\tau_i'} - W_{\tau_i''}$, we obtain

$$H_{sl}^{tetr} = \frac{4i\lambda b}{\Delta E'^2}(S_x Q_6 - S_y Q_5)\hbar\omega = \sum_k H_k Q_k. \quad (20)$$

In the third approximation (by taking the matrix elements of the operator H_{so} in the value of two factors H in the numerator, and the operator H_{ol} in the value of one), we have

$$H_{sl}^{tetr} =$$

$$- \frac{\lambda^2}{\Delta E'^2} a\left[\frac{1}{\sqrt{3}}(S_x^2 + S_y^2) Q_3 + (S_x^2 - S_y^2) Q_2\right] +$$

$$+ \frac{2\lambda^2}{\Delta E'^2} b[(S_x S_y + S_y S_x) Q_4 + (S_x S_z \quad S_z S_x) Q_5 +$$

$$+ (S_y S_z + S_z S_y) Q_6] = \sum H_k Q_k. \quad (21)$$

Comparison of formulae (20) and (21) shows that the value of the relaxation times τ [$\tau \sim H'^{-2}_{sl}$] in the third approximation is $\frac{\lambda^2}{|W_{\tau_i'} - W_{\tau_i''}|^2} \sim 10^4$

times greater than in the second. This is because $H'_{sl} = 0$ in the second approximation, if the modulated terms $h\omega = [W\eta' - W\eta'']$ are neglected in the denominators.

The fourth approximation can also be shown to be less than the third.

Further, in accordance with (16a) we obtain

$$\tau_{\text{tetr}} = \frac{8}{5}\frac{\dot{N}C_0}{T}\frac{\lambda^4}{\Delta E'^4}\left\{3(999b^2+512a^2)D^4 + \right.$$

$$+\left[(2718b^2+878a^2)(H_x^2+H_y^2)+\right.$$

$$\left.+(3294b^2+2304a^2)\frac{g_\perp^2}{g_\perp^2}H_z^2\right]\beta^2 g_\perp^2 D^2 +$$

$$+\left[(189b^2+56a^2)(H_x^4+H_y^4)+\right.$$

$$(189b^2+168a^2)\frac{g_\parallel^4}{g_\perp^4}H_z^4+(504b^2-7a^2)H_x^2H_y^2+$$

$$\left.\left.+(504b^2+26a^2)(H_x^2H_z^2+H_y^2H_z^2)\cdot\frac{g_\parallel^2}{g_\perp^2}\right]\beta^4 g_\perp^4\right\} \quad (22)$$

To find τ, b and c in (4) remain to be calculated. Neglecting exchange interactions, we have, when $S = 2$

$$b = b_{\text{el}} + b_{\text{magn}} =$$

$$= \frac{7ND^2}{10k} + \frac{Ng^2\beta^2H_i^2}{k},\ C = \frac{2Ng^2\beta^2}{k}. \quad (23)$$

where b_{el} and b_{magn} are parts of the thermal capacity constant b, dependent respectively on the electrostatic and electromagnetic interactions and D is the spin Hamiltonian constant (2).

The spin-spin interaction has to be taken into consideration before we obtain a final expression for τ. This is most easily obtained by introducing an internal magnetic field H_i [3]. Assuming that this internal field is distributed in accordance with Gauss'law, we obtain

$$H_k^2 = H_{ok}^2 + \frac{1}{6}H_i^2,\ H_k^4 = H_{ok}^4 + 2H_{ok}^2H_i^2 +$$

$$+\frac{1}{3}H_i^4,\ H_k^2H_l^2 = H_{ok}^2H_{ol}^2 + \frac{1}{3}(H_{ok}^2+H_{ol}^2)H_i^2 +$$

$$+\frac{1}{9}H_i^4;\ k, l = x, y, z.$$

In (22) and also in the formulae to be obtained below for a, it is to be understood that the field components H_K^2, H_K^4 and $H_K^2H_Z^2$ are average values.

Finally, we obtain from (3)

$$\tau = \frac{N\left[7D^2 + 20g^2\beta^2\left(H_o^2 + \frac{1}{2}H_i^2\right)\right]}{10kT^2\alpha_{\text{tetr}}} \quad (24)$$

(b) Processes of combined dispersion of phonons.

Of the second order processes we are concerned only with the processes of combined phonon dispersion since it is these processes which determine the lattice-spin interaction at high temperatures. Practically all the lattice vibrations will participate in the relaxation in this case.

To calculate τ we must now use the third approximation formula for H'_{sl}, and as a result take two matrix elements of the operator H_{ol} and one of H_{so} for the values of the H terms in the numerator.

If the expression for H_{sl} is resolved into a series and $\hbar\omega_{\text{res}} = [W\eta' - W\eta''] = \hbar\omega_j - \hbar\omega_i]$ is negligible in comparison with the lattice quanta (that is by putting $h\omega j \approx \hbar\omega_i = \hbar\omega$), then in the third approximation we obtain

$$H'_{sl} = \frac{8i\lambda h}{\Delta E'^3}\hbar\omega\left\{\left[\frac{1}{\sqrt{3}}a(Q_3Q'_6 - Q'_3Q_6) + \right.\right.$$

$$\left.+a(Q_2Q'_5 - Q'_2Q_5) + b(Q_4Q'_5 - Q'_4Q_5)\right]S_x +$$

$$\left[\frac{1}{\sqrt{3}}a(Q_3Q'_5 - Q'_3Q_5) - a(Q_2Q'_6 - Q'_2Q_6) - \right.$$

$$\left.\left.-b(Q_4Q'_6 - Q'_4Q_6)\right]S_y + [b(Q_6Q'_5 - Q'_6Q_5)]S_z\right\}$$

$$= \sum H_{km}Q_kQ_m \quad (25)$$

A co-ordinate is denoted by Q_k (without dash) if the ith lattice oscillator in superposition (9) achieves the transition $n_i \to n_i - 1$, and by Q'_m - if the j lattice oscillator achieves $n_j \to n_j + 1$.

It can be readily demonstrated that the fourth approximation gives a value for τ which is of the same order as the third approximation. Actually, by using the fourth approximation formula for H'_{sl} (in the numerator of which were the two matrix elements H_{ol} and the two H_{so}), and the matrix elements in (18), we obtain

$$H'_{sl} = -\frac{16\lambda^2}{3\Delta E'^2}\Big\{-3a^2\Big[\Big(Q_2Q'_2+\frac{1}{3}Q_3Q'_2\Big)(S_x^2+S_y^2)+\frac{1}{\sqrt{3}}(Q_2Q'_3+Q'_2Q_3)\cdot(S_x^2-S_y^2)\Big]+$$

$$+\frac{\sqrt{3}}{2}ab\,[Q_3Q'_4+Q'_3Q_4)(S_xS_y+S_yS_x)+$$

$$(Q_3Q'_5+Q'_3Q_5)(S_xS_z+S_zS_x)+(Q_3Q'_6+Q'_3Q_6)$$

$$(S_yS_z+S_zS_y)+b^2\,[(-Q_4Q'_4+Q_5Q'_5+Q_6Q'_6)$$

$$(2S_z^2-S_y^2)]\Big\} = \sum H_{km}Q_kQ'_m. \qquad (26)$$

When the formulae are in the forms of (16b), (17) and (3), it is easily seen that

$$\frac{\text{third appr.}}{\text{fourth appr.}} \sim \frac{\lambda^2 I_6}{h^2 I_8} = \frac{9}{7}\,\frac{\lambda^2}{(k\theta)^2} \sim 1.$$

Further,

$$\tau_3 = \frac{128\,NGI_8\lambda^2a^2b^2h^2}{5\,\Delta E'^6kT^2}[84D^2+10\beta^2$$

$$(\gamma g_\perp^2H_x^2+\gamma g_\perp^2H_y^2+g_\parallel^2H_z^2)]\cdot\Big(4+\frac{3b^2}{a^2}\Big)\cdot$$

$$\tau_4 = \frac{64}{15}\,\frac{NGI_6\lambda^4a^2b^2}{\Delta E'^6kT^2}\,[1044D^2+$$

$$+\gamma_1\beta^2g_\perp^2(H_x^2+H_y^2)+\gamma_2g_\parallel^2\beta^2H_z^2], \qquad (27)$$

where

$$\gamma = \frac{4+\frac{6b^2}{a^2}}{4+\frac{3b^2}{a^2}},\quad \gamma_1 = 252+546\,\frac{a^2}{b^2}+$$

$$+1134\,\frac{b^2}{a^2},\quad \gamma_2 = 252+504\,\frac{a^2}{b^2}.$$

and finally,

$$\tau = \frac{N\Big[7D^2+20g^2\beta^2\Big(H_0^2+\frac{1}{2}H_1^2\Big)\Big]}{10kT^2(a_3+a_4)}. \qquad (28)$$

THE OTHER IONS WITH AN EVEN NUMBER OF ELECTRONS

The remaining ions with an even number of electrons can be divided into two groups, (a) Ni^{++}, and (b) Cr^{++}, Mn^{+++}, V^{+++}. In Ni^{++} the ground state in the cubic field is nondegenerate, in the others degenerate.

The weak field with low symmetry in Ni^{++} salts does away with the degeneration of the excited levels: The value of $\Delta E'$ in it is much less than ΔE in the cubic portion. The value of $\Delta E'$ can be neglected in comparison with ΔE.

In contrast to the Ni^{++} salts, the field of low symmetry in the salts of Cr^{++}, Mn^{+++} and V^{+++} does away with the degeneration of the basic cubic level. Although in this case also, $\Delta E'$ is less than ΔE it cannot be neglected because the cubic sub-levels are also the intermediate states through which the lattice-spin interactions take place. In this case we neglect $1/\Delta E$ in comparison with $1/\Delta E'$ in the formulae for H'_{sl}, that is, in contrast to the Ni^{++} salts, we neglect the cubic portions in comparison with the parts with low symmetry (see following section).

The formulae for τ can be presented in the following general form: for the direct processes

$$\tau = F_1\,\frac{D^2+\delta g^2\beta^2H^2}{D^4+\delta_1D^2g^2\beta^2H^2+\delta_2g^4\beta^4H^4}, \qquad (29)$$

if the weak field has axial (tetragonal or trigonal symmetry), and for the second order processes

$$\tau = \tau_0\,\frac{\frac{b}{C}+H^2}{\frac{b}{C}+pH^2} \qquad (30)$$

The values of δ, δ_1, δ_2 and p for a weak field of tetragonal symmetry are given in Table 1.

DISCUSSION OF RESULTS

We have derived general formulae for the determination of the relaxation times of the salts of all ions of the iron group which have an even number of electrons in the incomplete $3d$ electron shell.

The following conclusions can be made from analysis of these formulae:

1. Dependence on the magnitude of spin.

This relationship has the general form:

VOL. 4 1957

TABLE I. Values of the constants δ, δ_1 δ_2 and p in formulae (29) and (30).

spin S	Ion	δ	δ_1	δ_2	p
1	V^{+++}	3	6	11	0.10
1	Ni^{++}	3	6	13	–
2	Cr^{++}, Mn^{+++}	$\frac{20}{7}$	0.87	0.04	0.9
2	Fe^{++}	$\frac{20}{7}$	0.97	0.08	0.4

$$\tau = \frac{C_H}{\alpha} \sim \frac{\sum_{\gamma_i'} \sum_{\gamma_i''} (W_{\gamma_i'} - W_{\gamma_i''})^2}{\sum_k \text{spur}\,[2WA_kW - W^2A_k - A_kW]^2}$$

for the direct processes, and

$$\tau = \frac{C_H}{\alpha} \sim \frac{\sum_{\gamma_i'} \sum_{\gamma_i''} (W_{\gamma_i'} - W_{\gamma_i''})^2}{\sum_k \text{spur}\,[A_kW - WA_k]^2}$$

for the processes of combined phonon dispersions where,

$$A_k = (S_x^2 - S_y^2),\ (S_x^2 + S_y^2),\ (S_kS_y + S_yS_x),$$

$$(S_xS_z + S_zS_x),\ (S_yS_z + S_zS_y).$$

and W is the spin Hamiltonian.

These formulae show that the spin components enter the coefficient of thermal conductivity (the diagonal totals) as the twelfth power if the direct processes cause the lattice-spin interaction, and as the eighth if the latter is due to the combination of dispersed phonons. In the numerator the spin components are in the fourth power. It is therefore only as a result of the value of the spin that the actual time of relaxation in Fe^{++} salts must be 2×10^2 times shorter than in V^{+++} salts at low temperatures, and 5×10 times at high temperatures, other conditions being equal.

Dependence on the intensity of the permanent magnetic field When $D \gg g\beta H$, formulae (29) and (30) show that the relaxation times do not depend on the intensity of the permanent field. If $D \sim g\beta H$, then the dependence on the field H is different at high and low temperatures since, at high temperatures, this dependence is expressed by a formula analogous to the Brons – Van Vleck formula [14]. Such a dependence of τ on the field intensity H appears in this work.

The dependence on temperature Formulae (22) and (24) for τ show that when relaxation is due to the direct processes, the dependence of τ on the temperature T is reversed: $\tau \sim T^{-1}$. Work on the saturation of paramagnetic resonance has shown such a dependence on temperature [17]. Measurements in parallel fields, however, show some of the relationships between τ and T to differ from this: in particular, at very low temperatures, it has been demonstrated that $\tau \sim T^{-n}$, where n varies from 1.7 to 3 [9], although this has been explained as due to other causes than the ineffectiveness of the mechanism of the lattice-spin interaction. In [12], for example, it has been shown that the dependence $\tau \sim T^{-2}$ can be obtained by examining a system of low frequency oscillators in resonance with a heat reservoir enclosing all the remaining lattice oscillations in liquid helium.

If the processes of the combined dispersion of phonons are responsible for the relaxation then a) at $T \gg \phi$, $\tau \sim T^{-2}$; b) when $T < \phi$, $\tau \sim T^{-7}$ (for Cr^{+++}, Mn^{+++}, Ni^{++} salts) or $\tau \sim T^{-9}$ (for salts of Fe^{++} and V^{+++}).

The anisotropy of the relaxation time The times of relaxation depend on the orientation of the magnetic field H in relation to the crystal axes, and all the formulae that we have derived indicate that there should be an anisotropy of these times.

Let us first examine a Ni^{++} ion. The ground orbital state of this ion in a crystal field of cubic symmetry appears to be nondegenerate, since the excited orbital state (levels) are higher by $\sim 10^4$ cm^{-1}. The weak fields of low symmetry formed by the slight splitting of these levels ($\Delta E'$) have therefore been neglected. This implies that we have neglected the modulations of the lattice vibration of the low-symmetry field in comparison

with the modulation of the basic (cubic) field. As a result, the interactions of the orbital shift of electrons with the lattice vibrations will be isotropic.

This is not enough to make the lattice-spin interaction isotropic. If the modulation of the low symmetry field can be neglected in practice, as argued above, then the fields themeselves can be neglected since it is on their size and symmetry that the splitting of the spin levels actually depends. The spin components S_x, S_y, S_z must contribute equally to the lattice-spin interaction in addition to the orbital-lattice interaction being isotropic, if the relaxation time is to be isotropic. It is easy to see that this can only be accomplished when the low-symmetry field is axially symmetrical about [111]. In this case the spin Hamiltonian has the form:

$$W = D\,(S_x + S_y + S_z)^2 + \beta g\,(H_x S_x + H_y S_y + H_z S_z)$$

(x, y, z are cubic co-ordinates) whence it is seen that all spin directions are equivalent. We have put $g_\perp = g_\parallel = g$, since we consider the low-symmetry field to be weak.

The salts of Cr^{++}, Mn^{+++}, Fe^{++}, and V^{+++}. In the cubic field, the ground orbital state of these ions remains degenerate. This basic cubic level then splits into sub-levels with low-symmetry fields, and these sub-levels, as previously described, are the intermediate states through which the lattice-spin interaction takes place, as a consequence of the modulation of the low-symmetry field. The fields superposed on the cubic field have either axial or orthorhombic symmetry, that is, they are anisotropic. The consequence is that the anisotropy in salts of this group of ions is due to the modulation of the low-symmetry fields.

In conclusion, the author thanks Professor Al'tshuler for directing this work.

REFERENCES

1. J. Wäller *Z. Phys.* 79, 370 (1932).
2. R. Kronig *Physica, Eindhoven* 6, 33 (1933).
3. J.H. Van Vleck *Phys. Rev.* 57, 426 (1940).
4. E.K. Zavoiskii *Doktorskaia dissertatsiia(doctor's thesis), FIAN,* (1946).
5. B. Bleany and K.W.H. Stevens *Rep. Progr. Phys.* 16, 108 (1953).
6. K. Ono, S. Koide and H. Sekiyama *Phys. Rev.*, 96, 38 (1954).
7. M. Tinkham *Proc. Phys. Soc.* A 68, 258 (1955).
8. S.A. Al'tshuler *Izv. Akad. Nauk SSSR, ser. fiz.* (1956 in press).
9. R.J. Benzie and A.H. Cooke *Proc. Phys. Soc.* A 63, 201 (1950).
10. H.B.G. Kasimir and F.K. Du Pre, *Physica, Eindhoven* 5, 507 (1938).
11. V. Gaitler *Kvantovaia teoriia izlucheniia (Quantum theory of radiation),* 107, 1940.
12. C.J. Gorter, L.C. Van der Marel and B. Bolger *Physica, Eindhoven* 21, 103 (1955).
13. J.H. Van Vleck *J. chem. Phys.* 5, 320, 1937.
14. K. Gorter, *Paramagnitnaiai relaksatsiia (Paramagnetic relaxation)* Izd. inos. lit. 131, 1949.
15. V.L. Avvajumov *(Candidates thesis),* Kazan, (1956).
16. A.H. Eschenfelder and L.C. Weidner, *Phys. Rev.* 92, 869 (1953).

VOL. 4 1957

EXCITON LIGHT ABSORPTION THEORY*

S.V. VONSOVSKII, V.I. CHEREPANOV AND V.S. GALISHEV

(Received 30 October 1956)

On the basis of a generalization of Frenkel's exciton theory of excited states [1] the probability of a photo-excited transition of a system of electrons from the ground to an excited state is calculated; it is found that the optical properties of such a system at the absolute zero are not quite analogous with the properties of a system of isolated atoms. When exchange and pairing processes in electron excitation are neglected, our theory reduces to Frenkel's.

1. INTRODUCTION

Seitz [2] has calculated the optical properties of solids at the absolute zero when the excited states of a crystal's electron system can be described by Frenkel exciton waves [3]. From his results it can be concluded that the optical properties of systems which can be described by such waves are analogous to those of isolated atom systems. Their light absorption spectra of discrete lines, not because the energy levels corresponding to the excited states do not form wide bands, but because of the selection rule, which only permits transitions into excited states with exciton wave-vectors zero.

We have also studied light absorption at the absolute zero but on the basis of the generalization of Frenkel's excited states theory developed by two of the present authors [1]. In contrast to all previous investigations of the subject [2–5] the calculations were based on secondary quantization which considerably simplified calculations and enabled us to treat a more general case, embracing exchange effects and electron pair excitations, not considered in the paper cited above. It turns out that the optical properties at the absolute zero are not completely analogous to those of systems of isolated atoms, although the absorption spectra remain line spectra.

2. THE INITIAL HAMILTONIAN PROBLEM AND ITS TRANSFORMATION

The model on which our calculations is based has already been discussed [1,6]. Following these previous papers we shall consider a crystal lattice with "frozen" positive ions with a completely homogeneous electron density and at each lattice site we must have in addition closed envelopes for each valency electron. Such an electron may be either in the normal, or one of the excited states. Spin electron characteristics are ignored, and excited states are considered non-degenerate.

The weakly excited state of a multi-electron system of a crystal in these approcimations was investigated in [1]. According to [1], the quantum levels of weakly excited states of a system are determined by assigning a complete sequence of occupation numbers N_k^0, using positive integral values; thus, the expression for energy of the system and the corresponding wave-function has the form·

$$H_0 = E(\ldots N_k^0 \ldots) =$$

$$\text{const} + \sum_k \sqrt{V_k^2 - U_k^2} \cdot N_k^0 \qquad (2.1)$$

$$C_{\{\ldots N_k^0 \ldots\}}(\ldots N_k \ldots) = \prod_k \delta_{N_k^0, N_k} \qquad (2.2)$$

where V_k and U_k are definite linear combinations of integrals dependent on electron interaction and the differences between energies in the excited and the ground "quasi-atomic" states (cf. Equation (3.7) in[1]), N_k = occupation number.

Hence the quantum states in the system of interacting electrons in a crystal under study can be interpreted as an association of individual "elementary excitations" or "quasi-particles" (excitons) obeying the Bose statistics. Each of these elementary excitations has an energy $(V_k^2 - U_k^2)^{\frac{1}{2}}$ in the state with quasi-momentum k. There is obviously here no interaction between

*Fiz. metal. metalloved. 4. No.2, 205–211, 1957 [Reprint Order No. POM37].

the elementary excitations, since the total energy is exactly the sum of the energies of the individual excitations, plus a constant.

The lowest state of a multi-electron system in a crystal realizable at absolute zero we define as that in which there are no elementary excitations.

The energy of this state is denoted $E_0 = E(....0....)$ and, generally speaking, it differs from the sum of the energies of isolated atoms since right from the start the theory embraces overlapping atomic wave-functions of adjacent sites. The wave function for the lowest state of the system is:

$$C_{\{...0...\}}(...N_k...) = \prod_k \delta_{N_k;\,0} \qquad (2.3)$$

The Hamiltonian of the multi-electron system in the field of a light wave can be written:

$$\hat{\mathbf{H}} = \hat{\mathbf{H}}_0 + \hat{\mathbf{W}}(t), \qquad (2.4)$$

where H_0 is the Hamiltonian in the absence of photoexcitation, whose proper values (2.1) were found in the previous paper [1] by a series of canonical transformations: $\mathbb{W}(t)$ is due to photoexcitation and is time-dependent (t = time). Photoexcitation is regarded as the cause of quantum transitions of the system from the lowest state into an excited one (exciton light absorption).

In co-ordinate representation the operator $\mathbb{W}(t)$ usually has the form:

$$\hat{\mathbf{W}}(t) = \frac{e}{\mu c}\sum_{j=1}^{N}(\vec{A}(t)\cdot\hat{\vec{I}}_j) \qquad (2.5)$$

Here e is the absolute electronic charge, μ its mass, c the speed of light;

$$\hat{\vec{I}}_j = -i(h/2\pi)\hat{\vec{\nabla}}_j, \quad \vec{A}(t)$$

$$\vec{A}(t) = \vec{A}_0[\exp(i\omega t) + \exp(-i\omega t)], \qquad (2.6)$$

where $\vec{A}_0$ is the amplitude, and $\omega = 2\pi\nu$ is the cyclic frequency of the light wave. Generally A depends on the space co-ordinates and time, but since in the visible range the wavelength of light greatly exceeds a lattice parameter, A can be taken as co-ordinate independent.

Hence we have for $\mathbb{W}(t)$ on the secondary quantization hypothesis the simple equation:

$$\hat{\mathbf{W}}(t) = \sum_{f,\lambda,\lambda'} W(f,\lambda;\, f,\lambda';\, t)\hat{a}^{+}_{f,\lambda}\hat{a}_{f,\lambda'}, \qquad (2.7)$$

in which the summation is extended over the numbers of all sites (f^1, f^2, f^3) and all states. In our model the subscript λ can only be 0 or 1 for the normal and excited states; $\hat{a}^{+}_{f,\lambda}$ and $\hat{a}_{f,\lambda}$ are the Fermi amplitude operators, and $W(f,\lambda;f,\lambda',t)$ is defined by:

$$W(f,\lambda;\, f,\lambda';\, t) =$$

$$= -\frac{ehi}{2\pi\mu c}\int \theta_{f,\lambda}(q)(\vec{A}(t)\cdot\hat{\vec{\nabla}}_q)\theta_{f,\lambda'}(q)\,dq, \qquad (2.8)$$

where h is Planck's constant, and $\theta_{f,\lambda}(q)$ are orthostandardized atomic functions, considered to act here as in the previous study. Then.

$$W(f,\lambda;\, f,\lambda';\, t) =$$

$$= -W(f,\lambda';\, f,\lambda;\, t), \quad W(f,\lambda;\, f,\lambda;\, t) = 0. \qquad (2.9)$$

By applying in succession to $\hat{\mathbb{W}}(t)$ defined as in (2.7) the same canonical transformations as to H_0 in [1] and by employing (2.9) we can easily show that $\hat{\mathbf{W}}(t) =$

$$= \frac{\sqrt{2N}\,ei}{\mu c}(\vec{A}(t)\cdot\vec{I}_{0,1})\sum_k a(k)\,\delta_{k;\,0}\,\hat{\mathbf{P}}_k, \qquad (2.10)$$

where

$$\vec{I}_{0,1} = -i\frac{h}{2\pi}\int \theta_0(q)\hat{\vec{\nabla}}_q\theta_1(q)\,dq, \qquad (2.11)$$

$$a^4(k) = \frac{V_k + U_k}{V_k - U_k}, \qquad (2.12)$$

and P_k is the momentum operator of the harmonic oscillator, corresponding to the wave-vector k.

Equation (2.10) shows that the sole possible transition of the multi-electron system from the ground to an excited state is that which satisfies the selection rule

$$\vec{k} = 0 \qquad (2.13)$$

3. PROBABILITY OF GROUND-EXCITED STATE TRANSITION OF THE SYSTEM

Our discussion is analogous to the semi-classical treatment of absorption in [2]. We adopt the time-dependent Schrodinger equation in the secondary quantization theory with the Hamiltonian (2.4):

VOL. 4 1957

$$\{\mathbf{H}_0 + \hat{\mathbf{W}}(t)\}\ C(\ldots N_k \ldots;\ t) =$$

$$= i\frac{h}{2\pi}\frac{\partial C(\ldots N_k \ldots;\ t)}{\partial t} \qquad (3.1)$$

Let us suppose that photoexcitation acts only from the moment $t = 0$. It then becomes of interest to find a solution of (3.1) equal at $t = 0$ to $C\ \{\ldots 0 \ldots\}(\ldots N_k \ldots)$. It can be put in the form of a series:

$$C(\ldots N_k \ldots;\ t) =$$

$$= C_{\{\ldots 0 \ldots\}}(\ldots N_k \ldots)\ \exp\left[-\frac{2\pi i}{h}E(\ldots 0 \ldots)\,t\right] +$$

$$+ \sum_{\{\ldots N_k^0 \ldots\}}{}' b_{\{\ldots N_k^0 \ldots\}}(t)\, C_{\{\ldots N_k^0 \ldots\}}(\ldots N_k \ldots)$$

$$\exp\left[-\frac{2\pi i}{h}E\cdot(\ldots N_k^0 \ldots)\,t\right], \qquad (3.2)$$

where the primes and the subscripts show that in summating over all possible collections $\{\ldots N_k^0 \ldots\}$ we exclude the collection $\{\ldots 0 \ldots\}$ and the coefficients $b\{\ldots N_k^0 \ldots\}(t)$ in (3.2) are considered to be small, approaching zero as $t \to 0$. If we put (3.2) into (3.1) and assume that the proper functions of H_0 satisfy the equation

$$\hat{\mathbf{H}}_0 C_{\{\ldots N_k^0 \ldots\}}(\ldots N_k \ldots) =$$

$$= E(\ldots N_k^0 \ldots)\, C_{\{\ldots N_k^0 \ldots\}}(\ldots N_k \ldots) \qquad (3.3)$$

and if we neglect terms containing the product of $b\{\ldots N_k^0 \ldots\}(t)$ by $W(t)$ we find:

$$\frac{ih}{2\pi}\sum_{\{\ldots N_k^0 \ldots\}}{}' \frac{db_{\{\ldots N_k^0 \ldots\}}(t)}{dt} C_{\{\ldots N_k^0 \ldots\}}(\ldots N_k \ldots)$$

$$\exp\left[-\frac{2\pi i}{h}E(\ldots N_k^0 \ldots)\,t\right] =$$

$$= \hat{\mathbf{W}}(t)\ C_{\{\ldots 0 \ldots\}}(\ldots N_k \ldots)$$

$$\exp\left[-\frac{2\pi i}{h}E(\ldots 0 \ldots)\,t\right]. \qquad (3.4)$$

If we multiply both sides of this equation by $C^*_{\{\ldots N_k^0 \ldots\}}(\ldots N_k \ldots)$, and summate over all possible combinations of occupation numbers and take into consideration the condition for orthostandardization of proper functions, we find:

$$\frac{ih}{2\pi}\frac{db_{\{\ldots N_k^0 \ldots\}}(t)}{dt} = (\ldots N_k^0 \ldots |\hat{\mathbf{W}}(t)| \ldots 0 \ldots)\cdot$$

$$\exp\left\{\frac{2\pi i}{h}[E(\ldots N_k^0 \ldots) - E(\ldots 0 \ldots)]\,t\right\} \qquad (3.5)$$

where

$$(\ldots N_k^0 \ldots\ \hat{\mathbf{W}}(t)| \ldots 0 \ldots) = \sqrt{2}\ W_0 |\exp(i\omega t) +$$

$$+ \exp(-i\omega t)](\ldots N_k^0 \ldots |\hat{\mathbf{P}}_0| \ldots 0 \ldots). \qquad (3.6)$$

Also

$$W_0 = \frac{\sqrt{N}\,ei}{2c}(\vec{A}_0 \cdot \vec{I}_{0,1})\ a(0). \qquad (3.7)$$

The matrix element in the right hand side of (3.6) can be calculated from the explicit equations (2.2) and (2.3) for the proper functions, and the property of the momentum operator P_0 (cf Frenkel, [7] p.646):*

$$(\ldots N_k^0 \ldots |\hat{\mathbf{P}}_0| \ldots 0 \ldots) = \frac{i}{\sqrt{2}}\,\delta_{N_0^0;\,1}\prod_{k\,(\neq 0)}\delta_{N_k^0;\,0}. \qquad (3.8)$$

Consequently, only those matrix elements of the excitation operator (3.6) are not zero which correspond to the formation of one exciton with a wave-vector $\vec{k} = 0$, so that for simplification we can put:

$$b_{\{0,\,0,\,\ldots,\,1,\,\ldots 0\}}(t) =$$

$$= b_1(t), \quad E(0, 0, \ldots, 1, \ldots 0) = E_1. \qquad (3.9)$$

Then the result of integrating (3.5) will be:

$$b_1(t) = -iW_0\left\{\frac{1 - \exp\left(\frac{2\pi i}{h}(E_1 - E_0 - h\nu)t\right.}{E_1 - E_0 - h\nu} + \right.$$

$$\left. + \frac{1 - \exp\left[\frac{2\pi i}{h}(E_1 - E_0 + h\nu)t\right]}{E_1 - E_0 + h\nu}\right\}. \qquad (3.10)$$

Since in our case $E_1 > E_0$, resonance can only occur for

$$E_1 - E_0 = h\nu \qquad (3.11)$$

which corresponds to induced light absorption.

The probability $P\nu(t)$ of absorption of a light quantum $h\nu$ close to resonance (3.11) is deter-

*In [1] the relation $q_0 p_0 - p_0 q_0 = i$ is deduced. Comparison of this with (423) in [7] shows that q_0 and p_0 are $1/\sqrt{2}$ of the corresponding Frenkel operators.

mined by the square of the modulus of $b_1(t)$:

$$P_\nu(t) = |W_0|^2 \Omega(E_1 - E_0 - h\nu). \quad (3.12)$$

According to Zeitz (page 233, Equations (43.19a) in [2]) The function $\Omega(\epsilon)$ can be replaced by the delta function $(4\pi^2 t/h)\,\delta(\epsilon)$ so that the final expression for the probability that at time t light quantum $h\nu$ will be absorbed, will be:

$$P_\nu(t) = \left|\frac{2\pi W_0}{h}\right|^2 \cdot t \cdot \delta(\nu_1 - \nu), \quad (3.13)$$

where $\nu_1 = (E_1 - E_0)/h$ is the transition frequency.

4. EXTINCTION COEFFICIENT ASSOCIATED WITH EXCITON EXCITATION IN A CRYSTAL

The loss of luminous energy per second through absorption per unit volume will be:

$$\frac{dP_\nu(t)}{dt} \cdot \frac{h\nu}{V} = \frac{h\nu}{V}\left|\frac{2\pi W_0}{h}\right|^2 \cdot \delta(\nu_1 - \nu), \quad (4.1)$$

where V is the volume of the main region of the crystal.

The square of the modulus for W_0 contains $|(\vec{A}_0 \vec{I}_{0,1})|^2$ in which the amplitude of the vector potential A_0 can be expressed by the amplitude of the electrical field potential E_0:

$$|(\vec{A}_0 \cdot \vec{I}_{0,1})|^2 = \frac{c^2}{16\pi^2\nu^2}|(\vec{E}_0 \vec{I}_{0,1})^2$$

$$\frac{c^2 E_0^2}{16\pi^2\nu^2}|(\vec{n}_0 \vec{I}_{0,1})^2, \quad (4.2)$$

where $\vec{n}_0 = \vec{E}_0/E_0$ is the unique light wave polarization vector. In addition, we can write:

$$E_0^2 = 2\overline{E^2}. \quad (4.3)$$

where E^2 is the mean square potential, so that:

$$\frac{dP_\nu(t)}{dt} \cdot \frac{h\nu}{V} =$$

$$= \frac{e^2 n}{2\mu^2 h\nu}|(\vec{n}_0 \vec{I}_{01})\, a(0)|^2 \cdot \delta(\nu_1 - \nu) \cdot \overline{E^2}, \quad (4.4)$$

where $n = N/V$ = the number of electrons per unit volume.

By comparing (4.4) with the phenomenological expression for the energy loss in light radiation (cf, e.g. [2]. p 661, Equations 147.6) we find an expression for the conductivity $\sigma(\nu)$ of the multi-electron system in the alternating electromagnetic field of a light wave of frequency ν:

$$\sigma(\nu) = \frac{e^2 n}{2\mu^2 h\nu}|(\vec{n}_0 \vec{I}_{01})\, a(0)|^2 \delta(\nu_1 - \nu). \quad (4.5)$$

For a comparison of the expression found for the conductivity with the corresponding expression deduced by Seitz ([2], p. 677. Equations (148.25)] let us use the explicity form of $\rightarrow I_{01}$ (2.11) and transform (4.5) to:*

$$\sigma(\nu) =$$

$$= \frac{e^2 nh}{2\pi^2\mu^2\nu}\left|\int \psi_0(q)\, \hat{\vec{\nabla}}_q \psi_1(q)\, dq\right|^2 \cdot |a(0)|^2 \delta(\nu_1 - \nu).$$

From the comparison we conclude that our conductivity expression differs from that of Seitz, in the coefficient $|a(0)|^2$, which is light-frequency independent. According to (2.12) and (2.13) and the definitions of V_k and U_k [1]:

$$a(0)|^2 = + \sqrt{\frac{M + 6(R + Q + A)}{M + 6(R + Q - A)}} \quad (4.7)$$

Here M is the difference in mean energies of a lattice electron in the excited and normal quasi-atomic states (without allowance for electron interaction), and R is defined as the difference in coulomb and exchange integrals in the approach of nearest neighbours [1]; Q as the difference in integrals for transfer of the excited state from one lattice site to another and of the analogous transfer with exchange in the approach of nearest neighbours, and finally A as the difference in integrals for simultaneous excitation of two electrons and simultaneous excitation with subsequent exchange.

Frenkel [3] treats wave excitation in a crystal as excitation of an electron of an individual atom inside the crystal and translation of this excitation through the lattice. The essential point is that the excited electron is always assumed in an environment of unexcited atoms. This is why light absorption by Frenkel type excitation waves

*Here we replace $|(\vec{n}_0 \vec{I}_{01})|^2$ by $1/3\,|\vec{I}_{01}|^2$ which constitues averaging along directions (cf. Equation (43.28) in [2]).

does not in essence differ from light atoms.

In the present paper the concept of the quasi-particle, the exciton (2.1), contains in addition to "single" electron excitations also "paired" excitation, although allowance for this is only necessary when both excited atoms are neighbours. If we neglect the integral A for this process, that is if we put $A = 0$, our equation (4.6) for conductivity is identical with (148.25) deduced by Seitz [2]. When $A>0$ the conductivity and therefore light absorption is greater in the presence of "paired" excitation than the absorption by a system of isolated atoms. But when $A<0$ light absorption is decreased when there is paired excitation. Which case arises depends on the ratio between the integrals in the definition of A (cf. (2.10) in [1]) that is, in the final analysis of the form of the atomic functions for the normal and excited electron states and the lattice parameters.

The expression for the conductivity (4.5) is easily converted to an expression for the apectral extinction coefficient, associated with exciton excitation in a crystal:

$$\eta(\nu) = \frac{4\pi\sigma(\nu)}{c} =$$

$$= \frac{2\pi e^2 n}{\mu^2 c h \nu} |(\vec{n}_0 \vec{l}_{01})\, a(0)|^2 \cdot \delta(\nu_1 - \nu). \quad (4.8)$$

Finally, it would be very interesting to study the optical absorption of light due to exciton excitation in a crystal with allowance for temperature effect.

REFERENCES

1. V.S. Galishev and S.V. Vonsovskii *Fiz. metal metalloved., 3,* 395 (1956).
2. F. Seitz *Sovremennaya teoriya tverdogo tela,* GITTL, 1949.
3. Ya. Frenkel *Phys. Rev., 37,* 17, 1726, (1931); *Phys. Z. Sowjet 9,* 158 (1936).
4. R. Peierls *Ann. Phys. Paris 13,* 905 (1932).
5. R.C. Slater and W. Shockley *Phys. Rev. 50,* 705 (1936).
6. Iu. M. Seidov and V.S. Galishev *Zh. eksp. teor. fiz. 30,* 695 (1956).
7. Ya. I. Frenkel *Volnovaya Mekhanika (Wave Mechanics),* Part II, 1935.
8. E.F. Gross *Izv. Akad. Nauk SSSR, ser. fiz. 20* , 89 (1956).

Note added in proof

With an accuracy to the fourth order of small numbers the transition frequency can be calculated from (3.9) and (2.1) as $V_1 = (E_1 - E_0)/h = V_\theta - 18A^2/h^2 V_\theta$ (4.9) where $V_\theta = M + 6(R+Q)$, the frequency obtained from [3]. V_1 can evidently be compared with the first (long-wave) line in the exciton absorption spectrum [8] because we have not considered exciton excitations due to disturbance of the homogeneity of electron density in a crystal. It is known that the frequency of this line is considerably less than the frequency calculated from the hydrogen-like equation. It is possible that one of the reasons for this is a displacement of V_1, due to the second term in the right hand side of (4.9).

ON THE FUNDAMENTAL POSSIBILITY OF "INTRAZONAL" MECHANISM OF LIGHT ABSORPTION IN SOLID MATERIALS*

V.I. CHEREPANOV

(Received 20 June 1956)

On the basis of the poly-electron selection rule for optical transitions in a system of interacting electrons in a crystal, an assessment is made of the theoretical possibility of "intrazonal" mechanism of light absorption in solids.

VOL. 4 1957

Absorption of the visible and ultra-violet light in solid materials is conditioned, in principle, by quantized transitions occurring in the electron system in a crystal under the action of exciting radiation.

Such transitions are considered by the single-electron zone theory as being in the nature of transition of single electrons from one energy band into another, either without taking into account the possibility of interaction between electrons, or by substituting for it by postulating a "self-co-ordinating" field. According to this theory, only the so called "optical" electron undergoes quantized transition in each case when one quantum of light radiation is absorbed by a crystal.

In reality, the electrons in a crystal are strongly interacting with one another and, therefore, the excitation of one of the electrons in a system should have a stronger or weaker effect on the state of the remaining ones.

In justifying the application to metals of the electron zone theory, it is sometimes pointed out [1] that the electron gas in metals is strongly degenerate and therefore, as a result of operation of Pauli's principle, weak external forces are incapable of changing the condition of a predominant number of electrons (with the exception of those which are situated close to the Fermi surface). Ginzburg and Silin [2] showed, in their study of electron interaction in metals in which the interaction was regarded as resembling collisions between individual particles, that there is no justification for postulating the occurrence of such collisions.

We shall remark that, in our opinion, this is correct but only in the case of a weak interaction between electrons. In the case of a strong interaction between electrons (non-ideal gas) it is not permissible to assume a priori that the electron gas in a metal is degenerate. Furthermore, in non-metallic materials, e.g. in semiconductors, the electron gas does not have to be degenerate at all. Finally, as already noted even by the authors [2], the postulate made above refers only to the region of low energy light quanta (long wave infra-red region of the spectrum). Thus, in general there is no justification for the interaction between electrons being ignored in a study of the optical properties of solid materials.

In addition, in our opinion, the poly-electron treatment of the problem as given in what follows, offers some new and interesting possibilities.

The selection principles for optical transitions in the framework of the poly-electron theory were deduced by somewhat different ways in [3-5].

Only the very general chacteristics of the wave-function of electrons in a crystal, as determined in [6], were used by the authors of investigations [3-5] in arriving at their deductions. Thus, it was shown that the known selection principle for optical transitions according to the single electron zone theory [7]

$$\vec{k}' = \vec{k} + \vec{K}_0, \qquad (1)$$

where $\vec{k}$ and $\vec{k}'$ are the wave-vectors of the "optical" electron in the initial and final states, and $\vec{K}_0$ is the wave-vector of the absorbed photon, is replaced by a more general relationship:

$$\vec{K}' = \vec{K} + \vec{K}_0, \qquad (2)$$

in which $\vec{K} = \sum_{i=1}^{N} \vec{k}_i$, the general wave-vector of the system [6]. The relationship (2) represents the poly-electron selection principle and means that

* *Fiz. metal. metalloved.* 4, No.2, 211-215, 1957 [Reprint Order No. POM 38].

not a single electron but a whole assembly of mutually interacting electrons participate in the process of absorption of one light quantum.

Since $K_0 \ll k, K$, we can, as is usually the practice, put instead of equations (1) and (2):

$$\vec{k}' = \vec{k} \qquad (1')$$

$$\vec{K}' = \vec{K} \qquad (2')$$

It is known that free electrons do not absorb light [8]. This follows from the laws of conservation of momentum and energy, and also from the identical dependence of both the momentum and energy of a free electron : $E(k) = \frac{h^2 k^2}{2m}$, where, E = energy, m = mass, $h\vec{k}$ = momentum of electron (Planck's constant divided by 2π, $\vec{k}$ = wave-vector of electron). During absorption of one quantum of light, there should be observed not only the law of the conservation of momentum(1'), but also the law of conservation of energy.

$$E(k') = E(k) + h\nu \qquad (4)$$

where ν – frequency of light. However, it follows from (1') that $E(k') = E(k)$, which contradicts equation (4) unless the quantized energy is negligibly small. Hence, a free electron is incapable of absorbing a quantum of light.

In the single-electron zone theory, the energy of an electronin a crystal depends on the wave-vector $\vec{k}$ as given above, and on the number of Brilliun's zone s:

$$E = E(\vec{k}; s), \qquad (5)$$

The identity of the relationship between energy and the wave-vector given above, is true in this case but only within the limits of one Brilliun zone. Hence, it follows from the selection principle (1) as used in the single-electron zone theory, and also from the law of conservation of energy (4), that quantized transitions are forbidden inside a zone although such transitions are possible from one zone into another. Consequently, a crystal can absorb light only if the frequency of light is suitable for transition of electrons from the zone corresponding to the valence band of the energy spectrum, to a zone corresponding to the next band.*

In the poly-electron theory of solid materials, the electrons are not regarded as being free to any degree. In this case, as it is shown in [6], the energy of the system is determined not only as a function of the generalized wave-vector $\vec{K}$, but also as that of the higher quantum numbers characteristic of the relative motion of electrons in a crystal. A part of these quantum numbers assumes discrete values,which is in accordance with the fact that, if the atoms in a crystal are sufficiently far away from one another, the energy spectrum of the various states of the system should be in the form of a number of discrete levels. If the assembly of the continuous numbers is denoted by l (pseudo-continuous quantum numbers), and that of the discrete quantum numbers by s, it is possible to express the energy of the system, for a general case, in the form of the following function:

$$E = E(\vec{K}, l; s). \qquad (6)$$

It will be assumed in our further considerations that two different states of a system belong to the same "zone" s, provided that the energy levels corresponding to such states were created from a single discrete energy level** with s number, at the stage when the atoms were condensed to form a crystal. Thus, there exists a genetic connexion between the states of a single "zone".

It is possible to divide all of the possible quantized transitions of a system into two types: (1) transitions which do not involve changes in the quantum numbers $l(\vec{K}' = \vec{K}, l' = l, s \neq s)$, and (2) transitions connected with a change in the quantum numbers $l(\vec{K}' = \vec{K}, l' \neq l)$. The transitions of the first type are analogous to those considered in the single-electron zone theory. If one is limited to a consideration of transition of this type only, it can be shown that the electron system behaves as a single particle with wave-vector $\vec{K}$, since the quantum numbers defining the degree of freedom with respect to the electron motion remain constant. Transitions of the second type have no analogy in the single electron zone theory.

The success of the single-electron theory in interpreting the optical characteristics of solid materials is clearly due to the fact that the probability of the second type transitions is very small in comparison with that of the transitions of the first type. It would be very desirable to try finding

* We are not concerned here with absorption of infra-red light, which is dependent on the movement of electrons in conductors.

** One should note that in this form our definition refers only to non-degenerat energy levels in isolated atoms.

a proof for the above concepts on the basis of an actual poly-electron model of a crystal, which we propose to do in future.

We shall remark that, among the second type transitions of a particular interest are those of the "intra-zonal" types which correspond to the relationships:

$$\vec{K}' = \vec{K},\ l' \neq l,\ s' = s.$$

This is because transitions within a zone are forbidden by the single-electron zone theory.

Although it is unreasonable to expect a noticeable occurrence of the second type transitions in a general case, since transitions will be masked by those of the first type having a much higher probability, their role should, nevertheless, be given due attention in some cases. This applies, first of all, to the spectrum region lying in the direction of long waves from the limit of "specific" light absorption. In this region of the spectrum, the energy of the light quanta is insufficient for bringing about a transfer from one energy level into another. According to the single-electron zone theory, no light absorption whatever should be detectable in the region of the spectrum, because transitions within a zone are forbidden. Light absorption in this spectral region is, however, possible according to the poly-electron theory owing to "intra-zonal" transitions. It is known that in both metals and semi-conductors (for instance, Si and Ge) there is actually observed in the spectral region in question some increase in the determined light absorption in comparison with the value derived from the single-electron zone theory [9].

Mention will also be made of an interesting "characteristic" of transitions in the case of semiconductors, which was pointed out to us by A.G. Samoilovich. This "characteristic" lies in the fact that the "intra-zonal" transitions should not be connected with the appearance of photoconductivity since, during such transitions, there is no change in the number of charge carriers in the semiconductor, and instead there is only a redistribution of the pseudo-impulses of the carriers. It is possible that this characteristic property may throw some new light on the photoelectrically inactive light absorption in semiconductors. The "exciton" theory is known to be insufficient for this purpose.

In conclusion we wish to emphasize that the present article is concerned only with the fundamental possibility of the occurrence of "intra-zonal" transitions, since before an attempt is made at explaining the real role of such processes it is necessary to calculate their probability on the basis of an actual poly-electron model.

The authors take this opportunity for expressing their gratitude to S.V. Vonsovski, correspondent member of U.S.S.R. Academy of Sciences, for his valuable guidance and interest taken in the work.

REFERENCES

1. V.L. Ginzburg and G.P. Motulevich *Usp. fiz. nauk* 55, 469 (1955).
2. V.L. Ginzburg and V.P. Silin *Zh. eksp. teor. fiz.* 29, No. 1 (1955).
3. A.V. Sokolov *Zh. eksp. teor. fiz.* 25, 341 (1953).
4. V.I. Cherepanov, Thesis presented for the scientific degree of candidate of phys. math. sciences, Chernovits State University, 1956.
5. N. Haken and W. Schottky *Z. Phys.* 144, 91 (1958).
6. N. Volz and N. Haken *Z. Phys. Chem.* 198, 61 (1951).
7. F. Zeits Modern theory of solids, GITTL, 1949.
8. R. Peierls Electron theory of metals, GITTL, 1947.
9. Fan and Bekker, *Poluprovodnikovye materialy (Semiconductor materials)*, p. 175, Izd. IL, 1954.

VOL. 4 1957

THE POSSIBLE FORM OF SURFACE OF CONSTANT ENERGY ELECTRONS IN A PERIODIC LATTICE-FIELD*

G.E. ZIL'BERMAN and Ya. AIZENBERG

(Received 24 May 1956)

An evaluation is made of the form of constant energy surface for the case of complex laws of electron dispersion in the lattice. It is shown that small electron groups can exist in the k-space for any degree of zone filling (typical form of equipotential surface is a multi-contact one), and that the existence of holes does not, in a general case, require a high zone filling.

The interaction of electrons in a metal can be substituted, from the thermodynamic viewpoint, by an assembly of any pseudo-particles obeying Fermi's statistics and carrying a charge that is approximately equal to the elementary charge[1].

The dispersion law of such particles should be periodic in the reciprocal lattice.

$$E = \sum_{\vec{n}} A_{\vec{n}} \cos \vec{k} \cdot \vec{n} \qquad (1)$$

where, $\vec{k}$ is the wave vector, $\vec{n}$ is the lattice vector.

From this point of view, the dispersion law of, for instance, strongly bound electrons having in a simple cubic lattice the form:

$$E = A_0 + A_1 (\cos k_1 a + \cos k_2 a + \cos k_3 a). \qquad (2)$$

contains the first members obtained by expanding expression (1).

The form of energy surface as defined by expression (2) is well known [2]. For a very small and a very high degree of filling, the surface defined by expression (2) is spherical in shape, and the spheres surround, in the two above cases, the central and the corner points of the elementary cell respectively, in the k-space and correspond to small groups of electrons and holes.

In what follows the term "electrons" will be used to define particles filling such a closed area of the k-space, whose cross-section area increases with increasing energy [3] (of the zone filling), and by "holes" are understood vacant positions in the closed area of k-space, but whose cross-section area diminishes with increasing energy.

Starting with the energy surface shape as defined by expression (2), it is usual to consider that small groups of particles (electrons or holes) can form only when the degree of zone filling is either very small, or very large, or if there is overlapping of energy zones. Furthermore, it is also usually assumed that small groups can appear only in the centre or at the corners of a reciprocal lattice cell.

It will be shown that the energy surface can have a shape that is much more complex than that arrived at from models of strongly bound electrons, and in order to do so, a detailed consideration will now be made of the electron dispersion law for the case of a simple cubic lattice**:

$$\left.\begin{aligned} E = {} & A_0 + A_1 (\cos k_1 a + \cos k_2 a + \cos k_3 a) + \\ & + A_2 [\cos (k_1 a + k_2 a) + \cos (k_1 a + k_3 a) + \\ & + \cos (k_2 a + k_3 a) + \cos (k_1 a - k_2 a) + \\ & + \cos (k_1 a - k_3 a) + \cos (k_2 a - k_3 a)] + \\ & + A_3 [\cos (k_1 a + k_2 a + k_3 a) + \\ & \quad + \cos (k_1 a + k_2 a - k_3 a) + \\ & \quad + \cos (k_1 a - k_2 a + k_3 a) + \\ & \quad + \cos (k_1 a - k_2 a - k_3 a)] + \\ & + A_4 (\cos 2k_1 a + \cos 2k_2 a + \cos 2k_3 a). \end{aligned}\right\} \qquad (3)$$

and the above will be put in the form:

$$\left.\begin{aligned} & \alpha = (3 - \cos x - \cos y - \cos z) + \\ & + \beta [6 - \cos (x + y) - \cos (x + z) - \\ & - \cos (y + z) - \cos (x - y) - \cos (x - z) - \\ & - \cos (y - z)] + \gamma [4 - \cos (x + y + z) - \\ & - \cos (x + y - z) - \cos (x - y + z) - \\ & - \cos (x - y - z)] + \delta (3 - \cos 2x - \cos 2y - \\ & \quad - \cos 2z) \equiv F(x, y, z). \end{aligned}\right\} \qquad (4)$$

* *Fiz. metal. metalloved.* 4, No.2, 216-221, 1957 [Reprint Order No. POM 39].

** Qualitatively, the results apply also to other lattice types.

VOL. 4 1957

If one starts with models of strongly-bound electrons, the dispersion law as given by expression (3) means that a consideration was made of the interaction with not only the closest neighbours but also with those situated at the diagonal ends of grains, on space volume diagonals and at distances from the central atom that are equal to the lattice constant.

The dispersion law as defined in equation (3) applies to one energy zone only.

INVESTIGATION OF SPECIFIC POINTS IN THE SURFACE AS DEFINED BY EXPRESSION (4)

Let us consider a section of surface as defined by formula (4) and by the planes x = const., y = const., and z = const. In each of these planes we have a curve of constant energy. Specific points in such a curve in a plane, for instance, $z = z_0$, represent, as is well known, the solution of the equation system:

$$\left.\begin{aligned} &\varepsilon = F(x, y, z_0), \\ &\frac{\partial F}{\partial x} = 0, \quad \frac{\partial F}{\partial y} = 0. \end{aligned}\right| \qquad (5)$$

In this particular case, we shall have nodal specific points, isolated specific points and spontaneous contact points. Among these, the isolated specific points are of greatest interest to us, since they behave as "growth nuclei" of smaller groups. In particular, the bottom of the energy zone (4) and its highest level will always behave as specific points of this type.

The system of equations as given in (5) was investigated in detail. In what follows, pictures will be given of typical energy surfaces corresponding to various degrees of α zone filling (from the zone bottom to total zone filling), for actual values of coefficients β, γ, δ. In Figs. 1-3 are shown surfaces drawn for the case of $\beta = 1$, $\gamma = -0.75$ and $\delta = 0.5$, and the surface shown in Fig.4 corresponds to $\beta = 0.8$, $\gamma = -0.75$ and $\delta = 0.4$.

As can be seen from Figs. 1-3, the initial moment of filling corresponds to nine isolated points in the centre and corners of the cell. The groups then continue to grow, and with the degree of filling equal to 1/3 of the zone, the central surface comes in contact with the cube face while the remaining groups are still in a form approaching the spherical one (Fig.1). As

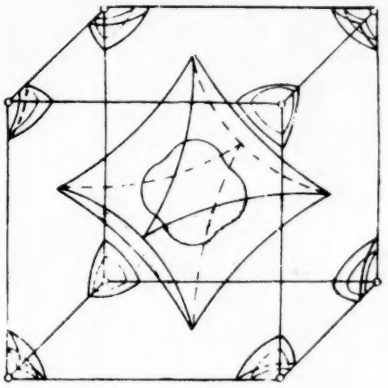

FIG. 1.

the filling progresses (Fig.2), the central surface intersects each of the other surfaces at three points (the degree of filling equals 16/21 = 0.756 of the zone). When the filling approaches

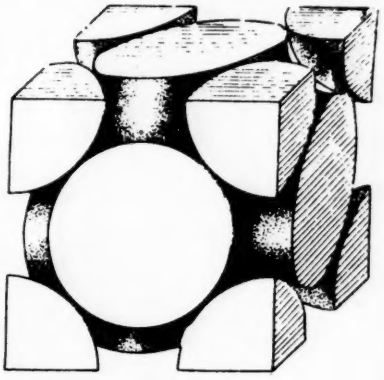

FIG. 2.

the highest zone level, there remain in the elementary cube, twelve areas of the shape shown in Fig.3. At the instant when the filling is close

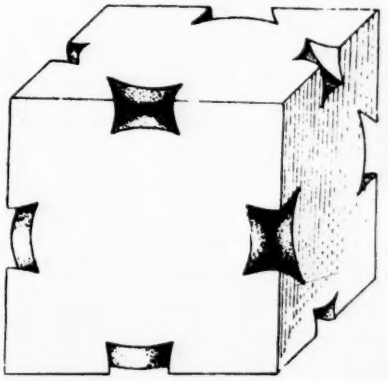

FIG. 3.

to saturation, each of the areas assumes a nearly spherical shape (or ellipsoidal one) and finally contracts to a point.

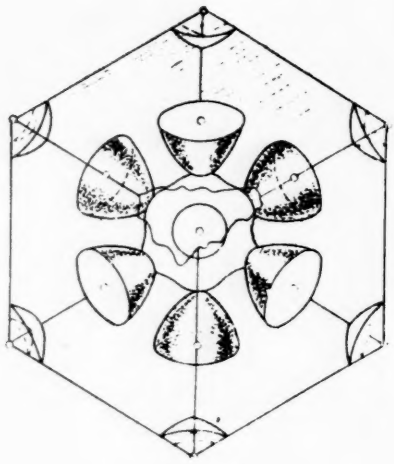

FIG. 4.

For different values of coefficients, e.g. β = 0.8, γ = -0.75 and δ = 0.5 (Fig.4), the zone begins to fill in in the same way as shown in Fig.1

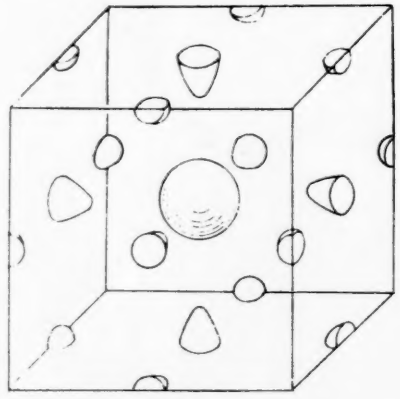

FIG. 5.

(9 small groups). Then, when the degree of filling equals 0.231 of the zone, the growth starts of 6 additional groups from the centre of each grain. For a degree of filling equal to 0.236 of the zone, the above 6 groups merge with the central one and a picture obtains as shown in Figs. 2 and 3.

In order to illustrate further the possibility of small group formation, use is made of Figs.5 and 6. In Fig.5 is shown the energy surface for coefficient values of β = -0.25, γ = 0.1, δ = 0.9 and for a low degree of zone filling (0.268). It

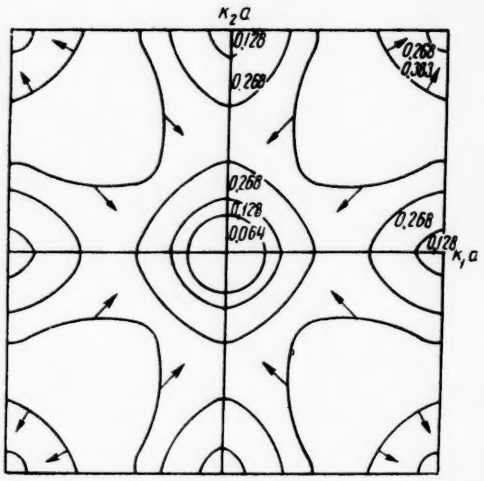

FIG. 6.

can be seen from the figure that, in this case, apart from the central group there now appear 16 small groups in the k-space. The central group appears first, then as the filling progresses, groups appear in the grain centres to be followed by those in the middle of cube sides. New groups situated at the cell corners appear with a still higher degree of filling. Fig.6 shows the energy surface section by plane z = 0 for various degrees of filling and the values of β = -0.25, γ = 0, δ = 0.9. The direction of energy reduction is shown by arrows.

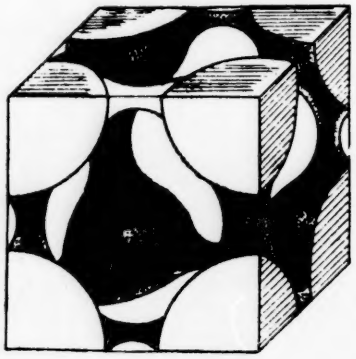

FIG. 7.

In Fig.7, which corresponds to β = 0, γ = 0, δ = 0.7 and to zone filling of 0.645, is shown a typical open surface corresponding to such conditions. With a further increase in zone filling, the area unoccupied by electrons gets smaller, and for the degree of zone filling equal to 0.667, bridging sets in in z = 0 and analogous sections,

which is followed by the area breaking down to 8 parts contracting to points.

$$\pm x = \pm y = \pm z = \cos^{-1}(-1/4\delta) = 0.622\,\pi.$$

In order to show that with a low zone filling the electron groups can appear at any point inside the cell, it is proposed to consider the case corresponding to $\beta = 0$, $\gamma = 0$ and $\delta = -0.5$. Then, with a low zone filling, there are formed immediately 8 small, closed areas (Fig.8). With a further increase in zone filling (see Fig.9 which corresponds to zone filling of approximately 0.1), these groups continue to grow and merge together so that an unoccupied area is created with its centre in the middle of the cell*.

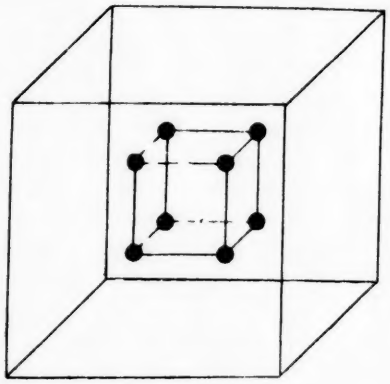

FIG. 8.

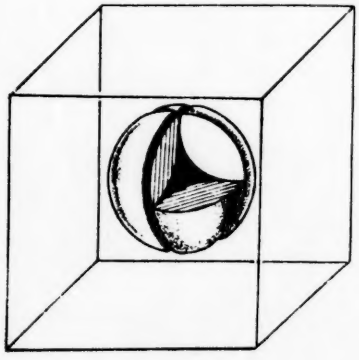

FIG. 9.

The shape of small areas is of a considerable interest. It can be easily shown that these areas, in a general case, represent second order surfaces since the closed areas in a simple cubic lattice are in the form of ellipsoids. The semi-axes ratio of these ellipsoids can have any large value even in the cubic lattice. And so, for instance the semi-axes ratio, this is the ratio of the axis perpendicular to the cube face to the second semi-axes, equals $\frac{(2\delta + \frac{1}{2})}{(2\delta - \frac{1}{2})}$ for the case of $\beta = 0$ and $\gamma = 0$. For δ values approaching 0.25, the above ratio is very big. In Fig.10 is shown the form of energy surface corresponding to 0.337 zone filling and $\delta = 1/3$.

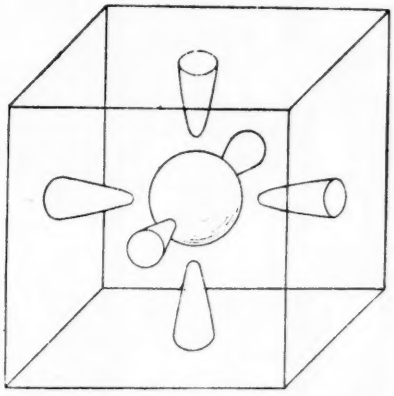

FIG. 10.

EVALUATION OF RESULTS

It is clear from what has been said above that the formation of small groups always corresponds to the bottom and highest levels of the energy zone. However, in addition to such characteristic zone points, small groups can also appear for very diverse zone fillings depending on the actual values of the β, γ, and δ coefficients. The case is possible of additional formation of small groups not at the zone bottom but somewhare near it. In general, the typical form of energy surface is a multi-contact surface consisting of numerous isolated groups. If such groups are small, they are in the form of ellipsoids.

The relationships between the β, γ, and δ coefficients can be easily established, such coefficients conditioning the appearance of separate groups at various points in the k-space of an elementary cell. It is found that the existence of the groups is possible for a very wide range of relationships between the β, γ, and δ coefficients. A decisive role is played here by the δ coefficient

* A part of the external surface in the Figure is cut out in order to show the inner unoccupied area.

VOL. 4 1957

and, in practice, the groups appear always provided that δ values are not very small.

Thus, it has been shown that separate electron groups, both spherical and strongly anisotropic, can exist inside a zone with various degrees of its filling, and at numerous points in the k-space (depending on the law of dispersion). We shall remark that it is usually assumed that electron groups appear only if there is overlapping of two energy levels, the upper one of which is unfilled in the absence of overlapping. Of course, this method of group formation is also possible.

All kinds of weak interactions, which are not taken into consideration in the derivation of dispersion law (1), represent a third reason for the formation of small electron groups. And so, for instance, if in a crystal there exist, in addition to the field with the lattice period, yet another electric field with a considerably greater period, frequent energy breaks will set in inside the crystal and these will also lead to the appearance of small electron groups.

The probability of small group formation can be evaluated for a given dispersion law and a normal level of zone filling. Let the zone width be denoted by $a_{\max}$ ($a_{\max} \sim 1$) (see [4]), and the energy interval at which a small group exist, by Δa. On the assumption of equal probability of all filling levels, the probability of existence of a group is given by $\frac{\Delta a}{a_{\max}} \sim \Delta a$. Since small groups obey the quadratic dispersion law, it can be easily calculated that $\Delta a \approx (a^3 n)^{2/3}$ where $N_1 = a^3 n$ –number of electrons per atom. Consequently the probability of the existence of any group with N_1 electrons per atom is $\approx N_1^{2/3}$.

If the dispersion law is such that small groups form at fillings of a_1, a_2, ..., a_m, the probability of group formation increases m times. It should be noted that the higher frequency terms in the dispersion law (1) favour generally an increase in the group number, i.e. they lead to an increase in m. If m is small, the probability of small group formation is low (the probability of the usual slight overlapping of zones is also low). Therefore, if it is assumed that the level of filling is a normal one, the cause of the very small group formation should be sought most probability in the weak interactions which are not accounted for.

However, the above conclusion should be anticipated if any other characteristics of the dispersion law, in addition to its periodicity, are known.

The groups of holes (particles with negative effective mass) can appear at low filling levels of surface zone (see Fig.9), and disappear during the further zone filling, Thus, zone overlapping or the existence of an almost completely filled zone are not absolutely necessary for hole formation.

Open surfaces (of the type shown in Fig.7) appear usually when the zone filling is not too big and not too small. In the case of cubic lattice, such surfaces are usually symmetrical with regard to axes k_1, k_2, and k_3, but in a lattice with a small number of symmetry elements, the open surfaces can be pulled down one or two axes (this is possible, for instance, in the hexagonal lattice, in which the properties along the 6th order axis are very much different from those along the binary axis).

In conclusion it should be noted that, in the light of the preceding considerations, the electron zone classification in terms of free atom (ns, np etc.) is completely unsatisfactory, since a gradual zone filling does not lead to a uniform filling of k-space areas. The existence of electron and hole groups, which it is usual to ascribe to zone overlapping, can occur also inside a given zone. The specific function of zone overlap lies in the removal of energy gaps in the spectrum and not in the formation of electron groups.

The authors are grateful to T.M. Lifshits and M.I. Kaganov for evaluation of the present work.

REFERENCES

1. L.L. Landau and E.M. Lifshits *Statisticheskaya Fizika* (*Statistical Physics*) M–L; I.M. Lifshits and A.M. Kosevich *Zh. eksp. teor. fiz.* 29, 730 (1955).
2. G. Bete and A. Zommerfeld *Elektronnaya Teoriya metallov* (*Electronic Theory of Metals*) Moscow, Leningrad, 1938.
3. I.M. Lifshits, M.Ya. Azbel and M.I. Kaganov *Zh. eksp. teor. fiz.* 30, 220 (1956).

ELECTRON EMISSION THEORY IN FERROMAGNETIC MATERIALS UNDER THE ACTION OF AN ELECTROSTATIC FIELD*

A.Z. VEKSLER

(Received 8 August 1956)

A calculation is made, on the basis of the $s-d$-exchange model, of the electron emission current in a ferromagnetic material in the presence of an external electrostatic field. It is shown that the current varies quadratically with spontaneous magnetization. The results agree with data reported in investigations quoted in [1,5].

INTRODUCTION

An investigation of electron emission in nickel [1] under the influence of an external electrostatic field, showed that there is a fairly strong dependence of the work function on temperature. This can be explained on the basis of the $s-d$-exchange model [2], which correlates the "anomalous" characteristics of ferromagnetic materials with peculiarities of the s-electron energy spectrum. In order to take account of such peculiarities in the determination of the current, it is necessary to introduce some corrections into the electron emission theory under the action of an electrostatic field [3]. The fact is, that the present theory neglects variations in the potential energy of electron inside a crystal by correlating all emission laws with the forces acting on the electron in an area outside the metal [3]. But, according to the $s-$ exchange model, the peculiarities in the $s-$electron energy spectrum originate from their interaction with $d-$electrons. In what follows, a theory is proposed for the electron emission in ferromagnetic materials, which takes into account the peculiarities mentioned above.

DETERMINATION OF $s-$ELECTRON WAVE FUNCTION

Let it de assumed that the half-space $x \leqslant x_0$ is filled with a ferromagnetic material, and the area corresponding to $x > x_0$ is a vacuum. We shall concern ourselves with the motion of $s-$electrons with "right" spin. The considerations given below can be applied equally well to $s-$electrons with "left" spin, and therefore no reference will be made to the orientation of the moment.

The condition of an $s-$electron within the ferromagnetic material is defined by a wave function of the following form:

$$\psi_k(\vec{r}) = \sum_{\vec{n}} \left\{ a_{\vec{n}} \exp\left[i(k_x + q_{n_1})(x - x_0) \right] + \right.$$

$$\left. + b_{\vec{n}} \exp\left[- i(k_x + q_{n_1})(x - x_0) \right] \right\} \cdot$$

$$\cdot \exp\left\{ i\left[k_y + q_{n_2} \right) y + \left(k_z + q_{n_3} \right) z \right] \}, \qquad (1)$$

where $\vec{k}$ is the pseudo-impulse of the electron, a is a lattice constant and

$$q_i = \frac{2\pi}{a} n_i \qquad (2)$$

According to the $s-d$-exchange model, the energy of $s-$electrons is determined by the expression

$$\epsilon = a - a'y + (\beta + \beta' y) a^2 k^2 \qquad (3)$$

where a, a', β, β' are parameters depending on the interaction of an $s-$electron with $d-$electrons and on the transfer energy of $s-$electrons [2]. In the area outside the ferromagnetic material, the wave-function satisfies the expression

$$\left[\frac{\hbar^2}{2m} \Delta + \varepsilon_1 - V(x) \right] \varphi(\vec{r}) = 0, \qquad (4)$$

where $V(x) = - eFx - e^2/4x$

and F is the field.

Solutions of this equation can be put in the form of the following series [4]:

$$\varphi(\vec{r}) = \sum_{\vec{g}} c_{\vec{g}} \varphi_{g_x}(x - x_0) \exp\left[i(g_y y + g_z z) \right], \qquad (5)$$

---

* *Fiz. metal. metalloved.* 4, No.2, 222-227, 1957 [Reprint Order No. POM 40].

VOL. 4 1957

where

$$g_y = k_y + q_{n_2},\ g_z = k_z + g_{n_3}. \tag{6}$$

$$g_x^2 = \frac{2m}{\hbar^2}\varepsilon - g_y^2 - g_z^2, \tag{7}$$

and the function $\phi_{g_x}(x)$ satisfies the equation

$$\frac{\hbar^2}{2m}\frac{d^2\varphi_{g_x}}{dx^2} + [\varepsilon_x - V(x)]\,\varphi_{g_x} = 0. \tag{8}$$

in which,

$$\epsilon_x = \frac{\hbar^2}{2m} g_x^2$$

Coefficients of c_g can be found from the continuity of the wave-function and its derivative on the crystal surface :

$$\left.\begin{aligned} \psi_k(\vec{r})\big|_{x=x_0} &= \varphi(\vec{r})\big|_{x=x_0}, \\ \frac{\partial\psi_k}{\partial x}\bigg|_{x=x_0} &= \frac{\partial\varphi}{\partial x}\bigg|_{x=x_0} \end{aligned}\right\} \tag{9}$$

Hence the following expression is obtained for the coefficients of c_g:

$$c_g = \frac{2i(k_x + q_{n_1})\,a_n}{i(k_x + q_{n_1})\,\varphi_{g_x}(0) - \dfrac{d\varphi_{g_x}(0)}{dx}} \tag{10}$$

CALCULATION OF CURRENT

The current density can be found by means of the formula:

$$j_x = \frac{eh}{2im}\left(\varphi\frac{\partial\varphi^*}{\partial x} - \varphi^*\frac{\partial\varphi}{\partial x}\right). \tag{11}$$

After neutralization along the y and z co-ordinates and substitution of (5) in (11), the following result is arrived at :

$$j_{x_{cp}} = \frac{eh}{2im}\sum_{\substack{n_1, n_1' \\ n_2, n_3}} c_n c^*_{n_1 n_2 n_3}|\varphi_{g_x}(0)|^2\cdot(\Omega^*_{g_x} - \Omega_{g_x}). \tag{12}$$

where

$$\Omega_{g_x} = \frac{\dfrac{d\varphi_{g_x}(0)}{dx}}{\varphi_{g_x}(0)} \tag{13}$$

During the calculation of the current density by means of formula (12), it is advisable to make use of relationships obtained by Nordheim [3], who considered that the wave-function of an electron in the area inside a metal can be represented as the superposition of two plane waves: the incident and the reflected waves. If the amplitude of the incident wave is denoted by ak and that of the other wave by c, then the limiting conditions for the case investigated by Nordheim leads to the following relationship:

$$\frac{c\varphi_{g_x}(0)}{a_k} = \frac{2ik_x}{ik_x + \Omega_{g_x}} \tag{10'}$$

After Ω_{g_x}, has been found from the above and substituted in (13), we obtain an expression for the current of the form :

$$j_{x_{cp}} = \frac{4eh}{m}k_x\sum_{n,n_1}\left|\frac{a_k}{c\varphi_{g_x}(0)} + \frac{a_k}{c^*\varphi^*_{g_x}(0)} - 1\right|$$

$$\frac{(k_x + q_{n_1})(k_x + q_{n_1}')\,a_n a^*_{n_1, n_2, n_3}}{\left(2k_x\dfrac{a_k}{c\varphi_{g_x}(0)} + q_{n_1}\right)\left(2k_x\dfrac{a^*k}{c^*\varphi^*_{g_x}(0)}\right) + q_{n_1}'} \tag{14}$$

We shall now consider two specific cases.

1. The case of weak electrostatic fields, where the following inequality is obeyed:

$$F \ll \frac{|\epsilon_0^2|}{e^3}$$

where $|\epsilon_0|$ is the work-function of electron. As shown by Nordheim, the coefficient of electron penetration approaches unity, when this inequality is obeyed, that is, the parameters a_k, c and $\phi_{gx}(0)$ are connected by the expression

$$a_k = c\ \phi_{gx}(0) \tag{16}$$

It should be noted, that only such terms in (13) for which $n_2 = n_3 = 0$ contribute to the current.

The remaining terms, which determine the transfer of electrons because of a tunneling effect at low fields, have an insignificant value.

On substituting (16) into (14), the following

form is obtained:

$$j_{11} = \frac{4eh}{m} k_x \sum_{n_1, n_1'} \frac{(k_x + q_{n_1})(k_x + q_{n_1}')\, a_{n_1 00}\, a^*_{n_1' 00}}{(2k_x + q_{n_1})(2k_x + q_{n_1}')} \qquad (14')$$

2. In the second case, when the field potential is very high,

$$F >> \frac{2\sqrt{2m|\epsilon_0|}}{he} kT, \qquad (15')$$

the escape of electrons is determined primarily by the tunneling effect. As shown by Nordheim, the following relation occurs in classical approximation:

$$\frac{\frac{c\varphi_{g_x}(0)}{a_k}}{x_2} = 2\left[1 - \frac{1}{4}\exp(-2K)\right] \qquad (16')$$

where,

$$K = \int_{x_1}^{x_2} \sqrt{\Phi(\xi)}\, d\xi, \qquad (17)$$

and x_1 and x_2 – are "points of reversal"

$$x_{1,2} = \frac{|\epsilon_x| \pm \sqrt{\epsilon_x^2 - e^3F}}{2eF},$$

$$\Phi(\xi) = \frac{2m}{h^2}\left[-eF\xi - \frac{h^2 g_x^2}{2m} - \frac{e^2}{4\xi}\right].$$

Substitution of (16′) into (14) leads after some rearrangement, to the equation:

$$j_{12} = \frac{eh}{m} k_x \exp(-2K_{0,0}) \sum_{n_1, n_1'} a_{n_1 00}\, a^*_{n_1' 00}, \qquad (14'')$$

where, $K_{0,0}$ is the interval, calculated from formula (17) for $n_2 = n_3 = 0$. Only the members corresponding to $n_2 = n_3 = 0$ remain in formula (14″) since the others are small because of the factor exp $[2K_{n_2 n_3}]$. In order to calculate the total current, it is necessary to integrate for all filled states. In the first case, when the current is determined by electrons escaping "above" the barrier, the expression for the current can be put in the following form

$$j_{11} = \frac{1}{8\pi^3} \int_{-\infty}^{+\infty}\int_{-\infty}^{\infty} dk_y\, dk_z \int_{\frac{-2m}{h^2}e^{3/2}F^{1/2}}^{\infty} \frac{h^2}{2m} \frac{j_{11}}{\frac{\partial \epsilon}{\partial k_x}} \frac{d(g_x^2)}{\exp\left[\frac{\epsilon - \epsilon_0}{kT}\right] + 1} \qquad (18)$$

If it is considered that in the area of integration we have that $\exp\left[\frac{\epsilon - \epsilon_0}{kT}\right] >> 1$, so that the slowly varying factor in the integral may be replaced by constant values, the following result is obtained:

$$j_{11} = \frac{e(kT)^2}{\pi^2 h\left(\frac{\partial \epsilon}{\partial k_x}\right)_0} \exp\left[\frac{\epsilon_0 + e^{3/2}F^{1/2}}{kT}\right] \cdot \sum_{n_1, n_1'} \frac{(k_{x_0} + q_{n_1}')(k_{x_0} + q_{n_1})\, a_{n_1 00}\, a^*_{n_1' 00}}{(2k_{x_0} + q_{n_1})\ 2k_{x_0} + q_{n_1}')}. \qquad (19)$$

Calculation of the total current for the case of stronger fields, leads to the expression:

$$J_{12} = \frac{e^3 hF^2 k_{x_0} \sum_{n_1, n_1'} a_{n_1 00}\, a^*_{n_1' 00}}{32\pi^2 m|\epsilon_0|\left(\frac{\partial \epsilon}{\partial k_x}\right)} \exp\left[-\frac{4\sqrt{2m}|\epsilon_0|^{3/2}}{3eFh}\right], \qquad (20)$$

where, k_{x_0} means that k_x is determined from the relationships:

$$\epsilon = \epsilon_0,\ k_y = k_z = 0.$$

COMPARISON WITH EXPERIMENTAL DATA

Expressions (19) and (20) determine the current of an s–electron with clockwise spin. The total current is found from the sum of currents of electrons with clockwise and anti-clockwise spins. Ignoring the slight dependence of the pre-exponentialterms on magnetization susceptibility, we find the following result (for the case of weak fields):

$$J_{x1} = A_1 T^2 \exp\left[\frac{\varepsilon_0(0) + \lambda y^2 + e^{3/2}F^{1/2}}{kT}\right]. \qquad (21)$$

VOL. 4 1957

In the presence of strong fields, the current is given by the following expression

$$J_2 = A_2 F^2 \exp\left[-\frac{4\sqrt{2m}\left\{|\varepsilon_0(0)|^{3/2} + \frac{3}{2}\lambda y^3\right\}}{3ehF}\right] \quad (22)$$

where,

$$A_1 = \frac{e(kT)^2}{\pi^2 h\left(\frac{\partial\varepsilon(0)}{\partial k_x}\right)_0} \sum_{n_1, n_1'} \frac{\left(k_{x_0}^{(0)} + q_{n_1}\right)\left(k_{x_0}^{(0)} + q_{n_1'}\right) a_{n,00}\, a_{n'',00}^{*}}{\left(2k_{x_0}^{(0)} + q_{n_1}\right)\left(2k_{x_0}^{(0)} + q_{n_1'}\right)}$$

$$A_2 = \frac{e^2 h k_{x_0}^{(0)}}{32\pi^2 m\,|\varepsilon_0(0)|\left(\frac{\partial\varepsilon(0)}{\partial k_x^{(0)}}\right)_0} \sum_{n_1, n_1'} a_{n,00}\, a_{n'',00}^{*}$$

$$\lambda = a^2(3\pi^2 n)^{2/3}\left(\frac{2}{3}k\beta' - \frac{1}{9}k^2\beta\right)$$

$\varepsilon_0(0) = \alpha + a^2\beta(3\pi^2 n)^{2/3}$ – value of ϵ_0 for $y = 0$.

The expression $k_{x_0}^0$ indicates that k_{x_0} corresponds to $y = 0$. If it is taken into account that the dependence of magnetizability on temperature in the region of the Curie point, has the form

$$y^2 = B(1 - T/\theta) \quad (23)$$

where, θ is the temperature of transition into the non-magnetic phase, it is then possible to write down expression (21) in the form:

$$\ln\frac{J_{x_1}}{T^2} = \ln C_1 + \frac{\varepsilon_{10}(0) + e^{3/2}F^{1/2}}{kT}$$

where,

$$C_1 = A_1 \exp\left(-\frac{B\lambda}{k\theta}\right)$$

$$\varepsilon_{10}(0) = \varepsilon_0(0) + B\lambda.$$

On the other hand, formula (21) can be applied to a temperature zones higher than θ. In doing so, itis necessary to assume that $y = 0$, and instead of (21′) we get:

$$\ln\frac{J_{x_2}}{T^2} = \ln' A_1 + \frac{\varepsilon_0(0) + e^{3/2}F^{1/2}}{kT}$$

Remembering that both expressions should give the same result when $T = \theta$, we find:

$$\ln\frac{A_1}{C_1} = \frac{\Delta\varepsilon(0)}{k\theta},$$

where, $\Delta\epsilon(0)$ is the difference in the effective work-functions, defined experimentally from the slope of Richardson's straight lines:

$$\Delta\epsilon(0) = \epsilon_0(0) - \epsilon(0) = B\lambda.$$

Values of A_1 and C_1 can also be found experimentally. We shall remark that the result obtained will be true also for $F = 0$. Thus it is possible to compare values of A_1, C_1 and $\Delta\epsilon(0)$ as obtained from measurements of thermionic emission currents. In the case of Fe, the following values were obtained [5]:

$$C_1 = 26\ \frac{a}{cm^2\,{}^\circ C^2},\quad A_1 = 1.4\ \frac{a}{cm^2\,{}^\circ C^2}$$

$$\Delta\epsilon(0) = -0.27\ \text{eV}.$$

Hence we find that:

$$\ln A_1/C_1 \cong -3.0 \text{ and } \Delta\epsilon(0)/k\theta \cong -3.0.$$

With greater values of field intensity, we get expressions approximating to (21′) and (21″):

$$\left.\begin{aligned}\ln\frac{J_{x_2}}{F^2} &= \ln A_2 - \frac{4\sqrt{2m}}{3ehF}|\varepsilon_0(y^2)|^{3/2} \text{ where } T \ll \theta,\\ \ln\frac{J_{x_1}}{F^2} &= \ln A_2 - \frac{4\sqrt{2m}}{3ehF}|\varepsilon_0(0)|^{3/2} \text{ where } T \gg \theta.\end{aligned}\right\} \quad (22')$$

Thus, in the case of stronger fields, the straight lines $\ln(j/F^2) = f(1/F)$, constructed for temperatures above and below the Curie point, should intersect the ordinate at a point with the co-ordinates $(0, \ln A_2)$, and the difference in the slopes should be $(2\sqrt{2m}/eh)\lambda y^2$.

Spivak and Gelberg [1] showed that the slope of the straight lines is different above and below the Curie point [1], and that the point of their intersection does not lie on the ordinate. One should remember, however, that their measurements were carried out at 20 and 400 °C, whereas the expressions deduced in the present work apply only to temperature regions close to the Curie point.

In order to investigate the dependence of work-function on temperature it is possible to measure the emission current at a constant field F and at various temperatures. In such a case, the follow-

ing relationship between J_{x_3} and T is obtained for temperature regions close to the Curie point:

$$\ln J_{x_3} = A_3 + b\frac{T}{\theta}\,(T \leqslant \theta), \tag{25}$$

where

$$A_3 = \ln A_2 F^2 - \frac{4}{3}\frac{\sqrt{2m}}{ehF}|\epsilon_0(0)|^{3/2} - \frac{2B\lambda\sqrt{2m}}{ehF}$$

$$b = \frac{2\sqrt{2m}B\lambda}{eh}$$

Thus, a plot of the function $\ln J_{x_3} = f(T/\theta)$ should be in the form of a straight line with slope

$$\frac{2\sqrt{2m}}{eh}B\lambda .$$

REFERENCES

1. G. Spivak and A. Gelberg *Dokl, Akad. Nauk SSSR* 94, 455 (1954).
2. S.V. Vonsovskii *Zh. eksp. teor. fiz.* 16, 981 (1946).
3. L. Nordheim *Proc. Roy. Soc.* 121, 626 (1928).
4. A.V. Sokolov and A.Z. Veksler *Zh. eksp. teor. fiz.* 25, 215 (1953).
5. H.B. Walbin *Phys. Rev.* 61, 509 (1942).

VOL.
4
1957

THEORY OF RESIDUAL ELECTRICAL RESISTANCE IN INTERSTITIAL TYPE ALLOYS*

A.A. SMIRNOV and I.A. STOYANOV

(Received 23 May 1956)

On the basis of a poly-electron model of metal, a determination is made of the dependence of residual electrical resistance in interstitial type alloys on the composition, distant order parameters on the centres and on correlation parameters, characteristic of the filling by various atoms of both the lattice sites and interstitial sites of the lattice.

Up to the present time, it is mainly the electrical resistance theory in substitutional type alloys [1-6] that has been the subject of development work. The present work has for its purpose an investigation of the dependence of residual electrical resistance in interstitial - type alloys on the composition, long range order parameters, and on correlation parameters (characteristic of short range order) between atoms of all types in the lattice sites and interstitial sites. The calculations were carried out within the framework of the poly-electron theory using the method as described in [3-5]. For the purpose of simplification, it was assumed that there is little difference in energy of conduction electrons in the field of ions of various types, which are used as subsituents in lattice centres, and that this difference is so small in the field of ions introduced into the interstitial sites that they can be regarded as but little excited.

The above assumptions are not true for all real interstitial-type alloys. However, the model chosen can be regarded as suitable for obtaining qualitative results only.

Let us consider an alloy in the process of ordering, with ions of various types α ($\alpha = 1,2, \ldots \zeta$) occupying various lattice sites, and with type β ($\beta = 1,2 \ldots \zeta$) ions occupying the interstitial sites. As a zero approximation, we shall choose an alloy that is fully ordered at both the lattice sites and interstitial sites, and which consists of effective ions in the field of which the electron has average potential energies $\bar{v}_x$ and $\bar{v}_x$ (in the lattice sites or a interstitial sites of a given type).

The matrix elements V'_{nm} of the excitation energy V', based on poly-electrons wave function ψ^0_n for a non-excited point, can be expressed in the form of

$$V'_{nm} = \int_{\Omega} \psi^{0*}_n V' \psi^0_m d\tau_1 \ldots d\tau N_e = N_e \Big/ \int_{\Omega} \Phi_{nm}(\vec{r}_i)\, \Delta V(\vec{r}_i)\, d\tau_i, \quad (1)$$

here,

N_e - number of conduction electrons, $\vec{r}_i$ - co-ordinate vector of ith electron, Ω - volume of the main crystal area,

$$\Delta V(\vec{r}_i) = \sum_{s=1}^{N} \Big\{ \sum_{x=1}^{\mu} [v_{sx}(\vec{r}_i - \vec{R}_{sx}) - \bar{v}_x(\vec{r}_i - \vec{R}_{sx})] + \sum_{\chi=1}^{\nu} [v_{s\chi}(\vec{r}_i - \vec{R}_{s\chi}) - \bar{v}_\chi(\vec{r}_i - \vec{R}_{s\chi})] \Big\}, \quad (2)$$

$$\Phi_{nm}(\vec{r}_i) = \exp(i\vec{q}\vec{r}_i)\, U_{nm}(\vec{r}_i), \quad (3)$$

$$\vec{q} = \sum_{i=1}^{N_e} (\vec{k}'_i - \vec{k}_i). \quad (4)$$

Here, $v_{sx}(\vec{r}_i - \vec{R}_{sx})$ and $v_{sx}(\vec{r}_i - \vec{R}_{sx})$ are the potential energies of ith electron in the field of ions situated in the lattice sites of number x and in the interstitial sites of number x of the sth elementary cell, and $\vec{R}_{sx}$ and $\vec{R}_{sx}$ are vectors passing from the first centre of first cell, used as the beginning of co-ordinates, to the lattice site x and interstitial site x of the sth elementary cell, N is the number of elementary cells in the crystal, μ and ν - numbers of lattice and interstitial sites in the cell (some interstitial sites may be vacant, when $v_{sx} = 0$), $\vec{k}'_i$ and $\vec{k}_i$ are vectors, characteristic of states ψ^0_n and ψ^0_m, $U_{nm}(\vec{r}_i)$ - periodic function of co-ordinates of an electron

* *Fiz. metal. metalloved.* 4, No. 2, 228 - 231, 1957 [Reprint Order No. POM 41].

with periods corresponding to the crystal lattice of zero approximation. By calculating the module square of matrix element excitation energy for alloys with body-centred face-centred cubic lattices, we get:

$$\frac{1}{N_e}|V'_{nm}|^2 =$$

$$= N\left(\sum_{\substack{\alpha,\alpha' \\ (\alpha<\alpha')}} \Delta^{nm}_{\alpha\alpha'} f^{nm}_{\alpha\alpha'} + \sum_{\alpha,\beta} \Delta^{nm}_{\alpha\beta} f^{nm}_{\alpha\beta} + \sum_{\substack{\beta,\beta' \\ (\beta<\beta')}} \Delta^{nm}_{\beta\beta'} f^{nm}_{\beta\beta'}\right), \quad (5)$$

$\Delta^{nm}_{\alpha\alpha'}$, $\Delta^{nm}_{\alpha\beta}$, $\Delta^{nm}_{\beta\beta'}$ — are values, in a chosen approximation, which do not depend on alloy composition or order parameters, and the function f is in the form:

$$f^{nm}_{\alpha\alpha'} =$$

$$= \sum_{L_y=1}^{Q_y} \lambda_{L_y} p_\alpha^{L_y} p_{\alpha'}^{L_y} - \frac{1}{2} \sum_{L_y=1}^{Q_y} \sum_{x_{L_y}=1}^{\lambda_{L_y}} \sum_{l=1}^{\infty} \sum_{L'_y=1}^{Q_y} \left[\varepsilon^{L_y L'_y}_{\alpha\alpha'}(\rho_l) + \right.$$

$$\left. + \varepsilon^{L_y L'_y}_{\alpha'\alpha}(\rho_l)\right] \sum_{m_{lL'_y}=1}^{z_{lL'_y}} \cos \vec{q}\vec{\rho}_{m_{lL'_y}}, \quad (6)$$

$$f^{nm}_{\alpha\beta} =$$

$$\sum_{L_y=1}^{Q_y} \sum_{x_{L_y}=1}^{\lambda_{L_y}} \sum_{l'=1}^{\infty} \sum_{L_M=1}^{Q_M} \varepsilon^{L_y L'_M}_{\alpha\beta}(\rho_{l'}) \sum_{m_{l'L_M}=1}^{z_{l'L_M}} \cos \vec{q}\vec{\rho} m_{l'L_M} \quad (7)$$

$$f^{nm}_{\beta\beta'} = \sum_{L_M=1}^{Q_M} \lambda_{L_M} p_\beta^{L_M} p_{\beta'}^{L_M} -$$

$$- \frac{1}{2} \sum_{L_M=1}^{Q_M} \sum_{x_{L_M}=1}^{'L_M} \sum_{l''=1}^{\infty} \sum_{L'_M=1}^{Q_M} \left[\varepsilon^{L_M L'_M}_{\beta\beta'}(\rho_{l''}) + \right.$$

$$\left. + \varepsilon^{L_M L'_M}_{\beta'\beta}(\rho_{l''})\right] \sum_{m_{l''L'_M}=1}^{z_{l''L'_M}} \cos \vec{q}\vec{\rho}_{m_{l''L'_M}} \quad (8)$$

Here, λ_{L_y} and λ_{L_M} are the number of L_y type centres and L_M type interstitial sites in the elementary cell; x_{L_y} and x_{L_M} are the number of L_y type lattice sites and L_M type interstitial sites in the cell; ρ_l and $\rho_{l'}$ are the radii of lth and l'th co-ordination spheres, formed by lattice sites and interstitial sites, respectively, around the central site of L_y type and of number x_{L_y}, $\rho_{l''}$ is the radius of the l''th co-ordinate sphere around the central site of type L_M and number x_{L_M}; $\vec{\rho}_{m_{lL'_y}}$, $\vec{\rho}_{m_{l'L_M}}$, $\vec{\rho}_{m_{l''L_M}}$ are vectors, drawn from the central site (interstitial site) of type L_y (L_M) and number x_{L_y} (x_{L_M}) respectively, into the site (interstitial site) of number $m_{lL'_y}$ ($m_{l'L_M}$, $m_{l''L_M}$), of type L'_y (L_M, L'_M) in co-ordination sphere number l (l', l''); $z_{lL'_y}$ ($z_{l'L_M}$, $z_{l''L'_M}$), are centre numbers (interstitial site numbers) of type L'_y ($L_M L'_M$) in co-ordination sphere of number l (l', l''); $p^{L_y}_\alpha$ and $p^{L_M}_\beta$ are probabilities of substitution at site of type L_y and of type L_M by atoms of types α and β, and finally, $\epsilon^{L_y L'_y}_{\alpha\alpha'}(\rho_l)$, $\epsilon^{L_y L_M}_{\alpha\beta}(\rho_{l'})$, $\epsilon^{L_M L'_M}_{\beta\beta'}(\rho_{l''})$ are parameters of correlation of the type considered in [3-5] between subsitution of a pair of sites and interstitial sites, the type of which is indicated by superscripts, by atoms, identified by subscripts, situated at distances of ρ_l, $\rho_{l'}$ and $\rho_{l''}$, respectively.

For the determination of residual electrical resistance use was made of the density matrix method W_{nm} [3-5], constructed for zero approximation wave-functions. The equilibrium condition obtained for a general case of a multi-component alloy is in the form of:

$$\sum_{n'm'} \sum_{n''m''} \left(\sum_{\alpha,\alpha'} M^{nmn'm'n''m''}_{\alpha\alpha'} f^{n'm'}_{\alpha\alpha'} + \right.$$

$$+ \sum_{\alpha,\beta} M^{nmn'm'n''m''}_{\alpha\beta} f^{n'm'}_{\alpha\beta} +$$

$$\left. + \sum_{\substack{\beta,\beta' \\ (\beta<\beta')}} M^{nmn'm'n''m''}_{\beta\beta'} f^{n'm'}_{\beta\beta'} \right) \Delta W_{n''m''}$$

$$= -\vartheta_{nm} F. \quad (9)$$

VOL. 4 1957

here $M_{\alpha\alpha'}$, $M_{\alpha\beta}$, $M_{\beta\beta'}$ and β_{nm} in the approximation considered are independent of the composition and order parameters; F is the electric field intensity; $\Delta W_{n''m''}$ is the difference in matrix elements $W_{n''m''}$ for an alloy in electrical field and outside it. Electrical resistance is calculated for a specific case of a substitution alloy of two metals A and B, in the interstitial sites of which are introduced atoms of one type C only.

At low concentrations of the penetrating atoms, a determination was made of the residual electrical resistance ρ_0, and without considering correlation. In this particular case, an admixture of interstitial atoms represents an additional part of resistance, proportional to the number of atoms C, N_c, which shifts the concentration curves of residual resistance for ordered and disordered binary alloy $A - B$, by a constant value of $\delta\rho_0$.

In a special case of the interstitial type alloy, in which C atoms are introduced into interstitial sites of a pure metal A, the expression defining residual electrical resistance ρ_0, (for any concentration of the solite atoms) is in the form:

$$\rho_0 = B c_3 (1 - c_3 \qquad (10)$$

here, c_3 is the ratio of the number of C atoms to the total number of octahedral sites; B is a constant. It is clear from formula (10), that in this case ρ_0 increases initially with increasing c_3, reaches a maximum when $c_3 = \frac{1}{2}$, and then decreases with a further rise of c_3 becoming equal to zero when $c_3 = 1$ (when all interstitial sites are occupied).

The influence of interatomic correlation on ρ_0 was explained in [3-5]. We shall, therefore, concern ourselves only with the effect of correlation between sites and interstitial sites on ρ_0. The formula for the measurement of residual electrical resistance in a disordered alloy with a face-centred cubic lattice, in which the disordered state is caused by correlation established between the sites and interstitial sites in the first co-ordination sphere, is in the form of:

$$\delta\rho^0_{\text{corr}} = D\varepsilon_{AC} = Dc_1c_2c_3 \frac{e^{\frac{a}{kT}} - e^{\frac{b}{kT}}}{c_1 e^{\frac{a}{kT}} + c_2 e^{\frac{b}{kT}}}, \qquad (11)$$

here, D is a constant, ϵ_{AC} is the correlation parameter between substitution of a site by atom A and that of the neighbouring interstitial site by atom C; c_1 and c_2 are corresponding concentrations of atoms A and B (ratio of the number of atoms A or B to the total number of atoms A or B); a and b are the interaction energies of atoms $A - C$ and $B - C$, taken with reverse sign.

A calculation of correlation between sites and interstitial sites shows that the change $\Delta\rho_0$, brought about by addition of atoms of C to the alloy $A - B$, is not constant, since now $\delta\rho^0_{\text{corr}}$, which depends on c_1 and is proportional to c_3 is added to the constant component. This part of resistance becomes zero for $c_1 = 0$ and $c_1 = 1$ and can be positive or negative. The presence of $\delta\rho^0_{\text{corr}}$ leads to a displacement of the maximum of curve ρ_0 (c_1) from its position, corresponding to $c_1 = \frac{1}{2}$ for an alloy in which there is no correlation. For $a = b$, the correlation correction $\delta\rho^0_{\text{corr}}$ becomes zero, as should be expected.

The displacement of the maximum in the concentration curve of electrical resistance depends on the annealing temperature at which the alloy was brought into the state of equilibrium, and its value is the higher the lower the annealing temperature. When $T \to \infty$, the position of maximum tends to $c_1 = \frac{1}{2}$, and the correlation correction approaches zero. In an alloy during the process of ordering, the value of correlation correction $\delta\rho^0_{\text{corr}}$ diminishes with increasing degree of order, and finally it becomes zero for a fully ordered alloy with stoichiometric composition. Analogous results were obtained also for alloys with body-centred cubic lattice.

REFERENCES

1. L. Nordheim *Ann. Phys, Paris* 9, 641 (1931).
2. A.A. Smirnov *Zh. eksp. teor. fiz.* 17, 743 (1947).
3. M.A. Krivoglaz and Z.A. Matysina *Zh. eksp. teor. fiz.* 28, 61 (1955).
4. M. A. Krivoglaz, Z.A. Matysina and A.A. Smirnov *Fiz. metal. metalloved.* 1, 385 (1956)
5. A.M. Dykhne, Z.A. Matysina and A.A. Smirnov *Fiz. metal. metalloved.* (in print).
6. M. A. Kirvoglaz and A.A. Smirnov *Voprosy fiziki metallov i metallovedeniya* (Problems in metal physics and metallography) Akad. Nauk SSSR. (in print).

THE ELECTRICAL AND MAGNETIC PROPERTIES OF THE INTERMETALLIC COMPOUND CdSb *

I.M. PILAT

(Received 28 November 1956)

The electric, magnetic and rectifying properties of the intermetallic compound CdSb are examined in relation to the excess of cadmium or antimony and also the concentration of impurities present, i.e. aluminium, tellurium, lead, tin and indium. The results are discussed from the point of view of their connexion with the cohesive forces in the crystal.

VOL. 4 1957

The system Cd – Sb has been studied by several authors [1-3]. X-ray analysis confirms that the intermetallic compound CdSb is the only stable phase of the system [4]. The CdSb lattice is rhombic with 16 atoms in the unit cell. Each atom is surrounded by four others one of which is of the same kind as the central atom. These surrounding atoms are placed at the apices of a deformed tetrahedron. The CdSb lattice can be described as a strongly distorted diamond lattice. The interatomic spacings in the lattice have the following values[5]:

$$\text{Cd}-\text{Cd},\ 2.99\ \text{Å};\quad \text{Cd}-\text{Sb},\begin{cases}2.80\ \text{Å}\\ 2.81\ \text{Å}\\ 2.91\ \text{Å}\end{cases}\quad \text{Sb}-\text{Sb},\ 2.81\ \text{Å}$$

The approximate values of the angles between the Sb – Sb and Sb – Cd bonds are given in Fig. 1.

Vol'fson and Rozhdestvenskii [1] studied several electrical properties of antimony-cadmium alloys, but they did not find any semi-conducting properties as they started with insufficiently pure metals and did not prepare the alloys by the most method.

V.A. Yurkov and N.E. Alekseeva [3] obtained a curve of the thermo-electric-motive-force against composition, whilst Justi and Lautz [2] studied the conductivity of the intermetallic compound CdSb. They found that in the temperature range 10-720°K the temperature coefficient of resistance remains negative if the composition of the CdSb alloy is within 0.5 per cent of the stoichiometric composition. The activation energy in the intrinsic conductivity range (above 100°C) was equal to 0.477 eV. At lower temperatures the following activation energies were obtained: 8.4×10^{-3} eV; 0.0210 eV; 0.0418 eV. The signs of the Hall coefficient and the thermo-e.m.f. at room temperature indicate a *p*-type or hole conductivity. They did not study the temperature dependence of the Hall coefficient and the thermo-e.m.f. The electrical properties of CdSb are greatly affected by the purity of the starting materials and the method of preparing the alloys. Justi and Lautz used insufficiently pure antimony (99.91 per cent Sb) which contained more than 0.1 per cent lead. Several specimens showed both *n*- and *p*-type conductivity.

In the present paper the electrical properties of CdSb are studied in relation to impurities. Some of the results were communicated to the 8th All-Union Conference on Semiconductors.

The cadmium and antimony were purified by vacuum distillation 3-4 times after which the impurities amounted to less than 0.0001 per cent. The results were checked by spectral analysis.

The test-specimens were prepared by alloying the respective amounts of cadmium and antimony in evacuated thick-walled Pyrex flasks. A special electrical vibrator was used to mix the molten components, and the cooled alloys were homogenized. Any deviation from the stoichiometric ratio was due to inaccuracy of weighing and to a slight oxidation of the cadmium during alloying. The object of the heat treatment was to prevent the formation of the metastable phase Cd_3Sb_2. Up to 250°C the measurements of the electrical properties were stable and reversible, but above this temperature some results were irreversible owing to the appearance of the metastable Cd_3Sb_2 phase which decomposed to CdSb and Cd or Sb. By special thermal treatment it might be possible to avoid this.

The alloys were also subjected to zone melting. Coarse CdSb single crystals and a more uniform

* *Fiz. metal. metalloved.* 4, No. 2, 232-238, 1957 [Reprint Order No. POM 42].

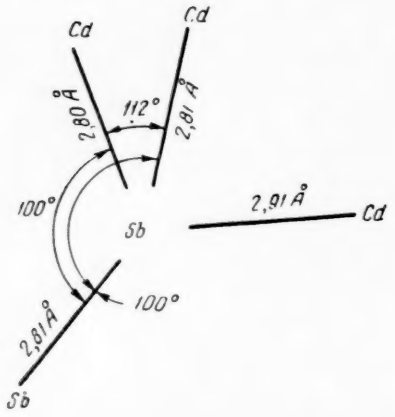

FIG. 1. Approximate angles of bonds between neighbouring atoms.

distribution of the added impurities were obtained in this way. Zone melting, however, did not remove impurities from the stoichiometric alloys.

The specimens had different contents of cadmium and antimony and also impurities such as of aluminium, tellurium, indium, lead and tin. The properties studied included the temperature dependence of the electrical conductivity, the thermo-e.m.f., the Hall coefficient, the coefficient of thermal conductivity and the magnetic susceptibility. Several tests were also made of the rectifying properties of CdSb at a CdSb – tungsten boundary surface and also in specially prepared alloys with $p-n$ junctions.

The electrical conductivity, thermo-e.m.f. and Hall coefficient were measured by the usual compensation method, and the magnetic susceptibility by the Gouy and Dorfman-Siderov methods [7]. The thermal conductivity was measured under steady state conditions in a high vacuum (8), covering the temperature range from -180° to +250°C.

The stoichiometric specimens were quite homogeneous, as proved by a micro-probe which was used cold and hot. No zones of different conductivity were found, as in [2] when the antimony contained traces of lead. With most of the specimens deviating from the stoichiometric composition by 0.5-0.6 per cent intrinsic conductivity began at 60-70°C,. Specimens closer to the stoichiometric composition were intrinsic at room temperature. The activation energy of the added impurity was between 0.07 and 0.03 eV.

When either component was present in an excess of more than 1 per cent, regions with a slightly positive temperature coefficient of resistance were formed (Fig. 2).

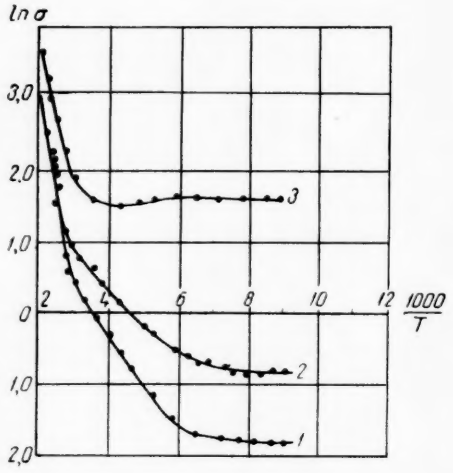

FIG. 2. Temperature dependence of electrical conductivity
1, stoichiometric
2, 0.5 per cent excess Cd
3, 1 per cent excess Sb

Table 1 gives some results of the effect of the additives on the electrical and magnetic properties. The activation energy was calculated from the temperature dependence of the electrical conductivity. The values for the Hall concentration of the carriers, the thermo-e.m.f., the thermal conductivity and the magnetic susceptibility are given for room temperature.

Deviation from stoichiometric composition does not alter the sign of the thermo-e.m.f. and the Hall coefficient.

Figs. 3, 4 and 5 show several characteristic curves of the temperature dependence of the electrical conductivity, the thermo-e.m.f. and the Hall coefficient.

With all samples the thermo-e.m.f. and the Hall coefficient are positive, though these change their sign with the Al-doped specimens near room temperature.

CdSb has a very low thermal conductivity, comparable with that of glass [9]. With increasing temperature the coefficient of thermal conductivity diminishes (Fig. 6).

The magnetic susceptibility measurements show

TABLE I

Stoichiometric	E (eV)	n (cm^{-3})	Q (V/°C)	κ ($W°C^{-1}\,cm^{-1}$)	χ ($\times 10^6$)
	0.43 –0.52	1.7 x 10^{16}	+ 700	0.00075	–0.30
	0.014; 0.03;		+ 420		–0.332
Pb	0.40 ;	5.65 x 10^{16}	+ 190	–	–0.48
	0.006; 0.042				
In	0.39 –0.40	2 x 10^{17}	+ 300	0.00095	–0.40
	0.016			0.00176	
Al	0.40 ;	4.7 x 10^{17}	+ 210	0.0015	–0.20
	0.025; 0.050			0.0019	
Sn	0.30 ;	10^{19}	–	–	–(0.5–0.75)
	0.47				
Te	0.40	1.2 x 10^{18}	–	–	–0.45
	–				+0.15 ·

that CdSb is weakly diamagnetic with a practically temperature-independent magnetic susceptibility. The latter decreases slightly with an excess of antimony (up to 0.1 per cent). In excess of 0.1 per cent, cadmium increases the diamagnetism. Specimens with lead or indium up to 0.1 per cent have a temperature-independent diamagnetism whilst the specimens with tin up to 0.1 per cent have a diamagnetism which increases linearly with rise in temperature. At low concentrations of aluminium (up to 0.4 per cent) or tellurium (up to 0.02 per cent) the specimens are diamagnetic, but become paramagnetic at higher concentrations.

The rectifying properties of CdSb were measured by the a.c. method using a cathode-ray oscillograph. The measurements were made on polycrystalline and single-crystal specimens the upper surface of which was raised and unworked. With a polished surface it was not possible to obtain rectification.

All specimens showed rectifying properties, though the rectification ratios were small. On single crystals obtained by zone melting the rectification ratio of the same order. As these specimens gave only a *p*-type characteristic, they obviously did not contain lead.

An excess of either cadmium or antimony of up to 1 per cent over the stoichiometric has hardly any effect on the rectifying properties, but these are considerably improved when even traces of an additive are present.

Specimens with up to 0.4 per cent aluminium give good diode characteristics, the rectification ratio reaching thousands (with direct and reverse voltages 1V). Specimens containing lead or tellurium also had good rectifying properties, but the rectification ratio, was slightly lower and reached only several hundred. These specimens showed current-voltage characteristics of both the *n*- and *p*-types. It is necessary to state that on one given specimen the oscillograms of the *n*-type gave a higher rectification ratio than the oscillograms of the *p*-type.

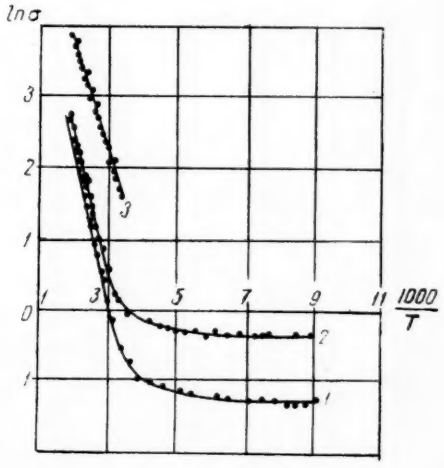

FIG. 3. The effect of lead additive on the temperature dependence of the electrical conductivity.
1, CdSb with 0.005 per cent Pb
2, CdSb with 0.015 per cent Pb
3, CdSb with 0.1 per cent Pb

The specimens containing tin had practically

no rectifying properties which is obviously due to the fact that even small additions of tin (up to 0.07 per cent) increase sharply the concentration of current carriers to 10^{18}-10^{19} cm^{-3} at room temperature. These specimens had electron conductivity.

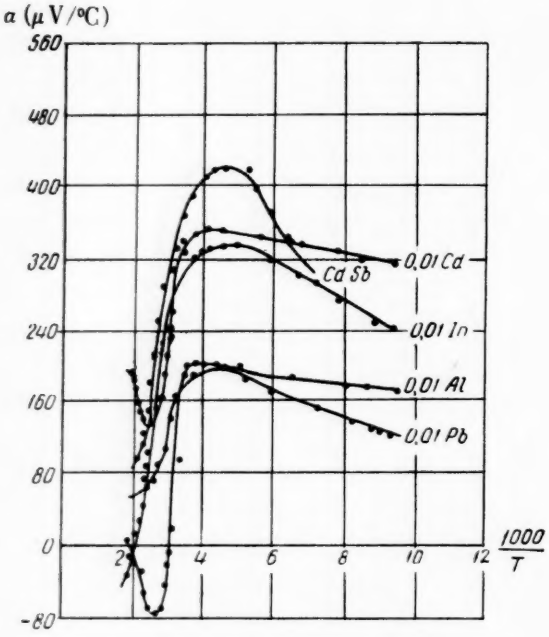

FIG. 4. Temperature dependence of the thermo-e.m.f. of CdSb.

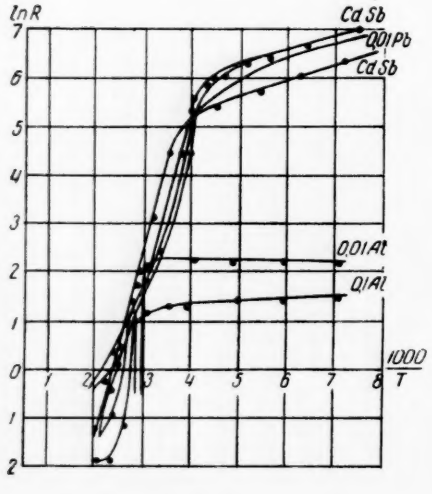

FIG. 5. Temperature dependence of the Hall coefficient.

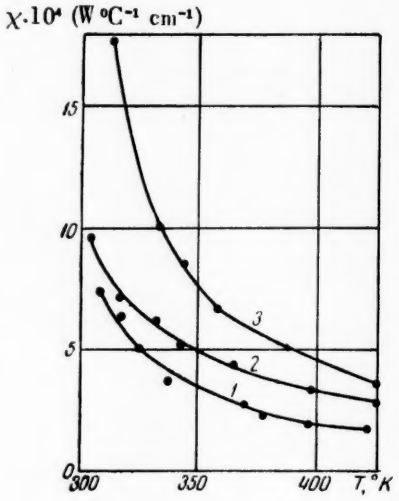

FIG. 6. Temperature dependence of the thermal conductivity.
1, CdSb
2, CdSb + 0.01 per cent In
3, CdSb + 0.1 per cent In

With reverse potentials up to 1 V, the current voltage characteristics were stable. When the stress was increased, the return trace of the characteristic deteriorated and a section with a negative resistance appeared of the same type as in germanium diodes.

Specimens containing up to 0.1 per cent indium, both as polycrystalline material and as single crystals, had excellent rectifying properties. The oscillograms were similar to those obtained with certain germanium diodes. On the unworked surface of the single crystals both n- and p-type characteristics were found. The best results were obtained with single crystals with a large concentration of indium (0.1 per cent).

To ascertain whether $p-n$ junctions could be fabricated in CdSb, single crystals of different composition were coated with certain metals under vacuum either molten or as powder. The surface of the single crystals was first etched with warm hydrogen peroxide. No $p-n$ junctions were obtained on single crystals of stoichiometric composition or with excess of either cadmium or antimony with coatings of indium, lead or tellurim, nor were positive results obtained with single crystals of CdSb containing up to 0.1 per cent lead or aluminium and treated with the same metals and different heat treatment.

The rectifying $p-n$ junctions were obtained

only on p-type single crystals of CdSb containing up to 0.1 per cent indium. With indium coatings the oscillograms of the $p-n$ junctions were stable and did not age, whilst the reverse breakdown voltage reached values of 2V; lead coatings gave a value of 4 V, but ageing occurred relatively rapidly.

Let us now summarize briefly. The experimental results discussed above undoubtedly confirm that CdSb is a semi-conductor, whilst its electrical properties indicate that it can be included among the semiconductors with good conductivity. This is very probably connected with the fact that the cohesive forces in the crystal are mainly covalent [10,11]. Another argument in favour of this is that the crystal lattice resembles that of diamond. CdSb has a deformed diamond lattice in comparison with Ge. Because first, it is a binary compound, and second, because a pair of cadmium and antimony atoms has only 7 valency electrons compared with 8 in the case of Ge or Si. This unsatisfied electron bond in the case of the CdSb crystal is evidently connected with the fact that CdSb behaves primarily as a p-type semiconductor, when either cadmium also or antimony is in excess. With tellurim as an additive the thermo-e.m.f. changed sign which is undoubtedly connected with the change in character of the lattice bond. This explains also the change of sign of the magnetic susceptibility which cannot be ascribed to the contribution to the susceptibility of the current carriers as their number is far too small – 1.2 x 10^{18} cm^{-3} (Table 1). The other additives obviously do not alter the character of the lattice bond since the thermo-e.m.f. in these cases does not change its sign. The exception is tin, but as Table 1 shows, this is connected with the increase in the concentration of the current carriers (when the magnetic susceptibility also begins to be temperature dependent).

The electrical and magnetic properties of CdSb, therefore, are closely connected with the nature of the cohesive forces in the crystal, but in contrast to germanium, we are not dealing here with a purely covalent type of bond. There still remain a whole series of complicating factors such as the difference in the valencies of the components which involves the unsatisfied electron bonds, the complexity of the structure, etc. A detailed study of the connexion between the electrical and magnetic properties of CdSb and the cohesive forces in its crystal will, therefore, be the subject of a further paper.

The author expresses his deep gratitude to Professor A.G. Samoilovich and to candidate in science L.L. Korenblit for their constant interest in this work and their valuable advice.

Translated by R.A. Hetherton.

VOL. 4 1957

REFERENCES

1. B.N. Vol'fson and V.N. Rozhdestvenskii *Zh. tekh. Fiz.* 3. 447 (1933).
2. E. Justi and G. Lautz Z. *Naturf.* 7a, 191 (1952). 7a, 602 (1952).
3. V.A. Uurkov and N.E. Alekseeva *Zh. tekh. Fiz.* 26, 911 (1956).
4. M. Hansen, *Struktura binarkhykh splavov (Structure of binary alloys)*,Metallurgizdat, 1941.
5. K.E. Almin *Acta. Chem. Scand.* 2, 400 (1948).
6. I.M. Pilat *Proc. 8th All-Union Conference on Semi-Conductors*, 1955.
7. Ya. T. Forfman *Magnitnye svoistva i stroenie veshchestva (The magnetic properties and structure of materials)*, Gostekhizdat, 1955.
8. A.F. Ioffe *Poluprovodniki v sovre mennoi fizike. (Semi-conductors in modern physics)*, Izd. Akad. Nauk, SSSR, 1954.
9. Eucken and Gehehoff, *Verh. dtsch. phys. Ges.* 14, 172 (1912).
10. N.A. Goryunova *Proc. 8th All-Union Conference on Semiconductors.* 1955.
11. E. Mooser and W. Pearson *Phys. Rev.* 101, 1608 (1956).

EFFECT OF ELASTIC STRESSES AND MECHANICAL HEAT TREATMENT ON THE MAGNETIC PROPERTIES OF CERTAIN HARD MAGNETIC MATERIALS*

M.G. LUZHINSKAYA and Ya. S. SHUR

(Received 16 October 1956)

The effect was investigated of elastic extension and torsion, and also of mechanical heat treatment, on the magnetic properties of alloys of the following composition: 8 per cent V, 52 per cent Co, balance Fe; 14 per cent V, 52 per cent Co, balance Fe; and 15 per cent Mn, balance Fe. Mechanical heat treatment consisted of applying unilateral tension loading to the specimens during annealing to give a state of high coercivity.

It was found that the agencies mentioned modify the magnetic properties of these alloys on account of a change in the magnetic anisotropy and magnetic texture.

INTRODUCTION

In previous papers [1,2] we showed that elastic stresses and mechanical heat treatment have a considerable effect on the magnetic properties of the high-coercive-force alloy Vicalloy. Elastic stresses were applied while the magnetic properties of specimens were being measured at room temperature. Mechanical heat treatment consisted of holding the specimen in an extended condition during annealing to give a high coercive force. The investigations conducted enabled it to be concluded that application of elastic stresses causes an increase in the magnetic anisotropy of an alloy having a single-domain magnetic structure. Consequently the coercive force increases both on extension and on torsion of specimens. Elastic stresses also bring about a change in the magnetic texture: extension helps to strengthen the longitudinal magnetic texture, and torsion to weaken it. In the first case, therefore, the residual flux density is increased, in the second it falls.

On mechanical heat treatment changes occur in the magnetic structure analogous to those found in the elastic extension of specimens, provided that this treatment is carried out with loads not exceeding a certain optimum size. Unlike elastic stresses, mechanical heat treatment brings about stable changes in the magnetic structure that do not disappear after the load has been removed. The effect of loading on mechanical heat treatment is due to the influence it has on the course of the structural transformations in the alloy Vicalloy.

The present work studies the effect of elastic stresses and mechanical heat treatment on the magnetic properties of certain other magnetically-hard ferromagnetic materials. Our object in this work is to determine experimentally how far the laws found for the alloy Vicalloy are general for other alloys and, in particular, for those in which a state of high coercivity is obtained as a result of structural transformations analogous to those taking place in Vicalloy.

MATERIALS AND SPECIMENS INVESTIGATED

Investigations were made into alloys of the system Fe–Co–V similar in composition to the alloy Vicalloy (8 per cent V, 52 per cent Co, balance Fe; 14 per cent V, 52 per cent Co, balance Fe) and also into an alloy containing 15 per cent Mn, balance Fe. These alloys have phase diagrams of the same type and attain a high coercive force after the same sort of treatment, consisting of cold deformation with subsequent tempering [3–5]. In the hardened condition these alloys contain a large quantity of non-ferromagnetic γ – phase, and also ferromagnetic α – phase. If the alloy is then subjected to cold deformation (rolling or extension), then during deformation the γ – phase changes into α – phase, with the result that the alloy attains a high magnetic saturation. Subsequent annealing at temperatures of 500–700°C causes the ferromagnetic phase to become partly non-ferromagnetic, as a result of which the structure of the alloy is very finely dispersed. Here the saturation falls, but the H_c reaches the highest values.

* *Fiz. metal. metalloved.* 4, No.2, 239-244, 1957 [Reprint Order No. POM43].

The specimens of the alloys investigated consisted of cold-drawn wires. The diameter of the specimens of the alloys containing 8 per cent V, 52 per cent Co, balance Fe and 14 per cent V, 52 per cent Co, balance Fe was 0.3 mm, that of the iron–manganese alloy was 0.24 mm. The reduction of area on cold drawing was 95 per cent.

The experimental method was described in the earlier papers [1,2].

RESULTS OF MEASUREMENTS

Alloy containing 8 per cent V, 52 per cent Co, balance Fe

The results of the measurements on these specimens, annealed by holding for 30 min at different temperatures and with different loads, are given in Figs. 1–3.

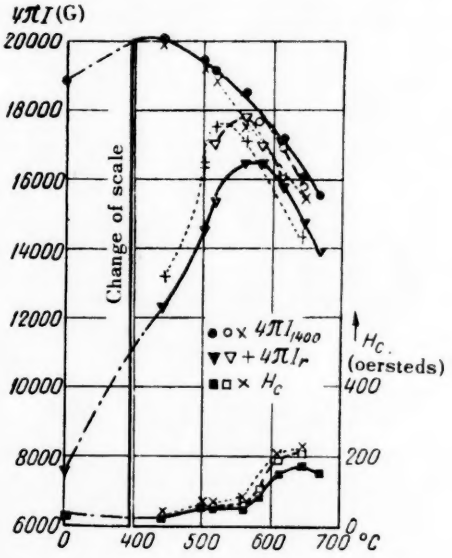

FIG.1 Variation in magnetic properties with annealing temperature for an alloy containing 8 per cent V, 52 per cent Co, balance Fe: not loaded, with a load of 26.5 kg/mm², with a load of 40 kg/mm²

Fig.1 shows the variation in magnetic properties of the specimens with annealing temperature. The dark signs and the thick lines relate to the results obtained from specimens annealed without loading, the light signs and the heavy dotted lines to specimens annealed with a load of 26 kg/mm², the crosses and fine dotted lines to specimens tempered with a load of 40 kg/mm². Fig.2 shows the variation in the properties of specimens annealed at temperatures of 515, 560 and 645° in relation to the load applied during annealing.

From Fig.1 it will be seen that on annealing without loading a noticeable change in the coercive force first appears at temperatures greater than 450°. It is at these temperatures also that the $4\pi I_{1400}$ (measured in a field of 1400 oersteds and near to saturation) starts to fall.

The maximum H_c – values are attained at annealing temperatures around 650°. Change in the residual flux density $4\pi I_r$, unlike the H_c, starts at lower temperatures and its maximum is reached at temperatures around 550°. The maximum H_c = 175 oersteds, where $4\pi I_r$ = 14700 G, and the maximum magnetic energy $(BH)_{max}$ = 2.10^6 G oersteds.

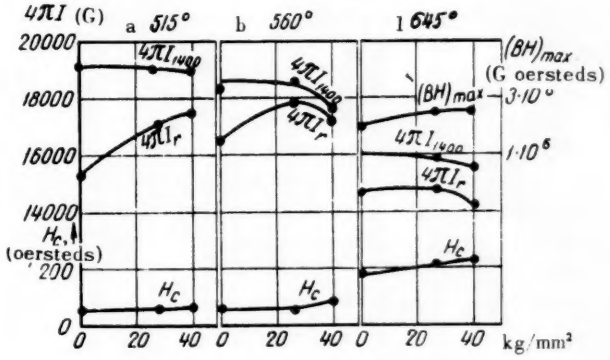

FIG.2 Variation in magnetic properties of specimens of alloy containing 8 per cent V, 52 per cent Co, balance Fe, annealed at temperatures of 515, 560 and 645°, with load applied during annealing

From Figs.1 and 2 it will be seen also that application of extending loads during annealing in a certain temperature range (around 500–550°) considerably increases the $4\pi I_r$, while H_c changes very little. Applying loads at higher temperatures causes a noticeable increase in the H_c, while $4\pi I_r$ here remains almost unchanged or falls. Loads causing a fall in $4\pi I_r$ also lower the $4\pi I_{1400}$. For a specimen annealed at a temperature of 645° with a load of 26.5 kg/mm², H_c = 205 oersteds, $4\pi I_r$ = 14700 G and $(BH)_{max}$ = $2.5 \cdot 10^6$ G oersteds. A specimen annealed at the same

temperature with a load of 40 kg/mm² has the same energy value, with a slightly lower $4\pi I_r$ and a higher H_c.

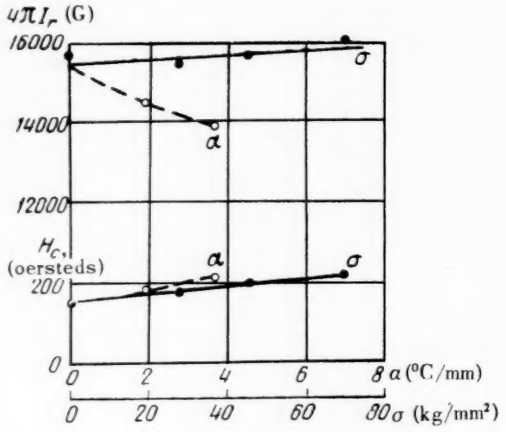

FIG.3 Effect of elastic stresses σ and torsion α on magnetic properties of alloy containing 8 per cent V, 52 per cent Co, balance Fe.

Fig.3 shows the effect of elastic stresses (extension and torsion) on the properties of a specimen annealed at 615° without loading. As can be seen from the figure, extension raises the H_c and $4\pi I_r$ of the alloy. Torsion increases the H_c but lowers the $4\pi I_r$.

Alloy containing 14 per cent V, 52 per cent Co, rest Fe

The measurements were made on specimens annealed at different temperatures by holding for 30 min with various loads.

The variation in the properties of the specimens with the annealing temperature is shown in Fig.4. The dark signs and the solid lines relate to the results obtained with specimens annealed without loading, the light signs and the heavy dotted lines to specimens tempered with a load of 26.5 kg/mm². The crosses indicate the $(BH)_{max}$ values for the specimens annealed without loading. It can be seen from the figure that the curves illustrating the change in properties with rise in annealing temperature for this alloy resemble those for an alloy containing 8 per cent V. The highest values H_c = 600 oersteds and $(BH)_{max} = 2.6 \cdot 10^6$ G oersteds are obtained after annealing at a temperature of 600°. Here $4\pi I_r$ = 7100 G and $4\pi I_{1400}$ = 7600 G.

In Fig.5 are shown results of measurements for specimens annealed at a temperature of 600° with loads of 0 to 40 kg/mm². From Figs.4 and 5 it will be seen that the effect of mechanical heat treatment on the properties of this alloy is much the same as for an alloy containing 8 per cent V, yet the change in properties as a result of mechanical heat treatment is very slight.

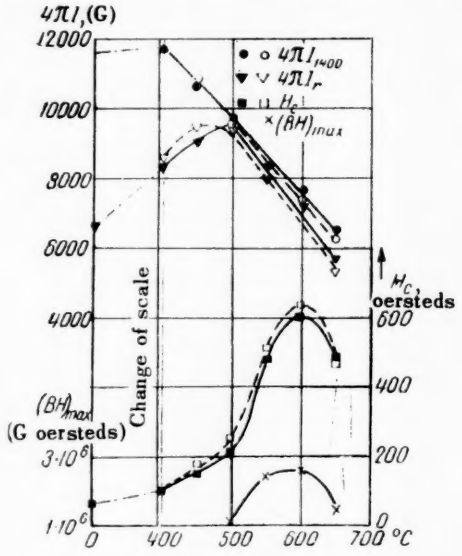

FIG.4 Variation in magnetic properties of an alloy containing 14 per cent V, 52 per cent Co, balance Fe, with annealing temperature: not loaded, with a load of 26.5 kg/mm²

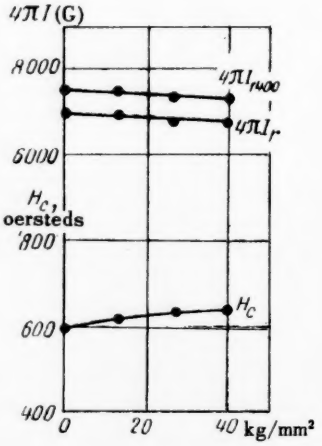

FIG.5 Vatiation in the magnetic properties of specimens of an alloy containing 14 per cent V, 52 per cent Co, balance Fe, annealed at 600°, with the size of the load applied during annealing

Fig.6 contains curves showing the change in H_c and $4\pi I_r$ in relation to the size of the elastic stresses applied at room temperature, for specimens annealed at 600° for 30 min. For this alloy also H_c and $4\pi I_r$ increase on elastic extension. On torsion its H_c increases, but the $4\pi I_r$ falls.

Alloy containing 15 per cent Mn, rest Fe

The properties of this alloy were measured on specimens that had been subjected to mechanical heat treatment at temperatures from 485 to 570° by holding for 10, 20, 40 and 60 min at loads of from 0 to 90 kg/mm.

Fig.7 shows the variation in the properties of the specimens in relation to the conditions of annealing without loading, on holding for 10 and 60 min. In the range of the conditions of mechanical heat treatment investigated Fig.4 and Fig.5 the H_c increases with rise in the tempering temperature, whereas the $4\pi I_r$ falls. The highest $(BH)_{max}$ occurs at tempering temperatures of about 520°. The maximum values of $(BH)_{max}$ = 0.8 . 10^6 G oersteds were obtained for specimens tempered at 525° for 1 hr, when H_c = 130 oersteds and $4\pi I_r$ = 11200 G. In order to illustrate the effect of mechanical heat treatment, in Fig.8 is shown the variation in the magnetic properties of specimens with the size of the load applied to the specimens during annealing at 505° for 40 min. On rise in the load, H_c increases, $4\pi I_{2500}$ remains unchanged at low loads, and then decreases.

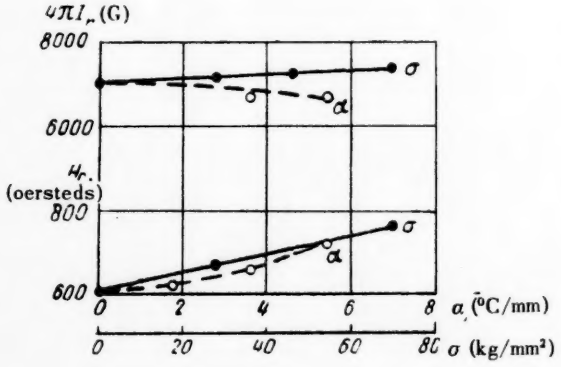

FIG.6 Effect of elastic tension σ and torsion α on magnetic properties of an alloy containing 14 per cent V, 52 per cent Co, balance Fe

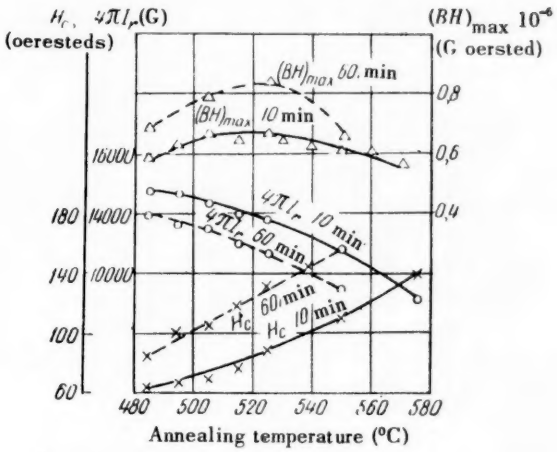

FIG.7 Variation in magnetic properties of specimens of an alloy containing 15 per cent Mn, balance Fe, annealed without loading, in relation to the annealing temperature
holding for 10 min
holding for 60 min

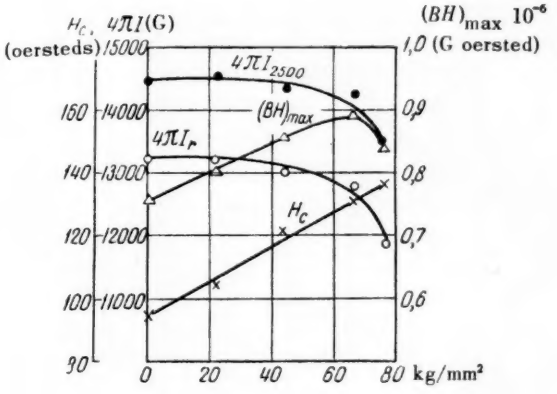

The effect of elastic stresses was measured on a specimen annealed at a temperature of 525° for 1 hr. It was found that both extension and torsion cause a rise in the H_c. For this specimen the $4\pi I_r$ on extension hardly changes and on torsion falls.

CONCLUSION

Comparison of the effect of mechanical heat treatment and elastic stresses on the magnetic

properties of the Fe – Co – V alloys studied in this paper, and also on those of the alloy Vicalloy, containing 12 per cent V, 52 per cent Co, balance Fe, previously studied shows that the change in properties as a result of the agencies mentioned is the same for all the alloys. Mechanical heat treatment has the greatest effect on the properties of an alloy containing 12 per cent V and having after ordinary annealing the highest properties of the alloys mentioned. For an alloy containing 8 per cent V, mechanical heat treatment causes slightly less change in the properties. For an alloy containing 1 per cent V, the effect of mechanical heat treatment is slight. It is interesting to note that the relative change in the magnetic properties under the action of elastic stresses is also the highest for an alloy containing 12 per cent V and lowest for an alloy containing 14 per cent V. Thus the laws governing the variations in the magnetic properties of an Fe – Mn alloy with mechanical heat treatment and elastic stresses are basically the same as for the Fe – Co – V alloys investigated.

The results obtained enable it to be supposed that the physical reasons for the change in properties under the effect of stresses applied during measurement or during heat treatment (mechanical heat treatment) for the alloys investigated in this paper are analogous to those governing the change in properties of Vicalloy alloy described in previous work [1,2]. It can be assumed that mechanical heat treatment must affect in the same way the magnetic structure, and therefore also the magnetic properties of other high-coercive-force alloys, in which a high H_c is obtained as the result of structural transformations similar to those in the alloys studied by us.

Mechanical heat treatment is one of the new methods of raising the magnetic properties of high-coercive-force materials.

REFERENCES

1. Ya. S. Shur, M.G. Luzhinekaya and L.P. Shubina *Fiz. metal. metalloved.* 4, (1957)
2. Ya. S. Shur, M.G. Luzhinekaya and L.P. Shubina *Fiz. metal. metalloved.* 4, (1957).
3. E.A. Nesbitt *Metals techn.* 13, 1973 (1946).
4. W. Jellinghaus *Teckn. Mitteil Krupp. Forschung.* 12, 257 (1941).
5. B.G.Livshits *Izv. Akad. Nauk SSSR ser. fiz.* 12, 116 (1948).

CERTAIN MAGNETIC PROPERTIES OF DISPERSION-HARDENING Fe–Mo AND Cu–Ni–Fe ALLOYS*

V.I. IVANOVSKII

(Received 6 March 1956)

As is known, in order to obtain high coercive forces, in addition to processes of ordering of atoms in the lattice, the decomposition of supercooled solid solutions is also used – i.e. dispersion hardening processes. Following dispersion hardening in certain alloys a structure forms in which particles of ferromagnetic phase are isolated from each other by non-magnetic or weakly-magnetic layers. According to present-day theories such a structure may give high coercive forces.

This paper studies the change in the magnetic properties during dispersion hardening. The alloys selected as objects of the investigation were Fe–Mo (18 per cent Mo) and Cu–Ni–Fe (52 atomic per cent Cu, 36 per cent Ni, 12 per cent Fe) alloys. The phase diagrams and physical properties of these alloys are given in [1,2].

KINETICS OF CHANGE IN COERCIVE FORCE OF ALLOY Fe–Mo (18 per cent Mo) AT DISSOCIATION TEMPERATURE OF SOLID SOLUTION

The specimens of the Fe–Mo (18 wt. per cent Mo) alloy investigated were rods 5 mm in diameter. In order to obtain a single-phase structure at low temperatures the specimen had to be quenched from a temperature of 1300°C. This was done as follows. Metal melted in a high-frequency furnace was drawn into porcelain tubes that were then quickly put in water so that the metal quenched almost from the melting point. The coercive force of the alloys treated in this way was almost 1.5–2 oersteds.

In an earlier paper [3] we showed that at the ordering temperature the coercive force of the alloy Fe_3Al increases with rise in the holding time. An analogous phenomenon is found in the Fe–Mo alloy at the dissociation temperature of the solid solution. The experiment was conducted as follows. Alloy quenched from a temperature of 1300°C, i.e. alloy with a single-phase structure, was placed in the furnace of a magnetometer heated to 650°C (the temperature at which the solid solution most effectively dissociates into two phases, liberating the chemical compound Fe_3Mo_2 from the matrix). At given intervals of time while at this temperature, the coercive force was measured. The results of the measurements are shown in Fig. 1. From curve *a* in this figure it is possible to observe graphically the increase in H_c during the process of dispersion hardening of the alloy.

MAGNETIC SUSCEPTIBILITY OF Fe–Mo ALLOY DURING DISSOCIATION OF THE SOLID SOLUTION

A specimen quenched from a temperature of 1300°C was placed in the furnace of a magnetometer heated to 650°C and its susceptibility was measured in relation to the holding time at this temperature. The results are shown in Fig. 1 (curves *b* and *c*). These curves differ fundamentally. Curve *c* illustrates the relationship of the susceptibility to the holding time in a furnace heated tp 650°C *in the presence of a magnetic field*. Curve *b* illustrates the same, but in the absence of a magnetic field. As can be seen from the figure, there is a great difference. Thus, for example, the susceptibility over a time $\tau = 60$ min measured according to method (*c*) has the value $\chi = 14.7$, while according to method (*b*) over the same time interval $\chi = 1.4$, i.e. less than one tenth as much. The difference in the susceptibilities was due to the fact that in the first case (*c*) the specimen was 60 min in an external magnetic field, while in the second it was not. The picture obtained was again of much the same type as that found for the alloy Fe_3Al [3].

MAGNETIC INTENSITY OF THE Fe–Mo ALLOY

It is of great interest to study the magnetic intensity of alloys capable of dispersion hardening. Judging from the curve of magnetization, at room temperature the Fe–Mo alloy investi-

* *Fiz. metal. metalloved.* 4, No.2, 245-248, 1957 [Reprint Order No. POM 44].

VOL. 4 1957

gated did not exhibit increased intensity. However at the dissociation temperature of the supercooled solid solution an increased intensity is seen. In Fig.1 (curve *d*) are shown the results of measurements of *I* in relation to the time *τ* after applying an external magnetic field of 120 oersteds. The measuring temperature was kept constant (650 °C) during the measurements. Thus at the dissociation temperature the Fe – Mo alloy exhibited very great intensity. The time during which ΔI is seen to increase with time may reach several hours.

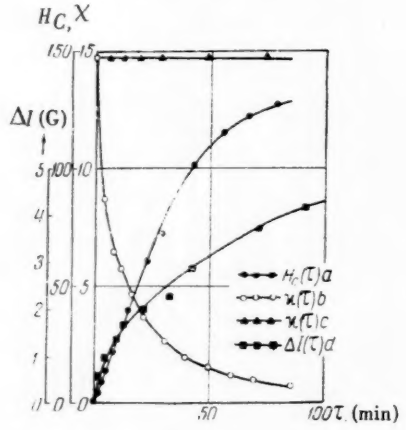

FIG. 1.

TEMPERATURE RELATIONSHIP OF COERCIVE FORCE OF Cu – Ni – Fe

Recently, in addition to Fe – Ni – Al alloys, Fe – Ni – Cu alloys have become important as permanent magnet materials. Alloys of this type have better plastic properties than Fe – Ni – Al alloys, as a result of which their magnetic properties can be improved by means of mechanical working. We shall confine ourselves here to studying the temperature dependence of the magnetic properties of the Cu – Ni – Fe alloy. Fig.2 contains curves illustrating the temperature dependence of the coercive force of the alloy mentioned above after various heat treatments. Curve I shows the relationship of H_c to *t* quenching the alloy from 850 °C, i.e. from a temperature at which the alloy has a single-phase structure. Curves II, III and IV show the relationship of H_c to *t* for the same alloy, which, however, had been subsequently annealed at 650° after quenching for different intervals of time: curve I - 5 hr,

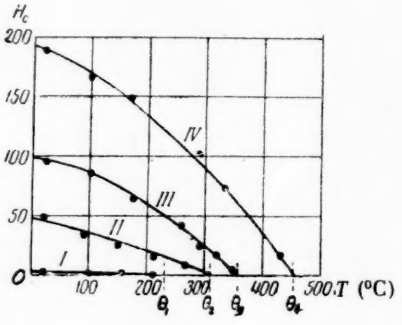

FIG. 2.

curve II - 10 hr, curve III - 10 hr and curve IV - 60 hr. As can be seen from the graphs, in the dissociation process the Curie point varies from 230 °C for the quenched alloy to 450 °C for alloy that has been subsequently annealed for 60 hr.

TEMPERATURE DEPENDENCE OF MAGNETIC INTENSITY OF Cu – Ni – Fe ALLOY

In the absence of any satisfactory theory concerning the mechanism of the occurrence of high intensity in a number of magnetically-soft materials, any new experimental data on this subject are of great interest. We conducted measure-

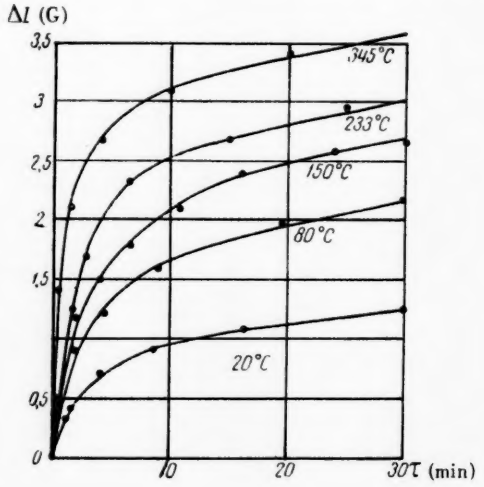

FIG. 3.

ments on the magnetic intensity of a Cu – Ni – Fe alloy that had been annealed for 60 hr at 650° C. The magnetic intensity was measured at different temperatures: 20, 80, 150, 233 and 345 °C. At all these temperatures the intensity was studied on the basis of a curve of magnetic intensity at one

and the same value of initial magnetic intensity $I = 30$ G. Both the values of I at $t = 0$ and the subsequent rise in ΔI with time were measured. The results are shown in Fig.3. It will be seen from the Fig.3 that with increasing temperature there is a rise both in the rate of increase in magnetic intensity and in ΔI in the same interval of time. Thus, for example, if at room temperature in 30 min the magnetic intensity ΔI increases by 1.25 G, then at $t = 345$ °C in the same interval of time ΔI will increase by 3.5 G.

KINETICS OF THE MAGNETIC INTENSITY OF Cu – Ni – Fe ALLOY DURING DISPERSION HARDENING

We made measurements of the kinetics of the magnetic intensity during dispersion hardening for different tempering at a temperature of 650 °C. The measurements were made at room temperature. In Fig.4 are given curves showing the relationship of ΔI to time for alloys that had been annealed at 650 °C for 5, 10 and 60 hr.

The quenched alloy did not exhibit elevated intensity. The highest ΔI in a period of 30 min is seen in the alloy annealed for 5 hr. The ΔI for this alloy is 6 G. With increasing tempering time, the ΔI for the alloy annealed for 60 hr falls to 1.25 G.

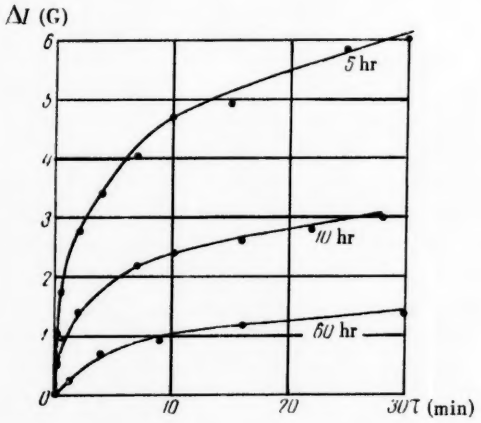

FIG. 4.

It is clear that at such a huge magnetic intensity the size of the coercive force must depend on the speed of measurement. If, as is usually the case in magnetometry, the specimen is brought to saturation, the magnetic field and the residual flux density are reduced to zero, then a single value is obtained for the coercive force (Fig. 5, thick curve). However, if account is taken in the measurements of the effect of the intensity, i.e. if the measurements are made in successive stages, holding the specimen a certain time at each value of H, then another, lower value of coercive force is found (Fig. 5, dotted curve). We made the following experiment: the coercive force of a specimen of Cu – Ni – Fe alloy annealed for 5 hr was measured "rapidly", i.e. the residual flux density was reduced to zero directly by means of a reverse field. The H_c after measuring in this equalled 49 oersteds. Then the coercive force was measured the other way. The residual flux density of the specimen was reduced in five successive stages. The specimen was held 30 min at each value of the magnetic field. In the course of this holding the magnetization of the specimen, owing to intensity effects, fell spontaneously, without any change in the size of the magnetic field. With this method of measurement the coercive force fell to 39 oersteds.

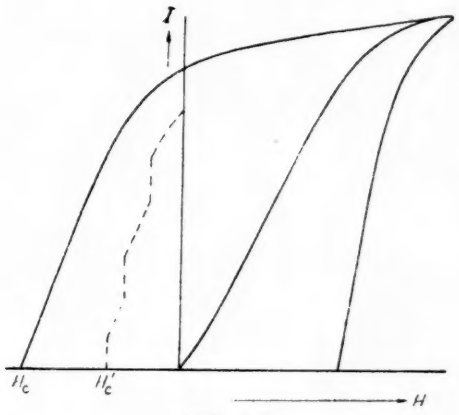

FIG. 5.

REFERENCES

1. A.S. Zaimovskii and V.V. Usov *Metally i splavy v elektrotekhnike* (*Metals and alloys in electrical engineering*), Gosenergoizdat, 1949.
2. P. Obergofer *Tekhnicheskoe zhelezo* (*Commercial iron*), Metallurgizdat, 1940.
3. V.I. Ivanovskii *Fiz. metal. metalloved.* 4, No.1 (1957).

THE HALL EFFECT AND THE INFLUENCE OF A MAGNETIC FIELD ON THE RESISTANCE OF MAGNETITE*

A.A. SAMOKHVALOV and I.G. FAKIDOV

(Received 5 October 1956)

A study was made of the Hall effect and the change in the electrical resistance of magnetite in magnetic fields, including the saturation zone of magnetite. It is shown that the electrical conduction in the galvanomagnetic effects mentioned is acted upon by an effective field equal to $H_{eff} = H_i + 4\pi\alpha M$, where the parameter of the effective field α changes in sign and magnitude in relation to the effect. An attempt is made to find a connexion between the Hall effect and the change of electrical resistance in a magnetic field in magnetite.

INTRODUCTION

From an investigation of the electrical and magnetic properties of magnetite and from determining the relationship between the various physical phenomena in magnetite, a better idea can be had of the mechanism of the phenomena governing its physical properties. The natural mineral magnetite $FeO.Fe_2O_3$ is in many ways similar in its physical properties to the synthetic ferrites widely used in present-day industry. Magnetite is a ferromagnetic semiconductor and a study of its galvanomagnetic properties may throw a certain light on its electron structure and enable a correlation to be made between the electrical and magnetic properties.

The results of such investigations may be useful also in the manufacture of ferrites with improved electrical and magnetic qualities.

Hitherto little has been done to study the galvanomagnetic properties of magnetite. The Hall effect in magnetite has only been investigated by Okamura and Torizuka [1]. Unfortunately there are a number of shortcomings in this work, of which the main one is the low magnetic field strength at which the Hall effect was studied (H_{max} = 2400 oersteds). For a specimen in the form of a lamina (demagnetization factor $N \cong 4\pi$), this magnetic field strength corresponds to the start of the magnetic intensity curve of magnetite. Therefore the laws applying in the saturation zone were left unexplained.

Below are the given results of an investigation into the Hall effect in magnetite for a field including the saturation zone. On the same specimens were studied the longitudinal and transverse effects of a change of resistance in a magnetic field, in order to enable the galvanomagnetic effects mentioned to be correlated.

SPECIMENS, METHOD OF MEASUREMENT

The galvanomagnetic effects were studied in two specimens of natural magnetite. Polycrystalline specimen No.1 was prepared in the shape of a parallelepiped measuring 6 x 12 x 52 mm. Specimen No.2 was cut parallel to the grain of an octahedral monocrystalline specimen of magnetite in plane (111) and was in the form of a lamina measuring 9.1 x 18.2 mm and 2.8 mm thick. The position of the specimens in relation to the magnetic field, and also that of the electrodes on the specimens are shown in Fig.1. It will be seen from the figure that on measuring the galvanomag-

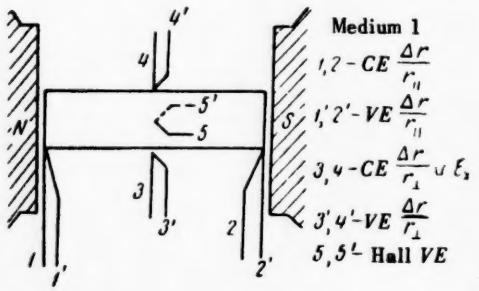

FIG. 1 (a)

*Fiz. metal. metalloved. 4, No.2, 249-256, 1957
[Reprint Order No. POM45]

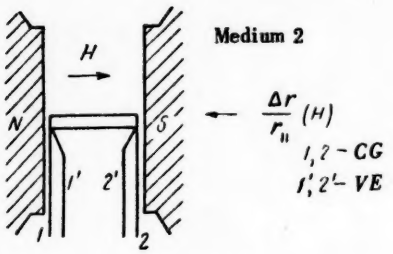

(b)

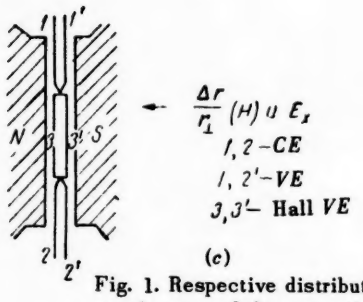

(c)

Fig. 1. Respective distribution of specimens and the magnetic field when measuring galvanometric effects (E = current electrodes VE = voltage electrodes)

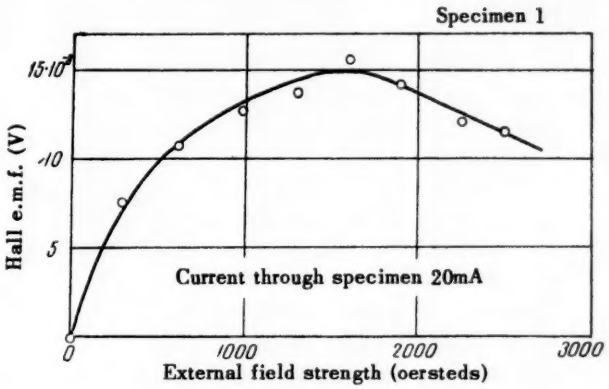

FIG. 2. Hall effect in magnetite (specimen 1)

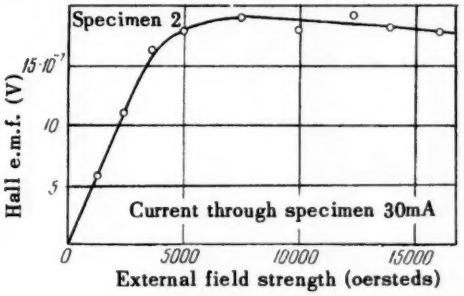

FIG. 3.Hall effect in magnetite (specimen 2)

netic effects (the Hall e.m.f., $\Delta r/r_{\parallel}$ and $\Delta r/r\perp$), the position of specimen No.1 relative to the magnetic field remained unchanged. On measuring the galvanomagnetic effects in specimen No.2 the longitudinal effect was measured in position 1, and the transverse effect $\Delta r/r_{\parallel}(H)$ and the Hall effect in position 2 (the areas marked in Fig.1 were galvanized by copper; then the current and voltage electrodes were soldered with tin). The specimens had the following specific resistance: specimen No.1, 1.63 Ω cm; specimen No.2, 1.27 Ω cm. Determining the sign of the thermal e.m.f. showed the electronic character of the conductivity of the specimens. The electrical measurements were carried out mainly on d.c. using a Dieselhorst potentiometer and a galvanometer with a sensitivity of scale 4.10^{-8} V/mm (the change in resistance in the magnetic field for specimen No.1 was measured by a.c.). The necessary precautions were taken in measuring the Hall effect: the measurements were made for different directions of the current and magnetic field, before measurement the specimens were carefully demagnetized etc.

The magnetic measurements - determination of the magnetic intensity curves of the specimens - were conducted ballistically in a Dewby electromagnet and a solenoid. Measurement was also made of the temperature dependence of magnetic intensity (for specimen No.1), which showed a characteristic rapid rise for magnetite at a temperature of around 114°K.

RESULTS OF MEASUREMENTS. HALL EFFECT

The results of measurements of the Hall e.m.f. in relation to the strength of the external magnetic field is shown in Fig.2 (specimen No.1) and Fig.3 (specimen No.2). It will be seen from the graphs that there is some similarity between the curves for specimens 1 and 2: on increase in the field strength the Hall e.m.f. increases, following the magnetic intensity curve, and then in the saturation zone it falls directly in proportion to the growth in the field. Thus the result may be expressed by the formula ordinarily used for ferromagnetic materials:-

$$E_x = R_0 (H_i + 4\pi a M) jb, \qquad (1)$$

where R_0 is the Hall constant of the "ordinary" part of the effect, aR_0 is the Hall constant of the "unusual" part of the effect, characteristic of ferromagnetic materials and directly proportional to the magnetic intensity (for magnetite a is negative), H_i is the field intensity within the specimen, M is the magnetic intensity of the specimen, j is the density of the primary current passing through the specimen and b is the thickness of the specimen (distance between the Hall electrodes).

The method of calculating the constants R_0 and a from the measurement results is given in the Appendix.

The values of R_0, a' and a'' calculated according to formulae (8), (11) and (13) are shown in Table 1.

TABLE 1.

Magnetite specimen	R_0(cm³/C)	a	
		a'	a''
1	$(2\pm0.3)10^{-4}$	1.3±0.3	1.4±0.3
2	$(1.7\pm0.1)10^{-2}$	17.8±1	21.2±1

Owing to the low value of the Hall e.m.f. measured, it was not possible to obtain the accuracy given in the above table. However, repeated measurements for other values of primary current passing through the specimen confirmed the result. The reliability of the result is also confirmed by the close coincidence of a' and a'' values found in other ways.

CHANGE OF RESISTANCE IN A MAGNETIC FIELD

The change of resistance in a magnetic field for specimens 1 and 2 is shown in Figs. 4 and 5. It will be seen from the graphs that for the two specimens both the longitudinal and the transverse effects correspond to a fall in resistance in the magnetic field.

In spite of the difficulties caused by the effect of the previous magnetic history of the specimen, the texture etc. on the course of $\Delta r/r_{\parallel}$ and $\perp = f(H)$, we still attempted to describe analytically the course of $\Delta r/r = f(H)$ found for magnetite. Here it appeared that the curves obtained can be expressed comparatively well by a formula as follows:- $\frac{\Delta r}{r} = A + B(H_i + 4\pi aM)^2$.

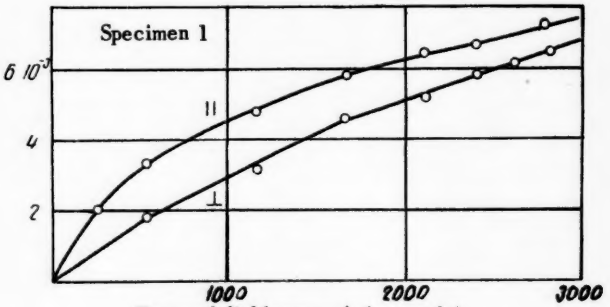

FIG. 4. Changes in resistance in a magnetic field (specimen 1)

In Fig.6 is given a graph of $\Delta r/r = f(H_i + 4\pi aM)^2$ for specimen No.1. From the graph it will be seen that the relationships

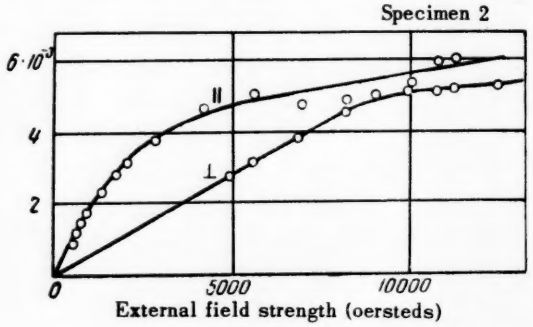

FIG. 5. Changes in resistance in a magnetic field (specimen 2)

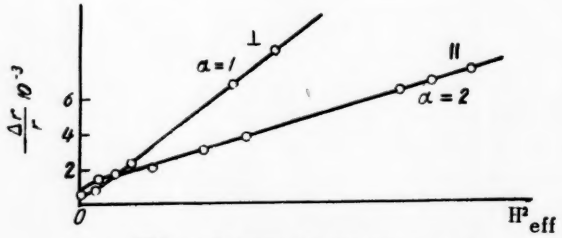

FIG. 6. Changes in resistance in a magnetic field of the function $(H_i + 4\pi aM)^2$

appear as straight lines (for specimen No.2 corresponding straight lines are obtained if $a_{\perp} = 7$ and $a_{\parallel} = 23$).

It should be pointed out that the theoretical equation in [2] gives an analogous relationship of $\Delta r/r$ to H_i and $4\pi Ma$. However, the coefficients must be analysed more closely theoretically

before we can talk of a direct connexion between these equations. Also the equation in [2] was derived for ferromagnetic materials (metals), while magnetite is a ferromagnetic semiconductor.

MAGNETIC CHARACTERISTICS OF SPECIMENS

In order to calculate the constants R_0 and a in the formula expressing the Hall effect in magnetite, and also in order to explain the connexion between the Hall effect and the change of resistance in a magnetic field, curves were drawn of the magnetic intensity of specimens 1 and 2. The magnetic intensity curve of specimen 1 is given in Fig.7, that for specimen No.2 in Fig.8 (the || magnetic intensity curve corresponds to the curve $\Delta r/r_{\parallel}$, the ⊥ curve to the curve $\Delta r/r_{\perp}$); in this case the magnetic intensity curves were measured in two directions perpendicular to the position of the specimen in relation to the direction of the magnetic field.

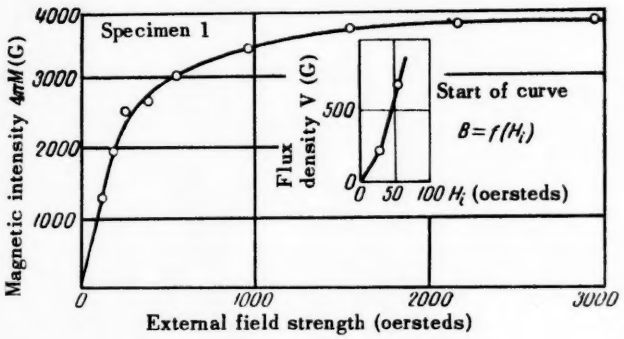

FIG. 7. Magnetic intensity (specimen 1)

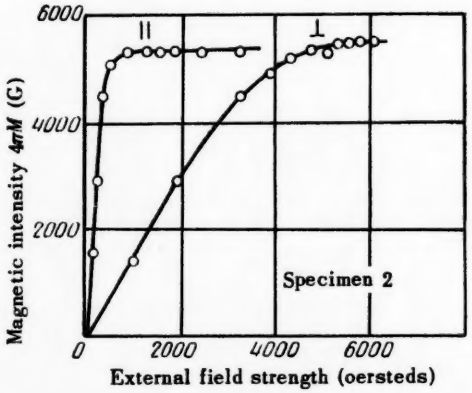

FIG. 8. Magnetic intensity (specimen 2).

The initial magnetic permeabilities and magnetic saturation intensity of specimens 1 and 2 are given in Table 2. The low magnetic saturation intensity of the polycrystalline specimen No.1 is clearly due to the presence in the specimen of impurities. In calculating the constant a'' for specimen No.1, the magnetic saturation intensity of the monocrystalline specimen of magnetite No.2 was used.

TABLE 2.

Magnetite specimen	Magnetic saturation intensity	Initial permeability
1	3800	6
2	5320	23

CONCLUSIONS

On the basis of the measurements the following can be concluded:-

1. The Hall effect in magnetite is expressed by the equation $E_x = R_0 (H_i + 4\pi a M)\, jb$ ordinarily valid for ferromagnetic metals.

The constants R_0 and a are opposite in sign, and in the saturation zone the Hall e.m.f. falls. This result agrees with data of the measurement of the Hall effect in nickel ferrite [3].

$R_0 \sim 10^{-1}$ to 10^{-2} cm³/C corresponds to a semiconductor concentration of conducting electrons of $\sim 10^{20}$ cm^{-3}. Here it should be said that it is not absolutely correct to estimate the concentration of the conductors in ferromagnetic materials according to the value R_0 in equation (1), since the "ordinary" part of the Hall effect in ferromagnetic materials is not absolutely similar to the Hall effect in non-ferromagnetic materials (cf. e.g. [4]).

2. Measurement of the resistance of magnetite in a magnetic field showed that it falls, both for longitudinal and transverse effects. This result agrees with published data for a number of ferrites (e.g. [5,6]) which was explained as "volume effect".

Experimental curves of $\Delta r/r_{\parallel \text{and} \perp} = f(H)$ are expressed satisfactorily by the equation

$$\frac{\Delta r}{r} = A + B(H_i + 4\pi a M)^2.$$

VOL. 4 1957

Thus here there is a square law of the relation of $\Delta r/r$ to the effective field H_{eff}, in this case $H_i + 4\pi\alpha M$.

3. Comparing the results concerning the Hall effect and change of resistance in a magnetic field, obtained in one and the same specimens of magnetite, it can be seen that in the galvanomagnetic effects referred to the conducting electrons are acted upon by an effective field, uniform in strength, $H_{\text{eff}} = H_i + 4\pi\alpha M$, where α is the parameter of the effective field, its magnitude and sign depending on the effect (cf. Table 3).

TABLE 3.

Hall effect	Parameter 6	
	Specimen No.1	Specimen No.2
	- 1.3	- 17.8
Change of resistance in magnetic field ⊥	1	7
" " " ∥	2	23

4. We intend to carry out similar investigations in the field of the low-temperature transformation of magnetite.

APPENDIX

Calculating the constants R_0 and α

In the formula

$$E_x = R_0 (H_i + 4\pi\alpha M) jb \qquad (1)$$

H_i and M are expressed through the following: the external field strength H_e, the demagnetization factor N and the permeability μ. We know that

$$H_i = H_e - NM, \qquad (2)$$

$$B = \mu H_i = \mu (H_e - NM), \text{ а также} \qquad (3)$$

$$B = H_i + 4\pi M = H_e - NM + 4\pi M. \qquad (4)$$

Adapting the last two expressions and solving them for M, we have

$$M = \frac{H_e (\mu - 1)}{\mu N - N + 4\pi} \qquad (5)$$

and accordingly

$$H_i = H_e - \frac{N H_e (\mu - 1)}{\mu N - N + 4\pi} . \qquad (6)$$

Inserting (5) and (6) in (1) we get $\frac{E_x}{jb} =$

$$= R_0 H_e \left[1 - \frac{N(\mu - 1)}{\mu N - N + 4\pi} + \frac{4\pi\alpha (\mu - 1)}{\mu N - N + 4\pi} \right]. \qquad (7)$$

Formula (7) enables R_0 and α to be calculated according to the experimental graph $E_x/jb = f(H_e)$ for a specimen with a demagnetization factor N and a magnetic characteristic μ.

Determination of R_0

Since the saturation zone $\mu \approx 1$, the two terms of expression (7) equal zero. Thus

$$R_0 = \left[\partial \frac{E_x}{jb} / \partial H_e \right]_{H_e > H_{es}} \qquad (8)$$

Determination of α

The angle of inclination of the start of $E_x/jb = f(H_e)$ is $\left[\partial \frac{E_x}{jb} / \partial H_e \right]_{H_e \sim 0} =$

$$= R_0 \left[1 - \frac{N(\mu_0' - 1)}{\mu N - N + 4\pi} + \frac{4\pi\alpha (\mu_0 - 1)}{\mu_0 N - N + 4\pi} \right], \qquad (9)$$

where μ_0 is the initial permeability. Dividing (9) by (8) we get $\frac{\left[\partial \frac{E_x}{jb} / \partial H_e \right]_{H_e \sim 0}}{\left[\partial \frac{E_x}{jb} / \partial H_e \right]_{H_e > H_{es}}} =$

$$= \left[1 - \frac{N(\mu_0 - 1)}{\mu_0 N - N + 4\pi} + \frac{4\pi\alpha (\mu_0 - 1)}{\mu_0 N - N + 4\pi} \right]. \qquad (10)$$

Solving (10) for α, we have $\alpha' =$

$$= \frac{\mu_0 N - N + 4\pi}{4\pi (\mu_0 - 1)} \left(\frac{\left[\partial \frac{E_x}{jb} / \partial H_e \right]_{H_e \sim 0}}{\left[\partial \frac{E_x}{jb} / \partial H_e \right]_{H_e > H_{es}}} - 1 \right) \qquad (11)$$

The constant α can also be determined another way. Extrapolating the rectilinear part of the graph $E_x/jb = f(H_e)$ along the ordinate, we have (cf.(1) and (2)):

$$\left[\frac{E_x}{jb} \right]_{\substack{\text{expt.} \\ H=0}} = R_0 (4\pi\alpha - N) M_s, \qquad (12)$$

where M is the magnetic saturation intensity.
From this we get:

$$\alpha'' = \frac{|E_x/jb|_{H=0}^{\text{expt.}}}{4\pi M_s R_0} + \frac{N}{4\pi}. \qquad (13)$$

(α calculated according to formula (11) is indicated by α' and according to formula (13) by α''). For the partial case of a thin lamina $N \cong 4\pi$ accordingly

$$\alpha' = \frac{\rho_0}{\rho_0 - 1}\left[\frac{\left(\partial \frac{E_x}{jb} / \partial H_e\right)_{H_e \sim 0}}{\left(\partial \frac{E_x}{jb} / \partial H_e\right)_{H_e > H_{es}}} - 1\right] + 1, \qquad (14)$$

$$\alpha'' = \frac{|E_x/jb|_{H_e \sim 0}^{\text{expt.}}}{4\pi M_s R_0} + 1. \qquad (15)$$

REFERENCES

1. T. Okamura and Y. Torizuca *Sci. Rep. Res. Inst. Tohoku. Univ.* A., *3* 352-60 (1950).
2. S.V. Vonsovskii, L. Ya. Kobelev and K.P. Rodionov *Izv. Akad. Nauk. SSSR, ser. fiz. 16*, 5, 569 (1952).
3. S. Foner *Phys. Rev. 88*, (4), 955 (1952).
4. D.I. Volkov *Vestnik Moskovskogo universiteta 3*, 65 (1954).
5. A.P. Komar and V.V. Kliushin *Izv. Akad. Nauk. SSSR, ser. fiz. 18*, 403 (1954).
6. N.A. Smol' Kov *Fiz. metal. metalloved. 2*, No.1, 10 (1956).

VOL. 4 1957

STUDY OF COERCIVITY OF COLD-WORKED AND ANNEALED IRON ALLOYS*

G.M. FEDASH

(Received 10 August 1956)

This paper presents the results of an experiment study of the variation of coercivity of iron alloys with alloying element content, percentage cold reduction, and annealing temperature. On the basis of these variations, the alloys fall into two groups; those alloyed with elements which raise, and with those which lower, the A_3 point. There are indications of segregation in cold reduction and partial annealing of iron–manganese and iron–nickel alloys.

At present coercivity is very widely used qualitatively as one of the criteria in magnetic analysis of purely metallurgical processes. It is therefore very desirable to establish the reasons for any changes in it. The general pattern of coercivity variation in the formation of solid solutions, cold straining and annealing of metals has been fairly well studied [1, 2]. It has been shown [3] that the coercivity of homogeneous solid solutions is independent of concentration and only increases sharply when a new phase appears. Hence the stresses arising through formation of solid solutions do not affect the coercivity of ferrite. However, in several ferrous alloys coercivity does change very considerably before appearance of a second phase, being raised more by elements which lower the A_3 point than by those which raise it [1]. Cold plastic deformation increases coercivity by creation of stresses. Annealing strained metals has the opposite effect. Changes in coercivity during straining and annealing of alloys may be complicated on the one hand by "uphill diffusion" because of stress gradients, and on the other hand by strain hardening, if the alloy is not sufficient homogeneous. In these cases, coercivity anomalies are found.

Thus in working iron-manganese alloys containing more than 3 percent manganese, there is a sharp fall of coercivity in the first stage of deformation [4].

In this paper we show that in alloys with elements which raise the A_3 point coercivity changes with cold straining and annealing in a different way from its change in alloys with elements which lower the A_3 point.

PREPARATION OF ALLOYS

The alloys were made from an Armco iron containing 99.65 percent iron, 0.03 percent silicon, 0.04 percent manganese, 0.12 percent nickel, 0.037 percent carbon, 0.02 percent phosphorus, 0.016 percent sulphur, and 0.077 percent copper. The alloys were melted in a high frequency induction furnace.

Alloys were prepared containing 1.17, 2.02, 3.96, 6.25, 8.04, 10.05, 12.12 and 15.52 percent nickel, 1.14, 2.07, 3.96, 6.00, 8.39, 10.54 and 12.20 percent manganese, 0.90, 1.98, 3.83, 5.71 percent silicon, 0.94, 2.01, 3.92, 6.09, 8.00 percent chromium 0.86, 3.08, 4.57, and 6.64 percent cobalt, and 0.05, 0.1, 0.2, 0.4, 0.6, 0.8, and 1.0 percent carbon.

The ingots were homogenized at 1100°C for 8 hr and furnace cooled, forged to 8 mm square billets, 200 mm long, which were homogenized at 50°C above furnace cooling. These specimens were used for studies of coercivity variation with alloying element concentration. See Fig. 1. They were reduced by rolling through a stand with 180 mm diameter rolls. After appropriate measurement, the rolled specimens were annealed for 30 min and at various temperatures above this at 100°C intervals. Annealing temperatures were measured

* *Fiz. metal metalloved.* 4, No. 2, 257-266, 1957 [Reprint Order No. POM 46].

VOL 4 195

to within ± 5°C. Coercivity was measured in an open magnetic circuit by the break method.

RESULTS AND DISCUSSION

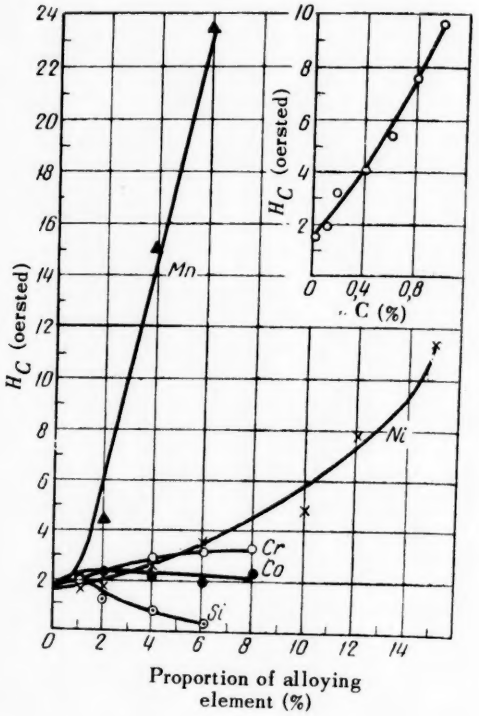

FIG. 1. Effect of alloying element concentration

Fig. 1 shows the variation of coercivity H_c with alloying element concentration. We see that it increases with concentration not only in carbon steels, which are 2 phase structures of ferrite and cementite, but also in alloys consisting of homogeneous α solid solutions. Manganese and nickel increase the coercivity of ferrite most, cobalt not at all, while silicon somewhat lowers it.

Since the atomic radii of chromium cobalt, nickel and manganese do not differ by more than 2 percent from the atomic radius of iron, [5,], these changes of coercivity cannot be due to lattice distortions through elements of different atomic dimensions. The atomic radius of silicon differs from that of iron by 8 percent but silicon lowers coercivity.

Metallographic study showed that manganese and nickel decrease the grain size of ferrite, while silicon increases it, but the changes in coercivity are too large to be explained entirely by a change in grain size. We must take into consideration which modification of iron a particular alloying element tends to form. Manganese and nickel expand the γ-range, and tend to form γ-iron and "force" iron to form a γ-lattice considerably below 910°C. If we assume that these structural peculiarities of manganese and nickel atoms are preserved at temperatures below the $\alpha + \gamma \rightarrow \alpha$ transformation temperature, we must also assume that at these temperatures manganese and nickel atoms are "unwilling" constituents of α-iron, preferring to form α-iron. This α-iron preference due to the configuration of the external electron shells of these elements should distort the force field of the lattice, and thus affect the coercivity of ferrite. Chromium, and particularly silicon, raise the A_3 point, consequently, they promote formation of α-iron, and therefore do not distort the force field so much. Cobalt at small contents does not affect the position of the A_3 point, nor the coercivity.

Differences in the interaction of solvent atoms with elements which raise (chromium, cobalt, silicon) and lower (manganese, nickel) the A_3 point are particularly pronounced in cold straining of the alloys. From Fig. 2, a-d

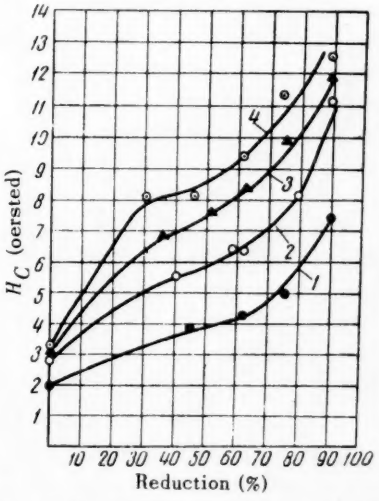

FIG. 2a. Variation of coercivity with percent reduction:

1 = 0.94 percent chromium,
2 = 3.92 percent chromium,
3 = 6.09 percent chromium,
4 = 8 percent chromium,

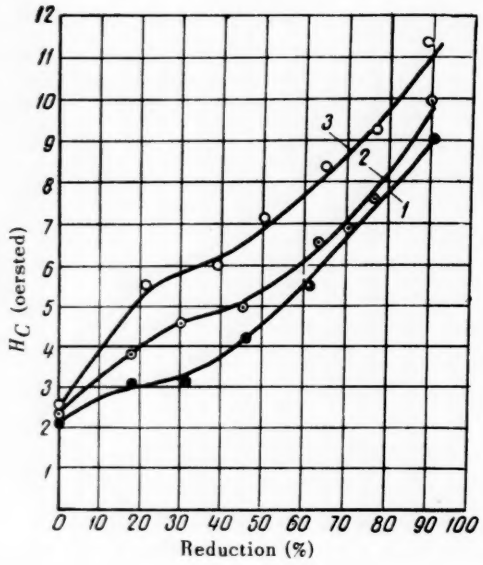

FIG. 2b. Variation of coercivity with percent reduction:

1 = 0.86 percent cobalt,
2 = 4.57 percent cobalt,
3 = 6.64 percent cobalt,

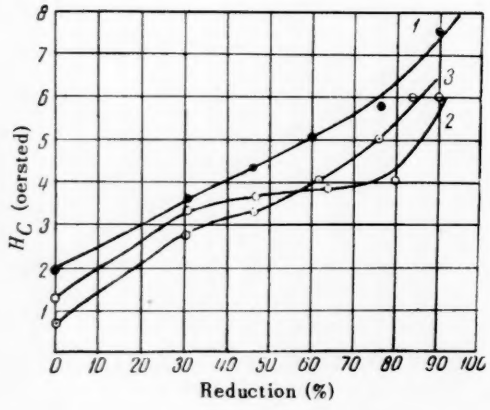

FIG. 2c. Variation of coercivity with percent reduction:

1 = 0.90 percent silicon,
2 = 1.98 percent silicon,
3 = 3.83 percent silicon.

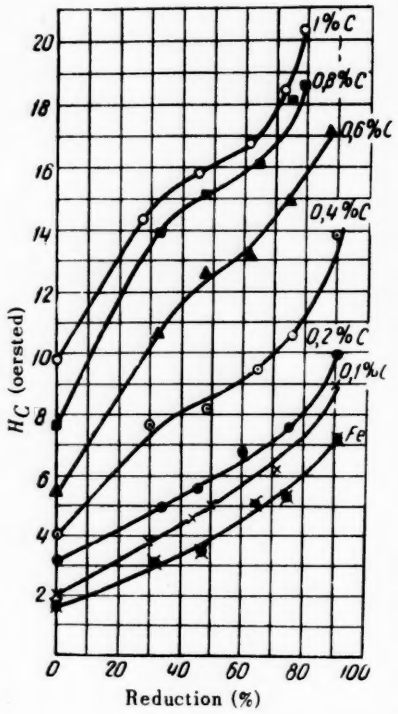

FIG. 2d. Variation of coercivity with percent reduction:

Iron – carbon.

we see that the variation of coercivity with reduction (in cold rolling) is very similar for alloys of iron with chromium, cobalt, silicon and carbon. The rate of increase of coercivity with reduction is greater at low and high than at intermediate reductions, so that the curves have inflexion points. Mes'kin [1] found the same thing for a plain steel containing 0.78% carbon. The more rapid rise of coercivity with reduction at low reductions in carbon steels is due to a decomposition of lamellar cementite. Apparently in homogeneous solid solutions also, individual grains, appropriately oriented to the deforming force, are broken up in the first stages of reduction, while during further reduction the grains can rotate and be stretched out along the rolling direction. At high reductions, microcracks appear, and coercivity again rises more rapidly. Fig. 2e shows curves for the variation of coercivity with reduction of iron-nickel alloys. Up to 8 percent nickel, the curves have the same shape as for alloys of the

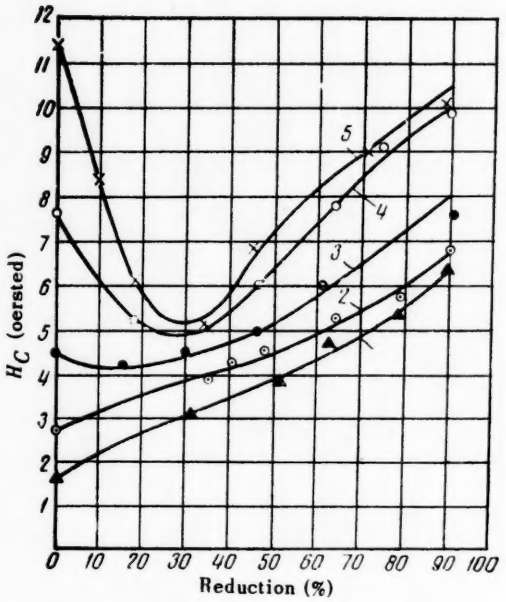

FIG. 2e. Variation of coercivity with percent reduction: for nickel

1 = 1.17 percent
2 = 3.96 percent
3 = 8.04 percent
4 = 12.12 percent
5 = 15.52 percent

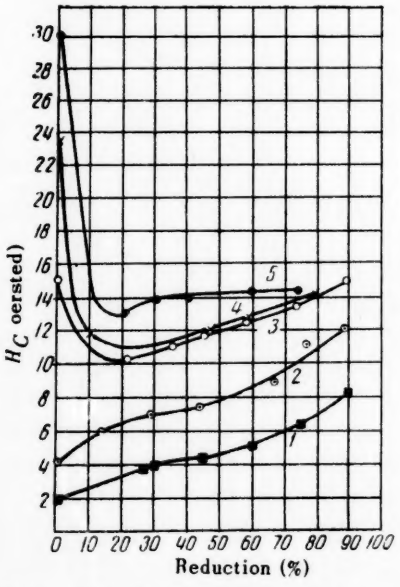

FIG. 2f. Variation of coercivity with percent reduction: for manganese.

1 = 1.14 percent
2 = 2.07 percent
3 = 3.95 percent
4 = 6 percent
5 = 8.39 percent.

first group, but above it there is an appreciable reduction of coercivity in the first stages of reduction. The lowering increases with nickel content. The same thing happens with iron–manganese alloys (Fig. 2f) containing more than 3 percent manganese [4].

This lowering of coercivity at low reductions may indicate relief of strain hardening. However, X-ray spectra of alloys with 8-15 percent of nickel did not reveal the presence of any γ-iron. On the other hand, the variation of coercivity in annealing of iron–manganese and iron-nickel alloys suggests the existence of diffusion processes, directed towards the separation of components, leading to chemical heterogeneity of specimens.

Fig. 3 shows the variation of coercivity with annealing temperature for alloys of the first and second groups. The coercivity of the first group alloys falls sharply towards the value for the initial specimens around the recrystallization temperature (300 – 550°C). The same thing happens with pure iron.

This sort of change occurs only at small concentrations of alloying elements which lower the A_3 point. The coercivity of alloys containing more than 2 percent manganese and 6 percent

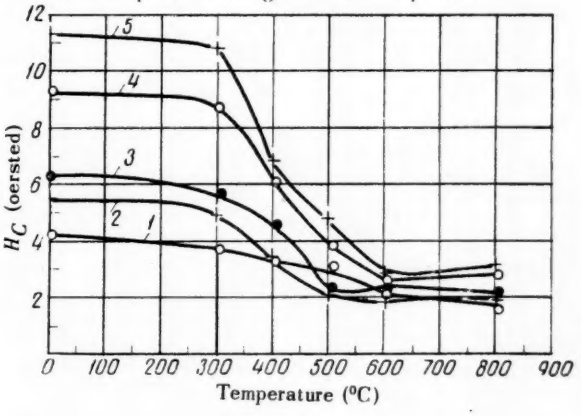

FIG.3a. Variation of coercivity with heat treatment temperature.

Curve	1	2	3
Percent Cr	0.94	2.01	3.92
Percent reduction:	61	51.5	57

Curve	4	5
Percent Cr	6.09	8.0
Percent reduction:	61.1	79

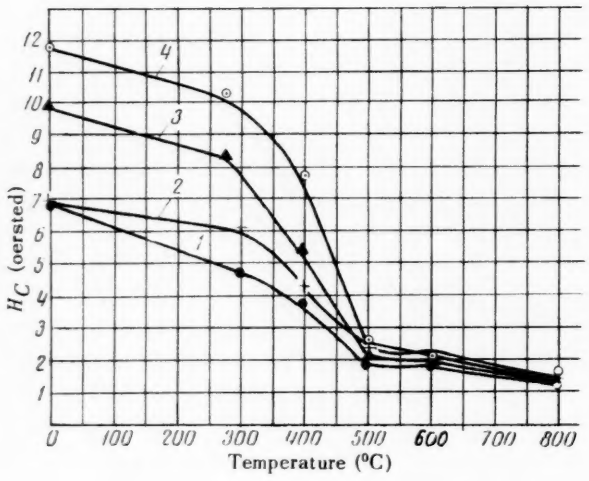

FIG. 3b.

Curve	1	2	3
Percent Co	0.86	3.0	4.57
Percent reduction	71	76.7	89.1

Curve	4
Percent Co	6.64
Percent reduction	89.1

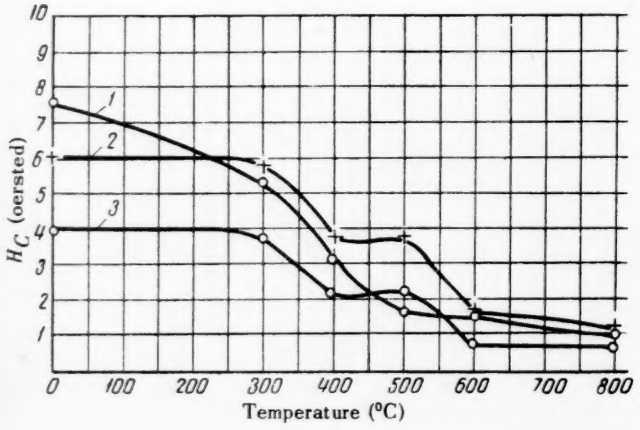

FIG. 3c.

Curve	1	2	3
Percent Si	0.90	1.98	3.83
Percent reduction	90	90	62

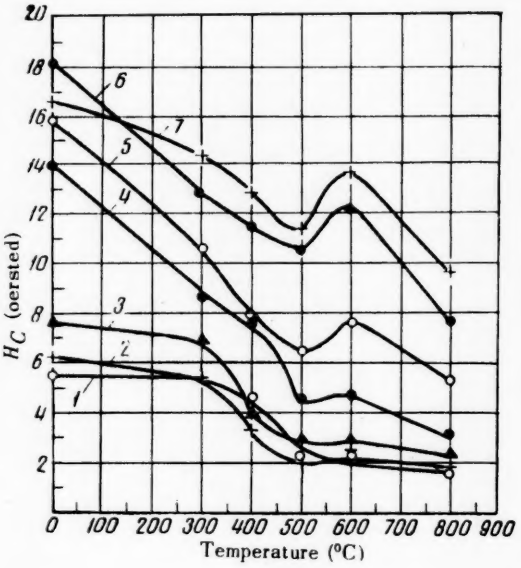

FIG. 3d.

Curve	1	2	3	4
Percent C	005	0.1	0.2	0.4
Percent reduction	75.0	71.6	75.6	90.6

Curve	5	6	7
Percent C	0.9	0.6	1.0
Percent reduction	76.6	72.2	61.9

nickel falls only during heating to 400°C, and annealing at 500–600°C sharply increases it. The coercivity maximum corresponds to the appearance of γ-iron at high alloying element contents. The X-ray spectra of these specimens shows γ-phase lines [6]. γ-iron is formed at temperatures below Ac_3 for corresponding initial concentrations. This tends to confirm that regions with an enhanced alloying element content are formed in the alloy, with a lower Ac_3 point on the constitutional diagram. As the alloying element content increases, the maximum coercivity appears at lower temperatures, i.e. the higher the concentration of solution, the lower the temperature at which γ-phase appears.

On full annealing (600–800°C), because of recrystallization and thermal motion, alloying elements become uniformly distributed, segregation of manganese and nickel disappears, and the coercivity falls to the values of the initial specimens. The lines for γ-phase should disappear from X-ray spectra after full annealing, and in fact they do [6, 7].

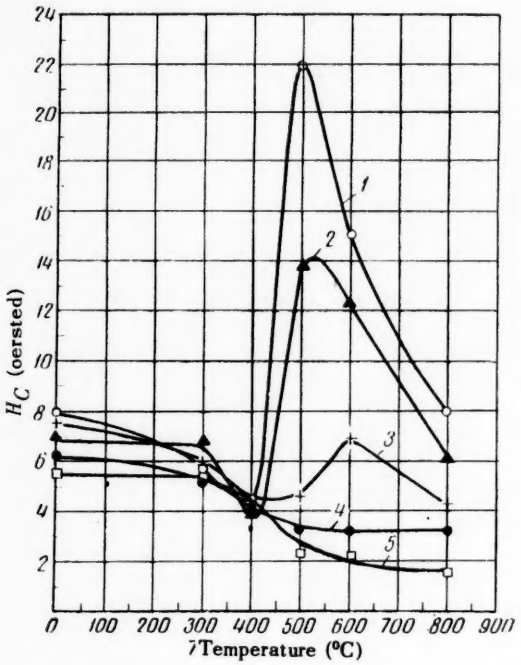

FIG. 3e.

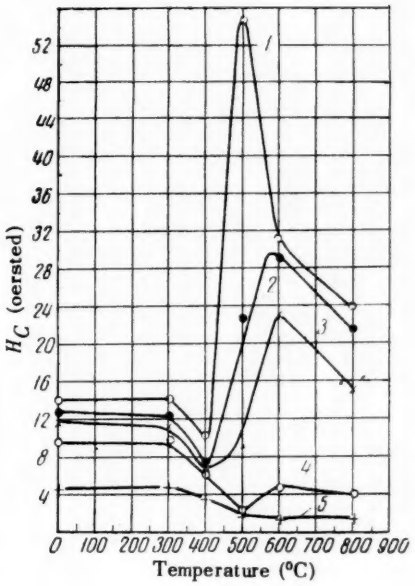

FIG. 3f.

Curve	1	2	3
Percent Ni	12.12	10.05	8.04
Percent reduction:	62.0	74.4	89.6

Curve	4	5
Percent Ni	6.25	Fe
Percent reduction:	88.5	75

Curve	1	2	3
Percent Mn	8.39	6	3.95
Percent reduction:	42.5	38.5	45

Curve	4	5
Percent Mn	2.07	1.14
Percent reduction:	43	45.5

When they are deformed, carbon steels behave like alloys of the first groups (Fig. 2d). Small maxima appear on the annealing curves, at 600° C (Fig. 3d) just as they do on alloys of the second group.

Our results show that on the basis of variation of coercivity of ferrite with concentration of alloying elements, reduction in rolling and annealing temperature, alloys can be divided into the same groups as they can on the basis of effect of alloying elements on the A_3 point.

The author thanks Lecturer B.G. Kurilekh for supplying the specimens and for the interest shown in the work.

REFERENCES

1. V.S. Mes'kin *Ferromagnitnye splavy (Ferromagnetic alloys)*, 1937.
2. S.V. Vonsovskii and Ya. S. Shur *Ferromagnetism*, 1948.
3. Kussmann and Sharnow *Z. Phys.* 54, 1 (1929).
4. D.G. Kurilekh and G.M. Fedash *Fiz.metal.metalloved.*2, 3 (1956).
5. I.I Kornilov *Zheleznye splavy (Iron alloys)* 2, 1951.
6. N.I. Varich, Thesis, Dnepropetrovsk State University, 1952.
7. N.I. Varich and D.G. Kurilekh, Nauchnye Zapiski Dnepropetrovsk State University, 11, 1953.

VOL. 4 1957

CONCERNING MAGNETIC EFFECT ON I_S (T°) CURVES IN THE TEMPERATURE RANGE 260-270° DRAWN FOR TEMPERED AND ANNEALED SPECIMENS*

B.A. APAEV

(Received 21 May 1956)

On tempering of hardened steel and on deformation of annealed steel the magnetic properties are found to change in a similar way: the magnetic intensity increases (compared with that in the annealed condition) and a kink appears on the I_S (T°) curves in the region 260-270° (in addition to the kink at the Curie point of cementite). The effects mentioned are due to one and the same thing, the presence in tempered and deformed steel of a carbide phase χFe_xC. Increase in the magnetic intensity is due to the chemical composition of this carbide ($x < 3$), and the second kink on the I_S (T°) curve is due to magnetic transformation (Curie point) in this phase.

In magnetic phase analysis conclusions concerning the presence of one or other ferromagnetic phase in a specimen being investigated are based on observations of the Curie point of the phase. Methods of determining Curie points according to the curve of magnetic susceptibility $\chi(T^\circ)$, the curve of heat capacity $c(T^\circ)$, the curve of magnetic intensity I_S (T°) are acknowledged as adequate [1]. In I_S (T°) curves the Curie point is indicated by a characteristic kink, resulting from a sharp fall in the intensity of the phase in the temperature region of this point. It is clear from the reversibility of the course of the $I_S(T^\circ)$ curve that this kink results from magnetic transformation and is not due to phase transformation occurring on heating.

$I_S(T^\circ)$ curves characterizing change in magnetic intensity on repeated heating of tempered specimens (when the heating temperature does not exceed the initial tempering temperature) satisfy the condition of reversibility. On the basis of this it has been concluded in magnetic phase analysis [2-4] that magnetic effect in I_S (T°) curves-a kink in the temperature region 260-270°-characterizes the Curie point of a high-temperature carbide phase that we shall indicate as χFe_xC.

K. Jack [5,6] and a number of other authors who have contributed to discussing the question of the phase composition of tempered carbon steel, have disagreed with this theory to explain this magnetic effect. They base their argument on the results of work [7,8] in which an analogous magnetic effect is reported on $I_S(T^\circ)$ curves drawn for plastically deformed specimens of annealed carbon steel. The authors of these reports have also found that in plastically-deformed specimens a rise in the magnetic intensity is observed.

D. Wilson [9], who investigated by means of X-rays and found no confirmation for the formation of new phases during plastic deformation, attributes the changes in the magnetic properties observed on plastic deformation to residual strains in cementite. He regards the kink on the curves in the temperature region 260-270° as due to "displacement" of the Curie point of cementite from its normal position 210 to 265° through the action of strains. He suggests that the amount of displacement of the Curie point (ΔT°) may alter with change in the residual strains in cementite [7].

Jack [5,6], in agreement with Wilson's conclusions, extends his theory to explain the change in the magnetic properties on plastic deformation to the tempered condition of steel as well. In view of the similarity in the magnetic effects (coincidence of the temperature of the kink on the $I_S(T^\circ)$ curves, higher magnetic intensity compared with that in the annealed condition) Jack explains these effects not by a difference in the phase compositions of tempered and annealed steel, but by residual strains in cementite.

The object of the present investigation was to study the validity of the theories presented by the authors of [5-7,9] concerning the nature of the magnetic effects being considered.

TEMPERED CONDITION OF STEEL

Jack's [5,6] views concerning the condition of

* *Fiz. metal. metalloved.* 4, No. 2, 267-277, 1957
[Reprint Order No. POM 47]

tempered steel and the processes occurring on tempering ($T > 250°$) can be stated as follows. Strains occur in cementite owing to compression by the surrounding α-phase. Under the action of these strains, though a change may occur in the cementite lattice parameters, its crystal structure remains the same. The degree of distortion of the cementite lattice depends on the magnitude of strain in the α-solid solution. With increasing tempering temperature there is a reduction in the strain of the cementite and its lattice condition approaches the equilibrium condition.

Since magnetic effects are connected with strain of cementite, it should be supposed that the kink on the I_s ($T°$) curve in the temperature region 260-270° will disappear and the magnetic intensity of steel will fall to the magnetic intensity in the annealed condition in exactly the same temperature interval as the strain is removed.

On the basis of the results of investigations [10-12] concerning change in the strained condition of the α-phase with increasing tempering temperature, it should be concluded that normal properties will be restored up to $T \leqslant 500°$. It is easy to see why Jack [6] doubted the reliability of Crengle and Sucksmith's data [3]. They observed a kink on the $I_S(T°)$ curve drawn for a specimen that had been tempered at a temperature of 509°. The persistence of this effect at high temperatures was also reported in [2]. We further illustrate this fact in Fig.1, from which it will be seen that the kink on the $I_S(T°)$ curves in the temperature region 260-270° is clearly found in the case of U 12 steel* after tempering for one hour at 450, 500 and 600°, i.e. at temperatures at which the strains in the α-phase can be reckoned to have practically disappeared. For this reason it is difficult to connect the magnetic effect on $I_S(T°)$ curves with strain in cementite.

At tempering temperatures > 400° the permanence of the magnetic effect on the $I_S(T°)$ curves is astonishingly great. Fig.2 shows three $I_S(T°)$ curves of U 12 steel specimens after tempering for 30 hours at temperatures of 300, 350 and 400°. Comparing these curves with $I_S(T°)$ curves for annealed specimens (dotted curves in Fig.2), we see that the magnetic intensity of the tempered specimens is greater than that of annealed specimens.

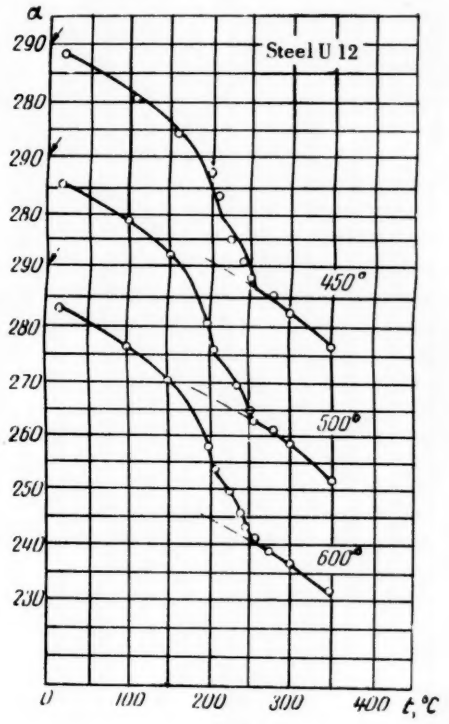

FIG. 1.

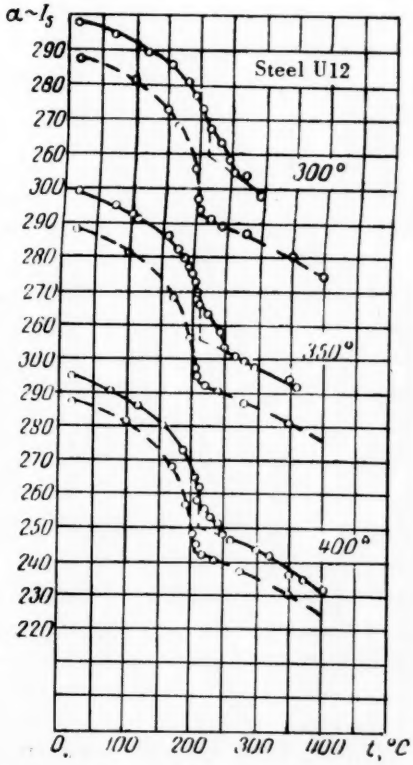

FIG. 2.

* The U 12 steel was hardened from a temperature of 1050°.

VOL. 4 1957

From Jack's viewpoint, the composition of steel after tempering in this way is characterized by the system $Fe_3C + Fe_\alpha$ (C), and the kink on the $I_s(T^\circ)$ curves in the temperature region 260-270° and the higher magnetic intensity result from strain in the cementite.

Comparing the magnetic intensities in relation to the temperature above 270°, then we see that the magnetic intensity of tempered specimens still remains greater than that of annealed specimens. After tempering at 300° it is about 6 per cent greater, after tempering at 400° - about 3 per cent (comparison in relation to a temperature of 300°). In the region of temperatures being considered (above 270°), the magnetic properties of the carbide phase already do not affect the magnetic intensity of the specimen, the latter depends only on the magnetic intensity of the α-solid solution and its volume.

$$I = \frac{P_\alpha}{100} I_\alpha$$

Since, after such prolonged tempering, the carbon concentration in the α-solid solution must be reckoned as being near the equilibrium concentration of carbon in the annealed ferrite [13, 14], it is impossible to relate the difference in the magnetic intensity of tempered and annealed specimens to the difference in the amount of cementite phase in these two conditions of the steel [15, 16].

Nor can this difference in the magnetic intensities be related to volume changes that might be expected to occur as a result of removing strain in the specimen with increasing tempering temperature. Relating the volume changes to the change in diameter only and taking as a gauge the change in density from the hardened condition to the annealed condition (1.5 per cent according to results in [17], then under these conditions on further heating of a specimen tempered at 300° for 30 hr the fall in intensity

$$\Delta I = I_{300^\circ} - I_{ann}$$

is altogether about 50 per cent of heat actually observed. According to results in [17, 18], in specimens tempered in this way on heating to higher temperatures, volume changes were not generally detected by dilatometry or by hydrostatic weighing.

According to Jack, this is due to the strain of the α-phase. Strains in a α-solid solution remaining after tempering for 30 hr at temperatures of 300-400°, having little effect on volume change, may strongly affect the magnetic properties, and thus the magnetic intensity of ferrite

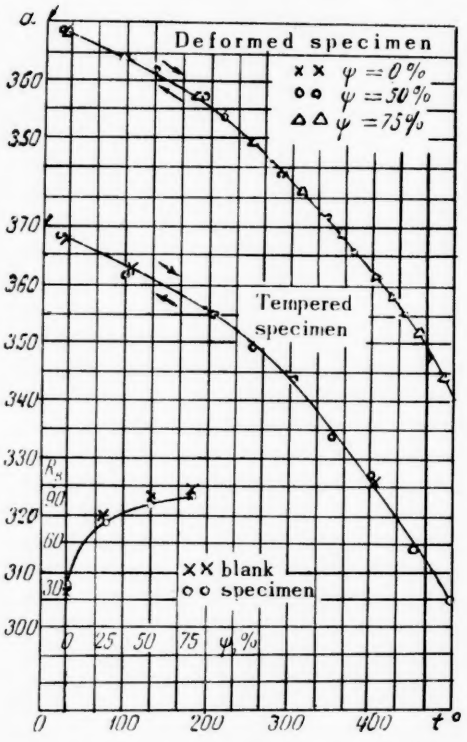

FIG. 3. Character of I_s (T°) curves on heating and cooling of hardened and deformed specimens of Armco-iron (heating was carried out to a temperature of 650°).

in the annealed condition cannot be reckoned identical with that of the α-phase in the tempered condition. With increasing annealing temperature, removal of strain in the α-solid solution leads to a fall in its magnetic intensity; on complete removal of strain the magnetic intensity equals that of annealed ferrite. But this contradicts the thermodynamic estimate of the sign of the change in magnetic intensity with reduction of strain in iron. Theoretically the magnetic intensity does not decrease, but increases when a ferromagnetic material approaches the equilibrium condition [19]. Nor is Jack's conclusion supported by the experimental data.

In order to check this conclusion we prepared specimens of Armco-iron by cold rolling with degrees of reduction of 75, 50 and 20 per cent. Blanks in the form of bars measuring 16 × 16, 8 ×

8 and 5 × 5 mm were cut from a single ingot and then rolled to strips 4 mm thick.

During preparation of the specimens, the necessary precautions were taken to prevent them from overheating. The hardness curve given in Fig.3 shows that the residual strains in the specimens were fully retained.

If the residual strains in iron affected the magnetic intensity, then it might be expected that the magnetic intensity of these three specimens would differ from that of a non-deformed specimen, and $I_S(T^\circ)$ curves drawn for these specimens on heating and cooling would be irreversible. Measurements showed that the scatter of the magnetic intensities of the specimens lies within the limits of accuracy of the experiment, and all the $I_S(T^\circ)$ are reversible (Fig.3). This same figure contains a $I_S(T^\circ)$ curve for an Armco-iron specimen alkali-hardened from a temperature of 1100°. The hardness of the Armco-iron after hardening ($H_B = 90$) was the same as that after high plastic deformation ($\psi = 75$ per cent). From the figure it will be seen that the strains resulting from hardening also do not affect the magnetic intensity and do not alter the reversibility of the $I_S(T^\circ)$ curve.

From what has been said it follows that none of the three causes mentioned [continuing dissociation of the α-solid solution, volume changes and the effect of strains on the magnetic properties of the α-phase] can explain the fall in magnetic intensity of the specimen with increasing annealing temperature.

It is easy to explain the fall in the magnetic intensity if the kink on the $I_S(T^\circ)$ curve in the temperature range 260-270° is connected with magnetic transformation in the intermediate carbide phase χFe_xC.

Since the phase composition of tempered specimens is characterized by the three phases $Fe_3C + \chi Fe_xC + Fe_\alpha(C)$, the relationship of the volumes of the phases in the specimen may be expressed as

$$P_c + P_\chi + P_\alpha = 100 \qquad (1)$$

and the magnetic intensity of the specimen (at $T > 270^\circ$)

$$I_{temp} = P_\alpha I_\alpha / 100 . \qquad (2)$$

For the annealed condition equations (1) and (2) take the form:

$$P_f + P'_c = 100, \qquad (3)$$

$$I_{ann} = P_f . I_f / 100 \qquad (4)$$

hence

$$\Delta I = I_{temp} - I_{ann} = P_\alpha I_\alpha / 100 - P_f I_f / 100. \qquad (5)$$

Owing to the α-solution becoming very impoverished in carbon after tempering for 30 hr at temperatures of 300 – 400° the approximation is allowable:

$$I_\alpha = I_f,$$

i.e. the magnetic intensity of the α-solid solution in tempered specimens can be taken as being equal to that of the annealed ferrite. On this basis we can write equation (5) as follows:

$$\Delta I = (P_\alpha - P_f) I_f / 100.$$

Since experiment shows that $\Delta I > 0$, then $P_\alpha > P_f$, or from (1) and (3) it can be concluded that

$$P'_c > (P_c + P_\chi),$$

i.e. the volume of the cementite phase in the annealed specimen exceeds the volume of the carbide phases in tempered specimens. Reduction in the volume of P_α is due to part of the iron atoms being used to form cementite from the phase χFe_xC, since it must be reckoned that the index x in the formula χFe_xC is less than three.

Thus we conclude that the kink on the $I_S(T^\circ)$ curve in the temperature region 260-270° indicates the Curie point of the carbide phase χFe_xC and the disappearance of this effect from the curve and the fall in the magnetic intensity of the specimen on further rise in tempering temperature are due to degeneration of this phase.

THE PLASTICALLY DEFORMED CONDITION OF STEEL

The material chosen for the investigation was hot-rolled 65 *GP* steel in the form of wire 6.5 mm in diameter. Plastic deformation was carried out in the cold state without intermediate annealing by drawing through dies. The degree of deformation, calculated from the reduction in diameter, covered an interval from 4 to 84 per cent (4; 14; 29; 62; 71 and 84 per cent). The character of the change in the magnetic properties of cold-deformed specimens was studied both in relation to the degree of deformation and to the heating temperature. A parallel investigation was carried out on

specimens tempered after hardening. The hardening temperature was 1050°, heating was done in a vacuum, and cooling was in aqueous 10% NaOH. All specimens were annealed in the temperature interval 300-650° with holding for 1 hr in Wood's alloy and tin.

4-14 per cent deformation does not cause any change in the magnetic properties of steel. After such deformation the magnetic intensity of steel remains the same as before and no changes whatever are seen on the $I_s(T°)$ curve. Nor are any changes seen subsequently on heating with specimens to a temperature of 300-650°. This conclusion is based on the fact that $I_s(T°)$ curves drawn for a specimen after deformation (ψ = 14 per cent) and after two subsequent heatings to 300 and 650° are similar to the $I_s(T°)$ curve for an annealed specimen (Fig. 4). Reduction by 29 per cent causes a noticeable change in the magnetic properties: the magnetic intensity of the specimen increases, and on the $I_s(T°)$ curve in addition to the kink at the Curie point of cementite there is a new one in the temperature region 260-270° (Figs. 4 and 5)*. This indicates that on plastic deformation not all the cementite but only some part of it is subjected to transformations.

In our arrangement there were no specimens with degrees of reduction between 14 and 29 per cent. Such specimens would make it possible to follow the development of the effect being observed [rise in magnetic intensity and kinking in the temperature region 260-270° on the $I_s(T°)$ curve] through the gradual increase in the strain. We therefore decided to observe these changes not on increase but on decrease in the strain in the deformed specimen, subjecting it to successive heatings. The specimens were heated in baths of Wood's alloy or tin, at temperature of 300, 350,

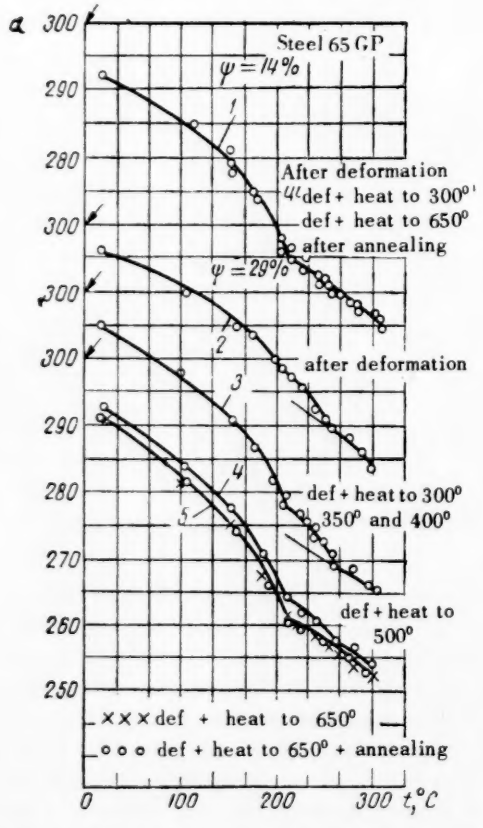

FIG. 4. Change in the characteristic of the $I_s(T°)$ curves in relation to the degree of deformation and the heating temperature after deformation. Heating time 60 min.

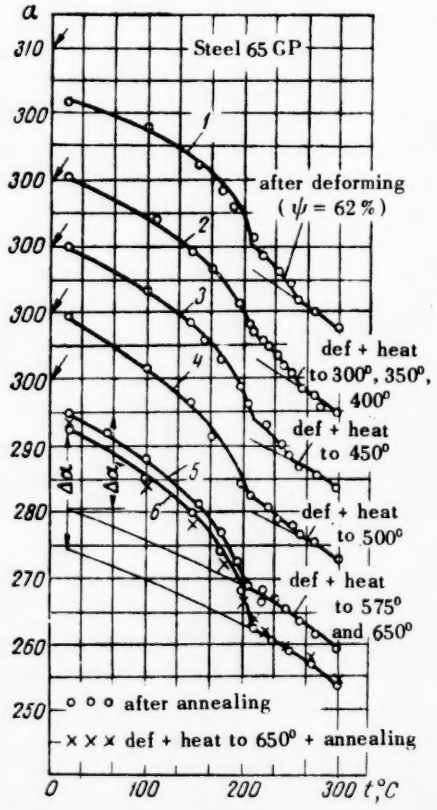

FIG. 5. Character of $I_s(T°)$ curves in relation to heating of deformed specimens ($\psi \approx 62$ per cent). Heating time 60 min.

* In the figures all the $I_s(T°)$ curves relate to specimens 4 mm in diameter.

400, 500, 575 and 650° with holding for 1 hr. Each time after the specimens had been heated an $I_s(T°)$ curve was drawn and by comparing them the nature of the changes taking place was analysed. Fig.4, curve 3 shows that heating a specimen to 300° causes a noticeable reduction in the magnetic intensity, that can be seen most clearly from the ferrite section of the curve, i.e. at $T > 270°$. Increasing the heating temperature to 350 and 400° causes no further change, and the $I_s(T°)$ curve after such heatings passes through the same points as after heating to 350°. After heating at 500° a further reduction is observed in the magnetic intensity and the effect on the curve in the region 260-270° (curve 4) almost completely disappears. On heating to 650° the magnetic intensity again falls a little and the kink in the region 260-270° disappears completely (curve 5). With further increase in temperature, up to the annealing temperature (950°), no changes are seen in the specimen and the course of the $I_s(T°)$ curve coincides with that of the curve after heating for one hour at 650°.

Investigation of the specimens subjected to greater reductions showed that with rise in the degree of deformation to 62 per cent the magnetic intensity continues to increase, while on further rise ($\psi = 71$ and 84 per cent) the magnetic intensity remains constant. We were unable to detect any differences in the character of the $I_s(T°)$ curves compared with the $I_s(T°)$ curve drawn for a specimen deformed to 29 per cent. The character of the change also remains the same on heating these specimens. The process is accompanied by a reduction in magnetic intensity; on heating in the region 300-400° the phase composition is seen to be stable: on heating to higher temperatures the kink on the $I_s(T°)$ curve in the region 260-270° clearly becomes weaker. The character of the degeneration of this magnetic effect remains the same as before: the temperature of the kink remains constant, but the slope of the section of the curve from 210-260° diminishes. Both in the deformed specimen and after heating, the presence of cementite is clearly seen from its Curie point (210°) which appears distinctly on all the curves in Fig. 5.

In comparing the $I_s(T°)$ curves in Figs. 4 and 5 it should be pointed out, however, that heating a specimen deformed to 62 per cent to a temperature of 650° does not bring the specimen into an annealed condition. After heating the specimen to 650° the $I_s(T°)$ curve goes higher than the curve for an annealed specimen. Comparison of the Δa and Λa, shows that in a specimen deformed and then heated to 650° the amount of cementite is less than in the annealed specimen (curves 5 and 6 in Fig. 5). This enables it to be concluded that graphitization takes place on heating of deformed specimens. This conclusion is confirmed by the fact that the original structure may be restored by annealing the specimen (the course of curve 6 after annealing, heating to 950° and cooling with the furnace, is shown in Fig. 5 by crosses). We further confirmed this by analysis of electrolytic precipitation from the specimen after deformation ($\psi = 62$ per cent) and heating to 650° by means of separating the free and combined carbon in Thoulet liquid [20].

The phenomenon of graphitization on heating of deformed specimens observed by us was noted by the authors of [8], who used the ordinary metallographic method to detect graphite.

The results of the investigation carried out can be summarized briefly as follows: At low degrees of deformation the magnetic intensity of steel does not change. On further increase in the degree of deformation the magnetic intensity of steel starts to rise. The rise continues to a certain limit, after which there is no change in magnetic intensity on further increase in the degree of deformation.

The general character of the relationship of I_s to the degree of deformation coincides with the results in [8], which gives this relationship for a steel of similar composition (C 0.70 per cent Mn 0.66 per cent). The only difference is that the authors of this work considered the increase in magnetic intensity at higher degrees of deformation ($\psi > 50$ per cent), whereas in our data an increase in I_s is seen already at deformation of 29 per cent.

Starting from this deformation, magnetic effect (a kink) is seen on the $I_s(T°)$ curves in the temperature region 260-270°. The effects of temperature on a plastically deformed specimen ($\psi = 29$ per cent) lead to a fall in the magnetic intensity and to disappearance of the effect in the temperature region 260-270°. With increasing heating temperature the character of the $I_s(T°)$ curves approaches that of the $I_s(T°)$ curve for an annealed specimen. On heating specimens with a degree of deformation > 62 per cent, graphitization is observed. After heating to 650° the $I_s(T°)$ curve for an annealed specimen.

VOL. 4 1957

Thus heating of deformed specimens (to $T^\circ < A_1$) with a degree of reduction of 29 per cent fully restores the original structure of the specimens prior to deformation. Heating of specimens with a high degree of reduction does not lead to restoration of the structure. Complete restoration is only obtained after annealing, i.e. on heating to $T^\circ > A_1$.

As a comparison for our results, it is interesting to give the results of the work of Wilson [9]. He studied the character of the changes occurring on the heating of deformed specimens of carbon steel containing 1.3 per cent carbon. The author notes that photographs of X-ray films of cementite made on plastically deformed specimens differ from those of annealed specimens by a considerable broadening of the lines, line shifts and a modification in the relative intensities. The change in the appearance of the X-ray photographs he attributes to the formation of plate-like crystals of cementite and residual strains in it. Heating of specimens leads to a gradual restoration of the cementite, as could be seen from a change in the X-ray photographs. Notable changes are seen on heating to 600°; on subsequently raising the heating temperature (to 750°) no changes occur. It is noted that cementite is not fully restored at temperatures of 600-750°, and the line intensity on the photographs is weaker than for an annealed specimen. The picture is fully restored only after annealing, i.e. after the deformed specimen has been converted into the austenite condition (heating to 900-950° with subsequent slow cooling).

We gave Wilson's results in order to show the similarity between descriptions of the process by means of X-ray photographs and $I_S(T^\circ)$ curves. It is interesting that the X-ray photographs and the $I_S(T^\circ)$ curve of cementite are only restored after annealing the deformed specimen. However we cannot agree with the author of [9] in his theory concerning the picture observed. As has already been pointed out he connects the reduced line intensity of the X-ray photographs of cementite after tempering (600°) and annealing (750°) with the plate-like form and strain in this phase, whereas in magnetic analysis the decrease in the slope of the $I_S(T^\circ)$ curve in the section 20-210° for deformed and tempered specimens compared with the slope of the curve in this section for an annealed specimen indicates that the amount of cementite decreases, i.e. that graphitization takes place.

Since $\Delta a' = I_f P_c / 100 = kP'_c$

where P'_c is the volume per cent of cementite in the deformed and tempered specimen, and

$$\Delta a = k P_c,$$

where P_c is the amount of cementite in the annealed specimen, then the difference

$$\Delta a - \Delta a' = k \Delta P_c$$

gives the amount of graphitized cementite. This process naturally causes the magnetic intensity to increase, as can be seen clearly from Fig. 5.

Jack [5,6], comparing the change in the picture of the X-ray structure on increase in the heating temperature of deformed specimens with change in picture of the X-ray structure in the interval of the third stage of tempering, notes the close similarity between these two changes. It is interesting to compare the character of the change in the $I_S(T^\circ)$ curves after tempering of hardened specimens with $I_S(T^\circ)$ curves after heating of deformed specimens. Fig. 6 contains curves of repeated heating after tempering of a hardened specimen. Comparison of the curves in Fig. 6 with those in Figs. 4 and 5 shows the identical character of the curves and the uniform character of the changes in them with increasing heating and tempering temperature. On comparing with the curves in Fig. 4 (ψ = 29 per cent), we see complete identity, on comparing with the curves in Fig. 5 (ψ = 62 per cent) there is some difference. The difference is that no graphitization is seen on heating a hardened specimen. Tempering at 650° brings steel into an equilibrium condition. On heating a deformed specimen graphitization processes occur. This result is further illustrated in Fig. 7.

Generalizing the experimental material obtained. we can draw the following conclusions. The character of the $I_S(T^\circ)$ curves after tempering of hardened specimens in a certain temperature interval is analogous to $I_S(T^\circ)$ curves for deformed specimens (ψ > 29 per cent). On the curves, in addition to the Curie point of cementite, a second kink is seen in one and the same temperature region 260-270°. It seems general also that the magnetic intensity of deformed and tempered specimens is greater than that of an annealed specimen (Fig.7). This relationship between the magnetic intensities is also maintained if this comparison is made at $T^\circ > 270^\circ$, i.e. at a temperature at which the mag-

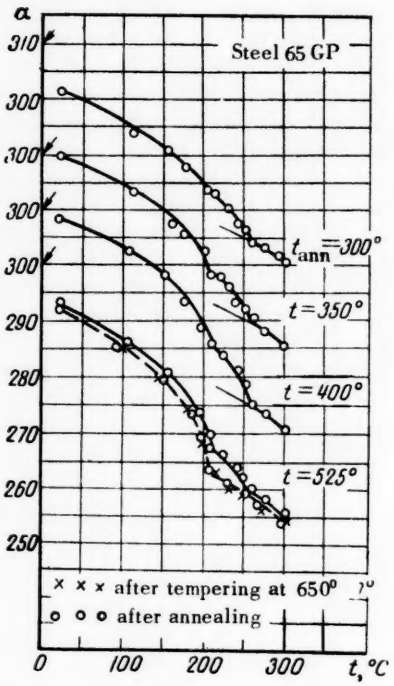

FIG. 6. Character of $I_s(T^0)$ curves in relation to annealing temperature. Heating time 60 min.

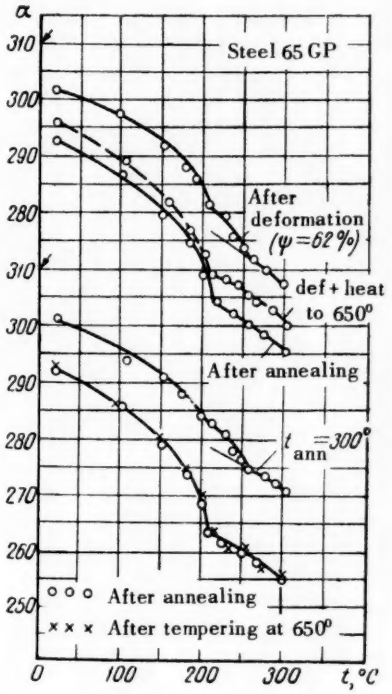

FIG. 7. Change in character of $I_s(T^0)$ curves on heating of specimen deformed and hardened on tempering. Heating time 60 min.

netic properties of the carbide phases do not affect the magnetic intensity of the specimen. With increasing heating temperature both in heat-hardened and deformed specimens the temperature of the kink in the region 260 - 270° does not shift. Damping of the magnetic effect with increase in heating temperature may be characterized as a decrease in the slope of the $I_s(T^0)$ curve in the section 210 - 265°.

On the basis of this, all the theories that we formulated to explain the nature of the magnetic effect on the curve in the region 260 - 270° for tempered specimens can be repeated in explaining this same effect for deformed specimens. From this it can be concluded that the nature of the magnetic effect in these two cases being considered is identical, and that the kink on the $I_s(T^0)$ curve for deformed specimens in the temperature range 260 - 270° also characterizes the Curie point of the carbide χFe_xC. The higher magnetic intensity of the deformed (tempered) specimen indicates greater carbon enrichment in part of the carbide phase.

Thus the phase composition of deformed specimens ($\psi > 29$ per cent) is similar to that of a specimen tempered after hardening at $T^0 > 300^0$ and may be characterized by three components:

$$Fe_xC + \chi Fe_xC + Fe(C).$$

Despite the identity of the phase compositions of tempered and deformed specimens. it should be noted that the condition of the system in these two cases is not the same. The difference is that on subsequent heating of a tempered specimen to higher temperatures the product of dissociation of the carbide χFe_xC is cementite alone, whereas in a deformed specimen (at any degree of deformation) dissociation of this carbide also leads to the formation of free carbon.

REFERENCES

1. S.V. Vonsovskii and Ya. S. Shur *Ferromagnetizm* (*Ferromagnetism*) GITTL, Moscow-Leningrad. 1948.
2. B.A. Apaev *Termicheskaya obrabotka metallov* (*Heat treatment of metals*), Collection of conference material, GONTI, Moscow, 1948.
3. J. Crengle and W. Sucksmith *J. Iron St. Inst.* 168, 2 (1951).
4. V.G. Permiakov *Zh. tekh. fiz.* 25, No. 5 (1955).

VOL. 4 1957

5. K.H. Jack *J. Iron St. Inst.* 169, 1 (1951).
6. K.H. Jack *J. Iron St. Inst.* 170, 3 (1952).
7. D. Wilson *Nature, Lond.* 169, 899 (1951).
8. J.H. Andrew and H. Lee *J. Iron St. Inst.* 165, 2 (1950).
9. D.V. Wilson *J. Iron St. Inst.* 165, 4 (1950).
10. E. Kaminskii, G. Kurdiumov and D. Leivikova *Zh. tekh. fiz.* 11, No. 12 (1941).
11. L.S. Moroz and Yu. S. Terminosov *Zh. tekh. fiz.* 19, No. 3 (1949).
12. A.P. Gulyaev and N.I. Burova *Metallovedenie i obrabotka metallov (Metallography and treatment of metals)*, No. 1 (1955).
13. G.V. Kurdyumov and L.I. Lysak *Zh. tekh. fiz.* 16, No. 11 (1946).
14. E.I. Kaminskii and G.I. Stelletskaya *Problemy metallovedeniya i fiziki metallov (Problems of metallography and physics of metals)*, Tsent. nauch. issled. inst. cher. metal. No. 1 (1949).
15. B.A. Apaev *Zh. tekh. fiz.* 23, No. 7 (1953).
16. B.A. Apaev *Fiz. metal. metalloved.* 1, No. 3 (1955).
17. E. Kaminskii and D. Katsnel'son *Zh. tekh. fiz.* 15, No. 3 (1945).
18. V.M. Yankovskii *Ismenenie svoish zakalennoi stali U8 pri otpuske (Change in properties of hardened U8 steel on annealing)*, Thesis.
19. K.P. Belov *Uprugie, teplovye i elektricheskie yavleniya v ferromagnitnykh metallakh (Elastic, heat and electrical phenomena in ferromagnetic metals)*, GITTL, Moscow-Leningrad, 1951.
20. Yu. A. Kliachko and M.M. Shapiro *Zav. lab.* 14, No. 5 (1948).

TEXTURE OF IRON SCALE x TEXTURE OF WUSTITE SCALE *

V.I. ARKHAROV and M.I. SIMONOVA

(Received 24 November 1956)

VOL. 4 1957

The texture of the scale formed on iron at low partial pressures, when the scale consists only of wustite, is of a crystallographic type which depends on the oxidation conditions. The common point of the sequence of textures is that the planes parallel to the external surface all belong to the same [001] crystallographic zone. The changes in textural type may be considered in terms of atoms in surface layers of crystals, regarded as "unscreened packets" of crystal lattices, on which oxygen is adsorbed. An explanation is presented of the observed changes in texture type, based mainly on lattice distortions in the surface layer-packets, endowing them with excess energy which increases with an increase of oxygen adsorption. This leads to a change in the relative surface energies of different packets.

High temperature oxidation of iron is a complicated case of diffusion-controlled reaction, complicated because iron, generally speaking, can form three oxides, so that iron scale consists of a series of layers, differeing in composition and crystalline character and in mechanism of formation. Each oxide is stable over certain ranges of temperature and partial pressure of oxygen.

Which oxide is formed is determined by the conditions in the reaction zone, which can differ from the average conditions in the bulk phase of the surrounding medium; hence the nature of the oxide formed is decided by the conditions for access of oxygen and iron to the reaction surface, i.e. by diffusion rates in the gas and solid phases, and by adsorption and desorption rates.

The scale formed on iron consists therefore of a variable number of layers, depending on these micro-conditions; the outside layer will be of an oxide which is in equilibrium with the surroundings, that iron oxide while is stable in composition and structure under the conditions prevailing in the surrounding atmosphere, while the internal layers are of lower oxides.

Among the characteristics by which one can elucidate the details of the mechanism of scaling of iron to this multilayer scale, texture is an important one. In several studies of texture we have been able to work out the details of iron oxidation [1,2] and of many other diffusion-controlled reactions [3-7]. We have studied the textures of scale formed under conditions in which higher oxides would be formed: ferric oxide in air and ferrosoferric (magnetite) in water vapour.

Under these conditions ferrous oxide (wustite) is formed as an internal layer in scale. To get a more complete insight into its mechanism, iron oxidation must be studied under conditions in which ferric and ferrosoferric oxides cannot be formed, but only ferrous oxide. Such conditions arise when iron is oxidized below a certain partial pressure of oxygen in the surrounding gas, and in particular in mixtures of water vapour and a fairly high proportion of hydrogen. This paper reports a study of the texture of the scale formed under such conditions.

EXPERIMENTAL

Cylinders of Armco iron, 110 and 30 mm long, 7 mm diameter and with recesses drilled in both ends for suspension, were used. Their surfaces were rubbed down well with emery paper and then washed with alcohol. They were oxidized in a vertical tubular furnace.

The oxidizing atmosphere with a low oxygen partial pressure was obtained by passing hydrogen at a constant rate through a water saturator in a heated thermostat and then through a tube provided with a heater and heat insulation connected to the lower end of the silica furnace tube, thus passing through the furnace upwards. The flow rate of hydrogen was metered and kept constant in all experiments. The volume of the saturator was so large that there were no significant changes in the conditions of water saturation of the hydrogen stream during the experiments. The composition (RH) of the gas mixture was controlled by thermostat temperature which was controlled within ± 0.2°C.

In preliminary experiments it was found that only wustite is formed on iron when the thermostat temperature is 80-90°C (This was proved by

* *Fiz. metal. metalloved.* 4, No. 2, 278-290, 1957 [Reprint Order No. POM 48].

using iron K radiation). In most experiments the thermostat was at 85°C, though in some it was at various other temperatures between 83 and 90°C. Since it was unnecessary to make accurate determination of the composition of the oxidizing atmosphere by the nature of the problem, the thermostat temperature was taken as a qualitative index of the oxidizing capacity of the atmosphere.

The following experimental procedure was used: the specimens were placed in the upper end of the silica tube which was also heated. Hydrogen was passed through the furnace tube while furnace and thermostat were being brought up to temperature, and then the furnace was switched over to water-saturated hydrogen which was passed through it for 1 hr. Then without interrupting the passage of gas the specimens were let down into the working space of the tube and oxidized for a certain period, at the end of which they were lifted again into the upper part of the tube and cooled there for 10 min. The passage of gas through the tube has stopped and the specimens removed from the furnace.

TABLE 1.

Oxidation temperature (°C)	Thermostat temperature (°C)	Oxidation time (hr)
800	85	1,4,7
900	85	2,4
1000	83	2,4
	85	2,4,7
	87	2
1150	85	1,2,4,
	87	2,4,
	90	2,4

The upper part of the silica tube with the specimens in it was kept throughout an experiment at 130-140°C to prevent condensation on the specimens of the tube walls; at this temperature the specimens did not oxidize appreciably. The furnace temperature was measured with a platinum-platinum/rhodium couple outside the tube at the level of the middle of the specimens inside it. Furnace temperature varied by ± 10°C. Table 1 shows the oxidation conditions.

Characteristic textures calculated from the X-ray spectra were obtained from the outside layer of scale by the method used previously [8]. One spectrum was obtained from the middle of each 30 mm long specimen, and from the 110 mm long specimens usually two 10 mm from each end and from some specimens spectra were obtained at 10-15 mm intervals along their length.

RESULTS

The texturograms revealed that the wustite forming the scale has a texture. The perfection of the texture is usually high on specimens oxidized at 1000°C and above; at 900°C it is less developed and there are only traces of it at 800°C. The crystallographic type of texture varied with the oxidation conditions, yielding different X-ray textural patterns. These patterns can be evaluated numerically on the assumption that to each of them there corresponds one type of texture, that is one particular crystallographic plane of wustite is parallel to the external surface in each case studied. In the various specimens textures were found whose (crystallographic) type can be characterized by the sequence: (100), (410), (210), (430), (110). The collection of lattice planes has a certain regularity; all of them belong to the same crystallographic zone with an [001] axis and from angles with the [100] directions in the indicated sequence increasing from 0° to 45° (Fig. 1).

One type of texture or another was obtained by small variations of the oxidation conditions and at first it seemed that complete experimental repeatability was absent. However, when a large number of experiments had been carried out, we found that, for the same oxidation temperature, as the atmosphere increased in oxidizing power

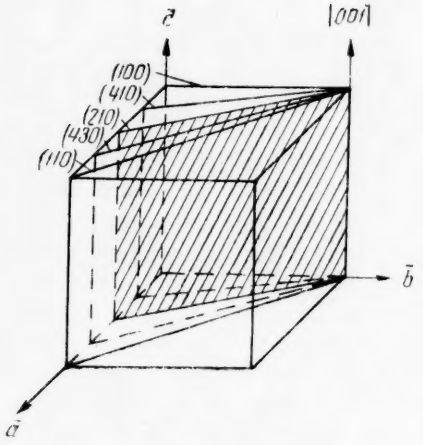

FIG. 1. Position of planes determining texture of ferrous oxide formed under different conditions.

the texture type tended towards that at the right hand end of the above sequence and vice versa.*

This correlation appeared most clearly from the analysis of the texture at various locations along the 110 mm specimens. Since the gas flowed upwards during oxidation, the lower ends of the specimens were subjected to the action of a somewhat more oxidizing mixture than the upper ends since by the time the gas had reached them it was somewhat impoverished in oxygen, and the lower ends were therefore always more strongly oxidized than the upper ends. On the same specimen it was always found that the texture of the scale on the bottom of these long specimens was always indexed by a type number to the right, and that at the top by one to the left, in the above sequence. Of course only in rare cases did we get specimens whose bottom end scale was of the (110) type, and whose top end scale was (100). Usually the textures were intermediate. When the bottom end scale was of the (210) type, the top end scale had a (100 or (410) texture, and in extreme cases (210), like the bottom scale. When the bottom scale was of (410) type, the top scale was (100) or (410). But when a (210) or (410) texture scale was formed on the top end, the bottom end scale had the same texture or (110). In no case was an inverse distribution of textures along a specimen found.

* That is the indices of the crystal planes, parallel to the external surface of the specimen in the crystallites of the texturized layer.

The same correlation (though less clear) was found when the saturator temperature was changed: when it was raised (oxidation temperature unchanged) the texture changed toward the right of the sequence; in some experiments when the saturator temperature was only slightly increased, the texture remained of the same type, but it never moved to the left.

Evidently the change is due to a change in the oxidizing capacity of the gas and this is connected with the experimental conditions affecting the access of oxygen to the specimens. In the experiments with change of saturator temperature it is more difficult to control these conditions than in the experiments with long specimens, because this temperature can only be varied by 6-8°C; if it is raised too much there is a danger of forming ferrosoferric oxide, which would distort the whole result, and if the saturator temperature is too low, the specimens oxidize wery slowly.

The variation of texture type with oxidation temperature is particularly interesting. At 900°C the predominant texture obtained is (110). Between 1000 and 1150°C a different texture predominated, and the already described correlation between texture and position on the specimen was also observed. At 1150°C the predominant texture was (410) or (100).

Figs. 2-6 show the theoretical texturograms for ferrous oxide for the various textures in the sequence given. Fig. 7 shows the theoretical texturogram for the (111) [ES] texture discussed below ([ES] = external surface). Figs. 2a-7a show the texturograms for wustite scale obtained under various oxidation conditions, the types of the textures studied being fairly close to the types in the corresponding diagrams Figs 2-7. This correspondence is confirmed by Tables 2-7.** Small divergences between the calculated and measured values of the angles ξ and ξ' are due mainly to errors in their measurement and, particularly, of the evaluation of the texture scattering angle α.

** In all tables [1] means the maximum lies outside the spectrum; [2] that measurement of ξ is impossible, because the large-angle end of the maximum is outside the spectrum; [3] that ξ' cannot be measured because of overlapping of the inner edges of the symmetrically placed maxima; and [4] that because of the overlapping of the edges of adjacent maxima only ξ' can be measured for one of them and ξ for the other.

A detailed examination of the divergence between the calculated and measured values of ξ' and ξ shows that in addition to textural scattering (a) another factor is at work: it would be more correct to describe the texture type by a positioning of the planes parallel to the external surface very close to that given in the sequence, but with more complicated indices and forming very small angles with the corresponding planes of the sequence. This should slightly lengthen the textural maxima assumed in Tables 2-7 as diatropic (increase of ξ), but affect other maxima less.

This fine detail does not change the basic crystallochemical character of the external surfaces of the crystals, forming the scale.

DISCUSSION OF THE RESULTS

Growth texture of course arises through anisotropy of the growth rate: crystals whose direction of maximum growth rate is at right angles to the external surface squeeze out their less favourably oriented neighbours during scale growth. This growth rate anisotropy is determined by the anisotropy of surface energy of crystals.

When crystals grow in a liquid of gas of the same substance as themselves their surface energy has a certain value which is constant for each face. If crystal growth is complicated by adsorption at some definite stage of growth: the surface energy of each face will vary with the degree of adsorption since adsorbed atoms change the composition and distort the crystal lattice of the surface layer.

This happens in the growth of wustite crystals: they grow through a diffusion-controlled reaction in one stage of which a certain quantity of oxygen atoms is adsorbed from the gas phase onto the growing surface which is a particular lattice plane of wustite. The surface concentration of these adsorbed atoms depends on the rate of supply of oxygen-containing molecules from the gas to the wustite surface and the rate of the reaction which incorporates these adsorbed atoms into the lattice. The supply rate depends mainly on the gas composition, and the reaction rate mainly on temperature. Hence, as a function of these two factors, the crystal faces of wustite on the external surface of the scale will be somewhat distorted.*

Correspondingly the surface energy of the various crystal faces of wustite will also change. Faces having a high density of lattice ions with a relatively low surface energy at low adsorption density will be strongly distorted at higher densities of adsorbed atoms, their surface energy will increase and may exceed the surface energy of another type of face, with a lower lattice density (and higher intrisic surface energy) and which is less distorted by adsorption for the same density of adsorbed atoms) than the first face.

Hence, as the crystal layer subject to adsorption grows, not only the absolute, but also the relative surface energies of the faces can change with the degree of adsorption. This means that the growth texture type can change with the external conditions of the diffusion-controlled reaction. These general consideration apply to the present study.

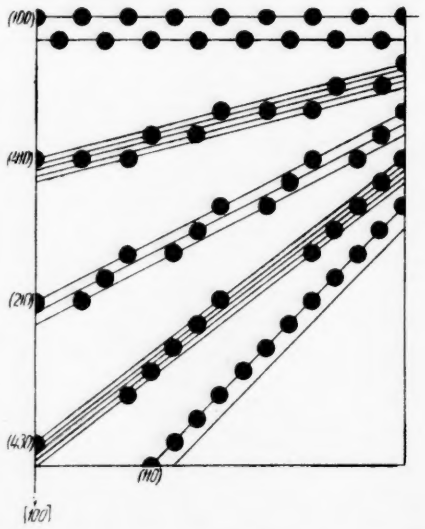

FIG. 8. Section on the (001) plane of "unscreened" packets, formed by atomic planes of the texture sequence given. In the packet for the (110) system atoms of the second plane are outside the plane of the paper. The diagram only shows the position of iron atoms.

* The thermodynamic concept of surface energy lowered by adsorption requires examination in a study of the atomistics of a surface layer. We must differentiate between the outer lattice layer (packet of crystal planes, containing uncreened atoms, see below) and the adorbed layer. Adsorption of atoms onto the extreme lattice layer displaces atoms in the latter, i.e. distorts the lattice, because of the strong interaction between them. This distortion inhibits lowering of the energy in the surface layer as a whole in later adsorption.

To explain the observed differences in texture of wustite scale it seems necessary to introduce a refinement into the picture of the phenomenon. Instead of basing our thinking on a purely geometrical conception of the faces making up the external surface of a crystal, we should consider the real physical form of the surface layer. Let us suppose that the effect of adsorbed atoms on the lattice is screened by the first atoms of the lattice, and consider the surface layer to be a region of such (*hkl*) planes in which the atoms do not mutually screen one another from the external surface. That is, all the atoms in such a packet are projected onto the general plane parallel to (*hkl*) without coincidence. In Fig. 8 are shown such packets for systems of planes comprising the sequence already given. Instead of lattice densities calculated for a two-dimensional image of a lattice, we calculate the density of filling by atoms of the unscreened packets, and characterize it by the area S in A^2 [effectively] occupied by one iron in the projection of the packet (*hkl*); corresponding values for the faces in which we are interested are

(*hkl*)	(100)	(410)	(210)	(430)	(110)
S	9,26	9,56	10,35	11,58	13,10

and increase from left to right, the order of (*hkl*) values being the same as in the sequence already quoted.

We can now put forward the following mechanism of change of texture type in our experiments.

At any constant temperature, when the oxygen partial pressure, and therefore the density of adsorbed atoms, is low the surface layer of crystals is only slightly distorted, and the face with the greatest "lattice packet density" (which in this case is the same as the ordinary lattice density) will have the least surface energy, that is the (100) face. As adsorption density increases (through increase of the concentration of oxygenated molecules in the surrounding gas) the (100) face begins to distort, and its "surface energy" becomes greater than that of the (410) face, whose surface energy changes more rapidly with change in adsorption, than that of (100). Under these conditions the external layer of wustite acquires the (100) [*ES*] texture. If the oxygen/partial pressure becomes higher still the plane which has the relatively greatest surface energy becomes (410) and it will determine the texture formed. Further increase of the oxygen partial pressure pushes the texture through the rest of the sequence, i.e. to (210), (430) and finally (110) [*ES*].

This is supported by the observed oxidation temperature dependence of the wustite scale texture type. Since temperature increase speeds up diffusion and the transfer of oxygen atoms from an adsorbed layer into the underlying lattice, it will decrease adsorption layer densities and therefore the distortion of crystal faces on the outside surface of scale. Under these conditions the face close to the left-hand end of the sequence given will have a relative minimum of surface energy, and, as we have seen, as the temperature rises the texture of wustite moves towards this end.

ADDITIONAL INVESTIGATIONS OF THE VARIATION OF WUSTITE SCALE TEXTURE WITH THE GAS COMPOSITION

The change of texture of wustite scale with slight changes of oxidation conditions suggests that the faces which figure in the sequence differ in comparatively little in surface energy when oxygen is adsorbed on them. To test this, iron specimens were oxidized under condition favourable for the formation of a certain texture and then under conditions favouring the formation of a different type; controls were put into the furnace during the second part of these experiments, to find out what texture was formed on fresh iron under the conditions.

In the first and second experiments the specimens were oxidized in a mixture of water and hydrogen with the saturator at 85°C. In the first experiment the specimen was initially oxidized at 1150°C for two hours, producing a (410) wustite texture at its lower and a (100) texture at its upper end; afterwards oxidation was continued at 1000°C (5 min, 1.5 hr) at which, in the main experiments, a (110) texture was formed, as was also confirmed by observations on the control put into the furnace in this second part of the experiment. However, the change in oxidation conditions did not produce

VOL. 4 1957

any change in the scale on the experimental specimen: at the end it still had the initially developed texture [(410) below and (100) above].

In the second experiment the experimental was first oxidized under conditions (100°C, 7 hr) producing on it a (110) texture, and it was then oxidized for 1.5 hours at 1150°C which produced a (100) texture on the control, but did not change the texture on the experimental specimen.

Next a specimen was oxidized for 5 hr at 1150°C in pure water vapour which produced on it a double-layer scale whose external layer was Fe_3O_4 with a (100) texture. Oxidation was then continued in a mixture of hydrogen and water vapour at 1000°C for 12.5 hr, which produced a (110) wustite texture scale on the control, but on the experimental specimen a (100) texture wustite scale, evidently under the influence of the texture in the ferrosoferric oxide which was converted to ferrous oxide when water vapour was replaced by hydrogen + water vapour.

This orienting effect was still more clearly in evidence in a fourth experiment, in which the experimental specimen was initially oxidized for 5 hours at 1150°C in air with formation of a scale whose external layer was of a ferric oxide with the usual (111) [ES] texture; oxidation was continued in a mixture of hydrogen and water vapour at 1000°C for 2 hours, a treatment which produced on the control the expected (110) texture wustite, but on the experimental specimen a (111) texture wustite (Fig. 7 and 7a, Table 7)

Evidently textures in wustite are stable in face of changes of oxidation conditions. This can be explained by the hypothesis that the various faces, more or less distorted by oxygen adsorption, differ little in surface energy.

In the presence of a pre-formed texture in a wustite layer already formed, wustite could grow on these crystallites although their orientation is not the most suitable energetically. The gain in total surface energy of the scale to be gained by change of texture would be less than the energy required to produce new three-dimensional nuclei, not connected with the substrate and mutually disoriented at later stages of growth preferential development of pre-existing crystallites having the most favourable orientation would determine the texture.

SUMMARY

1. When iron is oxidized under conditions which produce a purely wustite scale, this scale has a texture.

2. The type of texture depends on the oxidizing power of the gas and temperature. At a fixed temperature the texture changes in the sequence (100), (410), (210), (430), (110) when the oxidizing power increases or the temperature decreases from 1150 to 900°C.

3. The observed correlation between texture and oxidation conditions can be interpreted by considerations about oxygen adsorption. Increase of the amount of oxygen in the adsorption layer by an increase of the rate of supply from the surrounding gas and by a reduction of the rate of incorporation into the crystal lattice of the scale shifts the texture from left to right in the above sequence. The increased rate of supply is due mainly to an increase in oxidizing power of the gas (increased oxygen content of gas) and the reduction of rate of incorporation of oxygen into the scale. The effect of increased oxygen supply is greater than the decrease in the rate caused by decreased diffusion in the solid phase at lower temperature.

4. To interpret the observed changes of wustite texture with change of surface energy of the corresponding crystal faces, consideration should be given not to the usual lattice density but to the density of filling of a surface layer by atoms defined as a packet of planes parallel to the external surface of the crystal in which the atoms are not screened from one another. It is assumed that adsorption of oxygen more strongly distorts packets having a more regular atomic arrangement (and lowers their surface energy less) than packets with a more complicated configuration. This changes the relation between the surface energies of the various faces and therefore texture. The interpretation is deduced from the observed correlation between texture and oxidizing capacity of the gas.

5. It has been established that generally speaking the differences in relative surface energy of the various faces brought about by oxygen adsorption are small. When oxidizing conditions are changes wustite continues to grow, or is formed, with the pre-existing texture apparently because the gain in energy by a texture change is small compared with the energy required to create new three-dimensional nuclei, needed for a change of texture.

VOL. 4 1957

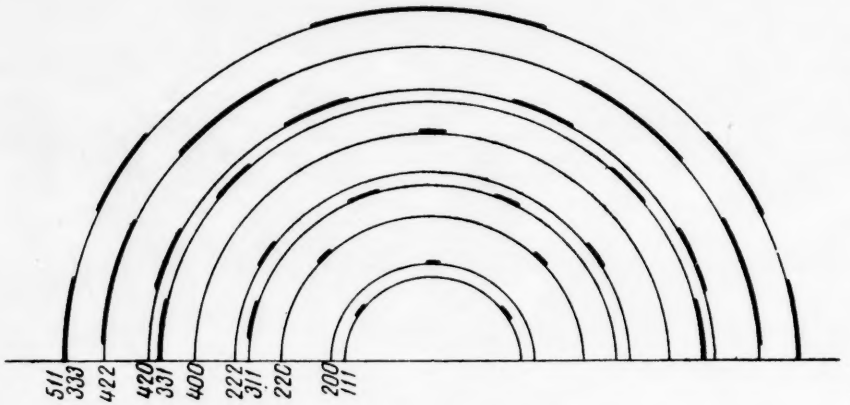

FIG. 2. Theoretical texturgram for ferrous oxide with (100) plane parallel to external surface of specimen.

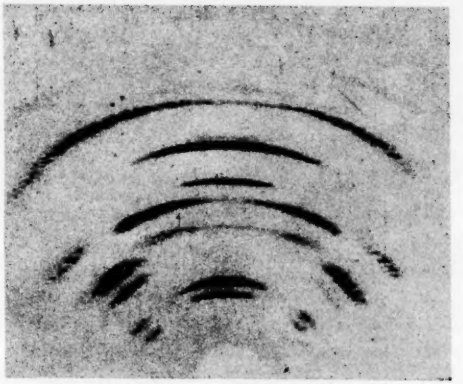

FIG. 2a. Texturogram of external layer of FeO. Oxidation temperature 1150°C, saturator temperature 87°C, time 4 hr.

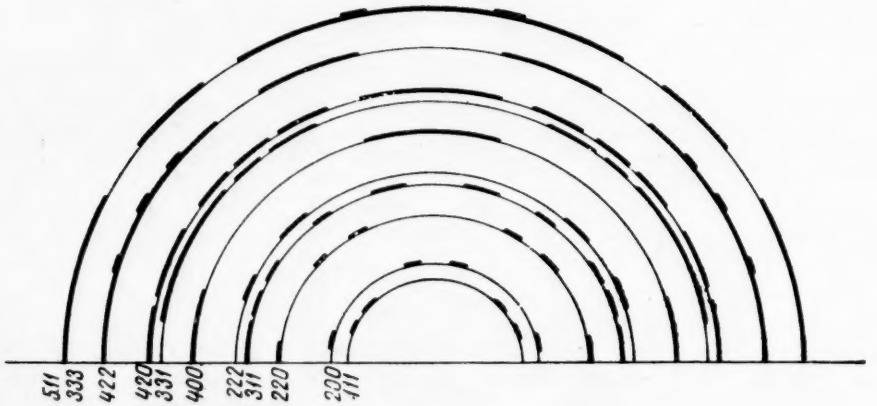

FIG. 3. Theoretical texturogram for FeO with (410) planes parallel to external surface of specimen.

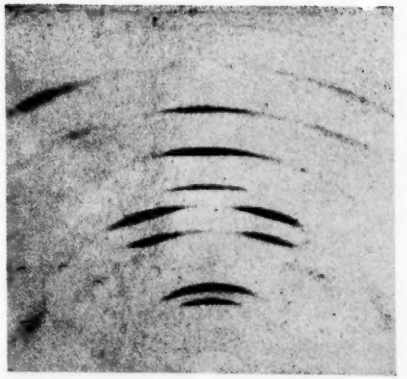

FIG. 3a. Texturogram of external layer of FeO produced by 4 hr oxidation at 1150°C, with saturator at 87°C.

FIG. 4a. Texturogram of external layer of FeO produced by 4 hr oxidation at 1000°C,-with saturator at 85°C.

FIG. 5a. Texturogram of lower end of external layer of FeO produced by 4 hr oxidation at 1000°C with saturator at 85°C.

FIG. 4. Theoretical texturogram of FeO with (210) planes parallel to specimens external surface.

FIG. 5. Theoretical texturogram of FeO with (430) planes parallel to external surface.

VOL
4
195

VOL. 4 1957

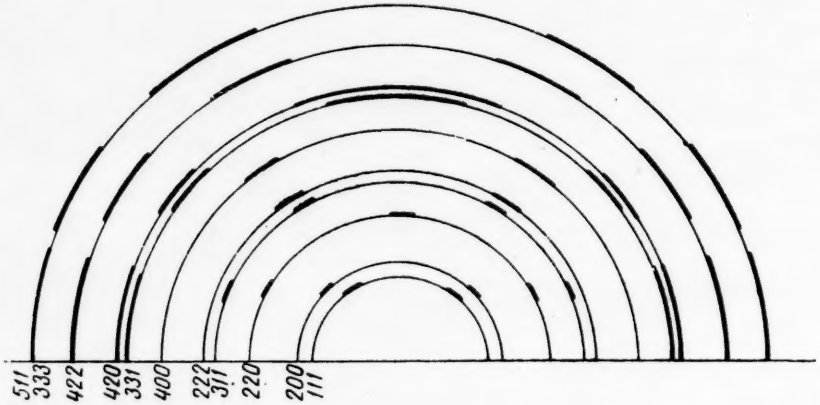

FIG. 6. Theoretical texturogram of FeO with (110) planes parallel to specimens external surface.

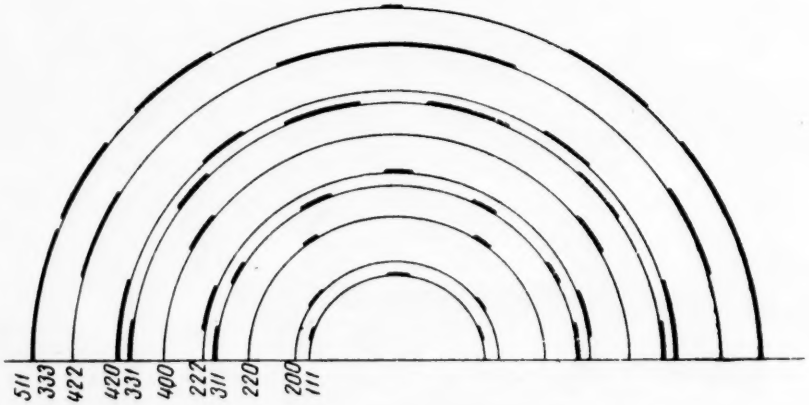

FIG. 7. Theoretical texturogram of FeO with (111) planes parallel to the specimens external surface.

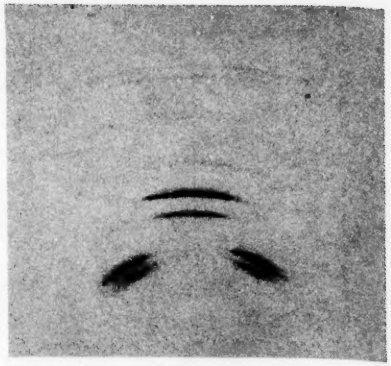

FIG. 6a. Texturogram of lower end of external layer of FeO produced by 2 hr oxidation at 1000°C with saturator at 85°C.

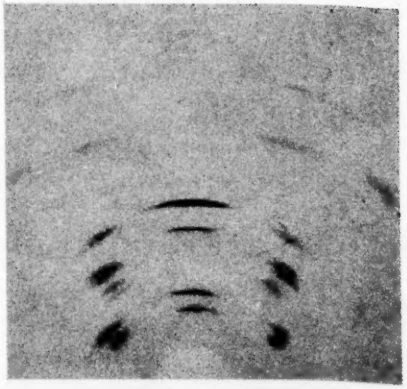

FIG. 7a. Texturogram of external layer of FeO, produced by reducing a-Fe_2O_3 for 2 hr at 1000°C with the saturator at 85°C.

TABLE 2. Calculation of X-ray spectrum for wustite (100) [ES]

Calculated					Measured					Notes
ϑ	*hkl*	ρ	ξ'	ξ	ϑ	ξ'	ξ	ρ	α	
8°14′	111	54°45′	54°20′	55°30′	8°26′	44°	61°	52°	8°	
9°30′	200	0°	0°	0°	9°31′	0°	20°	—	19°	
13°30′	220	45°	43°21′	46°39′	13°24′	34°	57°	45°	9°	
15°56′	311	25°15′	19°51′	26°20′	15°58′	7°	34°	25°	7°	
	113	72°27′	71°44′	82°30′		—	—	—	—	[1]
16°38′	222	54°45′	52°27′	58°29′	16°28′	41°	67°	53°	9°	
19°18′	400	0°	0°	0°	19°28′	0°	26°	—	22°	
21°07′	331	46°31′	42°29′	51°03′	20°58′	36°	65°	49°	7°	
	133	77°45′	76°51′	90°		—	—	—	—	[1]
21°40′	420	26°33′	15°48′	28°47′	21°48	0°	37°	29°	8°	
	240	63°26′	61°14′	74°12′		—	—	—	—	[1]
23°51′	422	35°17′	26°47′	39°10′	23°55′	15°	—	37°	—	[2]
	224	65°54′	63°29′	80°30′		—	—	—	—	[1]
25°24′	511	15°48′	0°	17°33′	25°32′	0°	25°	13°	—	[3]
	333	54°44′	50°16′	64°42′		—	—	—	—	[1]
	115	78°54′	77°42	90°		—	—	—	—	[1]
									$\alpha_m = 8°$	

TABLE 3. Calculation of X-ray spectrum for wustite (410) [ES]

Calculated					Experimental					Notes
ϑ	*hkl*	ρ	ξ'	ξ	ϑ	ξ'	ξ	ρ	α	
8°14′	111	45°34′	44°58′	46°11′	8°07′	40°	50°	45°	4°	
	$\bar{1}11$	65°09′	64°52′	66°29′		—	—	—	—	*
9°30′	200	14°00′	10°12′	14°12′	9°25′	0°	19°	16°	—	[3]
	020	75°58′	74°45′	79°42′		—	—	—	—	**
13°30′	220	30°57′	28°06′	31°56′	13°37′	30°	—	37°	—	[4]
	202	46°40′	45°06′	48°20′		—	53°	47°	—	[4]
	022	87°07′	80°51′	90°		—	—	—	—	[1]
15°56′	311	18°06′	8°42′	18°51′	15°55′	4°	31°	23°	7°	
	$3\bar{1}1$	36°26′	33°13′	38°09′		—	—	—	—	***
	131	59°12′	57°50′	63°18′		—	—	—	—	***
	113	68°33′	68°13′	75°24′		62°	77°	66°	4°	
	$1\bar{1}3$	78°20′	77°49′	90°		—	—	—	—	[1]
16°38′	222	45°34′	43°03′	48°12′	—	—	—	—	—	
	$2\bar{2}2$	65°09′	63°59′	71°18′	—	—	—	—	—	
19°18′	400	14°00′	0°	14°52′	19°18′	0°	19°	13°	—	[3]
	040	75°58′	74°09′	90°		—	—	—	—	[1]
21°07′	331	33°25′	26°33′	36°10′	21°13′	20°	—	34°	—	
	313	43°40′	39°11′	47°44′		—	—	—	—	[4]
	$3\bar{1}3$	52°16′	49°00′	57°58′		—	—	—	—	[2]
	$33\bar{1}$	59°57′	57°33′	69°03′		—	—	—	—	
	133	67°05′	62°19′	80°42′		—	—	—	—	[1]
21°40′	420	12°35′	0°	13°32′	21°40′	0°	—	—	—	
	402	29°48′	21°16′	32°16′		—	40°	32°	—	[4], [3]
	$4\bar{2}0$	40°36′	35°22′	44°20′	—	—	—	—	—	[4],
	240	49°16′	45°32′	54°28′	—	—	—	—	—	[3]****
	204	64°17′	62°13′	75°24′		—	—	—	—	[1]
	042	78°28′	77°32′	90°		—	—	—	—	[1]

* Isolated diffraction spots at 60-70° angles

** Isolated diffraction spots at 70-80° angles

*** Isolated diffraction spots at 30-40 and 50-60° angles

**** Intensity of maxima very small, ξ' and ξ cannot be measured.

TABLE 3 (contd.)

Calculated					Measured					Notes
ϑ	*hkl*	ρ	Ξ'	ξ	ϑ	Ξ'	ξ	ρ	α	
23°51′	422	27°00′	13°04′	29°39′		11°	—	30°	—	[4], [2]
	$42\bar{2}$	46°07′	40°43	52°00′	23°55′	—	—	—	—	
	242	53°33′	49°29′	61°35′		—	—	—	—	[1]
	224	60°20′	56°54′	71°44′		—	—	—	—	
	$22\bar{4}$	72°43′	71°03′	90°		—	—	—	—	
25°24′	511	11°24′	0°	12°38′		0°	—	—	—	[4], [2]
	$5\bar{1}1$	27°30′	10°54′	30°45′	25°19′	—	—	—	—	
	333	45°34′	39°11′	50°36′		—	—	—	—	[1]
	151	65°10′	62°17′	90°		—	—	—	—	
									$\alpha_m = 5°$	

TABLE 4. Calculation of X-ray spectrum for wustite (210) [ES]

Calculated					Measured					Notes
θ	hkl	ρ	ξ'	ξ	θ	ξ'	ξ	ρ	α	
8°14′	111	39°15′	38°30′	39°45′	—	—	—	—	—	
	111	75°02′	74°54′	77°30′	—	—	—	—	—	
9°30′	200	26°37′	25°00′	26°00′	9°22′	14°	40°	29°	9°	
	020	63°26′	63°02′	65°03′		54°	67°	59°	7°	
13°30′	220	18°30′	12°42′	19°03′	13°23′	0°	26°	20°	—	[3]
	022	71°34′	71°01′	77°21′		—	—	—	—	[1]
15°56′	311	19°18′	11°00′	20°06′	15°53′	0°	24°	22°	7°	
	131	47°37′	45°29′	50°11′		36°	59°	47°	9°	
	113	66°10′	65°11′	72°01′		—	—	—	—	
	131	81°15′	80°30′	90°		—	—	—	—	[1]
16°38′	222	39°15′	36°04′	41°20′	16°39′	36°	59°	43°	12°	
	222	75°02′	74°22′	90°		—	—	—	—	[1]
19°18′	400	26°35′	18°37′	28°18′	19°13′	0°	44°	33°	8°	
	040	63°26′	61°43′	71°24′		—	—	—	—	[1]
21°07′	331	22°26′	7°54′	22°58′	21°04′	0°	24°	20°	—	[4], [2]
	313	44°06′	39°41′	48°15′		—	—	—	—	
	133	59°55′	57°30′	68°00′		—	—	—	—	[1]
	331	72°04′	70°40′	90°		—	—	—	—	
21°40′	420	0°	0°	0°	21°41′	0°	—	—	—	[4]
	240	36°52′	30°36′	40°13′		—	44°	31°	—	
	420	53°09′	49°49′	59°25′		—	—	—	—	[1]
23°51′	422	24°06′	3°12′	26°31′	23°51′	0°	—	—	—	*
	242	43°05′	36°59′	48°21′		—	—	—	—	
	224	56°46′	52°12′	66°11′		—	—	—	—	
									$\alpha_m = 9°$	

* Intensity distributed over the whole ring: ξ' and ξ of individual maxima cannot be measured.

TABLE 5. Calculation of X-ray spectrum for wustite (430) [ES]

Calculated					Measured					Notes
ϑ	*hkl*	ρ	ξ'	ξ	ϑ	ξ'	ξ	ρ	α	
8°14′	111	36°07′	35°16′	36°34′	—	—	—	—	—	
	$1\bar{1}1$	83°22′	83°18′	90°	—	—	—	—	—	
9°30′	200	36°52′	35°48′	37°42′	9°28′	19°	—	32°	—	[4]
	020	53°08′	52°31′	54°12′		—	66°	53°	—	
13°30′	220	8°06′	0°	8°20′	13°28′	0°	23°	11°	—	[3]
	202	55°06′	53°58′	57°31′		40°	—	58°	—	[4], [2]
	022	64′54′	63°08′	68°38′		—	—	—	—	
	$2\bar{2}0$	82°52′	81°38′	90°		—	—	—	—	[1]
15°56′	311	25°15′	19°50′	26°20′	15°53′	0°	—	—	—	
	131	38°23′	35°24′	40°13′		—	—	—	—	[4]
	$3\bar{1}1$	57°08′	55°39′	60°48′		—	—	—	—	[3]
	$\bar{1}13$	65°02′	63°58′	70°32′		—	—	—	—	[2]
	131	72°27′	71°44′	82°36′		—	—	—	—	[1]
16°38′	222	36°07′	32°42′	37°58′	16°39′	20°	51°	37°	11°	
	$2\bar{2}2$	83°22′	83°06′	90°		—	—	—	—	[1]
19°18′	400	36°52′	31°58′	37°22′	19°14′	—	—	—	—	[4], [3]
	040	53°08′	50°32′	57°58′		—	—	—	—	
21°07′	331	15°38′	0°	16°41′	21°04′	0°	27°	14°	—	[2], [3]
	313	52°10′	48°53′	57°49′		—	—	—	—	
	133	57°53′	55°16′	65°11′		—	—	—	—	
	$3\bar{1}3$	68°24′	66°46′	85°18′		—	—	—	—	[1]
	$\bar{1}33$	79°13′	77°20′	90°		—	—	—	—	
21°40′	420	10°18′	0°	11°06′	21°39′	0°	—	—	—	[3]
	240	26°35′	15°48′	28°48′		—	—	—	—	[4]
	402	44°19′	39°40′	48°44′		—	—	—	—	[2]
	$4\bar{2}0$	63°26′	61°04′	71°14′		—	—	—	—	[1]
	204	69°02′	67°25′	90°		—	—	—	—	
23°51′	422	26°06′	10°57′	28°44′	23°54′	0°	—	—	—	[4], [3]
	242	35°17′	26°48′	39°10′		—	—	—	—	[2]
	$4\bar{2}2$	65°54′	63°30′	86°22′		—	—	—	—	[1]
25°24′	511	30°07′	16°46′	33°45′	25°32′	0°	—	—	—	[4]
	333	37°50′	29°01′	42°46′		—	—	—	—	[3]
	151	44°23′	37°42′	50°45′		—	—	—	—	[2]
	$5\bar{1}1$	50°16′	44°57′	58°23′		—	—	—	—	[1]
	$1\bar{5}1$	70°12′	67°59′	90°		—	—	—	—	

TABLE 6. Calculation of X-ray spectrum for wustite (110) [ES]

Calculated					Measured					Notes
ϑ	*hkl*	ρ	ξ'	ξ	ϑ	ξ'	ξ	ρ	α	
8°14′	111	35°17′	34°23′	35°42′	8°07′	28°	47°	38°	9°	
9°30′	200	45°00′	44°12′	45°48′	9°22′	26°	57°	42°	14°	
13°30′	220	0°	0°	0°	13°08′	0°	22°	—	—	[3]
	202	60°00′	59°03′	62°57′		—	—	—	—	*
15°56′	311	31°29′	27°39′	33°02′	15°40′	0°	50°	35°	—	[3]
	113	64°46′	63°41′	70°12′		—	—	—	—	*
16°38′	222	35°17′	31°34′	37°02′	—	—	—	—	—	*
19°18′	400	45°00′	41°29′	48°37′	19°00′	—	—	—	—	**
21°07′	331	13°18′	0°	14°16′	20°55′	0°	22°	10°	—	[3]

* ξ, ξ' cannot be measured because the maxima are of very low intensity

** β (420) in middle of spectrum. The line has an intensity distributed over the whole ring, so ξ' and ξ cannot be measured.

TABLE 6 (contd.)

Calculated					Measured					Notes
ϑ	*hkl*	ρ	ξ′	ξ	ϑ	ξ′	ξ	ρ	α	
	313	49°32′	45°57′	54°37′		—	—	—	—	[1]
	3$\bar{1}$3	71°05′	69°42′	90°		—	—	—	—	
21°40′	420	18°27′	0°	19°54′	21°31′	0°	36°	22°	—	[3]
	402	50°46′	47°08′	56°27′		—	—	—	—	[1]
	204	71°34′	70°07′	90°		—	—	—	—	
23°51′	422	30°00′	18°46′	33°08′	23°45′	—	—	—	—	[3], [4]
	224	54°46′	49°18′	63°17′		—	—	—	—	
	4$\bar{2}$2	73°13′	71°36′	90°		—	—	—	—	[1]
25°24′	511	35°20′	25°18′	39°48′	25°19′	10°	—	38°	—	[2]
	15$\bar{1}$	56°58′	52°53′	68°18′		—	—	—	—	[1]
	115	74°12′	72°27′	90°		—	—	—	—	
									$\alpha_m = 12°$	

TABLE 7. Calculation of X-ray spectrum for wustite (111) [ES]

Calculated					Measured					Notes
ϑ	*hkl*	ρ	ξ′	ξ	ϑ	ξ′	ξ	ρ	α	
8°14′	111	0°	0°	0°	8°07′	0°	16°	—	8°	
	1$\bar{1}$1	70°29′	70°48′	72°11′		61°	77°	68°	6°	
9°30′	200	54°41′	54°08′	55°54′	9°28′	47°	62°	54°	6°	
13°30′	220	35°13′	32°52′	36°22′	13°23′	23°	45°	35°	8°	
15°56′	311	29°25′	25°11′	30°40′	15°41′	22°	41°	32°	5°	
	3$\bar{1}$1	59°36′	57°11′	62°37′		54°	65°	58°	4°	
	3$\bar{1}\bar{1}$	79°59′	79°34′	90°		—	—	—	—	[1]
16°38′	222	0°	0°	0°	16°35′	0°	10°	0°	10°	
	22$\bar{2}$	70°29′	69°24′	79°44′		—	—	—	—	[1]
19°18′	400	54°41′	52°16′	59°46′	19°10′	50°	67°	56°	4°	
21°07′	331	22°03′	8°06′	23°39′	21°00′	0°	32°	24°	—	[4]
	33$\bar{1}$	48°19′	44°46′	22°57′		39°	—	49°	—	
	331	82°21′	81°50′	90°		—	—	—	—	[1]
21°40′	420	39°17′	33°42′	42°50′	21°40′	31°	51°	41°	5°	
	4$\bar{2}$0	73°03′	73°55′	90°		—	—	—	—	[1]
23°51′	422	19′17′	0°	21°32′	23°48′	0°	30°	21°	6°	[3]
	42$\bar{2}$	61°50′	58°56′	74°08′		—	—	—	—	[1]
25°24′	333	0°	0°	0°	25°19′	0°	10°	—	10°	[3]
	511	38°57′	30°32′	44°06′		—	—	—	—	[1]
	51$\bar{1}$	56°15′	52°02′	67°01′		—	—	—	—	[1]
	511	70°32′	68°21′	90°		—	—	—	—	
									$\alpha_m = 7°$	

VOL. 4 1957

REFERENCES

1. V.I. Arkharov and B.S. Borisov *Fiz. metal. metalloved.* 3, No. 3 (1956).
2. V.I. Arkharov Okislenie metallov pri vysokikh temperaturakh *(Metal Oxidation at high temperatures)*, Metallurgizdat, 1945.
3. V.I. Arkharov *Trud. Inst. fiz. Metal. Ural. Fil. Akad. Nauk SSSR*, No. 12 94, 1949.
4. V.I. Arkharov and S. Mardeshev *Fiz. metal. metalloved.* 3, No. 3 (1956).
5. V.I. Arkharov and S. Mardeshev *Fiz. metal. metalloved.* 1,281 (1955).
6. V.I. Arkharov and S. Mardeshev *Fiz. metal. metalloved.* 1,510; (1955).
7. V.I. Arkharov and S. Mardeshev *Fiz. metal. metalloved.* 1,517, (1955).
8. V.L. Arkharov *Zh. tekh. fiz.* 6, 1747 (1936).

THE OCCURENCE OF INTERNAL FRICTION PEAKS ASSOCIATED WITH THE STRESS-INDUCED DIFFUSION OF CARBON IN ALLOY STEELS HAVING A FACE-CENTRED CUBIC LATTICE *

KE T'ING – SUI and TSIEN CHIH-TSIANG **

(Received 18 January 1957)

Internal friction peaks associated with the stress-induced diffusion of carbon were examined in manganese steels of the four following different compositions

(1) Mn – 18.5 per cent (2) Mn – 25.4 per cent

(3) Mn – 36.0 per cent (4) Mn – 9.5 per cent, Ni – 8 per cent, Cr – 3 per cent.

(All these steels had a face-centred cubic lattice)

The maximum internal friction is observed in a temperature zone of 250°C with a frequency of vibration of about 2 c/s. Experimental results show that the height of the internal friction peak is in linear relationship with the concentration of carbon in solid solution.

The origin of these peaks is explained on the basis of the proposition that, in the course of alternating strain, carbon fills up the octahedral interstices of a face-centred cubic lattice. An allogenic atom (an atom of an alloying element or of a hole) produces with an atom of carbon an atomic pair which sets up distortion in the lattice, which differs in three crystallographic directions. The movement of these atomic pairs under stress produces internal friction. Formulae, derived from the assumption of such a pattern, can satisfactorily explain the linear relationship between the height of the internal friction peak and the content of carbon. The height of peak calculated in this way is found to approach closely to the value obtained experimentally.

Calculations of the concentration of holes in the lattice showed that the holes were responsible only for a tenth part of the observed internal friction. The atoms of alloying elements were held responsible for the remaining portion.

1. INTRODUCTION

Finkelstein and Rozin observed an internal friction peak in an alloy of 25 per cent Cu and 20 per cent Ni (γ – type), containing carbon. This peak was obtained by them in a temperature zone of 300°C with a frequency of vibration of about 1 c/s [1]. Similar peaks were observed by us in face-centred cubic alloys of certain types and in pure nickel, containing carbon. Systematic study that these peaks were associated with the stress-induced diffusion of carbon in face-centred cubic lattice [2, 3]. It was noted in [2] that if an atom of carbon in a solid solution with face-centred cubic lattice takes up an interstitial position, then the lattice assumes a condition in which micro-diffusion of carbon becomes possible, induced by stress in the lattice. These conditions can be of two types; (1) a condition of distortion caused by alloying elements; (2) a condition of distortion, caused by holes or vacancies in the lattice. To study the mechanism whereby this internal friction peak is produced, we undertook the following experiments on manganese steel of four types, having face-centred cubic lattice. We determined the relationship between the height of internal friction peaks and the quantity of dissolved carbon. On the basis of experimental results, we put forward a preliminary explanation of the origin of particular internal friction peaks.

2. PREPARATION OF TEST-PIECES

Internal friction was measured with an apparatus of the torsion-pendulum type, described earlier [4]. The length of the pieces was 200 mm, and the diameter 1.6 mm. The chemical composition of the test-pieces is given in Table 1.

X-ray analysis showed that the pieces had a face-centred cubic lattice both in the hardened

* *Fiz. metal. metalloved.* 4, No.2, 291-305, 1957 [Reprint Order No. POM 49].

** Translated into English by A.I. Moiseeva. First published in Chinese in *Acta Phys. Sinica* 12, No. 6 (1956).

condition and whilst being loaded with carbon after furnace quenching. All steps were taken to prevent the formation of carbides in the test-pieces intended for the measurement of internal friction. Each piece was first decarburized in an atmosphere of "wet hydrogen" at 1050°C and then loaded with carbon in a mixture of dry hydrogen and benzene vapour at 1050°C over varying intervals of time. Thus was obtained a series of pieces containing varied quantities of carbon. These pieces were homogenized in a vacuum furnace at 1100°C for 10 hr.. Metallographic tests showed that the carbon was evenly distributed over the cross-section of the homogenized articles. Indications that the carbon contained by the test-pieces was completely in solid solution were: (1) The absence of visible carbides under microscopic examination and the purity of the grain boundaries; (2) the increase of the height of the internal friction peak proportionally with increased carbon-loading. The very largest values for internal friction peaks obtained in each item which had been hardened after carbon-loading were not included in the total experimental results. The carbon content of the test-pieces was determined by the combustion method. Since only those pieces were used in the experiments which had a carbon content less than the pieces where internal friction peaks had a very high value, it can be concluded that in all the pieces tested carbon exists in solid solution.

VOL. 4 1957

3. MEASUREMENT OF ACTIVATION ENERGY

Curves of internal friction were plotted at three different frequencies of vibration for two test-pieces of 18.5 per cent manganese steel with a carbon content of 0.4 and 0.7 per cent in solid solution. In Table 2 are shown the optimum temperatures T (°K) for the maximum internal friction at each frequency of vibration and activation energy, as determined in these two pieces.

Blanter determined the activation energy and the coefficient of carbon diffusion in steel containing 19 per cent Mn by the macrodiffusion method in a temperature zone of 1000 – 1200°C. Activation energy was about 36,000 cal/mole with a carbon content of 0.4 per cent [5]. As is evident from Table 2, it is close to the value determined by the internal friction method. From the data obtained by the measurement of internal friction, coefficients of carbon diffusion were calculated in test-pieces containing 18.5 per cent Mn at optimum temperatures for internal friction peaks (200 – 300°C). The method of calculating these has been described in work [2]. The results of these calculations are shown in Table 3. The relationship of log D to $1000/T$ is shown in Fig.1;

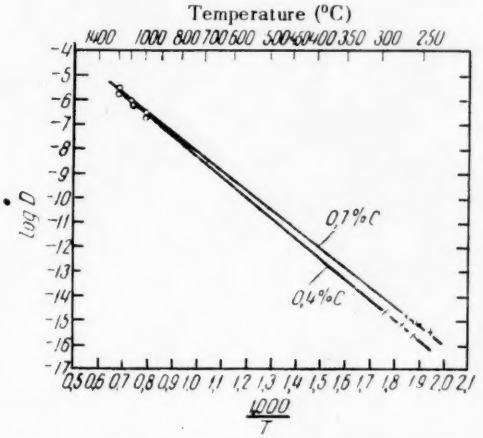

FIG. 1. Temperature relationship of the coefficient of diffusion D of iron in steel, containing 18.5 per cent Mn. o = data obtained by the macrodiffusion method. x = data obtained from the variation of internal friction.

just such results have been recorded as were obtained by Blanter in his measurements of macrodiffusion. Both series of data are set out in two straight lines (corresponding to 0.4 and 0.7 per cent C). The activation energy, calculated from the angle of gradient of these two straight lines, seems to be about 38,000 cal/mole for 0.4 per cent C and 36,000 cal/mole for 0.7 per cent C. These are close to the values obtained by the macrodiffusion method. This once again confirms that the observed peak of internal friction is associated with the diffusion of carbon induced by stress in test-pieces of manganese steel.

4. THE RELATIONSHIP BETWEEN THE HEIGHT OF THE INTERNAL FRICTION PEAK AND CARBON CONTENT IN SOLID SOLUTION

Before measuring their internal friction the test-pieces were given a preliminary heating up to 350°C inside the torsion apparatus, so as to remove cold working, which can be acquired by the pieces whilst being set up. Internal friction was always measured during a fall in temperature. Preliminary tests showed that in a region of temperature not exceeding 400°C the curve of internal friction obtained by measuring in rising tempera-

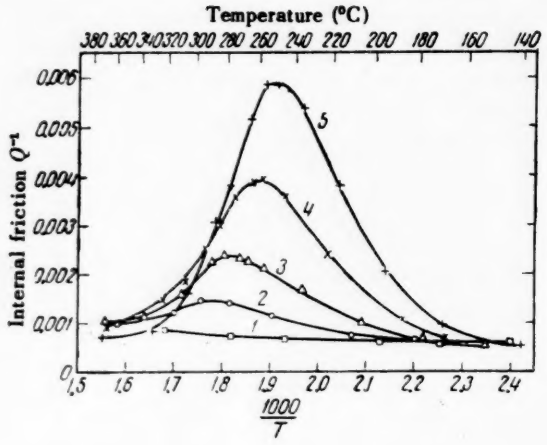

FIG. 2. Stress-induced internal friction peaks, associated with the diffusion of carbon, in steel having a Mn content of 18.5 per cent. Carbon content 1. – 0.12 per cent 3. – 0.70 per cent 2. – 0.37 per cent 4. – 0.95 per cent 5. – 1.34 per cent

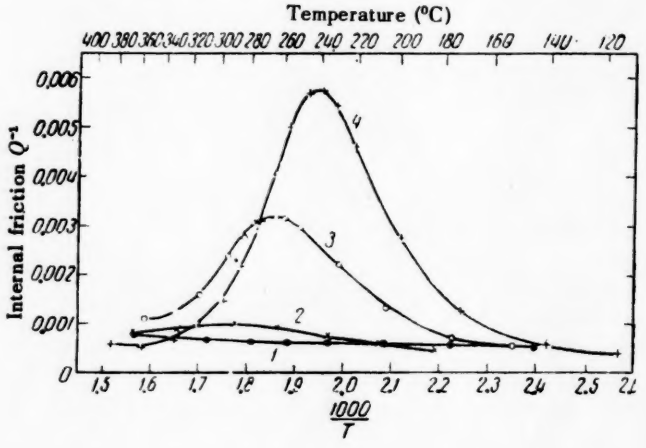

FIG. 3. Stress-induced internal friction peaks, associated with the diffusion of carbon, in steel containing 25.4 per cent Mn. Carbon content: 1. – 0.05 per cent 3. – 0.76 per cent 2. – 0.20 per cent 4. – 1.22 per cent

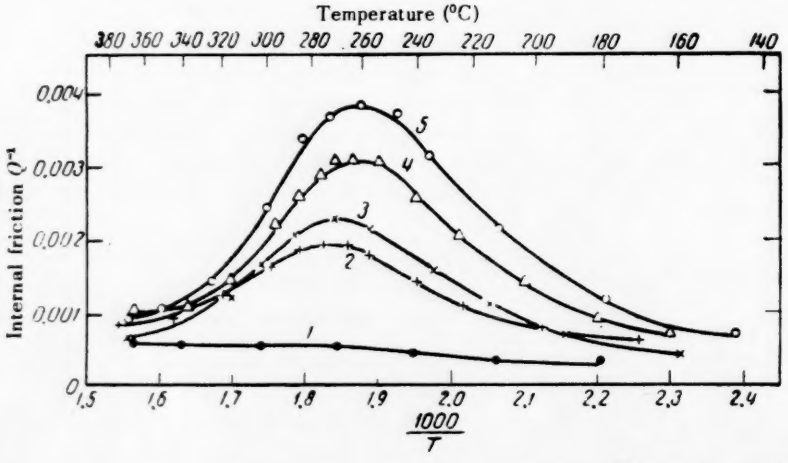

FIG. 4. Stress-induced internal friction peaks, associated with carbon diffusion, in steel containing 36 Mn. Carbon content: 1. – 0.12 per cent 3. – 0.65 per cent 2. – 0.42 per cent 4. – 0.75 per cent 5. – 0.97 per cent

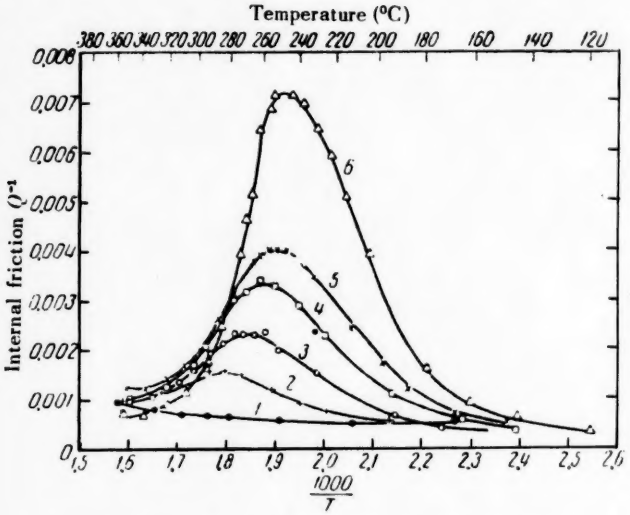

FIG. 5. Stress-induced internal friction peaks, associated with carbon diffusion, in steel containing 9.5 per cent Mn; 8.0 per cent Ni; 3.0 per cent Cr. Carbon content:

1. – 0.02 per cent 4. – 0.76 per cent
2. – 0.41 per cent 5. – 0.88 per cent
3. – 0.65 per cent 6. – 1.40 per cent

tures is identical with the curve obtained in falling temperatures.

Curves of internal friction for four types of manganese steel are shown in Figs. 2–5. The composition of the alloys and the frequency of vibration in which the measurement of internal friction was made are given below:

Fig. 2. Mn 18. 5 per cent; 2.0 c/s
Fig. 3. Mn 25. 4 per cent; 2.0 c/s
Fig. 4. Mn 36. 0 per cent; 2.2 c/s
Fig. 5. Mn 9. 5 per cent;
Ni 8. 0 per cent;
Cr 3. 0 per cent; 2.5 c/s.

The figures on the curves of internal friction indicate the order of sequence of carbon-loading.

The accuracy of measurement of internal friction was ± 0.0001 and the error in the chemical analysis of carbon was ± 0.03.

In Table 4 are shown data as to the height of internal friction peaks (background omitted) and of the content of carbon in solid solution (wt.%); the relationship between these has been shown in Fig. 6.

An analysis of the graphs in this figure leads to the following conclusions:

1. The height of the internal friction peak varies in linear relationship with the content of carbon in solid solution. This linear relationship is true

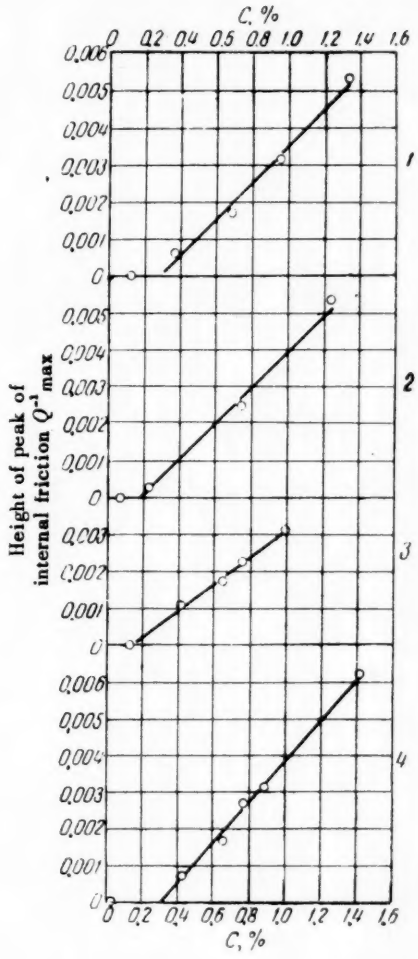

FIG. 6. Relation of internal friction peak height (background omitted) to content of carbon in solid solution (weight per cent):

1. – 18.5 per cent Mn 3. – 36.0 per cent Mn
2. – 25.4 per cent Mn 4. – 9.5 per cent Mn Ni; 3.0 per cent Cr.

even in the case of an alloy of complex composition, as, for instance, test-piece No. 4. From Fig. 6 (4) it is evident that this linear relationship is preserved in all cases of the stress-induced diffusion of atoms in alloys having face-centred cubic lattice.

2. The straight lines in Fig. 6 do not pass through the origin of co-ordinates. By producing each straight line to its intersection with the x-axis, we can ascertain the content of carbon at which the height of the internal friction peak is zero. These values are shown in the last column of Table 4. They decrease with an increase in the manganese content of the test-piece. Since all

TABLE 1.

No. of piece	Chemical composition of test-pieces (wt.%)					
	Mn	Ni	Cr	Si	S	P
1	18.5	—	—	0.39	0.006	0.068
2	25.4	—	—	0.57	0.004	0.081
3	36.0	—	—	—	0.005	0.032
4	9.5	8.0	3.0	0.41	0.005	0.032

TABLE 2. Optimum temperature for various frequencies of vibration

Frequency (c/s)	0,40	0,70
$1000/T$	3.12; 1.02; 0.46	2.16; 1.03; 0.46
Activation energy (cal/mole)	1.765; 1.835; 1.880 34000 ± 2000	1.850; 1.890; 1.945. 33000 ± 2000

TABLE 3. Coefficients of diffusion, calculated from the quantity of internal friction

C content %	0,4	0,7
$1000/T$	1.765; 1.835; 1.880	1.850; 1.890; 1.945
Relaxation time τ (sec)	0.051; 0.153; 0.346	0.074; 0.155; 0.346
$D \times 10^{-16}$ (cm^2 sec^{-1})	21.4; 6.98; 3.15	14.8; 7.05; 3.15
$\log D$	−14.67; −15.16; −15.50	−14.83; −15.15; −15.60

TABLE 4. Height of internal friction peak and content of carbon is solid solution

Test-piece	Sequence of carbon loading	Q^{-1}_{max}	Carbon content (%)	Critical carbon content (%)*
1 18.5% Mn	1	0.0000	0.12	0.29
	2	0.0007	0.37	
	3	0.0017_5	0.70	
	4	0.0031	0.95	
	5	0.0053	1.34	
2 25.4 % Mn	1	0.0000	0.05	0.18
	2	0.0003_5	0.20	
	3	0.0025	0.76	
	4	0.0053	1.22	
3 36.0 % Mn	1	0.0001	0.12	0.12
	2	0.0012	0.42	
	3	0.0017_5	0.65	
	4	0.0023	0.75	
	5	0.0031_5	0.97	
4 9.5 % Mn 8.0 % Ni 3.0 % Cr	1	0.0000	0.02	0.30
	2	0.0008	0.41	
	3	0.0016_5	0.65	
	4	0.0026_5	0.76	
	5	0.0031	0.88	
	6	0.0062	1.40	

* Obtained from intersection of straight lines with x – axis in Fig. 6.

existing carbon in the test-pieces is in solid solution, this shows that the internal friction peak can only show up when the content of carbon in solid solution exceeds a fixed critical value (other than nil) and this critical value decreases with the increase of the manganese content of the piece. Although the manganese content of test-piece No. 4 is less than that of test-piece No.1, the total quantity of alloying elements (Mn, Ni, Cr) constitutes 20. 5 per cent, which gives approximately the same value as the manganese content of test-piece No. 1 (18. 5 per cent Mn). The critical values of carbon content for these two alloys are also almost identical.

3. The slope of the straight lines decreases as the manganese content increases. This shows that with a high manganese content (or content of other alloying elements) a very high quantity of carbon is required to achieve the same values for internal friction peaks.

4. From the curves of internal friction shown in Figs. 2 – 5 the following additional conclusions can be reached :-

(a) The higher the manganese content of the test-piece, the less the internal friction peak shifts towards the side of low temperature with an increase of carbon content. This is the same relationship as was noted earlier [2]. According to the evidence from macrodiffusion experiments, the rate of carbon diffusion in γ – iron increases with an increase of carbon content and decreases somewhat with an increase of manganese content [5]. The effect of manganese is thus opposed to the effect of carbon. A high carbon content shifts the peak of internal friction to the low-temperature side, whereas a high manganese content will shift the peak to the high-temperature side. Since the effect of manganese is less marked than that of carbon, a blending of these two conflicting influences shows itself in a small shifting of the peak in the direction of very low temperature when carbon content increases.

(b) Where the test-pieces have the same manganese content the internal friction peak becomes narrower as the carbon content increases. Such behaviour is markedly expressed in curve 5 of Fig. 2, curve 4 of Fig. 3 and curve 6 of Fig. 5.

5. DETERMINATION OF THE LATTICE PARAMETER BY THE X-RAY METHOD

To confirm the linear relationship illustrated in Fig. 6, the X-ray method was used to determine the lattice parameter of the test-pieces employed in the measurement of internal friction. Under the conditions of our experiments, the lattice parameters were determined with an accuracy of ± 0.003 Å. Fig. 7 is a plot of the mean value of the lattice parameters of test-pieces containing 18.5 per cent Mn, with a varying carbon content. It is evident

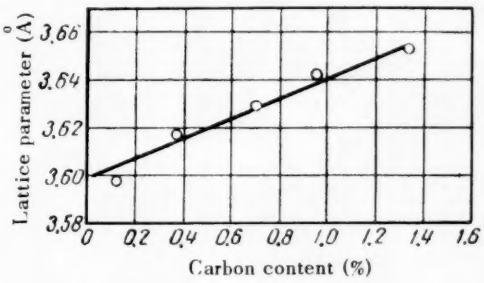

FIG. 7. Relation of lattice parameter to carbon content in steel containing 18.5 per cent Mn.

that the lattice parameter varies in linear relationship with the carbon content. The variation in the lattice parameter of dilute solutions is proportional to the concentration of dissolved atoms; therefore the linear relationship shown in Fig. 7 confirms the supposition that, as we found when measuring carbon by the combustion method, it exists in solid solution.

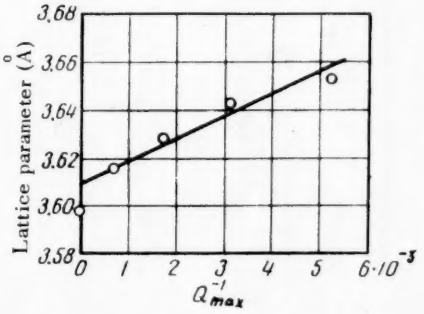

FIG. 8. Relationship between lattice parameter and height of internal friction peak (for steel containing 18.5 per cent Mn)

Fig. 8 shows that the lattice parameter also has linear relationship with the height of the internal friction peak. The intersection of these straight lines with the ordinate gives a value of

3.609 Å which is greater than the value of the lattice parameter of an object which contains no carbon (3.600 Å, Fig. 7). This once again confirms that an internal friction peak only occurs when a test-piece contains a critical quantity of carbon in solid solution.

6. POSSIBLE MECHANISM OF THE FORMATION OF A PARTICULAR INTERNAL FRICTION PEAK

The linear relationship between the height of an internal friction peak and the quantity of carbon in solid solution leads to the conclusion that the displacement of a single atom of carbon arises from the inherent nature of the process induced by stress. If a pair of carbon atoms were involved then, according to the calculations of Zener, Le Claire and others, the height of the internal friction peak would have a quadratic relation to the content of carbon in solid solution [6,7].

Fig. 9 shows a model which may explain the formation of an internal friction peak. *A* designates an atom of iron, *B* an allogenic atom (an atom of an alloying element or of a hole) and *C* an atom of carbon. With the arrangement of atoms shown in Fig. 9, an atom of carbon can form 5 links of the type *AC* and one link of type *BC*. I and II represent octahedral interstices of two possible types in the lattice. Let $BC > AC$*. If tensile stress is applied along the direction Z, an atom of carbon will tend to jump from position I (X – or Y – position), to position II (Z – position), so that the orientation *BC* would stand parallel to the direction of stress. This migration is indicated by a dotted line in Fig. 9. As a consequence of this migration additional strain in set up. In the same way an atom of carbon will tend to shift from position II to position I, when the applied exterior stress becomes compressive. Through the action of periodic stress an atom of carbon will shift from position I to position II and conversely. Since a certain interval of time is required to effect this stress-induced shift, this is the phenomenon of relaxation, in which strain lags behind stress, and which produces anelasticity and internal friction.

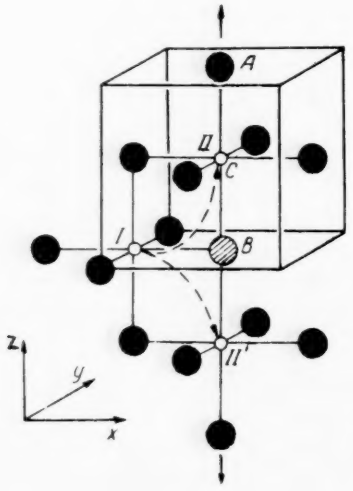

FIG. 9. Model giving a suggested explanation of the mechanism of the occurrence of stress-induced internal friction peaks, associated with carbon diffusion, in alloys having a face-centred cubic lattice. *A* – atom of iron; *B* – allogenic atom (atom of an alloying element or a hole); *C* – atom of carbon

The combination of links *BC* in the lattice must have two types of orientation. Let N_p and N_n be the magnitudes of the pair *BC* in a unit of volume of a test-piece, orientated conveniently parallel and perpendicular to the direction of the applied stress. During the action of uniaxial tensile stress part of N_n is converted to N_p which gives the increment of the number of pairs equal to dn_p. The anelastic strain obtained thereby will be equal to:

$$\varepsilon'' = \left(\frac{\partial \varepsilon}{\partial n_p}\right)_\sigma dn_p, \qquad (1)$$

where $(\partial \epsilon / \partial n_p)$ = anelastic strain resulting from the conversion of one pair *AC* into the pair *BC* in a unit of volume of a test-piece.

When conditions of equilibrium are reached [8], then

$$dn_p = \frac{2}{9}\, n\left(\frac{u}{kT}\right), \qquad (2)$$

where n = the total number of pairs *BC* in a unit of volume, u = the difference of energy between cases when the carbon atom is in the z – position, stress being applied along the z – direction. In the first approximation we can reckon u as independent of the temperature.

The complete change of energy from external stresses is

$$du = \sigma d\varepsilon + u dn_p,$$

whence

$$d(u - \sigma\varepsilon) = -\varepsilon d\sigma + u dn_p$$

* The situation is similar when $BC < AC$

Applying Kosh's ratio we get

$$\left(\frac{\partial \varepsilon}{\partial n_p}\right)_\sigma = -\left(\frac{\partial u}{\partial \sigma}\right)_{n_p}$$

If u is taken to be independent of n_p (i.e. ignoring interaction between BC pairs), then

$$u = -\left(\frac{\partial \varepsilon}{\partial n_p}\right) \cdot \sigma.$$

Substituting in equation (2) we get

$$dn_p = -\frac{2}{9} n \left(\frac{\partial \varepsilon}{\partial n_p}\right) \frac{\sigma}{kT}$$

The total strain resulting from the action of applied stresses will be

$$\varepsilon = E_u^{-1}\sigma + \varepsilon'' = E_u^{-1}\sigma - \frac{2}{9} n \left(\frac{\partial \varepsilon}{\partial n_p}\right)^2 \frac{\sigma}{kT},$$

where E_u = non-relaxation modulus of elasticity.

Let the relaxation modulus be E_R, then

$$E_R^{-1} = \frac{\varepsilon}{\sigma} = E_u^{-1} - \frac{2}{9}\left(\frac{\partial \varepsilon}{\partial n_p}\right)^2 \frac{n}{kT}.$$

The degree of relaxation will be

$$\Delta E = \frac{E_u - E_R}{E_R} = \frac{2}{9} E_u \left(\frac{\partial \varepsilon}{\partial n_p}\right)^2 \frac{n}{kT},$$

and the height of the internal friction peak will be

$$Q_{max}^{-1} = \frac{\Delta E}{2} = \frac{1}{9} E_u \left(\frac{\partial \varepsilon}{\partial n_p}\right)^2 \frac{n}{kT} \qquad (3)$$

If an atom of carbon has a position in the octahedral interstices, it will have 6 close neighbours. Suppose that the allogenic atoms are uniformly distributed within the crystal lattice; then, if the concentration of the alloying element is 1/6th or 17 at.% (i.e. 1 allogenic atom must be included in the 6 lattice atoms), an atom of carbon which has a place in the octahedral interstices will, on average, form one pair BC with one allogenic atom (see Fig. 9). We can therefore consider n in equation (3) i.e. the number of BC pairs in a unit of volume, as being the number of atoms of carbon in a unit of volume. Thus it follows from equation (3) that the height of the internal friction peak is proportional to the concentration of carbon.

In a case where the content of the allogenic element is more than 17 at.%, each atom of carbon can form more than one connexion BC in the lattice. Notwithstanding this, n, the number of BC connexions in a unit of volume, is always proportional to the concentration of atoms of carbon in a test-piece containing a specified quantity of the alloying element. Consequently, even if the alloy content exceeds 17 at.%, equation (3) still shows that the internal friction peak is proportional to carbon concentration. All test-pieces used in our investigation contained more than 17 at.% of alloy elements yet the linear relationship, illustrated in Figs 6 and 8, which we obtained, indicates that equation (3) fairly accords with experimental results.

7. CONSIDERATION OF RESULTS

Evaluation of the degree of relaxation and of the internal friction peak

The value $(\partial \varepsilon / \partial n_p)$ is calculated approximately from the results of changes in the lattice parameter. Thus, it seemed possible to compare the magnitudes of the degree of relaxation and of the height of the internal friction peak, calculated according to equation (3), with experimental findings.

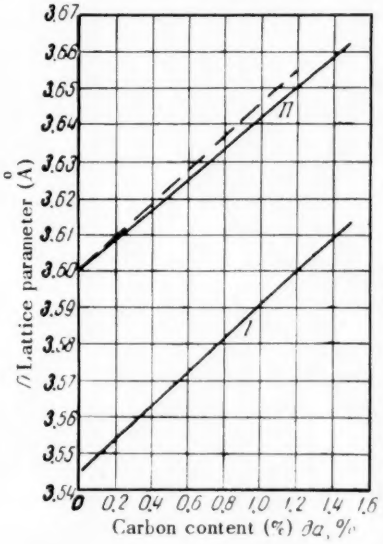

FIG. 10. Variation of lattice parameter in steel containing carbon. I – pure austenite; II – austenite containing 18.5 per cent Mn

Line I in Fig. 10 shows the relation of the lattice parameter of γ – iron to the carbon content [9]. Line II shows the relationship of the lattice parameter of γ – iron (containing 18.5 per cent Mn) to the carbon concentration (see Fig. 7). From the point of intersection of line II with the γ – axis a dotted line is produced parallel to line I (Fig. 10). This dotted line can be taken as representing the speed of change of the lattice parameter with carbon content in γ – iron having 18.5 per cent Mn, in a case where the atoms of carbon in the lattice

form only the connexions *ACA* (see Fig. 9). This line notably differs from the experimental line II, because the carbon atoms in reality form not only *ACA* but also *ACB* connexions.

Take a single cube of a test-piece and suppose that it has N cells, situated along each side of the cube, so that $aN = 1$ cm where a = a lattice parameter. Considering the dotted line in Fig. 10, we obtain with a carbon content of 1 per cent a length of cube side of $3.646\,N$ Å (if the atoms of carbon form only *ACA* connexions). But, according to line II, the length of cube side will only be $3.642N$ Å. The difference between these two values is $0.004N$ Å. This is because along the cube side part of the connexions *ACA* are converted into *ACB* connexions owing to the presence of the alloying element in the test-piece. As mentioned above, in a test-piece containing 17 at.% Mn, each carbon atom with a place in the octahedral interstices will form statistically one *ACB* and two *ACA* connexions. In the absence of stress the distribution of *ACB* connexions along three crystallographic axes is statistically uniform; consequently, it can be concluded that along each direction one third are *ACB* and two thirds are *ACA*. If, therefore, all *ACA* connexions along the cube sides are transformed into *ACB* connexions then the difference in length of a cube side will be three times greater than $0.004N$ Å i.e. it will be $0.012N$ Å. Hence the change in length of the cube side through the conversion of one *ACA* to *ACB* will be $0.012\,N/n_0$ Å where $n_0 = (N_0/M) \cdot \rho/100$, the number of atoms of carbon in a unit of volume of steel containing 1 per cent carbon, ρ – density of steel, 7.8g cm^{-3}; N_0 is Avogadro's constant, and M is the atomic weight of carbon.

According to determination, $\partial\epsilon/\partial n_p$ is the tensile strain resulting from the conversion of one connexion *ACA* (or of a pair *AC*) to one connexion *BCA* (or a pair *BC*) in a unit of volume; this is equal to $(0.012N/n_0)\ /3.600N = 0.85 \times 10^{-24}$. The number of atoms of carbon in unit volume of a test-piece containing x per cent by weight of carbon will be $n_0 x$. For an object containing 17at.% of manganese, we can count $n_0 x$ as being equal to n in equation (3); thus

$$\Delta E = \frac{2}{9} n_0 x E_u \left(\frac{\partial \varepsilon}{\partial n_p}\right)^2 \Big/ kT. \qquad (4)$$

Young's modulus for steel is 20×10^4 dynes/cm^2 and this value does not change noticeably in the various types of steel. The optimum temperature (T) for the internal friction peak can be taken as 550°K. Substituting these quantities in equation (4), we get

$$\Delta E = 2.29 \quad 10^{46} \cdot x \left(\frac{\partial \varepsilon}{\partial n_p}\right)^2. \qquad (5)$$

In Table 5 is given a comparison of the theoretical and experimental values of the degree of relaxation. "Critical carbon content" is subtracted from the total carbon content in arriving at the figures shown in Table 5.

TABLES 5. Comparison of theoretical and experimental values of degree of relaxation in test-pieces containing 18.5 per cent Mn.

Carbon content	ΔE (calc.)	$\Delta E = 2Q_{max}^{-1}$ (expt.)
1,05	0,017	0,0106
0,66	0,010	0,0063
0,41	0,0067	0,0035
0,08	0,0013	0,0012

The theoretical values of the degree of relaxation are adequately close to the experimental values. We must note that the error in determining the lattice parameter with our measurements is 0.003Å.which is slightly different from the lattice parameter figure applied in calculation. Consequently, these calculations can only be taken as an estimate. Nevertheless, it is fairly obvious form Table 5 that there is a quite satisfactory agreement between the theoretical and experimental figures.

EFFECT OF MANGANESE CONTENT

The slope of the lines given in Fig. 6 decreases as the manganese content increases, i.e., for one and the same carbon content in a test-piece the height of the internal friction peak decreases as the manganese content increases. A possible explanation of this phenomenon may lie in the following points. Since a test-piece contains more than 17 at.% of manganese, then each atom of carbon having a position in the octahedral interstices can have amongst its immediate neighbours more than one atom of manganese and consequently can form more than one *BC* – link. These *BC* – links are distributed along different crystallographic directions, with the result that the probability of an atom of carbon migrating from a position of one type to another is reduced. The internal friction is also reduced.

In an extreme case, when the manganese con-

tent reaches 50 at.%, there can be three atoms of manganese borrowing three of the six positions neighbouring on each atom of carbon. These three manganese atoms can be distributed along three mutually perpendicular directions. Under these conditions there cannot be any stress-induced jumping of carbon atoms, and there will be no internal friction peak.

In equation (3) n is the total number of BC pairs existing in a unit of volume. Even if the manganese content is more than 17 at.%, the number of BC pairs still remains proportional to the carbon content. Within the range of carbon content used in our experiments, only a very small portion of the octahedral interstices within the lattice were actually occupied by carbon atoms, which confirms the independence of $\partial\epsilon / \partial n_p$ from the carbon content. Furthermore, the internal friction peak is in linear dependence on the concentration of carbon in solid solution.

ALLOYING ELEMENTS AND HOLES

In section 6 the allogenic atom B is considered either as an atom of an alloying element, or as a hole. Let us now consider the relative significance of these and other matters in the causation of internal friction peaks.

Let n be the number of holes existing in a lattice comprising N atoms; then the equilibrium concentration of holes at temperature T will be

$$\frac{n}{N} = \exp\left(-\frac{u}{RT}\right), \qquad (6)$$

where u = energy of hole formation. On the basis of a series of tests on face-centred cubic metals Hertsriken made the suggestion that u is approximately equal to one third of the activation energy E_d in self-diffusion [10]. In γ – iron E_d equals 68,000 cal/mole [11], so that u can be reckoned to be approximately equal to 22,700 cal/mole. If a test-piece of γ – iron is hardened at a temperature of 1100°C (1375°K), the equilibrium density of holes which can be attained in a test-piece will be $\frac{n}{N} = \exp(-22700\ 2746) = 10^{-3.59}$ which works out at about 0.03 at.%. It is necessary to note that two corrections must be introduced in these values. The first correction is the change of entropy ΔS of hole-formation and this modifies equation (6) as follows:

$$\frac{n}{N} = \exp\left(-\frac{u}{RT} + \frac{\Delta S}{R}\right). \qquad (7)$$

According to an estimate made by Lumsden the term $\Delta S/R$ can increase the number of holes 10 – 100 times [12]. The second correction is for disappearance of holes, preserved during hardening at high temperature. At low temperature, holes can diffuse through nearby faults in the lattice, and thus the number of holes given in equation (6) can decrease. Nevertheless, the number of faults contained in a test-piece annealed at high temperature cannot be very great. Thus it can be taken that the density of holes in a test-piece hardened at 1100°C is approximately equal to one at.%, discounting both corrections considered above.

Supposing that the density of holes in a test-piece of γ – iron containing 18.5 per cent Mn is the same as in a test-piece of pure γ – Fe, which has undergone identical hot-working, then the hole-density in a test-piece of 18.5 per cent Mn, hardened at 1100°C, will also be approximately equal to one at.%. If we further suppose that the value $\partial\epsilon / \partial n_p$ is not very different in those cases where an allogenic atom is an atom of alloying element or of a hole, then that part of the internal friction which is induced by the presence of holes cannot be more than 1/10 of the internal friction actually observed, since the concentration of holes is over ten times less than the concentration of alloying elements in our test-pieces. Consequently the internal friction observed in test-pieces of manganese steel is principally associated with lattice distortion brought about by the inclusion therein of alloying elements.

In nickel the maximum stress-induced internal friction peak, associated with carbon diffusion, is only 0.007 [3]. This is one tenth the amount of internal friction than is observed in alloy steels. Obviously this is conditioned by the low concentration of holes in the lattice of pure nickel. The activation energy of self-diffusion in nickel is 60,000 cal/mole [13]. A test-piece of nickel whose internal friction was being measured was hardened at a temperature of 1100°C. The equilibrium density of holes, computed by means of our data, discounting the errors above noted, was about 2 at.%.

CRITICAL CARBON CONTENT FOR THE GENERATION OF INTERNAL FRICTION

One of the possible explanations or the existence of a critical content of carbon in the occurrence of internal friction is based on the presence of holes in the lattice. In the early stages of

carbon-loading a test-piece, atoms of carbon can enter the holes in the lattice. An atom of carbon, borrowing such a substitutional position, will not create observable internal friction. When the existing holes are completely filled, the remaining atoms of carbon can only be disposed of in the octahedral interstices. The critical carbon content for a test-piece containing 18.5 per cent Mn is approximately 0.29 wt.%, which approximately corresponds to 1.5 at.%. This value is close to that of hole-concentration in the lattice (approximately 1 at.%).

REFERENCES

1. K.M. Rozin and B.N. Finkelstein *Dokl. Akad. Nauk SSSR* 91, 811 (1953).
2. T.S.Ke and Ch. M. Wang *Acta Phys. Sinica* 11, 387 (1955).
3. T.S. Ke, Ch. T. Tsien and K.Misek *Acta Phys. Sinica* 11, 403 (1955): *Scientia Sinica* 4, 519 (1955).
4. T.S. Ke *Phys. Rev.* 71, 533 (1947), *Uprugost' i neuprugost' metallov (Elasticity and anelasticity of metals)* Izd. IL p. 198, 1954.
5. M.E. Blanter *Zh. tekh. fiz.* 21, 818 (1951).
6. C. Zener *Phys. Rev.* 71, 34 (1947).
7. A.D. Le Claire and W.M. Lomer *Acta met.* 2, 731 (1954).
   B.C. Childs and A.D. Le Claire *Acta met.* 2, 718 (1954).
8. C. Zener *Elasticity and anelssticity of metals.* Univ. of Chicago Press pp. 113-119, 1948. (Russian version). A.S. Nowick *Progress in metal physics* 4, 35 (1954).
9. S. Epstein *Alloys of iron and carbon* McGraw-Hill N.Y. Vol. 1, p. 212 , 1936.
10. C.D. Gertstriken *Dokl. Akad. Nauk SSSR* 98, 211 (1954).
11. P.L. Gruzin, I.V. Kornev and G.B.Kurdyumov *Dokl. Akad. Nauk SSSR* 80, 49 (1951);
    P.L. Gruzin *Izv. Akad. Nauk SSSR otd. tekh. nauk* 3, 383 (1953);
    F.S. Buffington, I.D. Bakalar and M. Cohen *Self-diffusion in iron, the physics of powder metallurgy.* McGraw-Hill N.Y. 92, 1951.
12. J. Lumsden *Thermodynamics of alloys,* Institute of Metals, Monograph and report series, London, No. 11, p. 347, 1951.
13. P.L. Gruzin Dissertation, Moscow, 1955 (Presented by K.A. Osipov, *Issledovaniya po zharoprochnym splavam, A study of heat-toughened alloys).* Institute of Metallurgy, Akad. Nauk SSSR, A.A. Vaikov P.p. 153, 1956.

VOL 4 195

THE MECHANISM OF PLASTIC DEFORMATION AND THE MECHANICAL PROPERTIES OF ALUMINIUM – III

THE ROLE OF PLASTIC DEFORMATION IN THE FORMATION OF THE MECHANICAL PROPERTIES OF ALUMINIUM*

E.S. YAKOVLEVA

(Received 28 June 1956)

VOL. 4 1957

The mechanical properties of metals and alloys vary with change in conditions of deformation. This is to a considerable extent determined by the fact that the cohesive strength also changes with the conditions of deformation, (for example, with temperature and pressure). The cohesive strength, however, is often insufficient for the explanation of the whole of the effect observed during the variation of one parameter. This happens not infrequently in alloys when the cohesive strength and the resistance to deformation vary inversely with the stresses [1]. Submicroscopic inhomogeneities then appear to be responsible for the mechanical properties of the metal.

There are different kinds of structural inhomogeneities in crystalline substances, for example, grain and block boundaries, foreign atoms, vacancies, dislocations. In metals, the amount and type of the different inhomogeneities vary with the temperature, so that the different types are responsible for the behaviour of a metal under load at different temperatures.

When conditions are dissimilar, so are the mechanisms which cause plastic deformation, and the deformation mechanism is determined by the magnitude and anisotropy of the effective cohesive forces and the inhomogeneities structure of the metal, that is, by just those parameters on which its mechanical properties depend. The change in the mechanism is usually related to the change in the behaviour of the metal under load, but to what extent the deformation mechanism determined the behaviour of a metal under load has not yet been sufficiently studied.

The present work endeavours to explain the relationship between the mechanism of plastic deformation and the mechanical properties of pure aluminium.

The aluminium used was of the type AVOOO which had been used for the deformation studies in the first two parts* of the present series.

The mechanical properties of the aluminium were determined from the stress diagrams obtained at temperatures – 196, + 18, + 250°C and at rates of 7.3×10^4, 73 and 2.3 per cent/hr. The deformations were carried out in a machine for drawing thin wires thus permitting the strain to be obtained on a photoplastic diagram [2].

Fig. 1 shows the strain diagrams for various conditions of deformation, showing that the deformation resistance of aluminium at all degrees of strain is greater the higher the speed and the lower the temperature of the test. It can also be seen that in the range of conditions studied, the temperature had a stronger effect on the deformation resistance than the rate of testing. For example, at a constant rate of extension of 2.3 per cent/hr and similar deformation of 30 per cent, the deformation resistance changed by a factor of 7.7 when the temperature rose from – 196 to 250°C. The greatest change in the deformation resistance occurs when the rate of extension is altered from 2.3 to 7.3×10^4 per cent/hr at a 30 per cent extension and a temperature of 250°C and is by a factor of only 2.

The almost eightfold change in deformation resistance on changing from – 196 to 250°C cannot be explained by a change in cohesion. In the temperature range – 196 to 600°C, the elastic modulus of aluminium which can be regarded as the neutralizing characteristic of the cohesion, changes by a factor of only 2 [3]. Thus the greater part of the variation in the properties of aluminium can be explained by the difference in the mechanism of the process of plastic deformation and by the type of inhomogeneities in its structure.

In part I of this series it was shown that the deformation of poly-crystalline aluminium takes

* *Fiz. metal. metalloved.* 4, No. 2, 306-309, 1957 [Reprint Order No. POM 50].

* *Fiz. metal. metalloved.* 4, No.1 (1957).

place in a different way. At low temperatures and high rates of strain, the deformation is achieved by displacement evenly distributed over a very great part of the glide plane. In order that the resistance to such deformation should be large the whole volume of the metal grain is involved in it to some considerable extent and large external strains are required to overcome this resistance. Fig. 1 shows that the resistance of aluminium to deformation at low temperatures and high rates of strain is in practice very great.

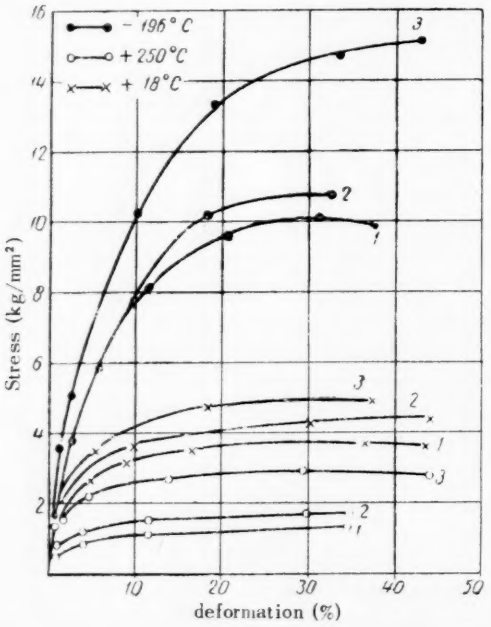

FIG. 1. Strain curve for aluminium taken at three rates and at three temperatures of deformation:
1. rate 2.3 per cent/hr.
2. rate 73 per cent/hr.
3. rate 7.3 × 10 per cent/hr.

With increased temperature and decrease in the rate of strain, the type of deformation undergoes a change. The movement is less uniformly distributed between the planes and in the actual glide planes, and a deformation takes place at the grain boundaries as well. There is at the same time a lowering of the metal's resistance to deformation (see Fig. 1) which is due to the increased probability of thermal fluctuations which give rise to local distortions of the lattice which in their turn facilitate the initiation of shear deformations. There can also be deformation at the grain boundaries since the resistance of the boundaries to deformation with increase of temperature is more quickly lowered than the resistance of the bulk of the grain.

With increasing degree of strain, the distribution of deformation in the grains is less uniform under all conditions. This is related to the development of heterogeneous strain formed in the grains as a result of interaction along their boundaries. As shown in part II of this series, a grain breaks down into randomly oriented blocks when subjected to inhomogeneous strain. The formation of these blocks can be seen in the very earliest stages of strain, sometimes earlier than the appearance of the slip lines in the grains. The dimensions of the blocks so formed are smaller, the higher the rate of deformation and the greater the degree of strain. The grain size increases with the testing temperature.

The boundaries of grains with distorted lattices seem to be an obstacle to the propagation of shear. Misorientation of the blocks themselves also hampers shear deformation. The formation of a great number of small misoriented blocks can explain the high coefficient of hardening of aluminium when strained at low temperatures and high rates of deformation. The hardening of aluminium does not depend only on the formation of misoriented blocks: pure shear unaccompanied by block formation also distorts the lattice and hardens metals. The magnitude of the hardening due to pure shear at room temperature is, however, less than that due to block formation [4].

Distortions due to shear fluctuate and can be completely removed by annealing without recrystallization. Hardening due to block formation is extremely stable and can be reduced only by increasing the blocks to grain size [5] or by recrystallization [6].

The lattice distortion due to plastic deformation in fine grained aluminium is well shown by the changes in the breadth and intensity of the lines in an X-ray diffraction diagram. Studies carried out by these methods disclosed distortions in aliminium deformed at room [7] and low [8] temperatures.

With increase of temperatures and decrease of rate of extension, the amount and misorientation of the blocks due to deformation decrease and the grain size increases. The hardening coefficient of aluminium decreases, which is probably connected with the coarsening of the blocks and the decrease in the proportion of the deformation which takes place by shear in the slip planes with increase of

temperature and lowered rate of strain.

The deformation of aluminium at 250°C at a rate of the order of 10 per cent/hr is not accompanied by hardening. In this case the blocks formed in the initial stages grow in the course of deformation to dimensions of the order of the original grain size and cannot therefore produce hardening. Deformation along the grain boundaries is also unaccompanied by hardening because of the intensive relaxation during strain [9]. Shear in the slip planes in conditions of creep, is insignificantly small and cannot give rise to any noticeable hardening.

CONCLUSIONS

1. Cohesive strength, inhomogeneity of structure and the mechanism of plastic deformation of the metal appear to be the factors which mainly determine the resistance of pure aluminium to deformation.

2. The differences in the resistance of aluminium to deformation at different temperatures and deformation rates is due principally to the variety of inhomogeneities in its structure and to the mechanism of plastic deformation.

REFERENCES

1. G. Kurdyumov, V. Kritskaya and N. Nodin *Problemy metallovedeniya i fiziki metallov (Problems in metallography and metal physics)* 4, 455 (1955).
2. V. Averkiev, V. Pavlov, G. Kolesnikov and M. Yakutova *Zh. tekh. fiz.* 16, 1349 (1946).
3. W. Koster *Z. Metallk.* 41, 39, 1 (1948).
4. A. Kochendorfer and F. Rohm *Z. Metallk.* 41, 215 (1950); H. Kanzaki *J. Appl. Phys.* 14, 4 (1953).
5. P. Beck *Phil. Mag.* 256, 3 (1953).
6. R. Honeycombe *J. Inst. Met.* 80, 45, 1 (1951).
7. S. Tsobkallo and V. Latsh *Izv. Akad. Nauk, ser. fiz.* 17, 3 (1953).
8. N. Noskova, V. Pavlov and B. Yunikov *Fiz. metal. metalloved.* 3, 3 (1956).
9. H. Chang *J. Inst. Met.* 5, 1175 (1953).

VOL. 4 1957

THE GROWTH OF LARGE SINGLE CRYSTALS OF ZINC OF KNOWN ORIENTATION *

B.N. BUSHMANOV

(Received 18 May 1956)

A method is described of obtaining large single crystals of zinc with orientation of the crystallographic axes as desired. A single crystal seed is passed through a flux into the molten metal and the upper end cooled.

Single crystals in which the orientation of the crystallographic axes within the actual specimen is known, are in demand for the study of the anisotropy of various physical properties. The single crystals should be big enough to give the faces of some five to ten square centimetres which are necessary in the study of such physico-chemical properties as adsorption, catalysis and exchange reactions.

The largest metal single crystals have been obtained by pulling out of a melt as suggested by Chokhral skii, and by progressive freezing in a tube, the method put forward by Tamman, Bridgman and Obreimov and Shubnikov [1-4]. The first of these methods achieves the single crystal with desired orientation by the very simple means of making the appropriate monocrystalline seed serve as the lifting tackle, [1, 2, 5]. Several methods of growing oriented single crystals by the tube method have also been suggested, but they do not guarantee that the crystals will be of large size and are quite complicated to use. Mention will be made of some of these methods in the sequel.

Glocker and Graf's method has been used to grow oriented single crystals up to 7.5 mm. diameter [6]. Palabin and Froiman's method [7], although hailed by Bakli [2] as "a highly ingenious contrivance", has been convincingly critized by Kuznetsov [1]. Shubnikov and de Haas [8] improved Kapitsa's method and grew crystals no bigger than the seed crystal (2.5 x 2.5 x 22 mm.) Tsinnamon's apparatus seems to be a further development of Kapitsa's, and allowed the growth of single crystals of zinc up to one square centimetre in cross-section, but the yield was low (5 percent) and the procedure comparatively intricate. The adaptation of Glocker and Graf's method by Takaki, Nakamura and their co-workers was considerably more complicated [9] and resulted in crystals only 3 mm in diameter. Other complicated methods are those of Chalmers [10] and of Chigvinadze; the latter did not intend to produce large crystals and his method allowed only one of the crystallographic axes of a zinc single crystal to be oriented [11, 12].

The aim of this paper is to put forward a simple method of growing a large single crystal of the required shape and with the desired orientation of the crystallographic axes.

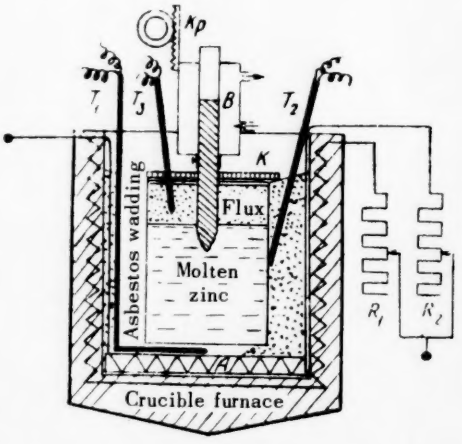

FIG. 1. Apparatus for growing large single crystals of zinc with a given orientation.
A.- additional heating element;
T_3, T_2, T_3, - thermocouples;
R_1, R_2, - rheostats;
Kp - rack for lowering the seed crystal;
K - asbestos lid;
B - condenser.

The apparatus [Fig. 1] consists of the usual

* *Fiz. metal. metalloved.* 4, No. 2, 310-314, 1957 [Reprint Order No. POM 51].

crucible furnace, but provided with an additional heating element fitted into the base, two rheostats connected to the heating elements, three thermocouples, a rack for inserting the seed crystal into the melt, and a stand with a contrivance for giving the required orientation to the seed crystal (not shown in the diagram). A glass vessel (beaker or flask) is placed in the furnace and the space between the walls of the vessel and the walls of

FIG. 2.

the furnace packed with asbestos wadding. The zinc is melted in another furnace and poured into the glass vessel (the crucible having been previously heated to 470 - 480°C), and the molten flux, zinc chloride, poured on to the surface of the molten zinc. The temperature of the zinc and flux was up to 50 or 60°C higher than the melting point of zinc. At this stage a rack was used to lower a single crystal seed through the flux into the melt. The seed has been grown separately by Bridgman's method, and was a cylindrical rod 100 to 150 mm. in length and 10 to 12 mm. diameter: the upper end was fitted into a condenser. The vessel was covered with an asbestos lid, water flowed through the condenser and the current through the heating elements adjusted by the rheostats so that there was a thermal gradient along the seed crystal only and not across the walls or the bottom of the vessel. The crystals thus grown were single crystals 45 to 83 mm. in diameter and weighing 0.6 to 2.1 kg. If these conditions were maintained there were hardly any unsatisfactory specimens.

Obreimov and Shubnikov mention [4] that Strelkov succeeded in crystallizing as a single crystal a whole crucible of zinc by pushing the seed into the melt from above, but unfortunately, more detailed description of Strelkov's work points out that under such conditions, shrinkage cracks are always obtained. It was to avoid these shrinkage cracks that Obreimov and Shubnikov suggested using the tube method.

The use of the flux in our method protects the metal from oxidation and completely excludes the possibility of the metal adhering to the glass. The preliminary experiments did not use the flux and were not successful: in only one case out of five was more than 90 percent of the volume of the specimen along the length a single crystal, but its orientation was not that of the seed. When the flux was used the seed's orientation was transferred to the metal.

The shrinkage cracks which occur do so on the lateral surfaces of the specimens. This is due to the fact that the vessel containing the zinc is heated somewhat more strongly from the side near the leads to the additional heating element and so the adjacent metal was the last

FIG. 4.

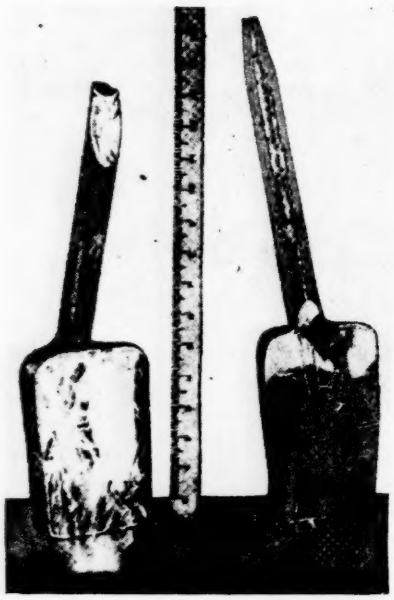

FIG. 5.

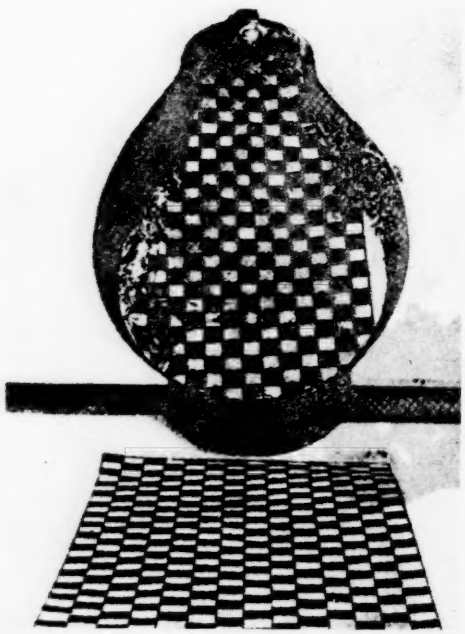

FIG. 6.

to crystallize, hence the shrinkage cracks.

Photographs of cleaned surfaces of some of the single crystals which have been grown by this method are seen in Figs. 2 - 6. The size of the specimens can be judged from the scale set up alongside. Fig. 5 shows that the orientation of the seed is transferred to the metal. In these specimens the basal plane was taken as lying along the axis of the cylinder so the seed had to be inserted at a corresponding angle. Figs. 3 and 5 show that there are no shrinkage cracks spoiling the interior of the specimens. The quality of the reflecting surface of a cleavage surface along the basal plane is shown by a checkerboard in Fig. 6. the size of the squares is 5 x 5 mm.

One seed crystal can be used to obtain two or three large single crystals, and specimens which are single crystal for only 20 or 30 mm. from one

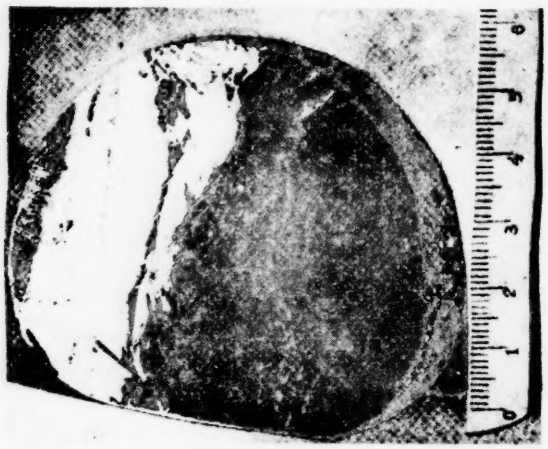

FIG. 3.

end can also be used as seeds: such a one is shown on the left of Fig. 5. By selecting the appropriate flux this method could probably also be used for other low melting metals.

This work has been carried out in the laboratory of the departent of general chemistry of the Kazan Aviation Institute, under the direction of Professor G.S. Vozdvizhenskii.

REFERENCES

1. V.D. Kuznetsov *Kristally i kristallizatsiya (Crystals and crystallization)* 333, GITTL, Moscow. 1954.
2. G. Bakli *Rost kristallov (Crystal growth).* Izd. IL. 62. 1954.
3. L.V. Shubnikov *Kak rastut kristally (How crystals grow) Izd. Akad. Nauk SSSR* 48 (1935).
4. I.V. Obreimov and L.B. Shubnikov *Trud. Leningr. fiz.-tekh. lab.* 21, 1925.

5. Rot and Taylor, Mel8 Mel'sh and Demelt, Lekhovek, Soled, Cox, Macdonald and Sterns, Horn and Neubauer *Sb. "Germanii" (A symposium on germanium).* Izd. IL. pp. 40, 55, 58 and 63. 1955.
6. R. Glocker and L. Graf *Z. anorg. Chem.* 188, 232 (1930).
7. P.A. Palibin and A.I. Froiman *Zh. eksp. teor. fiz.* 3, 162 (1933).
8. L.V. Shubnikov and V. de Haas *J. Soc. phys.-chim. russe* 62, 529 (1930).
9. H. Takiki, S. Nakamura, Y. Nakamura, J. Hayashi, K. Furukawa, and M. Aso, *J. Phys. Soc., Japan*, 9, 204, (1954).
10. B. Chalmers, *Canad. J. Phys.*, 1, 132, (1953).
11. D.M. Chigvinadze, *Soobshchen Akad. Nauk Truz. SSR*, 9. 19, (1948).
12. D.M. Chigvinadze, *Zh. tekh. fiz.* 25, 805, (1955).

VOL. 4 1957

CHANGES IN THE PROPERTIES AND STRUCTURE OF NICKEL - BASE SOLID SOLUTIONS *

Sh. Sh. IBRAGIMOV and B.G. LIVSHITS

(Reeeived 12 June 1956)

In the article a consideration is made of changes in the properties and microstructure of the Ni-Cr and Ni-Cr-Fe solid solutions subjected to thermal and cold-working treatments. Thermal treatment of the investigated alloys results in a considerable modification in the properties and microstructure of the alloys but it is not accompanied by the appearance or dissolution of any new phase. The curves of "properties vs. cold-working" have anomalous shape for normal solid solutions. This anomalous variation in the properties of alloys under investigation is explained by the setting in, in the solid solution lattice, of a process that is diffusion-like and results in modification of the atomic structure of solid solutions. A study is made of the kinetics and a determination given of the process activation energy.

In the investigation of ohmic resistance of alloys, which by their nature can be classified as solid solutions, an anomalous variation was found of the electrical resistance as a function of temperature. This points to a special condition of the alloys [2,4] in order to explain the nature of this condition. All of it points to the obvious lack of experimental data

The purpose of the present work was to study the phenomenon intensively in the Ni-Cr (21.4 per cent by weight of Cr) and Ni-Cr-Fe (57.4 per cent Ni and 16.55 per cent Cr, by weight) alloys using a variety of investigational methods: electrical resistance, dilatometry, microhardness and microstructure methods.

Depending on the rate of cooling from a temperature above 750° C, there is observed a considerable variation in the above mentioned properties of the Ni-Cr and Ni-Cr-Fe alloys, which is obviously connected with a modification in the atomic structure of the solid solutions. For instance, if an alloy of Ni-Cr is cooled at the rate of 25° C/hr, its electrical resistance increases by 5.5 per cent, microhardness by 20.8 per cent, and the lattice parameter of the solid solution is reduced by 0.003 Å in comparison with that of an alloy quenched in water.

The nature of curves obtained experimentally in order to show the variation in the electrical resistance and length of specimens subjected to heating and cooling, is anomalous. Ni-Cr alloy test-specimens, if heated after quenching to a temperature in the range of 420-530° C, show an intense increase in electrical resistance, which diminishes gradually, starting with the temperature of 530° C, until a minimum is reached, and then begins to increase again after passing the temperature of 750° C. During cooling, the electrical resistance of specimens of the same alloy changes in the opposite direction. The electrical resistance of alloy specimens cooled to room temperature at a rate of 100° C /hr exceeds that shown by quenched specimens by 4.3 per cent. Dilatometric curves show that, during heating of quenched test-specimens, the initial expansion is uniform because of thermal coefficient; a considerable contraction is observed in the range of temperatures characteristic of a rapid increase in the electrical resistance; this is followed again by expansion, but with a different thermal coefficient. The cooling curve lies below the heating one, which shows that there is a final reduction in the volume of alloys.

Such apparently anomalous variations in the electrical resistance and volume of Ni-Cr and Ni-Cr-Fe alloys test-specimens can be explained if one starts with Thomas's hypothesis [1]. According to this hypothesis the high temperature structural state of rapidly cooled test-specimensis fixed in such a way that the constituent atoms are distributed statistically over the lattice centres; during slow cooling, however, the distribution of atoms deviates from the statistical one, with consequent formation of "atom complexes" and the occurence of chemical hetero-

* *Fiz. metal. metalloved.* 4, No. 2, 315-318, 1957 [Reprint Order No. POM 52].

VOL 4 195

gencity inside the solid solution lattice, which is responsible for an increase in hardness and electrical resistance, for a reduction in the lattice parameter, and hence also for a reduction in the alloy volume. The above assumption makes it also possible to explain the shape of the electrical resistance and microhardness curves obtained with Ni-Cr and Ni-Cr-Fe alloys as a function of the degree of cold-working deformation (Fig.1).

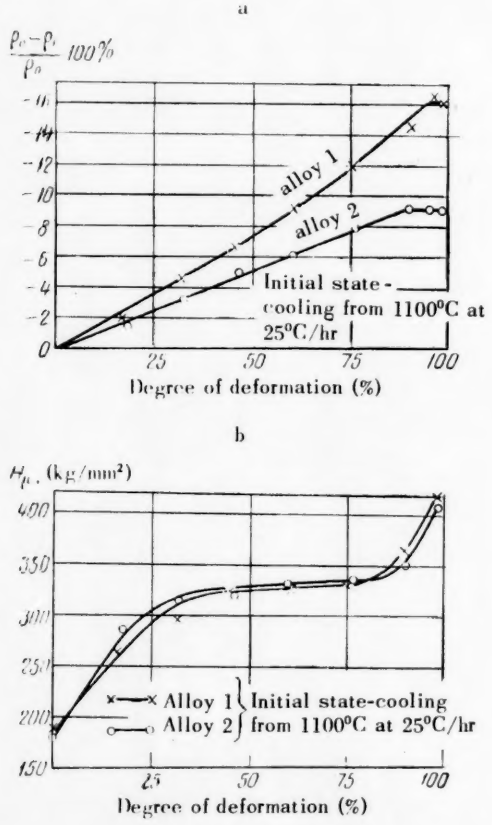

Fig.1. a – variation in electrical resistance, b – variation in microhardness of Ni.Cr and Ni-Cr-Fe solid solutions depending on the degree of cold deformation.

It is clear from Fig. 1 a and b, that the electrical resistance of the alloys reduces uniformly with increasing degree of cold deformation, and remains unaffected only if the degree of deformation exceeds 90 per cent. The microhardness of Ni-Cr and Ni-Cr-Fe alloys solid solutions increases initially with deformation, then remains almost steady for the range of deformations from 40 to 80 per cent, and finally increases again as the degree of deformation is increased to more than 80 per cent.

In all probability, the cold deformation of the alloys investigated, leads on the one hand, to an increase in electrical resistance and microhardness by causing deformation of the crystal lattice and creation of the first and second order stresses, and, on the other hand, it reduces them by destroying the "atom complexes" mentioned above. The reduction in electrical resistance of the alloys tested brought about by destruction of atom complexes (heterogeneity), is much higher than the increase in resistance due to cold working, and, therefore, the net result of cold deformation is a reduction in electrical resistance. With deformations up to 40 per cent, the first of these factors predominates and hence there is an increase in the microhardness, but as the degree of deformation is increased to 80 per cent, the two factors appear to compensate one another, with the result that the alloy hardness remains unchanged. At still higher degrees of deformation, the first of the factors becomes predominant again and leads to an increase in the alloy hardness, since the solid solution has again become statistically homogeneous as a result of deformation.

The heterogeneity in the solid solution lattice occurs within a defined temperature interval, and progresses by diffusion, as is clear from the nature of the curves for kinetics and activation energy of the process.

The activation energy of the process, calculated from variation in electrical resistance, was found to be 43,300 cal/g atom in the case of Ni-Cr alloy. Carbon atoms present in the solid solution crystal lattice were found to be responsible for an increase in the activation energy and consequently for a strong reduction in the process velocity. Thus, if the carbon content in Ni-Cr solid solution is 0.07 per cent, the energy of activation is 55,600 cal/g atom, whereas in the case of Ni-Cr-Fe alloy with a dissolved carbon content of 0.11 per cent, the activation energy amounts to 66,800 cal/g atom.

A study of process kinetics was made in the temperature range of 100-700° C. The specific electrical resistance and microhardness were taken as criteria of the degree of "heterogeneity" setting

in with the passage of time. The kinetic curves for Ni-Cr alloys are given in Fig.2 a and b.

It is clear that, in the temperature interval of 400-700° C, the velocity of the process is quite high, especially in the initial stage of "heterogeneity" formation. Thus, for instance, the specific electrical resistance and microhardness of the Ni-Cr alloy test-specimen at 450° C show a rapid rate of increase during a period of 5 hr (from 105.5 to 113 $\mu\Omega$/cm and from 156.5 to 200 kg/mm², respectively), and then increase but to an insignificant extent only: after a 500 hr period, the increase is 1.5 $\mu\Omega$/cm and 6 kg/mm² (114 $\mu\Omega$/cm and 206 kg/mm², respectively). As the temperature is increased from 300 to 700° C, the rate at which the process proceeds increases very considerably.

Some idea of the process kinetics can be gained from changes in the alloys' structure as shown during microscopic examination at comparatively small magnifications.

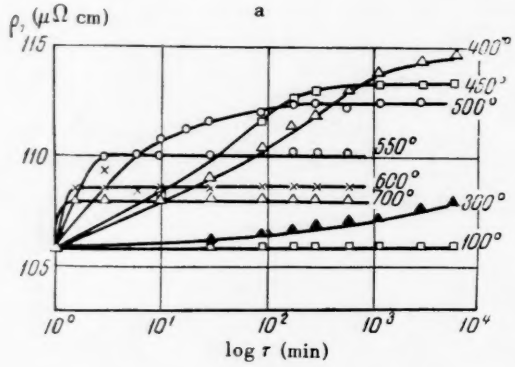

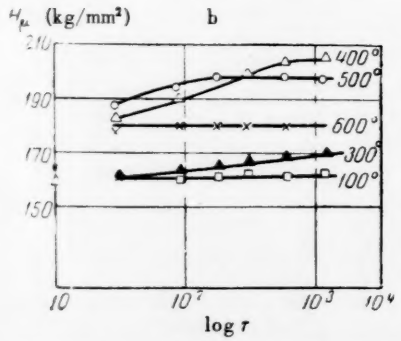

Fig.2. a – variation in specific electrical resistance, b – variation in Ni-Cr alloy microhardness at various temperatures. Values of the factors in the initial state (quenched from 770°C) are shown by triangles.

After quenching from a temperature of about 770° C, the microstructure of Ni-Cr alloy is characterized by the presence of the usual solid solution grains (grain boundaries are slightly contaminated by the separation of chromium carbide). Annealing at 350-550° C modifies the microstructure of the alloy as it is shown by the appearance, inside the solid solution grains, of parallel lines and of lines intersecting mutually at various angles (grooves). The direction of such grooves is different in different grains, and this points clearly to a connexion with the crystal orientation (Fig. 3a). The number of grooves, as well as many other properties of the alloy vary depending on the duration and temperature of the annealing treatment.

Fig. 3.a. Microstructure of Ni-Cr alloy after annealing at 770°C (x 320)

Fig.3. b. Microstructure of Ni-Cr alloy after quenching and annealing at 450°C (× 320)

VOL
4
195

As a result of microstructure investigations, by means of an examination under the optical and electron microscopes, and by X-ray analysis, it is concluded that there is no appearance of a second phase which could be held responsible for the above indicated variations in the alloy microstructure and properties.

Thus it can be concluded that two types of atomic structure are possible in the solid solutions of Ni-Cr and Ni-Cr-Fe alloys;

(1) a high-temperature structure, characterized by a statistically uniform distribution of the constituent atoms over the crystal lattice centres, and

(2) a low-temperature structure in which the constituent atoms differ, in their distribution, from the statistical distribution and form heterogeneous zones inside the solid solution lattice. It is clear that the size of the heterogeneous sections is of the same order as the wavelength of conducting electrons.

Heating above the temperature of 700° C and a subsequent cold-working deformation lead to the destruction of heterogeneity and to reversal to a statistical distribution of the constituent atoms in solid solutions of the alloys.

REFERENCES

1. H.Thomas *Z.Phys.* 129, 219 (1951).
2. A.Taylor and G.Hinton *J.Inst.Met.* 169 (1951).
3. B.G.Livshits and M.P.Ravdel *Dokl.Akad.Nauk SSSR* 93, 6 (1953).
4. I.I.Kornilow and R.S.Mints *Dokl.Akad.Nauk SSSR* 95, 3 (1954).

VOL.
4
1957

VOLUME CHANGES IN THE CARBIDE PHASE DURING ANNEALING OF STEEL *

N.N. LYULICHEVA

(Received 6 June 1956)

The volume changes in the carbide phase in steels with heterogeneous structure were studied by spatial metallography using the optical and electron microscopic methods. The study was made on carbon steel, chrome steel and manganese steel annealed in the temperature interval of 450-700° C. Determination was made of the carbide-phase volume variation as a function of temperature and duration of annealing. A theory is put forward for the structure of carbide phase at low annealing temperatures.

INTRODUCTION

It was found during electron microscopic examination of the structure of annealed steel, that the actual amount of the carbide phase present is higher than it should be expected according to the carbon content as given by the formula of Fe_3C [1-3]. The observed disrepancy is explained by some authors in terms of the ferrite being screened by carbide particles present and by other inaccuracies involved in electron microscopic photography, but no experimental or theoretical proof of such assumptions could be found.

On the other hand, many experiments are described in technical literature on the basis of which the conclusion was reached that the low temperature carbide contains more iron than required by stoichiometric ratio according to the formula Fe_3C.

As long ago as 1914, Baikov [4] found that the graphite present in high carbon alloys contains iron in an amount that is higher the lower the carbon content in pig iron. Since graphite results from decomposition, Baikov concluded that cementite represents a solid solution capable of existing with an excess iron content.

Test data are also available, on the basis of which it can be shown that the hardness of cementite varies in function of thermal treatment. Rozanov [5] made a study of cementite hardness in pure high-carbon alloys with a carbon content of 4.1-4.2 per cent and in the presence of impurities amounting to only 0.4 per cent.

As the quenching temperature is increased from 750-800°C to 1100°C, the cementite hardness drops from 750-800 H_B to 600-550 H_B. Rozanov concluded on the basis of his test data that cementite represents a solid solution deficient in carbon content. No determination was made by Rozanov of the total volume of the carbon phase.

Entia and others [6], having found higher ferromagnetic characteristics in low temperature carbide, and a higher velocity of its formation (while the diffusion velocity of carbon at these temperatures is low), also came to the conclusion that carbide contains an excess of iron.

Apaev [7], on the other hand, explained the lowering in the magnetization curves obtained after re-heating of an annealed steel by assuming that the carbon content in a low temperature carbide is higher than that in cementite, and that the carbide composition approaches that corresponding to the formula Fe_3C as the annealing temperature is increased, and is accompanied by a simultaneous increase in volume. Some other authors are of the opinion that the carbon content in low temperature carbide is higher than that in cementite [8,9].

To date there is no known determination of the carbide-phase volume by the metallographic method. The purpose of the present work is a systematic determination of the carbide-phase volume from the microstructure of steels with different carbon contents annealed at various temperatures.

PURPOSE OF INVESTIGATION

In this work, test results are given from an investigation carried out on steel grades 25, U7 and

* *Fiz. metal. metalloved.* 4, No. 2, 319-330, 1957 [Reprint Order No. POM 53].

U10, with carbon contents of 0.31, 0.68 and 1.06 per cent, respectively, as well as on chrome steel with 1.65 per cent Si and 0.6 per cent C contents (grade 60S2), and on manganese steel with 1.7 per cent Mn and 0.41 per cent C (grade 45G2).

In order to obtain structures as diverse as possible, the steels were subjected to quenching and subsequent annealing at temperatures in the range of 450-700°C, the duration of annealing being from 2-50 hr.

Polished samples of heat treated test-specimens were photographed under an optical metallurgical microscope with magnification of 1200, and under an electron microscope with magnification of 4500.

The plastic film technique was used for the making of electron microscope photographs, since the resolving power obtainable with this method is sufficient for the purposes of the present investigation.

VOL. 4 1957

TEST PROCEDURE AND ITS PRINCIPLE

For the purpose of calculating the carbide phase, use was made of A.A. Glogolev's point method, According to it, the percentage of a given phase in the structure is equal to the percentage of points, uniformly distributed over the microstructure, which fall on the phase. The accuracy of the method is the higher the greater the number of points distributed over the structure (not less than 200), and the greater the percentage content of the phase under investigation in a given structure [10].

In practice, the calculation of points falling on the carbide phase is done by means of a transparent plate having on its surface a photographically transferred square network which contains $27 \times 27 = 729$ intersection points of two sets of straight lines on an area of 80×80 mm. At least four counts were taken for each photomicrograph, the position of the network being different in each case. Measurement of the area occupied by the carbide phase in thin sections was made on both the optical and electron microscope photomicrographs.

Since an opinion is expressed in technical literature [1-3], that the carbide-phase volume, as observed on photomicrographs, differs considerably from the calculated value, it becomes necessary to consider this question in detail. A.I.Gardin [1] put forward a concept illustrating the appearance of new carbides with a more intense etching. In this way, the author explains the higher carbide phase content determined in electron microscopic micrographs. It is not difficult, however, to see that the explanation given by Gardin (see [1], Fig.97, p.156). is artificial and can be characteristic of an etching process occurring in a small section having only a few carbide particles. The artificiality of the idea proposed by Gardin can be seen from the fact that, if a fourth section is made on the diagram explaining his idea, so that it corresponds to a still greater depth of etching, there is only one carbide particle to be found in the section (instead of the eight particles as found by Gardin in the third section). Thus Gardin's diagram could illustrate with equal success both an increase as well as a reduction in the carbide phase, if it were observable. In real structures having hundreds of carbide particles in the field of vision, no sharp variation was ever noted in the number of carbide phase particles per unit thin section area for various depths of etching. According to the probability theory, there should be an identical number of carbide-phase particles in any section and, consequently, also in any layer of an etched thin-section specimen. With deeper etching and the removal of ferrite layer, there appears a certain number of new carbide particles, but, simultaneously, an identical number of carbide particles is dislodged from the ferrite, etched, and consequently removed from the thin-section during washing.

As far as the explanation in terms of the screening effect is concerned [1,2], it is quite clear that this phenomenon does take place although not to such an extent that it could be used as an explanation for the observed volume of the carbide phase (V_0) being greater than its theoretical value. An increase in V_0 by relief etching used for the preparation of plastic film, could occur but only because of an apparent increase in the size of such carbide particles whose maximum cross-section lies below the thin-section plane, or it could be due to ferrite screening by those carbide particles whose maximum cross-section lies, on the other hand, above the plane of thin-section. The maximum error in the determination of V_0 in both of these cases, can be calculated on the assumption that, instead of the average cross-section area, use is made of the maximum cross-section area of carbide particles. If an assumption is made that all carbide particles are in the form of equal spheres, the average carbide

particle section diameter in the thin section plane will be 0.875 parts of the maximum diameter, and the average area of cross-section will, consequently, be 0.62 parts of the maximum carbide particle cross-section area. This maximum error (about 40 per cent) in the determination of V_0 as a sum of the maximum cross-section areas of all the carbide particles, can occur only in the case of etching depth of the order of half carbide-particle diameter. First of all, such a depth of etching employed during the preparation of plastic films and, secondly, an increase in the value of V_0, even by 40 per cent as a result of screening is still incapable of explaining the considerable increase in the carbide-phase content as determined on electron microscope photographs.

In our investigations it was found that the observed value of V_0 was 4-5 times higher than the theoretical one.

In order to reduce the error due to ferrite screening, special attention was paid in our investigations to the etching of thin-sections. All such thin-sections, which were to be used for electron microscope study, were invariably subjected to examination under an optical microscope having in comparison with the electron microscope, only a small depth of sharpness. Etching was done in such a way that the smallest possible relief depth was obtained. Furthermore, the depth of etching could be controlled by studying the width of "shadows" near carbide particles, as visible in the enclosed electron micrographs. Since the vacuum deposition of chromium in the plastic films was done at an angle of 8°, the etching depth can be calculated as follows. The width of shadows obtained on all electron micrographs ($\times$ 4500) did not exceed 0.3 – 0.4500 mm, and hence the depth of etching h is given by:

$$h = \frac{0.3 \tan 8^\circ}{4500} = \frac{0.3 \times 0.14}{4500} = 9.3.\ 10^{-6}\ \text{mm}.$$

The diameter of carbide particles on the electron microscopic photographs of the steels investigated is of the order of 2.10^{-4} to 1.10^{-3} mm. Consequently, the etching depth was of the order of 0.05 – 0.009 of the carbide particle diameter. As it was shown above, the maximum error, because of screening, occurs during etching to a depth not less than half of the carbide particle diameter. The etching to a depth equal to several hundredths of the carbide particle diameter gives an error that is many times smaller. However, a theoretical calculation of the error brought about by the depth of etching in the measurement of V_0 is extremely difficult because of the irregular shape of carbide particles, and therefore only an experimental evaluation was made of the error that might be involved in the measurement of V_0.

An increase in V_0, as compared with its theoretical value, was observed also in our investigations under the optical microscope. A carbide detection method involving the use of sodium picrate staining was employed in investigating the effects exerted by the depth of etching. Etching with sodium picrate gives no relief on thin-section and, therefore, this method could not be used in the preparation of plastic films. Parallel calculations based on photomicrographs of thin-sections of test specimens, etched with sodium picrate and alcoholic 4% HNO_3, showed that the maximum discrepancy in the measured value of V_0 does not exceed 10 per cent of the figure obtained. In order to check that no distortions take place in the structure of specimens during the preparation of plastic films, photographs were made of some of the films, shaded with chromium, also under the optical microscope with magnification of 1200. Plastic film photography is rather difficult because, first of all, the films are not sufficiently flat for the comparatively large field of vision in the optical microscope, and therefore it is difficult to obtain good sharpness of the whole image simultaneously, secondly, the casts are transparent and only little light is reflected. The darker colour of carbides as obtained on optical photomicrographs of plastic films (Fig. 1b) is due to the fact that the semi-transparent films are coloured: carbides are shown in red and ferrites in blue.

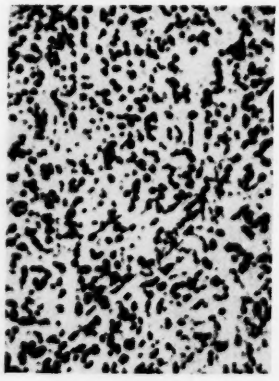

FIG. 1a.

b

c

FIG. 1. Microstructure of C10 steel. Annealing for 680°C for 5 hr, V_t = theoretical volume of the carbide phase = 16.3 per cent, (x 960).
a – sodium picrate etching, V_0 = 24.4 per cent
b – etching with alcoholic 4% HNO_3, V_0 = 24.8 per cent
c – plastic film from thin section etched with alcoholic 4% HNO_3 solution, V_0 = 27.0 per cent.

Values of V_0, as obtained from plastic film photographs, were analogous to those obtained from V_0 determinations on micrographs of thin-sections of test specimens etched with a alcoholic 4% HNO_3 solution (Fig. 1 a and b).

The fact that at least a double increase was found in the value of V_0, as compared with the theoretical value also in measurements obtained on the basis of optical photomicrographs, can be regarded as an additional proof that this increase in the V_0 value should not be explained as being due to inaccuracies inherent to electron microscope studies of structure. The microstructure of Y10 grade steel test-specimens, as seen under an optical microscope, is shown in Fig. 2. For the same annealing temperature, the value V_0 obtained after a 10 hr period of treatment is twice as high as that obtained after 51 hr treatment.

a

b

FIG. 2. Microstructure of steel Y10 with different observed carbide-phase volume. Etched with 4% alcoholic HNO_3.
a – annealed at 650°C for 51 hr, Y_0 = 16.3 per cent (x 960);
b – annealed at 650°C for 10 hr, V_0 = 37.5 per cent (x 1440).

In the light of the above considerations, the conclusion can be drawn that the higher observed volume of the carbide phase cannot be due to some sources of errors associated with the electron microscope study of structure, but that it must be caused by other factors, which will be evaluated in what follows. Since the relief etching brings no essential errors into the determination of V_0, only one type of etchant was used, alcoholic 4% HNO_3, for both the optical and electron microscope thin sections, so that only one etching process could be used in both cases. The photography of highly dispersed structures was done under the electron microscope, structures with an average dispersion were photographed under both the optical and electron microscopes, and coarsely dispersed structures were photographed under the optical microscope only, since in the case of these structures

VOL. 4 1957

the field of vision in the electron microscope did not contain carbide particles in a quantity sufficient for a statistical calculation of V_0.

EXPERIMENTAL RESULTS

Carbon Steels

Using the test procedure described above on both the optical and electron microscopic micrograms, the carbide phase volume V_0 was determined, the ratio of the experimentally determined carbide-phase volume V_0 to its theoretically calculated value was derived, and a calculation was made of the average cross-section area of a single carbide particle.

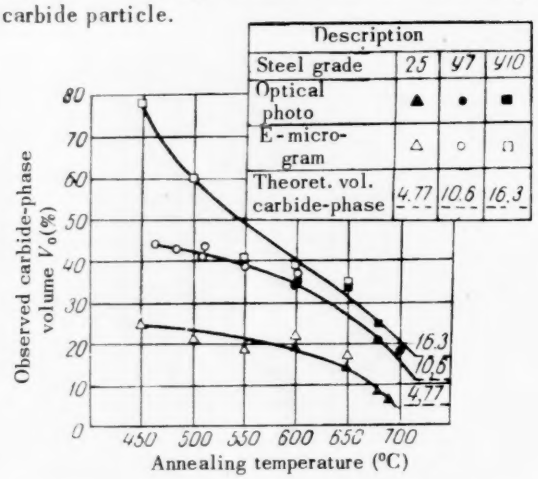

FIG. 3. Effect of annealing temperature on the change in carbide-phase volume for a 10 hr annealing period.

Results of V_0 determinations for steel grades 25, Y7 and Y10, annealed at various temperatures are given in Fig.3. It is seen from these curves that, as the temperature is increased, the observed value of the carbide-phase volume approaches its theoretically calculated value. The ratio V_0/V_t varies, for steel grades 25, Y7 and Y10 annealed during 10 hr, from 5.2, 4.2 and 4.8 at the temperature of 450 °C, to 1,3, 1.7 and 1.5 respectively, at the temperature of 680°C. Therefore, ratio of V_0/V_t is determined by the annealing conditions and is independent of the carbon content. For an identical duration of annealing, the observed carbon-phase volume increases with increasing carbon content in steel. In Fig.4 is shown the dependence of V_0 on the carbon content at various annealing temperatures.

As the annealing period is increased at any annealing temperature, the change in V_0 is most intense during the first 10 hr of annealing. The subsequent reduction in the observed carbide-phase volume takes place exceedingly slowly, as shown in Fig.5. At higher annealing temperatures, the initial change in V_0 is much more pronounced. In order to illustrate the effect of thermal treatment in the carbide-phase volume, photomicrographs are given in Fig.6 of test-specimens in Y10 steel with various V_0 values. The shorter the annealing period, the lower the annealing temperature and the higher the carbon content of steel, the greater is the volume of carbide phase observed in its microstructure.

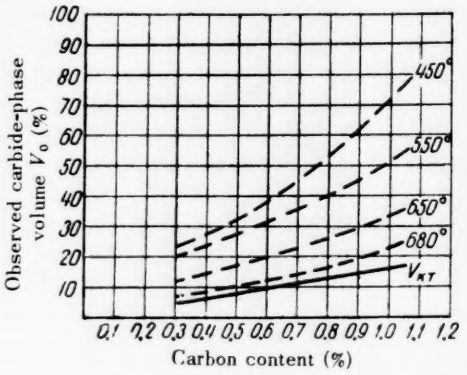

FIG. 4. Effect of carbon content in steel on the observed volume of carbide phase.

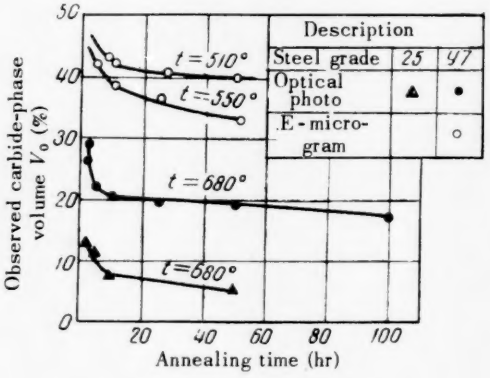

FIG. 5. Change in the carbide phase volume during annealing from various temperatures

a

b

c

FIG. 6. Electron micrographs of specimens in Y10 grade steel with various observed carbide-phase volumes; (x 4500):
a – annealing at 450°C, 12 hr, V_0 = 78 per cent
b – annealing at 550°C, 25 hr, V_0 = 37 per cent
c – annealing at 680°C, 5 hr, V_0 = 27 per cent.

Alloyed Steels

Two alloyed steels were investigated: 60S2 steel, alloyed with a non-carbide-forming element, and grade 45G2 steel, which was alloyed with a carbide-forming element. Test- specimens were annealed at temperatures of 500 – 600°C during 25 and 50 hr.

A study of the electron micrographs obtained with annealed chrome steel shows that chromium leads to a slight dispersion of the carbide phase. Thus, after annealing at 500, 550 and 600°C for 25 hr, the average surface area of the carbide particle in grade 60S2 steel specimens amounted to 0.53, 0.76 and 1.38 × 10^{-7} mm², and for steel grade Y7 – to 2.1, 2.9 and 5.1 × 10^{-7} mm² correspondingly.

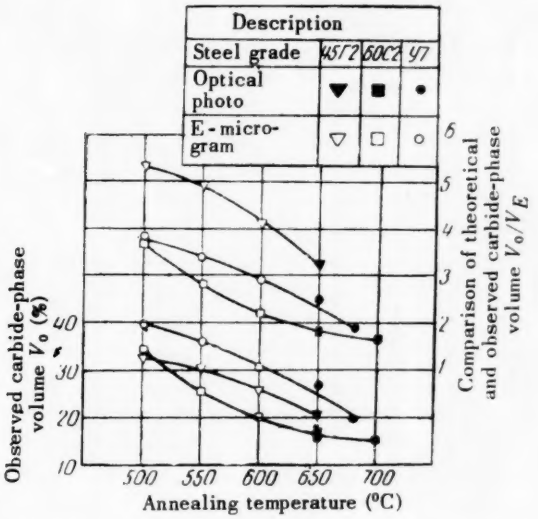

FIG. 7. Effect of manganese and silicon on the observed carbide-phase volume V_0 after annealing for 25 hr. For steel 6052, V_t = 9.25 per cent; for steel 45G2, V_t = 6.32 per cent.

Fig.7 shows the effect of chromium and manganese on the volume of carbide phase after an annealing period of 25 hr. In grade 60S2 chrome steel, the volume of carbide phase is slightly lower than that determined for Y7 grade carbon steel having numerically the same carbon content. In the case of manganese steel, the value of V_0 is lower than that for the grade Y7 carbon steel (0.68 per cent C), because of a lower carbon content (0.41 per cent), provided that the annealing conditions are identical in both cases. However, one can see from Fig. 7 that the relative increase in V_0, in comparison with its theoretical value, is greater for manganese steel than for both the carbon and chrome steels. Consequently, the carbide forming element (Mn) leads to an increase in the carbide-phase volume, and the non-carbide forming element (Si) reduces it.

EVALUATION OF TEST RESULTS

The test results given enable us to conclude that the observed carbide phase forming at low temperatures occupies a volume that is several times greater than its theoretical value. With increasing annealing temperatures, the observed carbide-phase volume gradually diminishes and coincides with the theoretical value for annealing

temperatures of 650-700°C. The regularity of variation in the carbide-phase volume during the annealing process points to the fact that the phenomena observed cannot be explained in terms of inaccuracies involved in the experimental procedure used, and that the carbides detectable microscopically were formed at low annealing temperatures and their composition does not correspond to the formula Fe_3C. This can be explained only if on assumption is made that the carbides detectable by metallographic methods contain less carbon than it corresponds to the formula Fe_3C.

The concepts advanced above can be confirmed by data reported in technical literature. According to the chemical [11] and X-ray [12] analyses, the carbide phase represents cementite, with the formula Fe_3C, over the whole range of the annealing temperatures investigated (starting with 200°C). As reported by Kurdumov, Isaichev, Apaev [7] and Permiakov [13], the carbide formed at low annealing temperatures corresponds to the formula Fe_xC, and as the temperature is increased, it passes into cementite Fe_3C (according to Permiakov, this transformation of Fe_xC into Fe_3C goes through an intermediate carbide stage). The mechanism of carbide-phase formation during the annealing of steel should not be decided soley upon on the strength of results obtained from metallographic investigations. The only certain thing that emerges from such investigations is that the hard, unetched carbide particles represent a structure with a carbon content that is lower than in cementite. However, it is still not clear in what combination carbon exists in the carbide phase.

If one considers Arbuzov's point of view [12], according to which cementite particles forming during annealing at temperatures between 200 to 700°C are in the form of flakes $2-9.10^{-5}$ mm in demensions, then the microscopically detectable carbides having linear dimensions $\sim 10^{-3}$ to 10^{-4} mm, should be regarded as conglomerates consisting of much smaller submicroscopic flakes of cementite and of particles of the solid solution. It is possible that during electrolytic separation of carbides from steel there occurs a breakdown of these conglomerates, the ferrite trapped inside the conglomerate particles dissolves, and only the undecomposed cementite particles, whose dimensions should be smaller than those of the initial large compounds, are deposited. Gardin's investigations [1] lend support to such a theory. The carbides formed after isothermal transformation in the Y12 steel grade have a diameter of $4.0.10^{-2}$ to $4.0.10^{-3}$ mm, [1] Fig. 147). On the other hand, electron micrographs of electrolytically separated cementite particles show particles with linear dimensions of $8.0\,10^{-5}$ to $4.0\,10^{-4}$ mm([1] Fig. 138)which are of a lower order. Furthermore, the carbide particles separated out at temperatures of 250 – 500°C have a porous, spongelike nature and hence the inner pores of the structure representing such a conglomerate must be filled with α - solid solution. It is only after an isothermal transformation at a much higher temperature, of the order of 600 – 680°C, that the carbides assume a dense structure and show no porosity ([1] Figs. 134-141).

The formation of carbides having within their structure blocks of α-solid solution can be represented as follows. The nuclei of cementite begin to form in places where, owing to changeable conditions, a concentration of carbon is created which approaches that present in cementite. The growth of individual nuclei is the faster the higher the temperature. Because of insufficient velocity of carbon diffusion at temperatures lower than 450 – 500°C, no coagulation of carbide particles sets in and, instead, zones are formed which contain cementite nuclei. It is probable that inside these zones which are within the observed carbide constituent, the diffusion of carbon can proceed much eaisier than in a homogeneous α-solid solution. As the temperature is increased from 200 to 500°C, the diffusion of carbon within these zones takes place in such a way that the number of individual cementite nuclei within the observed carbide constituent increases, the content of α-solid solution diminishes, and the amount of structurally-free α-solid solution increases.

If it is assumed that the carbide formation theory as advanced by Kurdyumov and others is true, it then becomes necessary to account also for the fact that carbides formed at low temperatures should have a larger volume, which reduces gradually as the temperature is increased. Thus, the carbide Fe_xC should contain more iron within its structure at the moment of its separation, than present in cementite with the formula of Fe_3C, i.e. the index x should be greater than 3. As the heating temperature is increased, the carbide Fe_xC should undergo a change in its composition and approach gradually that corresponding to Fe_3C, or the transformation $Fe_xC \rightarrow Fe_3C$ should proceed continuously in such a way that there would be a reduction in the in the overall volume of the carbide constituent

VOL
4
195

and its carbon content should be increasing.

Since at 500°C, the volume of the carbide phase is still different from the calculated one, the processes occurring within the carbide phase are not yet completed and continue to occur concomitantly with the coagulation which starts at this temperature. It should be remarked that the number of carbide particles diminishes before 500° is reached, but that there is no increase in their dimensions or, in other words, the process of coagulation has not yet become of predominant importance. At any temperature lower than 500°C, when carbon is still incapable of intense diffusion through the solid solution, i.e. when the extent of carbide coagulation is insignificant, there is possible an overall reduction in the carbide-phase volume because of a "shortening" of each carbide particle observed. Thus, the dimensions of carbide particles, as seen under a microscope, should decrease rather than increase as the annealing temperature is raised from 200 – 250 to 450 – 500°C. In our tests, no annealing was undertaken at temperatures below 450°C. However, with steel grades 25 and Y10 annealed at 450°C for 10 hr, the average cross-sectional area of carbide particle, as determined on thin sections, was greater than that found for specimens annealed at 500°C (Fig. 8). Photomicrographs of specimens in Y10 steel grade (see Fig.6) also show that a reduction in the size of carbide particles bebegins noticeably only at temperatures higher than 550 – 600°C.

Such "shortening" in the size of carbide particles with increasing temperature of annealing is also detectable on electron microscope micrographs Zemler [4]. In the table that follows, values are given of the observed carbide-phase volume V_o, the ratio of observed to theoretical volumes V_o/V_t, and the average cross-section area of a single carbide

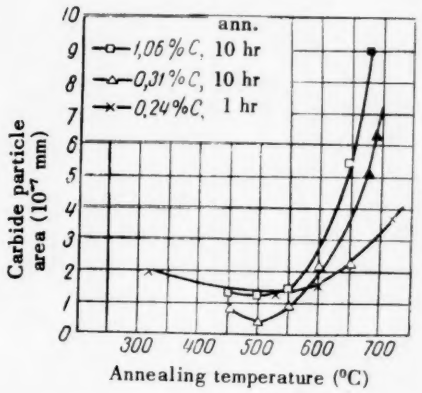

FIG. 8. Effect of annealing temperature on the size of carbide particles in carbon steels.

particle V_o/n (where, n = number of particles in 1 mm² of thin section), the data being calculated from Zemler's photomicrographs.

It can be shown by calculation that the size of carbide particles obtained with an annealing temperature of 320°C is greater than that for annealing temperatures of 530 and even 600°C. The total volume of the carbide phase at 320°C is nearly eight times greater than the theoretical volume.

Thus, no confirmation was found of B.A.Apaev's hypothesis that the low-temperature carbide with the formula of Fe_xC is richer in carbon than cementite Fe_3C, and that with increasing temperature of heating, the volume of carbide phase increases because of the transformation $Fe_xC \rightarrow Fe_3C$. The lowering of magnetization curves, observed by many investigators during the heating of annealed test-specimens, cannot be explained by an increase in the volume of the phase that is paramagnetic at temperatures higher than 210°C (cementite). Clearly, this lowering is accounted for by variation

TABLE 1. Effect of annealing temperature on the volume of carbide phase in steel containing 0.24 per cent C (calculation based on Zemler's electron photomicrographs)

Annealing temp. (°C)	Annealing period (hr)	Carbide-phase volume, observed (%)	Carbide-phase volume, theoretical (%)	Ratio V_o/V_t	No. of carbides in 1 mm² $n.\ 10^6$	Average cross-section area of carbide particles $V_o/n.\ 10^{-7}$ (mm²)
320	1.0	28.6	3.7	7.7	1.49	1.97
530	1.5	15.4	3.7	4.2	1.21	1.25
600	1.0	13.2	3.7	3.6	0.83	1.59
720	1.5	11.8	3.7	3.2	0.32	3.67

in the magnetic properties (including also the Curie point) of that carbide constituent in which there is a rise in the carbon content during the heating process. If, on the basis of the Apaev [7] curves, an approximate determination is made of the second Curie point A_x for the carbide phase in Y10 steel grade test-specimens subjected to a 5 hr annealing period, one finds that there is a simple linear relationship between the values of A_x and those of V_0 corresponding to the same temperatures. For annealing temperatures of 400, 500 and 600°C, it is possible to assume that the approximate values of A_x are 273, 261 and 248°C, respectively (on the basis of Apaev's curves); according to our test data, the values of V_0 for the same temperatures and for a 10 hr annealing period, are ~90, 60 and 39 per cent, respectively. In other words, the higher the iron content in the carbide phase the higher its magnetic properties.

With regard to hardness of the carbide phase, it can be assumed that it will be the higher the higher the carbon content in the carbide constituents. An increase in the annealing temperature in Rozanov's [5] experiment mentioned previously which leads to the formation of a more homogeneous austenite, obviously favoured the formation, after annealing, of a cementite that was strongly "diluted" with iron, and hence its hardness was also higher.

As regards the mechanical properties of a heterogeneous phase structures consisting of ferrite and carbide, it can be assumed that it is only the soft phase (the ferrite) that is capable of plastic formation. A variation in the carbide hardness occurring as a result of changes in its composition can, of course, be neglected since the hardness of carbide is always incomparably higher than that of ferrite. In such a case, the higher the amount of the plastic phase present, i.e. of the structurally free α-solid solution, the higher the plasticity of the whole alloy. The particles of the α-solid solution, which are included inside the carbide-phase structure, cannot take part in plastic deformation. Therefore, in calculating the volume of the hard phase it is necessary to use the value of volume V_0 as actually observed under a microscope and not the calculated one.

CONCLUSIONS

1. It was shown that the observed volume of carbide phase at low annealing temperatures is considerably higher than its theoretical value. This phenomenon cannot be explained by imperfectness of experimental procedure.

2. It was found that, as the temperature and duration of annealing are increased, the observed volume of the carbide phase diminishes regularly, but is always higher than the calculated values. Only if the annealing temperature is higher than 650°C and if the duration of annealing is 25-50 hr, the observed volume of the carbide phase approaches its theoretical value (corresponding to the formula (Fe_3C).

3. It was shown that carbide particles observed microscopically contain less carbon than is present in cementite. The low temperature carbide consists of either separate submicroscopic blocks of cementite and the α-solid solution, or it represents the solid solution of cementite and the α-phase. As the temperature and duration of annealing is increased, the carbon content in carbide also increases.

4. The generally accepted concept that there is a continuous rise in the size of the carbide particles with increasing temperature of annealing, was not confirmed. It was found that, as the annealing temperature is increased from 200 to 500°C, there is a reduction in the size of carbide particles, and that as the annealing temperature is raised to 500–700°C, the dimensions of the carbide particles observed increase.

5. It was found that manganese, a carbide forming element, increases (by comparison with carbon steel) the observed volume of carbide phase; however, silicon, a non-carbide forming element, reduces it.

REFERENCES

1. A.I. Gardin *Elektronnaya mikroskopiya stali (Electron microscopy of steel).* Metallurgizdat, 1954..
2. R.M. Lerinman, V.D. Sadovskii and A.M. Polyakov *Izv. Akad. Nauk SSSR, ser. fiz.* 15, 3, (1951).
3. N.N. Buinov and R.M. Lerinman *Zavod. Lab.* No.2 (1949).
4. A.A. Baikov and *Sb. Trud.* 2, pp.82-97 (1948).
5. A.N. Rozanov *Metallovedenie i termicheskaya obrabotka (Metal working and thermal treatment)* Symposium. GONTI, Moscow No. 1 (1954).
6. D. Entia, S. Fletcher and M. Cohen *Trans. Amer. Soc. Metals* 32 (1944).
7. B.A. Apaev *Zh. tekh. fiz.* 7 (1953).

8. O. Krisement, *Ark. Phys.* No.4, 353-355 (1954).
9. A.Z. Tsou, I. Nutting and I.W. Menter *J. Iron St. Inst.* 172, 12, 63 (1952).
10. S.A. Saltykov *Vvedenie v stereome tricheskuyu metallografiyu (Introduction to stereometric metallography)* Izv. Akad. Nauk Armyansk SSR, 1950.
11. N.M. Popova and M.F. Rybina *Zavod. Lab.* 3 (1950).
12. M.P. Arbuzov, *Voprosy fiziki metallov i metallovedenie* Akad. Nauk Ukr. SSSR, Kiev (1952).
13. G.B. Permiakov *Zh. tekh. fiz.* 25 (1955).
14. A. Semmler *Arch. Eeisenhuttenw.* 6, 223 (1942).

VOL.
4
1957

RECRYSTALLIZATION TEXTURE IN LOW-CARBON STEEL AFTER COLD ROLLING*

K.V. GRIGOROV and G.P. BLOKHIN

(Received 6 August 1956)

The development of recrystallization texture on low-carbon steel after cold-rolling has been studied by magnetization measurements over a wide range of previous deformation. An attempt is made to explain the observed correlations on the basis of a theory about nucleation in recrystallization.

The object of our work was to study the development and change of texture produced during recrystallization as a function of the annealing temperature and previous deformation, the latter being varied over a wide range.

The recrystallization texture developed on iron and low-carbon steels at large deformations has been established by X-ray studies [1-3]. It can be described by the following grain orientations:

1. The (001) plane is parallel to the rolling direction, and the [110] direction is at 15° to the rolling direction. In our paper we symbolize this as (001) [110] ~ 15°.

2. The (112) plane is parallel to the rolling plane, and the rolling direction is 15°nto the[110] direction, which we symbolize (112) [110] ~ 15°.

3. The (111) plane is parallel to the rolling plane, and the [112] direction is parallel to the rolling direction.

At large deformations the recrystallization texture in transformer steel is similar to that in iron and low-carbon steels [4, 5]. Let us call it a recrystallization texture of the second kind. The recrystallization texture formed in transformer steel at small deformations [6-10] can be represented as (100) [001] and (110) [001]. This we shall call a texture of the first kind.

To study the variation of recrystallization texture in low-carbon steel specimens whose cold-rolling texture has already been determined were annealed at various temperatures (in salt baths to protect them from oxidation). After annealing the specimens were cooled in air.

MEASUREMENT OF THE NORMAL COMPONENT OF MAGNETIZATION IN COLD-ROLLED SPECIMENS AFTER RECRYSTALLIZATION

The normal component of magnetization $I_n(\phi)$ as a function of the angle to the rolling direction ϕ was measured in recrystallized specimens of low-carbon steel having been cold-rolled to various percentage reductions. Figs. 1 and 2 show the variations of I_n with ϕ in cold-rolled specimens before and after annealing at 700°C. Curve 1 is for a specimen with a reduction $d_0/d = 3.54$, and curve 2 for the same specimen after 4 hr annealing at 700°C.

Fig.1 shows that the curves are quite different; this is because of differences in texture. After recrystallization we see that the minimum magnetization energy is at $\phi = 90°$, which means that crystal axes of the <100> type are perpendicular to the rolling direction.

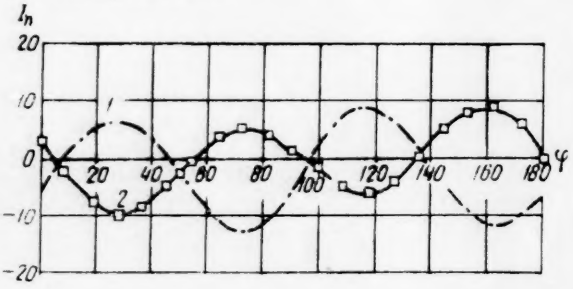

FIG.1. Variation of I_n with the angle of ϕ to the rolling direction in specimens of cold-rolled low-carbon steel with a small reduction, after recrystallization: 1: before annealing; 2: after annealing at 700°C for 4 hr.

Curve 1 of Fig.2 shows the variation of I_n with ϕ for a specimen cold rolled to $d_0/d = 230$, while curve 2 shows the variation for the same specimen annealed 1 hr at 700°C, during which initial recrystallization occurred. It will be seen that at large reductions the variations of I_n with ϕ are approximately the same before and after annealing, but the absolute value of I_n is considerably smaller after annealing. Here it may be con-

* *Fiz. metal. metalloved.* 4, No. 2, 339-343. 1957 [Reprint Order No. POM 54].

jectured that the recrystallization texture is very similar to the cold-rolling texture.

The $I_n - \phi$ variation, experimentally found for each specimen can be resolved by harmonic analysis [11] into the following Fourier series: for $d_0/d = 2.43$: $I_n(\phi) = 5.7 + 2.4\sin(2\phi + 169) + 4.0\sin(4\phi + 183) + 0.2\sin(6\phi + 210) + \ldots$ and for $d_0/d = 231$, i.e. specimens with large reductions: $I_n(\phi) = 31.4 + 4.2\sin(2\phi + 179) + 26.7\sin(4\phi + 2) + 0.4\sin(6\phi + 7) + \ldots$ which to a first approximation can be written:

$$I_n(\phi) = -2.4\sin 2\phi - 4.0\sin 4\phi$$

for small reduction, and:

$$I_n(\phi) = -4.2\sin 2\phi + 26.7\sin 4\phi$$

for large reduction.

The functional type is thus the same in specimens with small and large reductions prior to annealing. We see that at low reductions the initial phase angle for the fourth harmonic is approximately 180°, and at large reductions it is close to zero. We arbitrarily make A_4 in the first half-period negative at small, and positive at large, reductions. This indicates that the recrystallization texture at large reductions differs from that at small ones.

The dependence of the amplitudes of the fourth and second harmonics of I_n on d_0/d is shown in Figs. 3 and 4. The open, half and fully black circles are for values of A_2 and A_4 for specimens annealed at various temperatures between 700 and 820°C for various times between 1 and 5 hr. We see that these amplitudes are temperature and time-independent in the ranges studied.

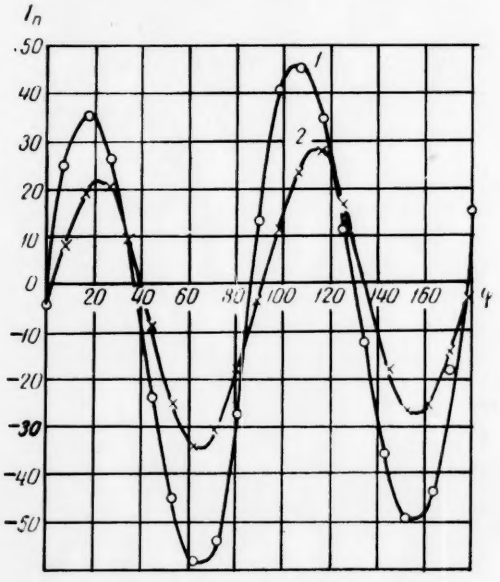

FIG.2. Variation of I_n with ϕ in specimens of cold-rolled low-carbon steel with a large reduction after recrystallization:
1: before;
2: after annealing 1 hr at 700°C.

The variation of A_2 with $\ln(d_0/d)$ is the same before and after annealing, so that we can conclude that the changes in texture due to recrystallization are characterized by the change of A_4 in Fig.3, and this is positive at small, and negative at larger, deformations. The absolute value of A_4 becomes a maximum at $\ln(d_0/d) = 1.5$, afterwards decreasing and passing through zero to become positive. At reductions for which $\ln d_0/d > 3$ it is a linear function of $\ln d_0/d$.

We may assume that the positive value of A_4 at low reductions is due to some initial texture. For example, to obtain small deformations the billet initially was rolled to thin dimensions and since it was, therefore, greatly deformed, the corresponding initial texture was fairly well developed. Even several annealings above the temperature of the allotropic transformation could not completely destroy it. Were there no initial texture the initial value of A_4 in Fig. 3 would be zero, and this gives us the basis for correcting the experimental curve at low reductions.

The corrected curve has been drawn in broken line in Fig.3; we see that after recrystallization not only the degree of perfection of texture, but also its character depends on the degree of deformation.

The variation of A_4 with $\ln d_0/d$ shown in Fig.3 can be regarded as produced by the superposition of two textures. At low reductions (d_0/d not more than 10-14) the texture of the first kind predominates, but there is some texture of the second kind, and at large reductions, the latter predominates.

The linear portion of the curve in Fig.3, extrapolated backwards, goes through the origin, proving that there is texture of the second kind at low reductions. The variation of A_4 with $\ln d_0/d$ at high reductions proves there is some texture of the first kind in this region also.

The curves for A_2 and A_4 for recrystallized low-carbon steel do not differ in shape from those for transformer steel [12] and the changes in texture in these two steel types during cold rolling are approximately the same. Recrystallization of a 3 per cent silicon transformer steel at low reductions produces a (100) [001] and (110) [001] tex-

VOL. 4 1957

ture, which is a texture of the first kind; at large reductions the recrystallization textures of transformer iron and low-carbon steel are identical. In cold rolling, the texture and the variation of the percentage of texturization with reduction are the same for these two materials also. Hence it is natural to suppose that recrystallization textures at low reductions will also be the same for both materials, i.e. (100) [001] and (110) [001]. This is supported by the identity of the crystal lattice of both metals. The slip planes and directions during deformations of the grains are also identical (for a transformer steel containing 4 per cent silicon).

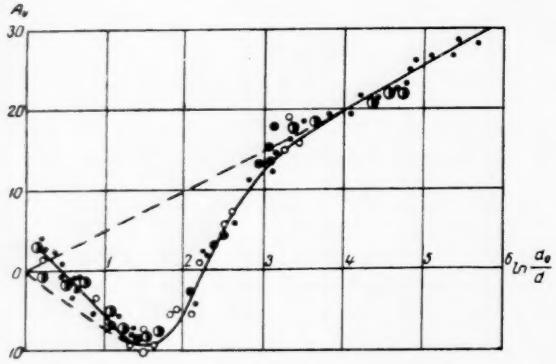

FIG.3. Variation of A_4 with ln d_0/d for cold-rolled low-carbon steel after recrystallization.

CALCULATION OF THE RELATIVE GRAIN VOLUMES OF LOW-CARBON STEELS, HAVING RECRYSTALLIZATION TEXTURES

The relative grain volumes must be calculated differently for low and high reductions. At low reductions the (100) [001] and (110) [001] texture predominates; let W_3 be the relative volume of grains with the (100) [001] orientation, and W_4 that for grains with the (110) [001] orientation. At high reductions the texture of the second kind predominates, and we will denote by W_5 the relative volume of grains having the (100) [011] $\sim 15°$ orientation, and by W_6 that of grains having the (112) [1·10] $\sim 15°$ orientation. W_3 and W_4 have been calculated [12] between $d_0/d \sim$ 1-4.5, and W_5 and W_6 at and above $d_0/d = 2$, from the corrected (broken-line) curves for A_2 and A_4 in Figs. 3 and 4 with Akulov's theory [13]. Figs. 5 and 6 show the variations of the relative grain volumes, for the orientations mentioned, with the reduction.

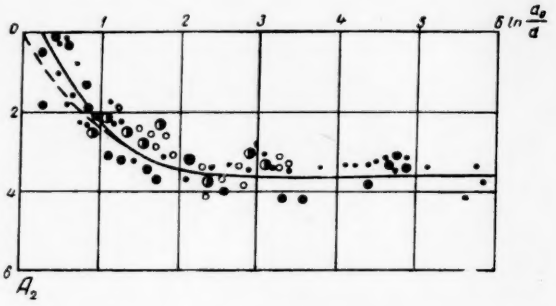

FIG.4. Variation of A_2 with ln d_0/d for cold-rolled low-carbon steel after recrystallization.

From Fig. 5 we see that the number of grains with (001) [100] and (011) [100] orientations produced during recrystallization increases between d_0/d = from 1.0 to 4.5, approximately proportional to the reduction criterion. W_5 increases linearly with ln d_0/d while W_6 is independent of it. (Fig. 6).

Let us assume that for d_0/d between 5 and 20 the texture of the first continues to develop as indicated by curve 3 in Fig.5, and the secondary texture of the second kind as indicated in Fig.6. Then at ln $d_0/d = 2.25$, where $A_4 = 0$, an extrapolation of W gives W_6 for grains with texture of the second kind about twice (actually 26-28/13-14) that of grains with a texture of the first kind.

DISCUSSION OF RESULTS

The main features of the formation and development of a recrystallization texture can be depicted thus [12]. The orientations (100) [001] and (110) [001] are stable in the deformation texture; then deformation occurs by twinning. The individual grain fragments not only preserve their orientation but it is probable that among these fragments or blocks there is a large number with comparatively little lattice distortion.

Such fragments, surrounded by strongly deformed material, are the centres for formation and growth of new crystals, that is recrystallization centres in annealing. If the reduction in rolling is slight, the deformation texture will contain both the first and second orientations indicated as stable. Crystals or their fragments having the second orientation, strain harden more rapidly than those having the first orientation, so that in the recrystallization of weakly deformed iron grains with the second orientation (110) [001] grow preferentially.

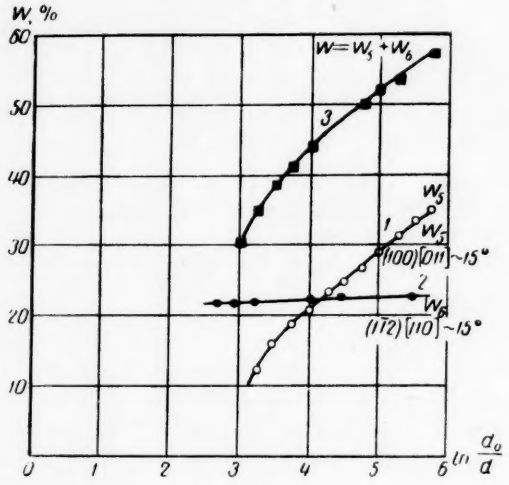

FIG.6. Variation of W_5, W_6 and $W_5 + W_6$ with ln d_0/d for cold-rolled low-carbon steel after a annealing (secondary recrystallization texture).

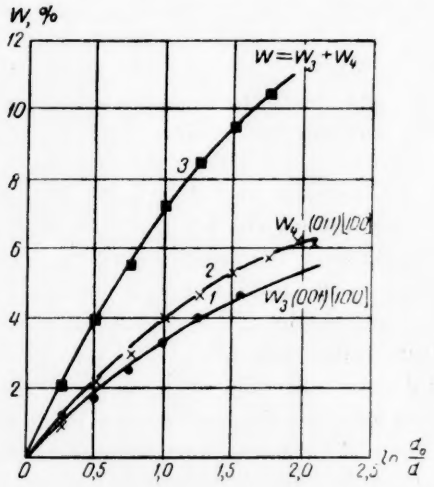

FIG.5. Variation of W_3, W_4 and $W = W_3 + W_4$ with ln d_0/d for cold-rolled low-carbon steel after annealing (primary recrystallization texture).

Actually, among the strain-hardened fragments, those having the most regular lattice may be preserved. The greatest stress gradient is then created, and the portions with the (110) [001] which are least distorted (have the least free energy) but are in a distorted environment, whose free energy is higher, will grow during recrystallization, that is will act as recrystallization nuclei [14]. From similar considerations one may also conceive of the presence of another orientation 100 <001> in the primary texture.

This scheme has many points of similarity and difference with and from the scheme of "magnetic orientation" which has been proposed by Decker and Harker [15] for transformer steel. At large reductions in rolling fragments with the first (or close to the first) orientation are the main ones which are stable, and grow preferentially in annealing, forming a recrystallization texture of the second kind.

SUMMARY

1. The nature and degree of development of recrystallization texture depends on the degree of deformation. A (001) [100] and (110) [001] texture develops strongly at low reductions. As the reduction increases a (001) [110] ~ 15°, (112) [110] ~ 15° texture comes to predominate.

2. Saturation of the recrystallization texture is not attained even at 99 per cent reductions.

3. The relative volume of grains with (112) [110] ~ 15° orientations is independent of reduction at high reductions.

4. The character and degree of development of recrystallization texture is temperature independent between 700 and 820°C.

REFERENCES

1. G.Kurdyumov and G.Sachs *Z.Phys.* 62, 592 (1930).
2. M.Gensamer and B.Justman *Trans. Amer. Inst. Mech. Engrs.* 125, 501 (1937).
3. R.Gloker *Rentgenovskie luchki i ispytaniya materialov (X-rays and material testing)*, GTTI Moscow-Leningrad, 1932.
4. C.Barrett, G.Ansel and R.Mehl *Trans. Amer. Inst. Mech. Engrs.* 125, 516 (1937).
5. Z.P.Tarasov *Trans. Amer. Inst. Mech. Engrs.* 135, 353 (1939).
6. K.I.Sixtus *Physics* 6, 105 (1953).
7. R.M.Bozort *Trans. Amer. Soc. Metals* 33, 1107 (1935).
8. G.M.Fromin and *Sb. Trud. Mosk. Inst. Stali* Issue 10, p.149 (1948).
9. J.T.Burwell *Metals Tech.* 7 (1940).
10. V.I.Smirnov *Kurs Vysshei metematiki (Course of higher mathematics)*, GITTL, 1939.
11. K.V.Grigorov, G.P.Blokhin, E.A.Korsun and M.Ya.Zakutner *Fiz. metal. metalloved.* 1, No.1 36 (1955).
12. N.S.Akulov *Ferromagnitizm (Ferromagnetism)* GITTL, 1939.
13. M.O.Kornfeld *Zh. tekh. fiz.* 4, 235 (1934).
14. B.E.Decker and D.J.Harker *J. Appl. Phys.* 22, No.7, 900 (1951).

VOL. 4 1957

THE EFFECT OF INTERMEDIATE ANNEALING ON COLD ROLLING AND RECRYSTALLIZATION TEXTURE *

K.V. GRIGOROV and G.P. BLOKHIN

(Received 20 August 1956)

Given below are some experimental findings, obtained by the magnetometer method, concerning the effect of intermediate annealing on the mechanism of changes in the cold-rolling and recrystallization texture in transformer iron and low-carbon steel.

Methods of obtaining transformer steel with high magnetic qualtities by means of cold-rolling intermediate and final annealing have been described in the group of works [1–5].Conflicting opinions are found amongst the various authors as to the effect of intermediate annealing on coldrolling and recrystallization texture.

Goss [1], studying the texture of transformer steel, came to the conclusion that intermediate annealing between two stages of cold-rolling destroys the texture which is set up in the course of the first rolling.

The appearance in Bozorth's experiments [6] and Sixtus's investigations [7] of texture of the type (110) [001] quoted by Tarasov [8] is explained only by the effect of intermediate annealing.

There has, however, been no systematic study of the effect of intermediate annealing on texture.

In this work a study is made of the effect of intermediate annealing on the development of cold-rolling and recrystallization texture.

The investigation was carried out on low-carbon steel and transformer iron having a silicon content of 3 per cent.

Blanks of low-carbon steel of thickness d_0, practically isotropic, following multiple annealing at a temperature of 1050–1100°, were rolled to a specified thickness. After this they were annealed in a salt bath at a temperature of 800° for 1 hr, then again rolled to a thickness of ~ 0.2mm . To obtain varying degrees of strain the initial thickness d_0 was varied. The degree of straining during the first rolling (up to intermediate annealing) was constant, but the degree of straining during the second rolling (after intermediate annealing) was varied. The final degree of straining was varied with indefinite limits.

The blanks of transformer steel had an initial thickness of 7.3 and 1mm. The preparation of this material for studying texture differs from the preparation of test-pieces of low-carbon steel only in the omission of the preliminary multiple annealing. It is known that in alloys of iron and silicon, where the silicon content is 3 per cent, there is no allotropic transformation $\alpha \rightarrow \gamma$. To obtain varying degrees of straining after intermediate annealing the blanks were planed to various thicknesses.

The intermediate annealing of test-pieces of transformer steel was carried out at 800–1000°. The first cold rolling with a degree of straining $\frac{d_0}{d} = 4$ (in which the quantity A_4 = the amplitude of the fourth harmonic of the normal component of magnetization, has considerable significance after recrystallization.

After the second rolling test-pieces were prepared from strip in the form of disks with a diameter of 30mm. Their normal component of magnetization I_n was measured [9], and by means of harmonic analysis [10] the amplitudes of their second and fourth harmonics were computed (A_2 and A_4). The test-pieces then underwent multiple annealing at the same temperature as that at which they had been intermediately annealed; their normal component of magnetization was again measured and the amplitudes A_2 and A_4 were computed.

By Akulov's theory [11], calculation was made according to the value of A_2 and A_4 of the relative volumes of crystallites having one and the same orientation; this is determined by direct methods (X-ray and optical). Thus, the values A_2 and A_4 are the characteristics of the

* *Fiz. metal. metalloved.* 4, No. 2, 339-343, 1957 [Reprint Order No. POM 55].

degree of perfection and to some extent of the type of texture.

RESULTS OF EXPERIMENTS

1. *Transformer steel (3 per cent Si).*

The relationship of amplitude A_2 and A_4 of the second and fourth harmonic of the normal component of magnetization to overall relative strain

$$D = \int_{l_0}^{l} (dl/l) = \ln (l/l_0) = \ln (d_0/d)$$

where l and d are finite, but l_0 = original length and thickness of the rolled sheet) is shown in Figs. I and 2.

degree ($d_0/d = 1.5$) the value of A_4 changes from a negative to a positive quantity. The variation of the first phase of the fourth harmonic shows this: in the second cold rolling the positive value of the quantity A_4 furthermore, increases proportional with the degree of strain.

The relationship of A_4 to overall relative strain, illustrated in curves 1 and 2 of Fig. 2, is similar to the relationship of A_4 set out in curves 3 and 4. Here the picture is as if curves 1 and 2, as a result of intermediate annealing, shift to the area of high strains, as a result of which curves 3 and 4 were also obtained.

From Fig. 1 (the symbols are the same as in Fig. 2) it follows that intermediate annealing does not change the relationship of A_2, typical

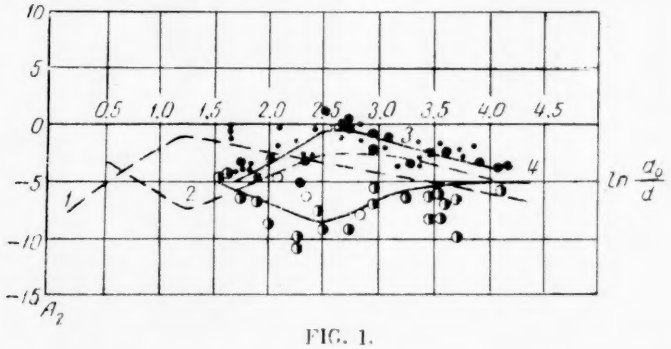

FIG. 1.

In Fig. 2, curve 1 sets out the relationship of the value of A_4 to overall relative strain, in (d_0/d) for test-pieces strained by cold rolling without intermediate annealing [9]. Curve 2 expresses the relationship of A_4 for transformer steel recrystallized by cold rolling (without intermediate annealing). Curve 3 indicates the relationship of A_4 to overall relative strain in the case of test-pieces of transformer steel cold-rolled with intermediate annealing. In these curves the values of A_4 are indicated by dots for those materials which were rolled with intermediate annealing at a temperature of 800°, and by open circles for materials in which intermediate annealing was given at a temperature of 1000°C.

Curve 4 in Fig. 2 sets out the relationship of A_4 to overall relative strain in the case of test-pieces which had passed through cold rolling with intermediate annealing, and which had undergone recrystallization under the second rolling.

It is evident from Fig. 2 (curve 3) that where the second straining is of a very insignificant

of cold rolling without intermediate annealing but, as it were, shifts it to an area of heavy strains.

In the course of second rolling, strain texture develops in materials which already possess a recrystallization texture of the first kind [9, 12]. The rapid increase of the quantity A_4 in Fig. 2 (with slight second straining) is an indication of the rapid growth of strain structure. This shows that recrystallization structure of the first kind - (100) [001] and (110) [001] – is not very stable, but nevertheless is most advantageous in transformer steel. In steel having such a texture there is an improvement of magnetic qualities.

As regards textural instability of the first kind it can be concluded from this that a small amount of cold strain leads to a rapid growth of strained structure.

There is no evidence that varying the temperature of intermediate annealing over a range of 800 – 1000° has any substantial effect on the values of A_4 and A_2 for alloys of iron and sili-

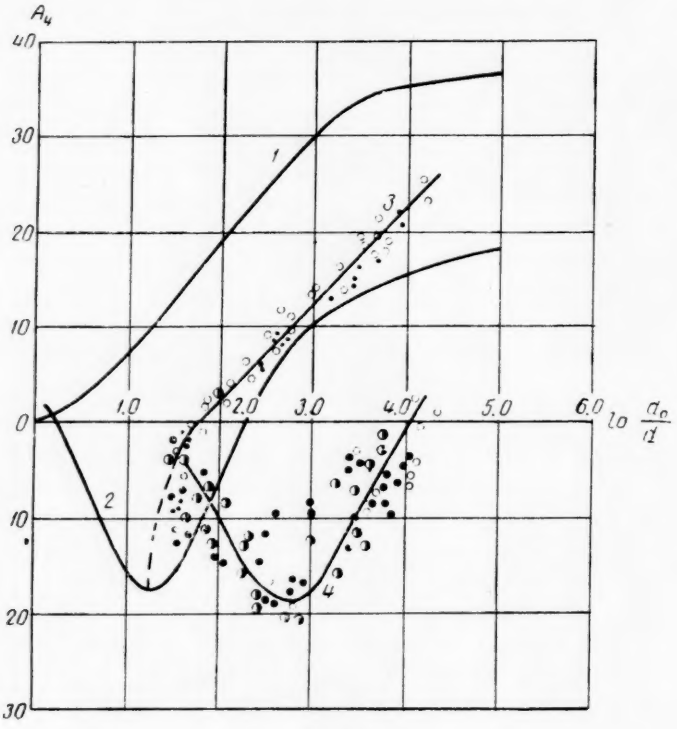

FIG. 2.

con, and consequently on the character and degree of perfection of texture.

From the graphs Figs 1 and 2 it is evident that in rolling with intermediate annealing the recrystallization texture, corresponding to slight straining under cold rolling without intermediate annealing, is, as it were", transferred" to an area of heavy strain.

In the case of "triple" rolling with two intermediate and a third and final annealing, the greatest "transfer" of curves A_2 and A_4 is obtained and consequently also of texture corresponding to slight strain, to an area of still greater strain.

This points to the possibility of controlling, within definite limits, the formation of texture by means of an appropriate selection of the number of intermediate annealings and of the degree of straining between annealing. For example, there can be obtained in this way recrystallization texture of the first kind ("cubic" structure) not only under conditions of light strain, but also with any amount of heavy straining during the rolling process.

2. Low-carbon steel

In Figs. 3 and 4 are shown the relationships of the quantities A_2 and A_4 to overall relative strain for low-carbon steel, rolled with intermediate annealing.

Comparison of Fig. 4 with Fig. 2 shows that the relationship of A_4 for low-carbon steel is the same as the relationship for transformer steel.

The order of change in the quantity A_4 with an

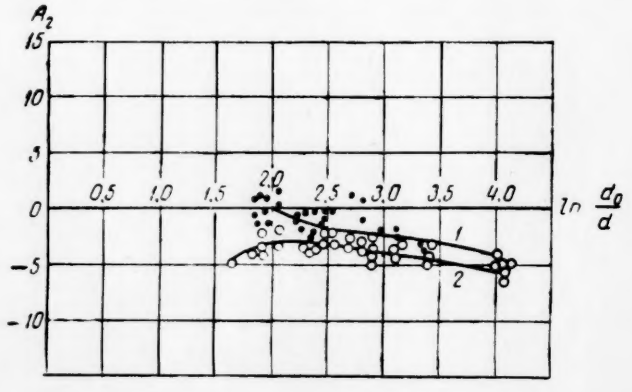

FIG. 3.

increase in the degree of straining after intermediate annealing and then after recrystallization annealing (following the second rolling) is one and the same for low-carbon steel as for transformer steel.

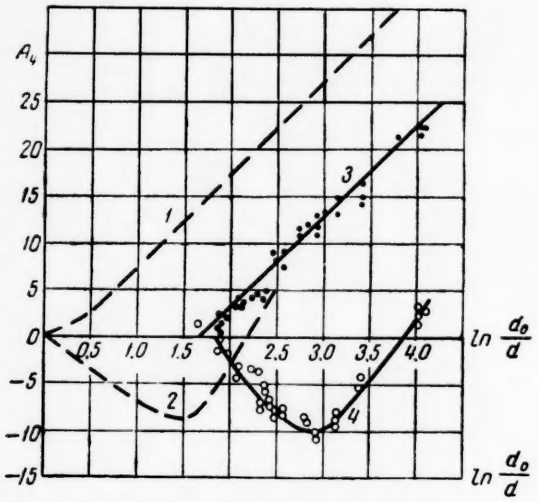

FIG. 4.

As regards the relationship of A_2 to overall relative strain, it is evident from a comparison of Figs 3 and 1 that this relationship does not differ very much in transformer steel from the relationship A_2 in low-carbon steel.

Nevertheless, in the case of both alloys intermediate annealing, as it were, "transfers" this relationship to an area of heavy strain.

The similarity of the effect of intermediate annealing on the order of change in the quantities A_4 and A_2 in low-carbon and transformer steel leads up to the fact that all the aforementioned findings are true both for transformer and for low-carbon steel.

CONCLUSIONS

1. The effect of intermediate annealing on cold rolling and recrystallization texture is that in cold rolling with large reduction stages and with intermediate annealing the same texture is produced as in rolling with small reduction stages, but without intermediate annealing. This permits textural control by combining cold rolling with intermediate annealing.
2. Goss's assertion [1], that intermediate annealing destroys texture in transformer steel, is unwarranted.
3. Tarasov's explanation [8] of a new type of texture (110) [001] occurring in Bozorth's experiments [6] in the course of intermediate annealing is not confirmed.

REFERENCES

1. N.F. Goss *Trans. Amer. Soc. Metals* 23,511 (1935).
2. A.L. Goldman, R.M. Grobman and E.S. Chernobrov E.S. Chernobrovkina *Stal'* 3,231 (1947).
3. F.P. Lybalko and M.V. Yakutovich *Zh. tekh. fiz.* 17, 1503 (1947).
4. A.L. Goldman and V.V. Druyhinin *Elektrichestvo* 10, 39 (1946).
5. A.S. Zaimovikii and L.S. Kayarnovrkii *Kachestvennaya stal'* 89, 19 (1936).
6. R.M. Bozorth *Trans. Amer. Soc. Metals* 33, 1107 (1935).
7. K.I. Sixtus *Physics* 6, 105 (1935).
8. L.P. Taresv *Trans. Amer. Soc. Metals* 35, 353 (1939).
9. K.V. Grigorov, G.P. Bloklin, E.A. Koryun and M.I. Zakutner *Fiz. metal. metalloved.* 1, No.1, 36 (1955).
10. V.I. Smirov *Kurs uysshei matematiki (Course in higher mathematics)*, GITTL, 2, 1951.

VOL. 4 1957

THE TEMPERATURE DEPENDENCE OF INTERNAL FRICTION IN SEVERAL PURE METALS*

V.S. POSTNIKOV

(Received 15 May 1956)

Variations in the internal friction of aluminium, copper, nickel, iron, cobalt, titanium, molybdenum, tungsten (measured by the author) and tin, lead, magnesium, silver, gold and platinum (measured by other authors) with temperature were determined by the low-amplitude torsional oscillation method.

All pure metals which do not undergo allotropic modifications on heating have the same temperature/internal friction relationship which can be explained by existing relaxation theory supplemented by conceptions of the author in regard to the behaviour of internal friction at high temperatures.

INTRODUCTION

The damping of oscillations and, in particular, the determination of internal friction by torsional oscillation have been studied very many times, beginning with Kelvin (1865) and Focht (1892) in the last century and continuing with Weinberg (1904) and Kuznetsov (1913).

This quite complex relaxation property, therefore, has been of considerable interest since the kinetics of many physico-chemical processes in solids and liquids can be understood by a study of the internal friction. Such processes include dispersion-hardening, particularly in the early stages of precipitation, the range of temperature stability of a given phase and its structural constituents, intercrystalline corrosion, the presence of gases in metals, etc.

A particularly interesting problem is the temperature of internal friction since the level of the internal friction is connected with the hardness of the metal and alloy at elevated temperatures. Other workers have also studied this problem, but not sufficiently.

The present paper contains the results of experiments on pure metals and also similar results obtained by other authors, and it has been possible to draw tentatively certain general conclusions from them.

THE SPECIMENS AND THE MEASURING METHOD

The experiments were made on aluminium, titanium, cobalt, nickel, copper, molybdenum and tungsten.

The internal friction Q was measured in units represented by the logarithmic decrement of damping found in the free torsional oscillation of wire specimens 300 mm long and 0.7 mm thick. The period of the free oscillations was approximately 1 c/s. The torsional deformation did not exceed 10^{-5}, nor the elongation 10^{-6}. The measurements were made in a special apparatus [1] under a vacuum of 10^{-4} to 10^{-5} mm Hg. The test-specimens (Table 1) were prepared from pure metals provided by the Moscow Scientific Research Institute for Treating Light Metals, the Leningrad Institute of Nickel and the Institute of Metal Physics and Metallography of the Central Scientific Research Institute for Ferrous Metallurgy. All specimens were annealed in a vacuum of 10^{-4} to 10^{-5} mm Hg for 3 hr at different temperatures, e.g. aluminium at 450°, copper at 600°, nickel, cobalt, titanium and iron at 800°, molybdenum and tungsten at 900°.

TABLE 1

Metal (in order of m.p.)	Purity (per cent)	Reduction of Area (per cent)
Aluminium	99.98	95
Copper	99.992	95
Nickel	99.99	98
Cobalt	99.98	13
Iron	99.67	95
Titanium*	98.00	92
Molybdenum	99.92	98
Tungsten	99.61	98

*Titanium was drawn at 700°C.

* *Fiz. metal. metalloved.* 4, No. 2, 341-351, 1957 [Reprint Order No. POM 56].

VOL 4 195

VOL. 4 1957

EXPERIMENTAL RESULTS

The results obtained by the author are given in Figs. 1–4, and those of other authors in Figs. 5–6.

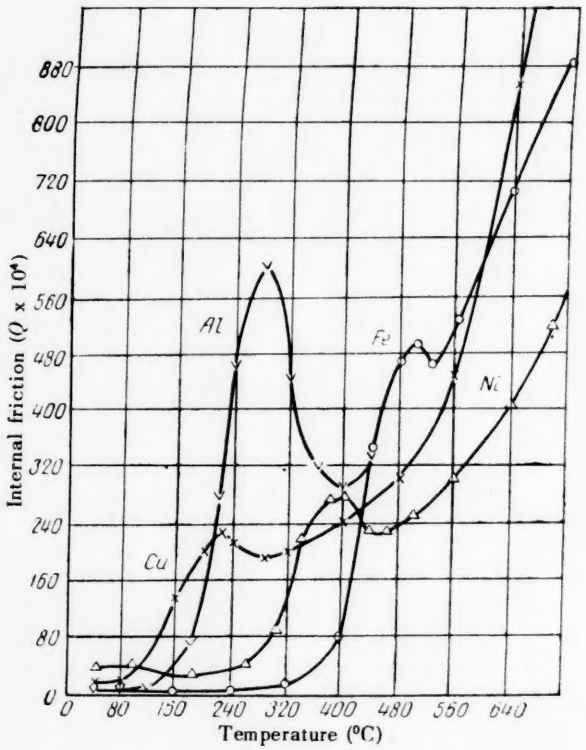

FIG.1. Temperature dependence of internal friction for aluminium, copper, nickel and iron.

Titanium, molybdenum and tungsten have no maxima, as shown in Fig.2, but only arrest-points. Those for molybdenum and tungsten are not shown, as they lie above 700°. Cobalt, on the other hand, has a most interesting internal friction vs.

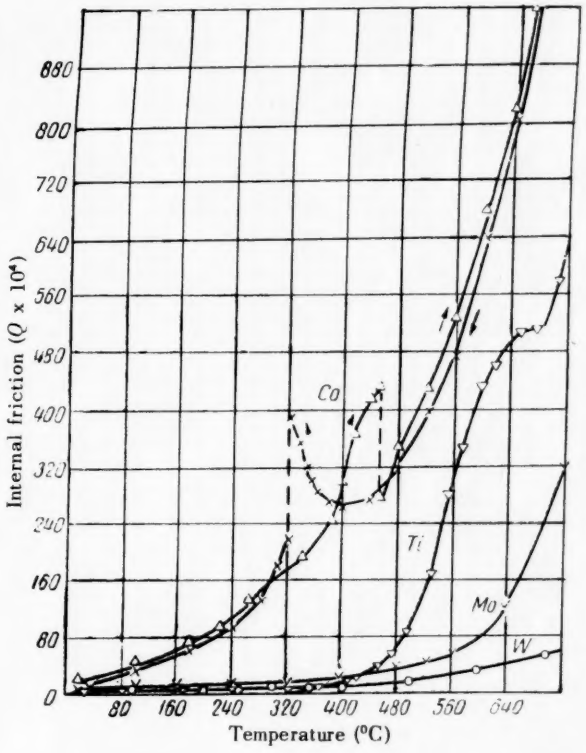

FIG.2. Temperature dependence of internal friction for cobalt, titanium, molybdenum and tungsten.

Fig.1 shows that the changes in internal friction with temperature are similar for aluminium, copper, nickel and iron, a distinct maximum occurring at a certain temperature: 224°, for copper, 280° for aluminium, 390° for nickel and 500° for iron. However, the level of the maximum is different in each case. With aluminium it is more than 240 times greater than the internal friction at room temperature (equal to 2.6×10^{-4}), whilst with copper, for example, it is only 22 times greater. The results for aluminium, copper and iron are in good agreement with those obtained by Ke Ting-Sui [2, 3] since the slightly higher values which he obtained for aluminium and iron are obviously due to the higher purity of the metals used.

temperature curve: the internal friction increases rapidly up to a maximum at 450°. Near this temperature, under isothermal conditions, it rapidly falls to a stable value for approximately 30 min. When the temperature is then further increased, the internal friction also increases without any further irregularities. On cooling, the internal friction decreases almost down to 400° after which it rapidly increases to a maximum at 320°. Under isothermal conditions (for 30 min.) at this temperature the internal friction falls to a stable value, and further decrease in temperature produces a proportional decrease in the internal friction to a value of approximately 20×10^{-4} at 20°. In the 300–450° range a particular form of "hysteresis" occurs.

Figs. 3 and 4 show internal friction vs. temperature curves for pure nickel and solid solutions of carbon and chromium in nickel. As the amount of the alloying element is increased, the maximum moves towards higher temperatures and is gradually converted to an arrest-point. Ke T'ing-Sui [4] obtained quite similar results for aluminium and copper.

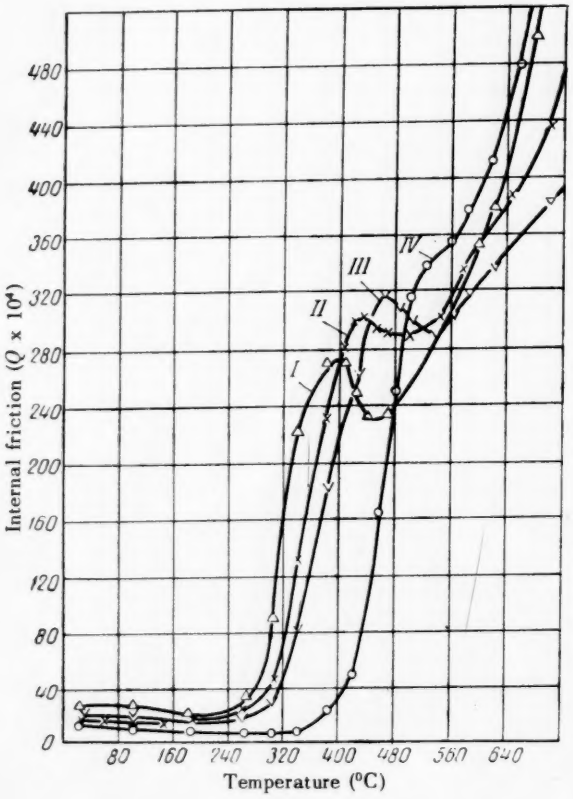

FIG.3. Temperature dependence of internal friction for pure nickel (I); for a solid solution of 0.04 per cent C in Ni(II); 0.07 per cent C (III); 0.21 per cent C (IV).

Figs. 5 and 6 give internal friction/temperature curves for tin, lead, magnesium, silver, gold and platinum [2, 5, 6, 7, 8]. With the exception of silver and platinum, the same relationship is found as for the metals represented in Fig.1. However, silver and platinum have only been studied once (in 1920) and, unfortunately, at relatively low temperatures. At higher temperatures they would probably give curves similar to those of gold.

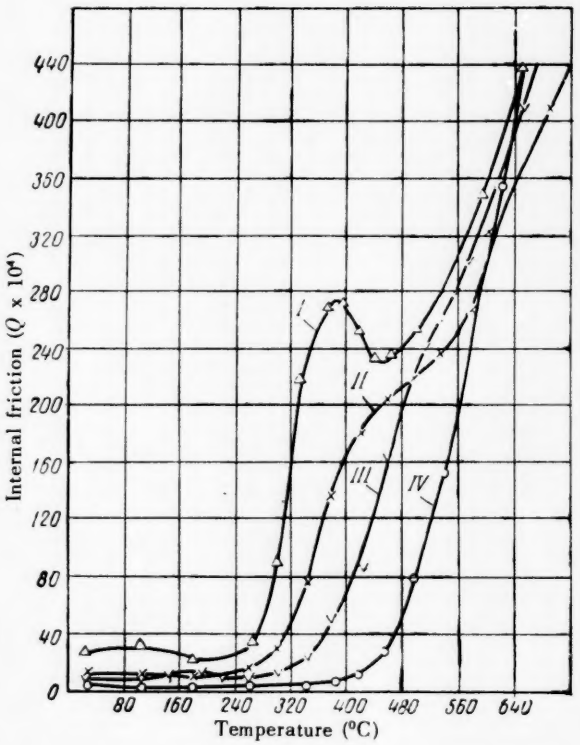

FIG.4. Temperature dependence of internal friction for pure nickel (I); for a solid solution of 0.72 per cent nickel in chromium (II); 1.19 per cent Ni (III); ordinary Nichrome.(IV).

The following conclusions can be drawn from the curves given in Figs. 1–6.

1. The temperature dependence of internal friction is constant with time for well-annealed metal specimens in that it is reproducible if oxidation is kept to a minimum.

2. The temperature vs. internal friction curve of every polycrystalline metal has at least one maximum or arrest-point provided it does not undergo allotropic modifications on heating and assuming a constant frequency of the free oscillations.

3. Those metals which undergo allotropic modifications on heating, e.g. cobalt, have an irregular (with time) internal friction in the temperature range in which the allotropic modification occurs. The internal friction shows a particular type of "hysteresis".

4. The internal friction maximum (or arrest-point) lies in the range of recrystallization of the

metal, the position depending on the degree of previous plastic deformation: an increase in the degree of plastic deformation produces a shift of the maximum towards lower temperatures. At equal degrees of plastic deformation the position of the maximum or arrest-point is some function of the melting point of the metal: the higher the melting point of the metal, the higher the temperature at which the maximum is observed.

5. At a given temperature, higher melting-point metals have a lower internal friction than lower melting-point metals.

6. The internal friction of binary alloys and impure metals increases with temperature much more slowly than that of pure metals.

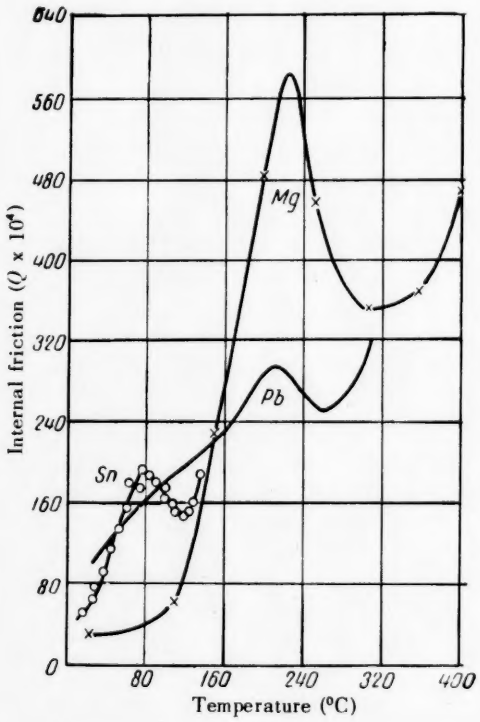

FIG.5. Temperature dependence of internal friction for tin, lead and magnesium.

DISCUSSION OF THE RESULTS

It is at present generally accepted that internal friction is produced by different types of relaxation phenomena which occur in metals or alloys as a result of a stress field due to periodical external working [9–13]. According to this relaxation theory it is suggested that the metal or alloy system passes from a metastable to a stable state, under the given conditions, in one or several relaxation times τ. If such a system is subject to a periodically changing stress, the dissipation of the elastic energy will depend on the frequency ω of the stress change. Existing theories show that the energy dissipation is a function of the parameter $\omega\tau$.

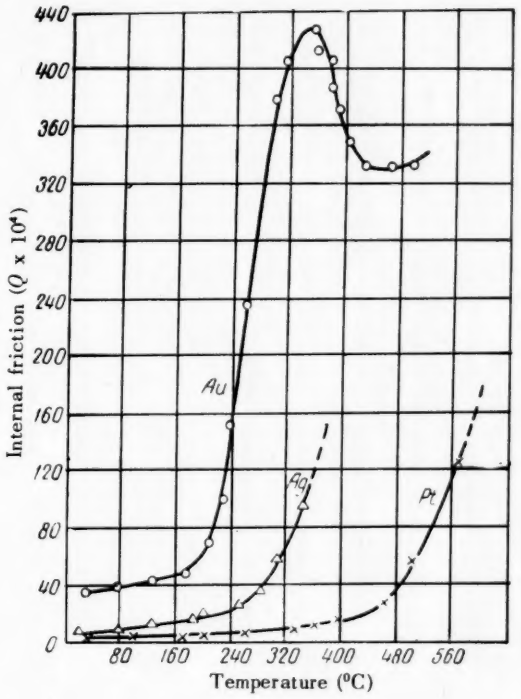

FIG.6. Temperature dependence of internal friction for silver, gold and platinum.

For example, it follows from relaxation theory on the basis of general thermodynamic considerations [10] that for a system with one relaxation time:

$$Q = \frac{\Delta_0 \cdot \omega \cdot \tau}{1 + \frac{M_\infty}{M_0} \cdot (\omega \cdot \tau)^2} \qquad (1)$$

If Q is plotted in a graph against the parameter $\omega\tau$, the curve will have a maximum [12] when $\omega\tau = 1$, in other words, when the frequency of the stress change ω is equal to the inverse of the relaxation time. This deduction affects the whole of relaxation theory.

However, real bodies do not have one relaxation time, but a whole number of them or even a

continuous spectrum. If several relaxation processes, each of which has its own relaxation time τ_i, occur in a body simultaneously, the internal friction in such a body will be determined by the equation:

$$Q = \sum_{i=1}^{n} \frac{\Delta_i \cdot \omega \cdot \tau_i}{1 + \frac{M_\infty}{M_0} \cdot (\omega \cdot \tau_i)^2} \qquad (2)$$

The internal friction will have not one maximum but several maxima, or if the times τ_i are centred around a certain average value τ_{av}, one fairly "diffuse" maximum [12, 13].

Lastly, if the distribution of the relaxation constants is continuous, the internal friction will be determined by the equation:

$$Q = \int_{-\infty}^{+\infty} \frac{\Psi(\tau) \cdot \omega \cdot \tau}{1 + \frac{M_\infty}{M_0} (\omega \cdot \tau)^2} \cdot d(\ln \tau) \qquad (3)$$

where $\Psi(\tau)$ is an unknown function of the distribution (which is difficult to determine experimentally). It can also be determined from the condition:

$$\Delta_0 = \int_{-\infty}^{+\infty} \Psi(\tau) \cdot d(\ln \tau) \qquad (4)$$

where Δ_0 is an experimentally known fault in the elastic modulus.

In both cases the integration introduces a considerable source of error.

All existing theories explain the origin of internal friction and the appearance of maxima on the temperature vs internal friction or frequency vs. internal friction curves, but they do not explain the behaviour of internal friction at highly elevated temperatures. For example, all the maxima in the curves of Figs. 1, 5 and 6 are explained by viscous sliding along the grain boundaries. Since the grains are not of equal size [12, 13], the relaxation of stresses along grain boundaries will not have one value of time, but several, and the greater their number, the more "diffuse" the maximum will become.

At a certain distribution of the relaxation times the maximum may expand to an arrest-point, as in the case of titanium, molybdenum and tungsten.

The author has made an attempt to explain the change in internal friction at highly elevated temperatures and has derived [13] the following equation:

$$Q = (\alpha \cdot \beta \cdot a \cdot \bar{\Theta} / \omega \cdot kT) \exp(-H/RT) \qquad (5)$$

where $\bar{\Theta}$ is the mean shear stress; H the energy parameter which defines the possibility of atom transitions inside the metal lattice; α, β, a, k, R are constants, ω is the cyclic frequency of the free oscillations of the specimen; and T is the absolute temperature.

The paper [13] also shows that internal friction can be represented as the sum of the partial internal frictions produced by the different relaxation processes, the main part at high temperatures, however, being determined by equation (5).

SUMMARY

1. New experimental data obtained on titanium, nickel, iron, molybdenum and tungsten as well as literature data on tin, lead, magnesium, silver, gold and platinum give quite good support for the author's theory of the temperature dependence of internal friction as described in [13].

2. The temperature vs. internal friction curve of pure metals can be explained by relaxation theory and the ideas developed in [13].

3. At elevated temperatures the presence of impurities in a metal reduces the internal friction found at a given temperature.

In conclusion, I would express my gratitude to Miss A. Ya. Samoilova, assistant in the Physics Department, for carrying out a number of control experiments and preparing the graphs.

Translated by R.A. Hetherton

REFERENCES

1. V.S. Postnikov *Trud. Kemerovskogo gorrogo in-ta* 1, 221 (1954).
2. Ke T'ing Sui *Phys. Rev.* 71, 533 (1947); *J. Appl. Phys.* 20, 274 (1949).
3. Ke T'ing Sui *Metals Tech.* 15, 2370 (1948).
4. Ke T'ing Sui *J. Metals* 188, 575 (1950); *J. Appl. Phys.* 20, 274 (1949).
5. L.R. Rotherham, B.A. Smith and G.B. Greenough *J. Inst. Metals* 79, 439 (1951).
6. J. Barducci *Ric. Sci.* 24, 2025 (1954).
7. K. Iokiba and S. Sakai *Phil. Mag.* 42, 397 (1921).

8. R.M. Donald and D.H. Lewis *J. Metals* 5, 937 (1953).
9. Co Zener *Elasticity and anelasticity of metals*, 1948.
10. B.N. Finkelstein and N.S. Fastov *Dokl. Akad. Nauk SSSR* 21, 875 (1950); *Problemy metallovedeniya i finiki metallov*, IL, 1954.
11. A.S. Nowick *Progr. Metal Phys.* 4, 1 (1953).
12. V.S. Postnikov *Usp. fiz. nauk* 53, 87 (1954).
13. V.S. Postnikov *Zh. tekh. fiz.* 24, 1599 (1954).

VOL.
4
1957

THERMAL CONDUCTIVITY OF ORDERED ALLOYS IN STATIONARY THERMAL EQUILIBRIUM* †

G.E. ZOLOTUKHIN

(Received 26 March 1956)

Results of an experimental study of thermal conductivity of gold–copper and platinum–copper alloys as a function of the length of annealing below the critical temperature are reported. An attempt is made to extend the Smirnov - Ryzhanov theory to the phenomena of thermal conductivity in ordered structures.

1. Theories of close and long-range order in the arrangement of atoms in the lattice of solid solutions find application in the study of a number of physical phenomena. In particular, the theory of Bragg and Williams has been successfully used by Smirnov [1] in solving the problem of the motion of an electron within a crystalline lattice of an alloy of arbitrary composition and degree of long-range order.

Using the theory of electron motion, Smirnov arrived at the following expression for electrical resistance ρ of such alloys as a function of the concentration of components c and degree of long-range order s

$$\rho = A[c(1-c) - \frac{\nu}{1-\nu}(q-c)^2 S^2],$$

where A is a quantity independent of S, c is the relative concentration of atoms of the first species N_1/N; and ν is the relative concentration of nodes of the first species $aq = c/\nu$.

The results of theoretical calculations of ρ are in general agreement with experimental data of Johanson – Linde and Komar [2]. The latter work contains values of ρ for alloys close in composition to $AuCu_3$ and AuCu.

It was shown that this relation agrees well with the Smirnov – Ryzhanov theory and contradicts the theory of Mito.

2. One can expect that the thermal conductivity, similar to the electrical conductivity of ordered alloys, will change with the change in concentration and degree of long-range order. However, no sufficiently accurate experimental study or sufficiently rigorous theoretical treatment of this relationship has been made. The study of thermal conductivity of ordered alloys could help in improving our understanding of the ordering process and its mechanism. In order to fill somewhat this gap we have carried out a number of experiments studying the thermal conductivity of ordered alloys of copper with gold or platinum as a function of the composition and of the degree of long-range order.

Among the alloys studied by us were alloys corresponding to the stoichiometric composition AuCu, $AuCu_3$, PtCu, $PtCu_3$ and also alloys of intermediate composition. Joint study of the ordered and disordered structures by the same method enabled us to compare closely the properties of these structures.

The coefficient of thermal conductivity was determined in the condition of thermal equilibrium by the method described ealier [3].

A definite order in the arrangement of atoms was obtained by annealing for a given time in a muffle furnace at temperatures below the critical. During annealing the temperature was controlled by a recording potentiometer. After a predetermined interval of time the current supply to the furnace was turned off and the specimens were left to cool in the furnace at the rate of 10-12°C/min.

The thermal conductivity measurements of the whole range of alloys was carried out after annealing. The influence of ordered arrangement of atoms in the lattice on the value of the thermal conductivity coefficient was studied by alternating annealing with thermal conductivity measurements. The annealing of platinum-copper alloys was carried out at 400°C. and of gold-copper alloys at 400 and 200°C.

The degree of long-range order in the ordered structures of the AB type was found by using our formula which relates thermal conductivity to the order in atom arrangement.

---

* *Fiz. metal. metalloved.* 4, No.2 352-359, 1957 [Reprint Order No. POM 57].

† Z. Krupskaya also took part in this work

3. The equilibrium diagram shows that gold and copper form a continuous series of solid solutions [4]. According to Grube [4] during the cooling a decomposition of solid solution corresponding to a given composition occurs with the formation of intermetallic compounds AuCu and $AuCu_3$.

The separation of the first of these occurs at 425°C. and of the second one at 395°C. On rapid cooling from the temperature above the critical, the atoms of gold and copper arrange themselves at random in a face-centred cubic lattice. During annealing at temperatures below the critical, atoms of gold tend to move into the corners of the cube and atoms of copper into the centres of faces. As a result of this a superstructure is formed in alloys with equal content of copper and gold. The arrangement of atoms in the ordered structure of $AuCu_3$ is more complex.

Copper alloys containing 20.0, 25.0, 35,0, 50.0 and 65.0 at.% of gold were prepared. Among the alloys studied were some corresponding to intermetallic compounds and some of intermediate composition. In the preparation of alloys assay grade gold and electrolytic copper were used. The constituents were placed in a graphite crucible and melted in an arc furnace. The specimens were of cylindrical shape suitable for the subsequent thermal conductivity measurements. The coefficient of thermal conductivity at thermal equilibrium was calculated from the formula

$$\chi = (q' + q)/F \cdot \partial T/\partial x,$$

where $q' = (\partial T'/\partial t + \partial T''/\partial t)\ c\rho\ F.h'/2$

correspond to the component of the heat flow through cross section F required to maintain the established temperature gradient between the cooling surface and the electrode section at a distance h'; $\partial T/\partial x$ = the temperature gradient corresponding to the given cross-section (Fig. 1);

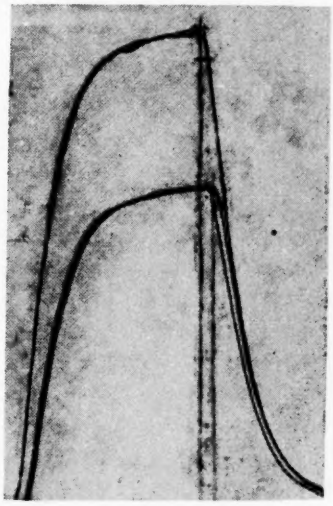

FIG. 1. Thermograms of Au-Cu (20 per cent Au) alloys after annealing for 10 hr at 200°C.

and q the amount of heat received by the cooler.

In order to measure the temperature and to find $\partial T/\partial x$, two holes 0.5 - 0.8 mm. in diameter and reaching to the centre were drilled in the side surface of the cylindrical specimens.

Table 1 gives the dimensions of the specimens; height H, cross-sectional area F, distance between the cooling surface and the first thermocouple Δx_1, distance between the thermocouples Δx, and also specific heat c and density ρ.

The results of thermal conductivity measurements in relation to the length of annealing at 200°C. are given in Table 2 and are represented graphically in Fig. 2. Apart from the coefficient of thermal conductivity Table 2 gives also the temperature interval $T_1 - T_2$ in which the thermal conductivity was measured, the average value of the temperature gradient and the total heat flow Q through the cross-sectional area studied situated between the two thermocouples (Q was determined by means of "thermograms" and by measuring the

TABLE 1

Alloy	Gold content (%)	Dimensions of electrodes				c	ρ
		H (cm)	F (cm²)	Δx (cm)	Δx_1 (cm)		
1	20.0	1.43	0.63	0.68	0.20	0.060	14.30
2	25.0	1.49	0.63	0.72	0.20	0.058	15.05
3	35.0	1.45	0.63	0.68	0.20	0.051	16.70
4	50.0	1.30	0.63	0.75	0.20	0.045	18.34
5	65.0	1.30	0.63	0.59	0.20	0.040	19.40

amount of heat taken away by the cooling liquid).

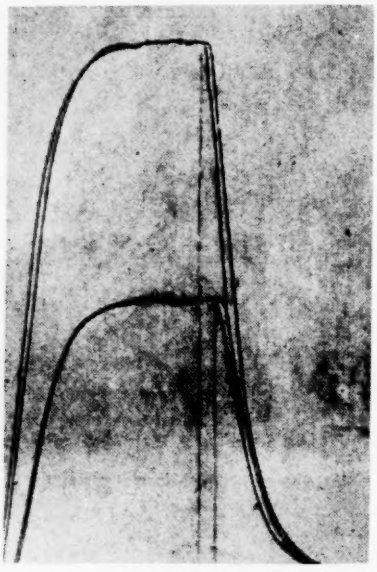

FIG. 2. Thermograms of Au-Cu (20 per cent Au) alloy after annealing for 20 hr at 200°C.

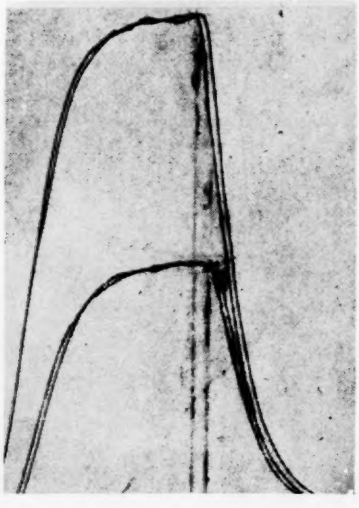

FIG. 3. Thermograms of Pt-Cu (35 per cent Pt) alloy after annealing for 10 hr at 400° C.

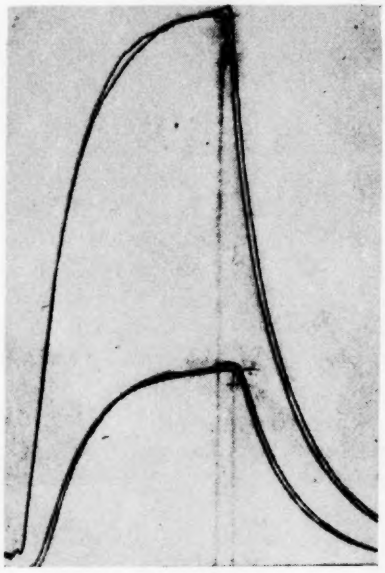

FIG. 4. Thermograms of Pt-Cu (50 per cent Pt) alloy after annealing for 50 hr at 400°C.

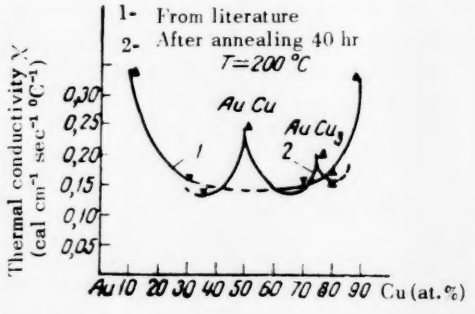

FIG.5. Thermal conductivity of gold-copper alloys based on own experiments and literature data.

Table 2 shows that the thermal conductivity of the metals studied varied with the annealing time. The conductivity of alloys approaching the composition corresponding to AuCu and $Aucu_3$ increased on annealing and reached a definite value. On the other hand the conductivity of alloys containing 20, 35 and 65 at.% Au decreased after annealing. The conductivity of the alloy containing 50 at.% Au was 0.134 before annealing and 0.236 after annealing for 40 hr.

The conductivity of alloys containing 35 and 65 at % Au decreased after 40 hr annealing from 0.210 to 0.136 and from 0.194 to 0.135 respectively.

TABLE 2. Thermal conductivity of gold-copper alloys

State and composition of alloys	T_1 (°C)	T_2 (°C)	$\partial T/\partial x$ (°C cm^{-1})	Q (cal sec.$^{-1}$)	χ (cal cm^{-1} sec^{-1} °C^{-1})
I. 20 at.% Au, 80 at.% Cu					
cast	181	118	92	14.1	0.244
after 10 hr annealing	210	140	103	14.9	0.250
after 20 hr annealing	182	94	130	14.0	0.164
after 30 hr annealing	244	144	147	13.1	0.145
after 40 hr annealing	205	93	165	15.8	0.152
II. 25 at.% Au, 75 at.% Cu					
cast	204	141	87	13.3	0.210
after 10 hr annealing	246	194	72	14.0	0.320
after 20 hr annealing	172	85	121	13.0	0.178
after 30 hr annealing	248	146	142	13.4	0.155
after 40 hr annealing	174	87	121	17.1	0.226
III. 35 at.% Au, 65 at.% Cu					
cast	254	195	100	13.2	0.210
after 10 hr annealing	260	105	161	14.4	0.142
after 20 hr annealing	216	113	175	14.7	0.134
after 30 hr annealing	255	114	188	15.0	0.132
after 40 hr annealing	226	117	185	16.1	0.136
IV. 50 at.% Au, 50 at.% Cu					
cast	286	145	188	15.6	0.134
after 10 hr annealing	254	166	117	14.1	0.192
after 20 hr annealing	195	100	126	14.5	0.185
after 30 hr annealing	246	155	121	14.8	0.195
after 40 hr annealing	155	89	101	16.0	0.236
V. 65 at.% Au, 35 at.% Cu					
cast	230	156	109	13.2	0.194
after 10 hr annealing	273	190	122	14.6	0.190
after 20 hr annealing	204	102	150	13.4	0.144
after 30 hr annealing	259	158	149	13.4	0.143
after 40 hr annealing	256	119	195	16.4	0.135

VOL. 4 1957

TABLE 3.

Content of platinum at.%	Dimensions of electrodes				c	ρ
	H (cm)	F (cm^2)	Δx (cm)	Δx_1 (cm)		
20.0	1.35	0.63	0.65	0.15	0.074	14.4
25.0	1.40	0.63	0.85	0.12	0.062	15.0
35.0	1.32	0.63	0.83	0.15	0.054	16.7
50.0	1.36	0.63	0.78	0.12	0.046	18.4
65.0	1.30	0.63	0.70	0.15	0.041	19.6

After long annealing at 400°C. the thermal conductivity of the alloy containing 50 at.% Au reached the value 0.186, but the conductivity of the 25 at.% Au alloy did not change. The change of thermal conductivity of gold-copper alloys with the time of annealing at 400 and 200°C. is in full agreement with the theory of ordered state.

Fig. 5 shows literature data regarding the thermal conductivity of disordered structures [5] which agree closely with our results obtained with alloys in disordered state. The alloys of copper with platinum were studied in a similar way.

4. Chemically pure platinum and electrolytic copper were mixed in predetermined quantities and melted in an arc furnace. On solidification the specimens assumed cylindrical shape. The chemical composition and the dimensions of the specimens studied are reported in Table 3.

As the equilibrium diagram [6] shows platinum and copper form a continuous series of solutions, similar to gold and copper. During slow solidification of alloys in the neighbourhood of equal atomic contents of platinum and copper the decomposition of the homogeneous solid solution takes place with the formation of the intermetallic compound PtCu.

Also, a second compound corresponding to the composition $PtCu_3$ is known. The ordered state in the arrangement of atoms is reached after 5 – 10 hr annealing at 400°C.

The results of thermal conductivity measurements of alloys after various times of annealing are given in Table 4 and are represented in Fig. 6.

TABLE 4. Thermal conductivity of copper-platinum alloys

State and composition of alloy	T_1 (°C)	T_2 (°C)	$\Delta T/\Delta T$ (°C cm^{-1})	Q (cal sec^{-1})	χ (cal cm^{-1} sec^{-1} °C^{-1})
I. 20 at.% Pt, 80 at.% Cu					
cast	276	108	259	13.2	0.081
after 10 hr annealing	270	150	155	14.5	0.125
after 20 hr annealing	262	155	164	13.9	0.135
after 40 hr annealing	264	155	168	16.8	0.154
after 50 hr annealing	270	185	131	14.4	0.175
II. 25 at.% Pt, 75 at.% Cu					
cast	374	139	276	11.7	0.062
after 5 hr annealing	318	146	202	11.4	0.090
after 10 hr annealing	324	166	186	11.5	0.098
after 20 hr annealing	320	172	174	14.2	0.127
after 100 hr annealing	297	179	210	16.7	0.126
III. 35 at.% Pt, 65 at.% Cu					
cast	395	117	385	9.40	0.044
after 10 hr annealing	522	184	408	10.2	0.039
after 20 hr annealing	542	169	453	14.4	0.049
after 40 hr annealing	487	155	400	12.4	0.049
after 50 hr annealing	506	256	301	12.4	0.050
IV. 50 at.% Pt, 50 at.% Cu					
cast	472	154	407	11.5	0.036
after 10 hr annealing	350	192	202	12.0	0.103
after 15 hr annealing	302	157	186	13.6	0.140
after 50 hr annealing	290	144	174	15.3	0.137
after 100 hr annealing	262	108	185	17.14	0.147
V. 65 at.% Pt, 35 at.% Cu					
cast	465	156	444	13.0	0.046
after 10 hr annealing	388	171	310	10.2	0.052
after 20 hr annealing	386	180	297	12.6	0.067
after 50 hr annealing	407	187	315	13.0	0.065
after 100 hr annealing	428	124	435	13.5	0.055

VOL 4 195

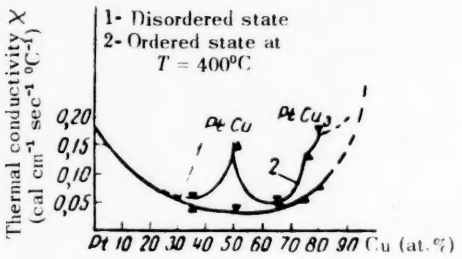

FIG. 6. Thermal conductivity of platinum-copper alloys based on own experiments and literature data.

The results show that during annealing the thermal conductivity of structures undergoing ordering increases and the conductivity of those which remain in the disordered state practically does not change. The thermal conductivity of alloys containing 35 and 65 at.% Pt is on average 0.049 and 0.057 respectively.

The conductivity of ordered structures PtCu and $PtCu_3$ increased with the annealing time and reached, at equilibrium, a limiting value. Fig. 6 shows the sequence of the changes of χ as a function of the annealing time. In the disordered state the conductivity of alloy corresponding to the formula PtCu is 0.036. After annealing for 100 hr χ reaches a limiting value of 0.147.

The coefficient of thermal conductivity of alloys corresponding to the formula $PtCu_3$ increases in a similar way. In the disordered state χ of this alloy is 0.062 and after annealing for 100 hr. 0.126.

The increase of thermal conductivity with the annealing time was observed also in the alloy containing 20 at.% Pt because of the closeness to the composition of the ordered structure.

5. By analogy with the electrical conductivity the thermal conductivity of ordered alloys can be expressed as a function of the composition and of the long-range order. This relationship can be represented for the simple structure of the *AB* type, where the number of nodes is equal to the number of atoms of one species ($\nu = c$) by the expression $\chi = \chi_0 [1/(1 - S^2)]$, where χ_0 is the thermal conductivity in the disordered state and S the degree of long-range order. We have calculated S using the above expression for the ordered structures AuCu and PtCu as a function of the annealing time. The results of these calculations are given in Tables 5 and 6.

TABLE 5. Alloys of gold with copper

Disordered state	Length of annealing at 200°C (hr)			
	20	30	40	
S 0.134	0.185	0.195	0.236	
τ 0.00	0.52	0.56	0.66	

TABLE 6. Alloys of platinum with copper

Disordered state	Length of annealing at 400°C (hr)					
	5	10	15	20	50	100
χ 0.036	0.093	0.103	0.140	0.138	0.137	0.147
S 0.00	0.75	0.80	0.86	0.86	0.86	0.86

The equilibrium in the ordered structure of PtCu was established after annealing for 15 hr at 400°C and the degree of order S, reached was 0.86.

In the case of AuCu equilibrium was not attained even after annealing for 40 hr at 200°C.

Our study of the order-disorder transformation in PtCu enables us to estimate the order of magnitude of the potential barrier energy (W) of Pt and Cu atoms exchanging places.

Assuming, after Bragg and Williams, [7] $A = 10^{-12}$ sec and taking $S = 0.86$, W can be calculated from the known expression $S = A \exp(W/kT)$. According to our calculation this energy is 46 k cal/g atom.

CONCLUSIONS

1. The change of the thermal conductivity coefficient of ordered gold-copper and platinum-copper alloys was studied as a function of the length of annealing below the critical temperature.

2. The interdependence between the thermal conductivity coefficient of the ordered alloys of the *AB* type and the degree of long-range order was demonstrated.

3. A method was examined for the determination of the thermal conductivity coefficient of metals and alloys at the condition of thermal equilibrium by using an a.c. arc as a heat source.

We take this opportunity to express our gratitude to V.A. Zhdanov for reading the manuscript.

REFERENCES

1. A.A.Smirnov *Zh. eksp. teor. fiz.* 17, No.8 (1947).
2. A.P. Komar *Zh. eksp. teor. fiz.* 17, No.8 (1947).

VOL. 4 1957

3. G.E. Zolotukhin *Fiz. metal. metalloved.* 3, 508 (1956).
4. A.V. Boitsov, G.F. Boitzova and N.A. Avdorina *Blagorodnye metally (Precious metals)* p. 33. Metallurgizdat, Moscow, 1946.
5. F. Barrett and H.B. Nettletone The thermal conductivity of liquids and solids *International Critical Tables* 5, 218 (1929).
6. N.S. Kurnakov and V.A. Nemilov *Izv. platinovogo in-ta.* 17, 1931.
7. D.U. Niks and I.V. Shokli *Usp. fiz. nauk* 20, No.3 (1938).

THE REDISTRIBUTION OF CARBON DURING THE TRANSFORMATION OF AUSTENITE IN THE MIDDLE TEMPERATURE RANGE*†

L.I. KOGAN and P.I. ENTIN

(Received 24 July 1956)

The results are given of an experimental study of the carbon redistribution during austenite transformation in the middle range as a function of steel composition and also of the temperature and duration of transformation.

VOL. 4 1957

INTRODUCTION

The kinetics of austenite transformation in the middle (intermediate) range is characterized by the combination of such features as the diffusion (pearlitic) and diffusionless (martensitic) transformations [1]. Because of that there appeared several times statements that the transformation in the middle range is essentially a combination of diffusional processes and martensitic transformation of austenite [2-5].

However, these statements were not sufficiently well founded, because of the lack of data on the structure and composition of phases which are formed during the transformation. Within the last few years the position changed substantially. There exist experimental data which enable us to describe in the following way the various elementary processes of which the transformation of austenite in the middle range is composed.

1. The transformation of austenite in the middle temperature range occurs without a noticeable redistribution of the alloying elements. This conclusion follows from numerous analyses of the structure and composition of the carbide phase which show that, without the dependence on the structure of the equilibrium carbide phase, the content of alloying elements in cementite which forms in the middle temperature range is the same as their average content in steel [6-8].

2. The change of the lattice spacing of the crystalline austenite indicates that the transformation in the middle temperature range is connected with the redistribution of carbon [9-11]. It was established during the study of steels containing various alloying elements that the intermediate transformation can be accompanied by an increase or decrease in the amount of carbon in the residual austenite.

A substantial enrichment of the residual austenite in carbon was found to occur in steels containing 0.3-0.6 per cent carbon and alloyed with chromium, nickel and vanadium. A decrease in carbon content in the residual austenite during the intermediate transformation was observed in our work [11] and in the work of Jellinghaus, Rose and Holetzko [12] in hyper-eutectoid manganese steels containing 1.0-1.4 per cent C and 2-3.5 per cent Mn. However, in the presence of silicon even the specimens of the high-carbon steel 100S2 show a marked enrichment of the residual austenite in carbon during the transformation in the middle temperature range.

The redistribution of carbon in austenite makes it possible for the martensite transformation to take place above the point M_S for the given steel in various parts of austenite which have a low carbon concentration. Carbon can separate in the cementite form or accumulate in the residual austenite [11].

3. The transformation of austenite in the middle range is accompanied by the appearance of a characteristic relief on the surface of the polished specimen which is a proof of the regular character of atom movements on the phase boundary and of the cohesion of phases [13]. The formation of the relief during the transformation is common to the alloyed and carbon steels [11].

It was shown too that the transformation $\gamma \rightarrow \alpha$ occurring in practically carbon-free alloys of iron with various elements can assume a martensitic character below 500-400°C [16].

Kurdyumov and Perkas have established during their study of austenite transformation in monocrystals of steel containing 1.0-1.2 per cent C and 1.4 per cent Cr or 2.0 per cent Mo that α-phase which forms little above the point M_S has a tetra-

---

* *Fiz.metal.metalloved.* 4, No.2, 360-368, 1957 [Reprint Order No. POM 58].

† Yu. P. Gull' and I.V. Kekalo took part in carrying out various experiments.

gonal crystalline lattice [14]. Austenite and α-phase formed during the middle range transformation have regular mutual orientation.

All these facts in addition to the already known kinetic details of the austenite transformation point, in our opinion, to the martensitic mechanism of the $\gamma \rightarrow \alpha$ transition in the middle temperature range.

4. The middle range austenite transformation can be explained on the basis of the existing data as a combination of the diffusional redistribution of carbon in austenite and of the martensitic $\gamma \rightarrow \alpha$ transformation occurring in parts of the austenite with lower carbon content.

In the present work, some experimental data on the redistribution of carbon as a function of the steel composition (content of carbon and of alloying elements) are reported as well as results of study of the change in carbon concentration in austenite in relation to the temperature and duration of the middle range austenite transformation.

The measurements of the lattice spacing after partial austenite transformation were carried out on a number of steels, the chemical composition of which is given in Table 1.

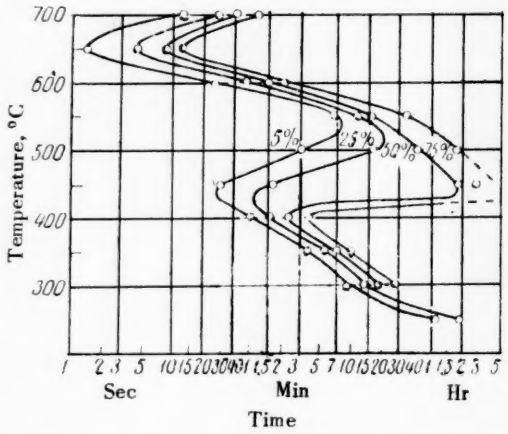

FIG. 1. Isothermal transformation of austenite in the steel 144K3.

using the (311) line was ± 0.004-0.005 kX.

1. The measurements of the average lattice spacing of austenite undertaken in conjunction with the study of the middle range transformation were performed on steel specimens containing approximately the same amount of chromium but different amounts of carbon - 144K3, 98 K3 and 54K3.

TABLE 1.

Grade of Steel	Composition (%)					
	C	Si	Mn	Cr	Al	Ni
144 Kn 3	1.44	0.21	0.36	3.45	—	—
98 Kh 3	0.98	0.28	0.32	3.15	—	—
54 Kh 3	0.54	0.23	0.32	3.54	—	—
118 G 3	1.18	0.18	3.58	—	—	—
48 G 4	0.48	0.26	4.33	—	—	—
30 Yu 2	0.30	0.30	0.42	—	2.90	—
79 Yu 2	0.79	0.29	0.31	—	2.86	—
55 N 8	0.55	0.21	0.21	—	—	8.87
53 KhN 3	0.53	0.28	0.32	1.16	—	3.44
139 G 2	1.39	0.34	2.74	—	—	—
61 S 2	0.61	2.33	0.22	—	—	—
100 S 2	1.0	2.08	0.36	—	—	—

The X-ray photographs were taken by the X-ray apparatus URS-50I. The absolute error in the determination of the austenite lattice spacing using (200) and (111) lines was less than ± 0.003 kX. In some cases the photographs were taken at the transformation temperature by means of a special high-temperature X-ray camera of Kaminskii and Stelletskaya and an ionic X-ray tube with a manganese anode [15]. The absolute error in the determination of the lattice spacing of austenite

Fig. 1 shows the diagram of austenite transformation in 144 K3 constructed on the basis of magnetic measurements after a preliminary heating to 980°C.

In order to obtain a complete solution of carbides in austenite during heat treatment before taking the X-ray photographs, a higher preheating temperature (1100°C) was used. After heating to 1100°C and keeping at this temperature for 10 min the specimens were transferred into a bath main-

tained at 300 or 400°C and kept there for various lengths of time before cooling in water.

In the second case the specimen was quenched in water directly after heating to 1100°C. In this way the austenitic structure was completely fixed-Isothermal treatment was carried out directly in the high-temperature X-ray camera.

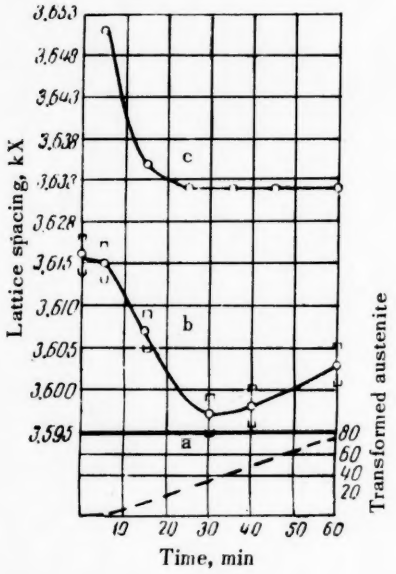

FIG. 2. Steel 144K3. Isothermal treatment at 400°C.
a - curve of the isothermal austenite transformation
b - change in lattice spacing of the residual austenite
c - change in lattice spacing during the transformation (high-temperature photographs).

The results of the lattice spacing determinations of the residual austenite at room temperature and directly at the transformation temperature are shown in Fig. 2 (b, c). Fig. 2 (a) which was constructed on the basis of micro-structural analysis represents isothermal austenite transformation at 400°C.

The austenite transformation at 400°C is connected with the rapid decrease of the lattice spacing by 0.017 kX which corresponds to the decrease in carbon concentration of austenite by 0.4 per cent. This decrease occurs mainly during the initial stage of the transformation. If the isothermal treatment at 400°C lasts longer than 30 min the lattice spacing measured at the transformation temperature remains practically unchanged (Fig. 2, curve c).

When the X-ray photographs were taken at room temperature a certain increase of the lattice spacing was observed in the later transformation stages (curve b). The comparison of curves b and c (Fig. 2) shows that the increase of the lattice spacing is connected with the transformation of parts of the austenite of lowest carbon content into martensitic on cooling.

The isothermal treatment at 300°C leads to the decrease of the lattice spacing by 0.008 - 0.010 kX which corresponds to the diminution in the carbon content of austenite by 0.18 - 0.20 per cent.

The lattice spacing of the residual austenite in the steel 98K3 (isothermal treatment carried out at 250 - 350°C) increases from 3.608 to 3.611-3.613 kX. These changes are close to the limits of the experimental accuracy which shows that the average value of the lattice spacing remains virtually unchanged in this case.

The lattice spacing of the residual austenite in the steel 54 K3 (isothermal treatment at 350°C) increases from 3.584 to 3.600 kX which corresponds to the decrease in carbon concentration by 0.3 per cent.

2. The measurements of the average lattice period of austenite undertaken in conjunction with the study of the middle range transformation were carried out on specimens of the steel 118G3 (1.18 per cent C and 3.58 per cent Mn) and 48G4 (0.48 per per cent C and 43 per cent Mn).

It was found that the isothermal treatment of the steel 118G3 at 350°C leads to the decrease of the lattice spacing from 3.603 to 3.583 kX. This corresponds roughly to the decrease in carbon content of austenite from 1.2 to 0.8 per cent [11].

The transformation occurring at 275°C in the specimens of steel 48 G4 shows a considerable incubation period (about 5 hr) and is finished after 22 - 23 hr of treatment. During this time about 65 per cent of austenite is transformed (Fig. 3, curve a). The measurements of the lattice spacing of the residual austenite were carried out using line (200). The specimens heated to 900°C were transferred into a bath at 275°C where they were kept for various lengths of time (2 to 50 hr) before cooling in water.

The curve representing the change of the lattice spacing of the residual austenite with the length of isothermal treatment has the same shape as the kinetic curve (Fig. 3, curve b). The lattice spacing of the residual austenite does not change during the incubation period of the transformation. During

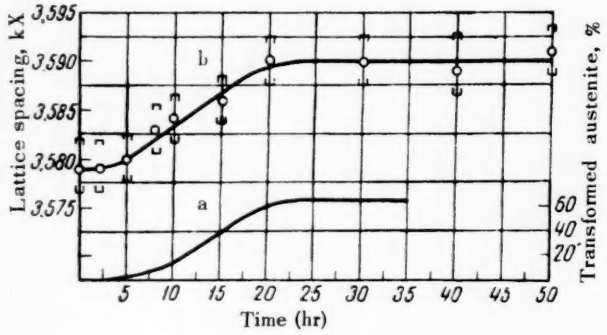

FIG.3. Steel 48G4. Isothermal treatment at 275°C.
a - curve of the isothermal austenite transformation
b - change in lattice period of the residual austenite.

the transformation the lattice spacing increases from 3.579 to 3.591 kX which corresponds to the increase in carbon content by 0.25 - 0.30 per cent. After 20 - 25 hr the limiting transformation for the given temperature is reached and there is no further change in the lattice spacing of the residual austenite.

3. The measurements of the lattice spacing of austenite in the middle range transformation were carried out on specimens of the steels 30YU2 (0.3 per cent C and 2.9 per cent Al) and 79YU2 (0.79 per cent C and 2.86 per cent Al).

The specimens of the steel 30YU2 were heated to 950°C and transferred to a bath at 450°C, where they were kept for various lengths of time before cooling in water. The results of lattice spacing measurements of the residual austenite and the kinetic curve of the transformation at 450°C are shown in Fig.4. The lattice spacing of the residual austenite increases from 3.619 to 3.647 kX which corresponds to the increase of the average carbon concentration in austenite by 0.6 per cent.

The curves representing the change in the lattice spacing of the residual austenite (Fig.4, curve b) and the kinetics of austenite transformation at 450°C (curve a) have a similar character. After 1 - 2 min of treatment the transformation rate drops off, and during further treatment the lattice spacing does not change substantially.

The pearlitic transformation which begins after 20 min is not accompanied by changes of the lattice spacing. No residual austenite remains after 8 hr 40 min at 450°C.

The partial transformation of austenite in the specimens of the steel 79YU2 at 300 - 450°C does not lead to a substantial change in the lattice spacing of the residual austenite. Treatment for 1 hr at 350°C causes an increase in the spacing from 3.644 to only 3.653 kX.

4. It is interesting to compare the changes in the lattice spacing of the residual austenite during the middle-range transformation in steels of the same carbon content: 54 K3, 55N8 and 53KN3.

As already stated the lattice spacing of austenite in the steel 54K3 increases during transformation at 350°C from 3.584 to 3.600 kX. This corresponds to an average carbon content increase by 0.3 per cent.

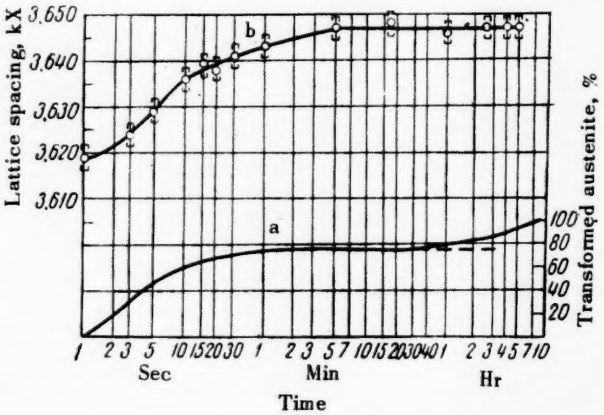

FIG.4. Steel 30YU2. Isothermal treatment at 450°C.
a - curve of the isothermal austenite transformation
b - change in lattice period of the residual austenite.

In the steel 55N8 the 2 hr treatment at 350°C leads to an increase in the spacing from 3.577 to 3.587 kX, which corresponds to an increase in carbon content by 0.25 per cent; after 3 hr treatment at 400°C the lattice period changes from 3.577 to 3.591 kX and the average carbon content increases by 0.3 per cent (Fig.5).

In the quenched specimens of the steel 53KN3 the lattice spacing of austenite is 3.573 kX. The specimen heated to 950°C was placed in an oil bath maintained at a temperature somewhat higher than the beginning of martensitic transformation (190°C) where it was kept for 2 min before cooling slowly to the room temperature. This heat treatment was chosen in order to increase the amount of the residual austenite and make sure that X-ray determination of the lattice spacing was possible. The results of these determinations are given in Table 2.

TABLE 2. Steel 53 KhN3

Preheat temperature, (°C)	Conditions of isothermal treatment (temp. and time)	Cooling	Austenite transformed (%)	Lattice spacing of the residual austenite a (kX)
950	190 – 2 min	with the furnace	–	3.573
950	400 – 2 hr	in air	28	3.588
950	300 – 40 min	in air	67	3.586
950	250 – 90 min	in air	45	3.584

The partial transformation of austenite between 250 and 400°C leads to the increase in the lattice spacing of the residual austenite from 3.573 to 3.586 - 3.588 kX which corresponds to an increase in carbon content by 0.3 per cent.

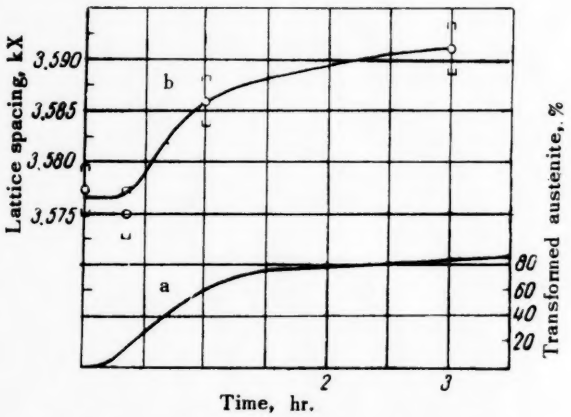

FIG.5. Steel 55N8. Isothermal treatment at 400°C.
a - curve of the isothermal austenite transformation
b - change in lattice period of the residual austenite.

5. Figs. 6 and 7 show the variation of the austenite period of the steels 55N8 and 100S2 with the isothermal transformation temperature for approximately the same degree of transformation. The higher the transformation temperature the greater the increase in the austenite lattice spacing and greater the enrichment of the residual austenite in carbon. If a decrease in the carbon content is observed during the transformation then the higher the temperature the greater the decrease in carbon content. For instance, in the case of the steel 144K3 the maximum decrease in carbon content is 0.2 per cent at 300°C and ~ 0.4 per cent at 400°C; and for the steel 139G2 about 0.13 per cent at 300°C ~ 0.4 per cent at 350°C and ~ 0.5 per cent at 400°C [11].

6. The self inhibiting of the austenite transformation is observed in steels in which the carbon content in the residual austenite is lower (118G3, 139G2 and 144K3) higher (48G4, 54K3) or the same as before the transformation (98K3, 79YU2).

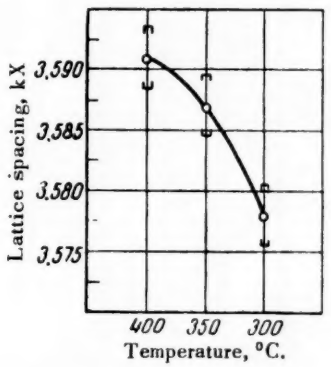

FIG.6. The relation between the lattice spacing of the residual austenite in the steel 55N8 and the isothermal transformation temperature in the middle range (for 85 per cent transformation).

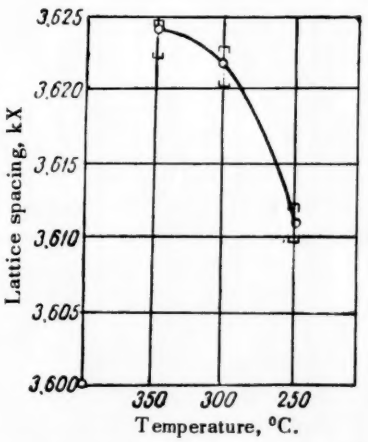

FIG.7. The relation between the lattice spacing of the residual austenite in the steel 100S2 and the isothermal transformation temperature in the middle range (for 75 per cent transformation).

The results of this study enable us to make the following conclusions.

a. The degree of enrichment of the residual austenite in carbon during the middle-range transformation is determined in steel containing chromium, manganese and nickel by the content of carbon in the given steel.

In the steels 55N8, 54K3 and 53K3 of about the same carbon content a similar enrichment in carbon was observed during the transformation at 350-400°C.

On the contrary, the comparison of results obtained with steels of approximately the same content of alloying elements (54K3, 98K3 and 144K3; 118G3 and 48G4; 301Yu2 and 79Yu2) shows that with the increase of carbon content the direction of the carbon redistribution changes. For instance, in the steels 54K3, 48G4, 30Yu2 a marked increase of lattice spacing is observed during the transformation; in the steels 98K3 and 79Yu2 the average lattice spacing of austenite virtually does not change and in the steels 144K3, 118G3 and 139G2 the transformation of austenite is accompanied by a considerable decrease in the carbon content of austenite. Steels containing silicon are to a certain extent exceptional. In the steels 61S2 and 100S2 the carbon concentration in the residual austenite increases considerably to 1.6 per cent during the transformation.

The changes in the lattice spacing and carbon content of austenite occurring during the transformation and quoted in this work are average values. The experimental results show a marked lack of homogeneity in the carbon content of the residual austenite [11].

b. The degree of change in the carbon content (whether enrichment or depletion) is higher the higher the transformation temperature.

c. The curves representing the change of the lattice spacing during transformation with time and the kinetics of the transformation have a similar character for steels in which the enrichment in carbon occurs. In the steels which show a decrease in carbon content of austenite the most marked change (decrease) in the lattice spacing is observed before the deposition of the α-phase (steel 139G2) [11] or during the initial stages of transformation (steel 133K3). This follows clearly from the X-ray photographs taken at the transformation temperatures.

d. The austenite transformation in the middle temperature range is characterized by the redistribution of carbon in austenite and the following martensitic transformation in the austenite regions of lower carbon concentration.

The appearance of heterogeneity in carbon concentration in austenite (regions of higher and lower carbon concentration) at the middle range temperatures is thermodynamically possible and corresponds to a decrease of the free energy of the system. The regions of lower carbon content are transformed into martensite. The middle range transformation in steels of high average carbon content (1.2-1.4 per cent) can begin with direct formation of cementite which also causes the appearance of austenite regions of low carbon concentration where the martensite transformation can occur.

The removal of carbon from the regions where its concentration diminishes into other parts of austenite (accompanied by an increase in the lattice spacing of the residual austenite) or separation of cementite (accompanied by a decrease in the lattice spacing) leads to the formation of austenite regions of low carbon content and creates the possibility of martensite transformation occurring at temperatures above M_S.

The direction of the carbon redistribution in austenite at the middle temperature range is determined obviously by the kinetic factors.

In steels containing 0.3-0.6 per cent carbon its removal into the residual regions of austenite is kinetically more favorable than the formation of cementite which needs an increase in carbon concentration to 6.7 per cent and hence requires diffusion through longer distances.

In steels containing 0.7-1 per cent carbon in which there is no change in the average spacing during transformation, the removal of carbon into the residual austenite regions and the separation of cementite are equally probable.

The interaction of atoms of iron, carbon and alloying elements can change substantially the degree of redistribution of carbon in austenite. For instance, the addition of silicon leads to an appreciable enrichment of the residual austenite in carbon. Even in the high carbon steel 100S2 the austenite transformation is connected with an increase in carbon content of the residual austenite by 0.5-0.6 per cent. The specific effect of silicon is explained by its ability to inhibit carbide formation.

The higher the middle-range transformation temperature the lower the resultant concentration of

carbon in the austenite regions which undergo later martensite transformation. This conclusion is confirmed by the relation between the amount of change in the carbon concentration and the transformation temperature (for the same percentage transformation).

The self-inhibiting effect discovered in the middle temperature range is not connected with the redistribution of carbon, but is a result of the martensitic mechanism of the $\gamma \rightarrow \alpha$ transformation.

The influence of the alloying elements on the middle range austenite transformation is determined mainly by their effect on the rate and path of carbon diffusion.

REFERENCES

1. V.D.Sadovskii *Trudy instituta metallofiziki i metallurgii* 3 (1945).
2. S.S.Shteinberg *Metallurg* Nos. 9-10 (1937).
3. N.A.Minkevich *Kachestv. stal* 5 (1936).
4. F.Wever *Arch. Eisenhüttenw.*7 (1932).
5. G.V.Kurdyumov *Izv. Akad. Nauk SSSR ser. khim.* 2, 271 (1936).
6. R.I.Entin *Prob. metalloved. fiz. metal.* 3 (1952); 4 (1955).
7. A.Hultgren *Rev. Metall.* 11, 12 (1953).
8. S.V.Tsivinskii, L.I.Kogan and R.I.Entin *Prob. metalloved. fiz. metal.* 4 (1955).
9. L.M.Pevzner, G.M.Rovenskii and T.D.Kubyhkina *Dokl. Akad. Nauk SSSR* 4, 85 (1952).
10. F.Wever, A.Rose and W.Peter *Arch. Eisenhüttenw.* 21, 11,367 (1950).
11. L.I.Kogan and R.I.Entin *Izv. Akad. Nauk SSSR otd. tekh. nauk* 1 (1955).
12. W.Jelinghaus, A.Rose and H.Holetzko *Arch. Eisenhuttenw.* 5-6 (1954).
13. T.Ko and S.A.Cotrell *J. Iron St. Inst.*·172, 3, 307 (1952).
14. M.D.Perkas and G.V.Kurdyumov *Prob. metalloved. fiz. metal.* 2 (1951).
15. E.Z.Kaminskii and T.I.Stelletskaya *Prob. metalloved. fiz. metal.* 2 (1951).
16. L.I.Kogan and R.I.Entin *Dokl. Akad. Nauk SSSR* 73, 1173 (1950).
17. W.Hofmann and G.Schumacher *Arch. Eisenhüttenw.* 26, 2 (1955).

VOL. 4 1957

CRITICISM

LIMITS OF UTILITY OF REPEATED MEASUREMENTS*

R.I. YANUS

(Received 8 October 1956)

It is shown that Gogoberidze and Kirillov's opinion, that repeated measurements of the same quantity with the same apparatus can lower the probable random error of the measurement only to the error of reading the instrument, is true only for those trivial cases in which the numerical results of all measurements are the same.

Gogoberidze and Kirillov [1] have recently criticized one of the important tenets of the statistical theory of errors, namely that by increasing the number of measurements n of one quantity M with the same apparatus the deviation of the arithmetic mean of the results M_n from the true value tends to zero at any sensitivity of the apparatus:

$$\lim_{n\to\infty} |M_n - M| = 0. \tag{1}$$

They assert that although this tenet appears obvious to many, it is actually untrue because all the readings m_i are subject to an uncertainty δ (which the authors call the apparatus sensitivity, but which would be better called the reading error**) which would give a similar uncertainty in the value of M_n:

$$\frac{1}{n}\sum_{i=1}^{n}(m_i \pm \delta) = \frac{1}{n}\sum_{i=1}^{n} m_i \pm \delta = M_n \pm \delta. \tag{2}$$

Assuming that the differences in m_i, due to random measurement errors can be recorded and fitted by some distribution equation (e.g. the Gauss distribution) only when they exceed $\pm\,\delta$ the authors deduce:

$$|M_n - M| \geqslant 2\delta. \tag{3}$$

Assuming that the error in M_n (let us call it μ_n) is:

$$\mu_n = \sqrt{\frac{\sum_{i=1}^{n}(m_i - M_n)^2}{n(n-1)}}, \tag{4}$$

with

$$\mu_n > 2\delta, \tag{5}$$

and that the limits of μ_n are given by (3), the authors conclude that to increase n so as to reduce the measurement error is justified only up to some value $n = N$ at which (4) gives:

$$\mu_N = 2\delta. \tag{6}$$

It is easy to find N_m known to be larger than N. Let us denote the largest of the differences $|m_i - M_n|$ obtained in the measurement by Δ. With the inequality:

$$\sum_{i=1}^{n}(m_i - M_n)^2 < n\Delta^2, \tag{7}$$

we find

$$\sqrt{\frac{\Delta^2}{N_m - 1}} > 2\delta, \tag{8}$$

$$N < N_m < 1 + \left(\frac{\Delta}{2\delta}\right)^2. \tag{9}$$

Without concerning ourselves with the correctness of (3) given in the original***, we can indicate a case which clearly contradicts it. For instance, if the measurement is made with an apparatus and in conditions so that the same value is obtained for the quantity in all the multiple measurements (all the m_i's equal to one another) then the systematic errors of measurement, which are not allowed for in (3) we have the inequality:

$$|m_i - M| = |M_n - M| \leqslant \delta. \tag{10}$$

If in deducing (8) we used (10) instead of (3), we obtain instead of (9):

---

* *Fiz. metal. metalloved.* 4, No.2, 369-374, 1957 [Reprint Order No. POM 59].

** The sensitivity of an apparatus is the name usually applied to the reciprocal of one scale division. But because the instrument can be read to within some fraction of a scale division, depending on the degree of uniformity of the scale, the quality of the reading devices used, etc., the ratio of δ to the sensitivity is not always the same.

*** Unfortunately, the text of paper [1] contains so many typographical errors and inaccuracies in formulations, that in parts we really cannot make sense out of it. The reason is apparently that the final preparation of the manuscript for publication was interrupted by the death of Gogoberidze. It is really unfortunate that the second author did not even correct printers' and authors' errors.

$$N < N_m < 1 + \left(\frac{\Delta}{\delta}\right)^2. \qquad (11)$$

The limits of value of repeated measurements is very important in much research work, so that the paper under consideration deserves careful study. From such a study we have concluded that the authors' assertion that increasing n beyond N cannot in any way increase the accuracy of the result is a wrong generalization of a conclusion, correct only for certain cases, to all cases of repeated measurements.

We shall show that the basis of this assertion, (2), requires substantial correction. Also in the original paper [1], the right-hand side of (4) is regarded and used as an accurate expression of the true error of the result M_n, though actually it is only the most probable error (within known factor). The true error may be up to a large multiple or down to a small fraction of the most probable, so that it can exceed the limit δ (or 2δ) even when the most probable error does not. The probability that the true error is substantially larger than the most probable decreases rapidly with increase of n (even with $n > N_m$), hence increase of n beyond the limit given by (9) or even (11) undoubtedly increases the accuracy and reliability of the approximate equation:

$$M \simeq M_n. \qquad (12)$$

Since N and N_m do not have the properties attributed to them in [1], the "criticism" of Millikan's determinations of the electronic charge [2] and of some other measurements used to illustrate the paper, is inconsistent*.

Let us examine in more detail the foundation of (2), which is of more importance than (9) or (11). (2) is the authors' answer to the problem which, I think, can be formulated thus: suppose the result of the i the measurement is composed of the true value of the quantity being measured M, the random error of the particular observation x_i, denoted by $\pm\Delta$, and the error in reading for this observation ξ_i, denoted by $\pm\delta$:

$$m_i = M + x_i + \xi_i; \quad -\Delta \leqslant x_i \leqslant \Delta;$$

$$-\delta \leqslant \xi_i \leqslant \delta. \qquad (13)$$

The sequence of possible values for m_i is a discrete one with intervals of 2δ, x_i can have any values; ξ_i is the difference between $M + x_i$ and the nearest possible value of m_i**. The mathematical probability of x_i is zero (i.e. x_i is not an "entirely" random error). It is required to calculate the mathematical probability for M_n (we will denote it by M_0) and to find the conditions in which $|M_0 - M|$ can be considerably less than δ (it is desirable to come as close as possible to the equation $M_0 = M$).

Let us solve this problem numerically in the following example. It is required to determine the possible accuracy of determination of the mean voltage in an electrical network after a certain interval of time from the readings m_i of a voltmeter, read during this period of time n times at equal intervals in whole tens of volts with an error of reading $\delta = 5$ V. We will suppose n large enough that the probability of substantial deviations of M_n from its mathematically probable M_0 will be fairly small. We will also assume that the voltmeter has been so carefully calibrated that systematic errors in its readings do not exceed 0.1 V.

Let us assume, to simplify numerical calculations, that the true average voltage in the line is a whole number (e.g. $M = 118$ V) and that the x_i's are also whole numbers and distributed uniformly in the range $-\Delta$, Δ. Then the minimum value m_i (m'_Δ) is equal to the difference $M - \Delta$, rounded to the nearest ten (applying the "rounding to an even number rule" when $M + x_i$ ends with a five); the maximum values (m''_Δ) will be equal to $M + \Delta$, rounded in the same way. For M_0 we find:

$$M_0 = \frac{1}{2\Delta + 1} \sum_{\kappa=-\Delta}^{\Delta} m_\kappa. \qquad (14)$$

* The authors consider that instead of making 58 series of observations, Millikan should have contented himself with only 8, and that the final result should have been given only to 3, and not to 4 significant figures. In their calculations about this work, the authors made a remarkable simplification. Later an error was discovered even in the third significant figure of Millikan's figure for the electronic charge, but this does not justify the simplification indicated because this error was the result of systematic errors which were not taken into consideration in the author's calculations.

** For a definite selection m_i when $|\xi_i| = \delta$ one can make use of, for instance, "the rounding off to an even figure rule": of 2 values m_i deviating equally from $M + x_i$ we choose that in which the last significant figure is even. This rule is acceptable when the last significant figures of successive "m's" form the natural series of numbers.

VOL. 4 1957

Simple calculations give the following Table:

$\Delta = 0$	1	2	3	4	5	6	7	8	9
$M - \Delta = 118$	117	116	115	114	113	112	111	110	109
$M + \Delta = 118$	119	120	121	122	123	124	125	126	127
$m_\Delta = 120$	120	120	120	110	110	110	110	110	110
$m''_\Delta = 120$	120	120	120	120	120	120	120	130	130
$\sum_{\kappa=-\Delta}^{\Delta} m_\kappa = 120$	360	600	840	1070	1300	1530	1760	2000	2240
$M_0 = 120$	120	120	120	118.9	118.2	117.7	117.3	117.6	117.9

$\Delta = 10$	11	12	13	14	15	16	17	18	19
$M - \Delta = 108$	107	106	105	104	103	102	101	100	99
$M + \Delta = 128$	129	130	131	132	133	134	135	136	137
$m'_\Delta = 110$	110	110	100	100	100	100	100	100	100
$m''_\Delta = 130$	130	130	130	130	130	130	140	140	140
$\sum_{\kappa=-\Delta}^{\Delta} m_\kappa = 2480$	2720	2960	3190	3420	3650	3880	4120	4360	4600
$M_0 = 118.1$	118.3	118.4	118.1	117.9	117.7	117.6	117.7	117.8	117.9

From these figures we see that, at small Δ's, all the m_i's are identical ($m'\Delta = m''\Delta$) and that any increase in the number of measurements obviously cannot decrease the error of the result which may be up to $\pm\,\delta$ (when, for example, M = 115 or 125 V). Thus if $\Delta > \delta$ then $|M_0 - M| < \delta$; when Λ increases without limit, $|M_0 - M|$ tends to zero, completely damping out any variations around its limiting value. Thus as n and Λ increase beyond a certain value, the probable error of the result decreases below δ without limit*

It is obvious that a similar result is obtained when the distribution of x_i values is not uniform within the interval $(-\Delta, \Delta)$ but is some other distribution (for instance, Gaussian) but necessarily symmetrical around zero (so that the mathematical probability for x_i is zero).

Gogoberidze and Kirillov categorically deny the possibility that with any value of n the probable error of the result will be less than δ. They also attribute this opinion to Bernshtein and quote from his book [3] to support the contention, but the citation is so short that the exact sense of the original is not reproduced faithfully. I feel it necessary to reproduce here the complete section of the original text, from which the authors quoted a passage, since the quotations made by G and K ignore important fine details.

"Without dwelling in more detail on this problem (the theoretical impossibility of decreasing the effect of systematic measurement errors on the error of the result by repeated measurements with the same apparatus – R. Yanus) we would note that even in the absence of systematic errors, it is impossible with measuring instruments of limited accuracy to obtain by repeated measurement a value of the quantity to be measured with any accuracy desired. If, for example, I read from Tables of 5-figure logarithms the mantissa of any number ending in a 5, and propose to 100 of my audience to discard the last figure keeping unchanged or increasing by 1 unit the fourth figure of the mantissa, by the usual rule for approximate calculations, it would obviously be absurd to suppose that an arithmetic mean of the 100 mantissas so obtained which is expressed to the sixth significant decimal, would have greater chances of corresponding to the actual value of the 6-figure logarithm of the number in question, than if I myself attached to a 5-figure mantissa a sixth figure at random: the result would depend entirely on the imagination of my audience, which is in no way governed by the true value of the logarithm, and we would obtain the same result if the proposed figure had been taken from any other tables.

Generally, an arithmetic average, in virtue of the law of large numbers, comprises the deviation of individual observations x_i from their mathematically probable a,

* It may seem paradoxical that an increase in random errors of individual measurements can decrease the error of the result. But an increase of Λ requires a corresponding increase of n so that the probability of substantial deviations of M_n from M_0 is fairly small. If n is not sufficiently large, then increase of Λ, decreasing the probable error of the result due to instrument reading errors, but simultaneously increasing the probable error because of random errors in the individual measurements, may be harmful and not useful.

but if the x_i's contain inherently a certain indeterminacy $\pm \delta$, then according to the definition of mathematical probability a will have the same indeterminacy; hence, in computing an arithmetic mean we can replace x_i by $x_i + \theta_i$ $(-1 < \theta_i < 1)$. The problem of determining a (or of the physical quantity x, putting $a = M.O.x_i$) with an error less than δ is devoid of meaning".

It is easy to see that the problem examined by Bernshtein is not identical with the problem examined in paper [1], and is only a limiting case of it when all the θi's within the limits indicated by Bernshtein are absolutely equal. A somewhat similar situation may obviously sometimes arise in measurements with apparatus whose reading accuracy is determined not by the error of reading, (which should be fairly small) but an indeterminacy due to friction in the moving parts (as for instance in the suspension of high sensitivity balances from their balance arms, if the readings of these balances are determined not by the more accurate "method of swings" but by the final position of the balance arm) or to hysteresis, and after effects (magnetic, dielectric, elastic). Even in these cases correct measurement differs fundamentally from the situation in Bernshtein's example in that the imagination of his audience is not governed at all by the true value of the logarithm, while the readings of even the crudest instruments to some measure (we may suppose it small, but it will differ from zero) are governed by the true values of the quantity measured. But if this governing action is very small, then only with a very large number of measurements could we obtain tangible results of its action. Thus, only technical difficulty or expense, and not theoretical impossibility can sometimes make research workers limit the number of repetitions of measurements, and to content themselves with an error of $\pm \delta$ in the result obtained. Formally, the example adduced by Bernshtein is close to the problem examined above, but differs from it in the following particulars:

a. The presence of a non-eliminated systematic error (equal to the error due to rounding the true value of the mantissa of a logarithm of the number taken within five tenths of one place);

b. The absence of "entirely" random errors $(\Delta = 0)$;

c. The absence of a determinancy in the selection of the sign (plus or minus) $\xi_i = \pm \delta$ in (13).

If we take these into consideration the conclusions to be deduced from Bernshtein's example do not differ from the more general conclusions indicated by the above examination of our problem. For instance, if the conditions of the experiment given in Bernshtein's example are supplemented by any source of numbers, however small but symmetric with respect to zero ("random errors") added to the 5-place mantissa before it is rounded off to 4 places, then the arithmetic mean of a fairly large number of 4-place mantissas obtained this way will be very close to the original 5-place mantissa, that is to the accurate value of the logarithm of the number taken, apart from the already mentioned systematic error (due to rounding to the fifth place). Thus here also the random "errors" regularly modifying the value of the quantity "being measured" in the individual "measurement" can increase the accuracy of the result of repeated measurements.

I think, therefore, we can draw the following conclusion: increasing the number of repetitions of a measurement to increase the accuracy and reliability of the result can profitably be continued without limit if the results of the individual measurements show a scatter, within which the governing action of the true value of the quantity measured on the result of measurement differs from zero*.

REFERENCES

1. D.B.Gogoberidze and V.V.Kirillov Symposium *Fizika tverdogo tela (Physics of solids)* in memory of D.B.Gogoberidze, Published by the Leningrad Institute of Fine Mechanics and Optics, No.18, p.64, 1955.

2. R.Millikan Electrons, protons, photons, neutrons and cosmic rays (Translation) ONTI, 1939

3. S.N.Bernshtein *Teoriya Veroyatnostei, (Theory of Probability)*, GITTL, Moscow-Leningrad, p.225, 1946.

* To prevent misunderstandings, we would remind our readers that what has been said above relates only to random errors of measurement and has no bearing on systematic errors. Gogoberidze is undoubtedly right in directing attention to cases of underestimation of the latter, and of the inapplicability of the statistical theory of random errors to them. It is also obvious that in absolute (not comparative) measurements there is no great sense in expending much effort on making the probable random error of a measurement result extremely small, compared with the possible systematic error of the measurements.

VOL. 4 1957

LETTERS TO THE EDITOR

THE PROBLEM OF MAGNETOSTRICTION IN HEXAGONAL SYSTEM FERROMAGNETICS*

Yu.B. KOSTYANITSYN

(Received 3 March 1957)

Some research has been done into an expression for the magnetostriction of monocrystal ferromagnetics of the cobalt type, and the physical significance of the constant of magnetostriction has been explained, The constants of magnetostriction in cobalt have been evaluated by comparing theoretical formulae with experimental data on the dependence of magnetostriction on magnetization in the region of magnetization rotation.

(1) The tensor of magnetostriction in hexagonal system ferromagnetics is as follows:-

$$\begin{gathered}\tau_{11} = \varkappa_1 s_1^2 + \varkappa_0, \quad \tau_{12} = \varkappa_4 s_1 s_2, \\ \tau_{22} = \varkappa_2 s_2^2 + \varkappa_3 s_3^2 + \mu, \quad \tau_{13} = \varkappa_4 s_1 s_3, \\ \tau_{33} = \varkappa_3 s_2^2 + \varkappa_2 s_3^2 + \mu, \\ \tau_{23} = (\varkappa_2 - \varkappa_3)\, s_2 s_3,\end{gathered} \tag{1}$$

where τ_{ik} = the components of the tensor of magnetostriction, s_i = the projection of the single vector in the direction of magnetization, and x_i and μ are the constants of magnetostriction. Hence it follows that the linear magnetostriction in the direction of the single vector $\vec{v}$ is equal to

$$\begin{gathered}\Delta = \left(\varkappa_1 s_1^2 + \varkappa_0\right) v_1^2 + \left(\varkappa_2 s_2^2 + \right. \\ \left. + \varkappa_3 s_3^2 + \mu\right) v_2^2 + \left(\varkappa_3 s_2^2 + \varkappa_2 s_3^2 + \mu\right) v + \\ + 2\varkappa_4 s_1 s_2 v_1 v_2 + 2\varkappa_4 s_1 s_3 v_1 v_3 + \\ + 2\left(\varkappa_2 - \varkappa_3\right) s_2 s_3 v_2 v_3.\end{gathered} \tag{2}$$

In order to obtain the isothermal magnetostriction λ, the thermostriction Δ_t must be subtracted from equation (2). For crystals of the cobalt type with a direction of easy magnetization along the hexagonal axis we have

$$\Delta_t = \mu + (\varkappa_1 + \varkappa_0 - \mu)\, v_1^2 \tag{3}$$

and consequently,

$$\begin{gathered}\lambda = \varkappa_1 \left(s_1^2 - 1\right) v_1^2 + \left(\varkappa_2 s_2^2 + \varkappa_3 s_3^2\right) v_2^2 + \\ + \left(\varkappa_3 s_2^2 + \varkappa_2 s_3^2\right) v_3^2 + \\ + 2\varkappa_4 s_1 v_1 \left(s_2 v_2 + s_3 v_3\right) + \\ + 2\left(\varkappa_2 - \varkappa_3\right) s_2 s_3 v_2 v_3.\end{gathered} \tag{4}$$

In order to investigate this expression it is convenient to transfer to spherical co-ordinates. Then

$$\lambda = g \cdot \sin^2\theta + \frac{h}{2} \sin 2\theta, \tag{5}$$

where

$$\begin{gathered}g = \left[\varkappa_2 \cos^2\left(\varphi - \varphi_2\right) + \varkappa_3 \sin^2\left(\varphi - \varphi_2\right)\right] \cdot \\ \sin^2\theta_2 - \varkappa_1 \cos^2\theta_2, \qquad (6)\end{gathered} \tag{6}$$

$$h = \varkappa_4 \cdot \sin 2\theta_2 \cdot \cos\left(\varphi - \varphi_2\right). \tag{6a}$$

Here the angles θ and ϕ relate to the direction of magnetization, and θ_2 and ϕ_2 relate to the direction of measurement (θ and θ_2 equal latitude, ϕ and ϕ_2 equal longitude, calculated from the plane passing through axes 1 and 2). From (6) and (6a) it is evident that magnetostriction depends only on the differences of the longitudes $\phi - \phi_2$: consequently, in this approximation it is isotropic in the basal plane. Moreover, the directions of magnetization and dimension do not occur symmetrically in (5), which is not the case in cubic system crystals. The physical significance of the constant of magnetostriction may easily be explained from (5), as follows: x_2 is the longitudinal magnetostriction in the basal plane, x_3 is the latitudinal magnetostriction when there is magnetization in the basal plane, measurable in this same plane, and $-x_1$ is the latitudinal magnetostriction when there is magnetization in the basal plane, measurable along the hexagonal axis. The constant x_4 has no such simple interpretation.

It follows from (5) that the volumetric magnetostriction is as follows:

$$\frac{\Delta V}{V} = \left(\varkappa_2 + \varkappa_3 - \varkappa_1\right) \cdot \sin^2\theta. \tag{7}$$

The elimination of θ from (7) gives the following volumetric magnetostriction of the polycrystal

$$\left(\frac{\Delta V}{V}\right)_n = \frac{2}{3}\left(\varkappa_2 + \varkappa_3 - \varkappa_1\right). \tag{8}$$

(2) The curve of magnetostriction $\lambda = \lambda(H)$ in the region of magnetization rotation, (where H = the outer field, the direction of which is given by the angles θ_1 and ϕ_1), can be found at once, if the curve of magnetization $\theta = \theta(H)$ is known (in the

---

* *Fiz. metal. metalloved.* 4, No.2, 375-376, 1957 [Reprint Order No. POM 60].

case of cobalt it can be calculated that $\psi = \psi_1$ during rotation). The curves $\lambda = \lambda(j)$, where $j = I_0/I_p$ the relative magnetization, are found directly by substituting the value $\theta = \theta_1 - \cos^{-1} j$ in (5). For example, when there is magnetization in the basal plane the longitudinal magnetostriction is:-

$$\lambda = \varkappa_2 j^2, \qquad (9)$$

the latitudinal magnetostriction in the basal plane is:-

$$\lambda = \varkappa_3 j^2 \qquad (10)$$

and the latitudinal magnetostriction on the hexagonal axis is:-

$$\lambda = -\varkappa_1 j^2. \qquad (11)$$

The linear dependence of the magnetostriction on j^2 in these instances can be checked by comparison with the experimental data; such a comparison also enables the constants $\varkappa_1$, $\varkappa_2$ and $\varkappa_3$ to be evaluated. We made use of Nishiyama's data on the magnetostriction of monocrystal disks and cobalt bars at room temperature.

In order to obtain the dependence $\lambda = \lambda(j)$ the curve of magnetization must also be known. We took Honda and Masumoto's [4] data for bars with an axis (1010) and (1120).

The results of the experimental values j^2 and λ for the four values of the effective field are reproduced in the table.

It can be seen from the table that the experiment well confirms the linear dependence λ on j^2 in the region of magnetization rotation.

In view of the considerable differences when magnetostriction is measured in different specimens, the value of the constant can only be evaluated very approximately. On the basis of (9-11) and of the experimental data produced by Nishiyama, Honda and Masumoto we have adopted the following approximate values of the constant:

$$\varkappa_1 = -80 \cdot 10^{-6}, \quad \varkappa_2 = -30 \cdot 10^{-6}, \quad \varkappa_3 = -60 \cdot 10^{-6}.$$

In order to evaluate the constant $\varkappa_4$ we took Nishiyama's value of the latitudinal effect with magnetization in the direction $\theta_1 = 67.5^\circ$. By substituting in (5) $\theta_2 = \theta_1 + 90^\circ = 157.5^\circ$, and the adopted values $\varkappa_1$ and $\varkappa_2$ (where $\psi = \psi_2$) we obtained

$$\lambda = 64 \cdot \sin^2\theta - 0.7 \sin\theta \cdot \cos\theta. \qquad (12)$$

θ is found from the ratio $j = \cos(\theta_1 - \theta)$, and j from Kaya's (5) experimental data for $\theta_1 = 70^\circ$. The calculation for the four values of the effective field gives an average magnitude $\varkappa_4 \sim -130.10^{-6}$.

Approximately the same magnitude is obtained from calculation in the case $\theta_1 = 45^\circ$ (latitudinal magnetostriction). Thus it can be tentatively accepted that $\varkappa_4 = -130.10^{-6}$.

TABLE 1.

H_{eff} (oersted)	j^2	λ ($\times 10^6$)		
		Direction of dimension		
		Longitude [$10\bar{1}0$]	Latitude [1120]	Latitude [0001]
2000	0.13	- 5	- 7	10
3000	0.22	- 9	-13	13
4000	0.30	-13	-19	23
5000	0.40	-18	-25	33

A knowledge of the four constants enables the course of magnetostriction to be calculated in the region of magnetization rotation with any direction of magnetization and measurement. Evidently, a calculation of the terms of the second degree in the tensor of magnetostriction is sufficient in the case of cobalt. A calculation of the terms of a higher degree should give the anistropy of magnetostriction in the basal plane, which, as the experiment shows, is very insignificant in cobalt.

REFERENCES

1. S.V.Vonsovskii and Ya.S.Shur *Ferromagnetizm (Ferromagnetism)*, GITTL, 1948.
2. N.S. Akulov and Ya.I. Fel'dshtein *Vestn. Mosk. gos. univ.* 2, 73 (1950).
3. Nishiyama *Sci. Rep. Tohoku Univ.* 18, 341 (1929).
4. Honda and Masumoto *Sci. Rep. Tohoku Univ.* 20, 323 (1931).
5. Kaya *Sci. Rep. Tohoku Univ.* 17, 1157 (1928).

VOL. 4 1957

MAGNETIZATION OF OBJECTS WITH ALTERNATING CURRENT FOR DEFECTOSCOPY AND OTHER PURPOSES*

N.M. RODIGIN

(Received 27 September 1956)

In connexion with the wide-scale adoption of magnetic defectoscopy in industry a problem has arisen as to the creation of a cheap, portable and reliable installation for the magnetization of objects.

This problem became particularly acute when circular magnetization began to be adopted, carried out either by passing current through objects (in the case of strips), or by passing current through bars, placed inside objects (in the case of hollow cylinders). For circular magnetization, as a rule, high currents are demanded (hundreds and thousands of amperes).

The use of dynamos and still more so of storage batteries as sources of power makes the cost of the installation too high for defectoscopy. The adoption of alternating current for the magnetization of objects, however, has enabled as easily accessible method of magnetic defectoscopy to be carried out, since current of this kind is always available in any works and, moreover, there is no difficulty in obtaining large currents.

The only factor impeding the adoption of alternating current is that there is no certainty of obtaining the same residual induction in objects with each act of magnetization.

In this connexion some research has been carried out both into phenomena occurring during magnetization with alternating current and into the laws governing the decrease of residual induction when repeated magnetization of one and the same body is effected [1 – 4].

This research established the influence on magnetization of a number of factors, in particular the speed of breaking contact, the moment of breaking contact, the conditions under which the electric arc is formed, the parameters of the magnetization circuit, and so on.

This research enabled the process of magnetization of objects with alternating current to be more accurately comprehended.

However, the shortcomings indicated earlier which exist in the magnetization installations now in wide use were not eliminated, and further work was needed on the problem of using alternating current for the magnetization of objects. The present work is devoted to this problem.

When the changes in the ordinary sinusoidal alternating current at different times are observed, it is apparent that there are intervals of time, equal to a half-period, when the current flows in one direction only. Magnetization with alternating current in one of these intervals of time will be analagous to magnetization with direct current.

This idea is put into effect in the apparatus which we have devised.

A plan of the apparatus is shown at Fig. 1. Magnetization in the apparatus of the object 1 is carried out only for a quarter of a period, when the voltage of the alternating current circuit is changing from maximum to nil.

The basic elements of the apparatus are an ignitron, a thyratron, a peak transformer and a condenser.

The ignitron 2 is intended for connecting and disconnecting the magnetization circuit. The ignition of the ignitron is effected by current discharged by the condenser. 3.

The thyratron 4 serves for closing the circuit to which the condenser is connected. The thyratron circuit receives voltage from the secondary winding of the peak transformer 5 and the battery 6.

The transformer 5 is so calculated that its peak voltage which compensates the biasing battery voltage would be sufficient for opening the thyratron.

In order to ensure the working of the apparatus it is essential that the ignitron should be ignited at the moment when there is a positive po-

* *Fiz. metal. metalloved.* 4, No. 2, 377-378, 1957 [Reprint Order No. POM61].

tential of a certain magnitude on its anode. This is done by phasing, that is by the appropriate choice of phases in the alternating current circuit, to which the circuits of magnetization and of the peak transformer are connected.

The closing of the anode circuit of the thyratron, to which is connected the ignition mechanism of the ignitron, is done at the moment of peak voltage on the secondary winding of the peak transformer. This peak voltage is reached when the magnetic current in the iron of the transformer is close to nil.

Since the vector of the e.m.f. of the transformer lags behind the vector of the magnetic current by 90°, the closing of the anode circuit of the thyratron, and consequently the closing of the ignition mechanism of the ignitron, is done at the moment when the voltage in the circuit is close to maximum (amplitude), which is also essential for closing the anode circuit of the ignitron.

In addition to the appropriate magnitude of voltage between the anode and the cathode of the ignitron, a positive potential on the anode in relation to the cathode is also demanded. There is no difficulty in securing this.

If the potential on the anode is negative, then it is sufficient to connect leads to the peak transformer unchanged, in order to obtain the correct phasing.

The extinguishing of the ignitron, and the disconnexion of the magnetization circuit connected with this are in fact carried out at a strictly determined moment when the voltage is close to nil.

Thanks to the use of the peak transformer the connexion of the magnetization circuit is also carried out at a determined moment. Thus identical magnetization of similar objects is achieved.

The ignition of the ignitron with current discharged by the condenser is done with the purpose of bringing about simultaneous connexion of the magnetization circuit, which also facilitates identical magnetization of objects.

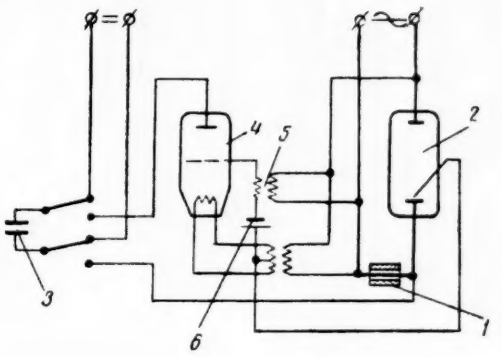

FIG. 1.

In comparison with the installations at present existing for the magnetization of objects, the apparatus which we have evolved has the following advantages:-

1. It ensures identical magnetization (as to magnitude and charge) of the same objects.
2. It reduces the time taken for the magnetization of objects (to a quarter of a period).
3. It reduces the amount of electric power used.
4. It enables the gauge of the supplying leads to be reduced.

The disadvantage of the apparatus is that it employs short-lived gas-discharging equipment.

REFERENCES

1. A.V. Al'tman and R.I. Yanus *Zh. tekh. fiz.* 17, No. 2 (1947).
2. A.V. Al'tman and R.I. Yanus *Zh. tekh. fiz.* 17, No. 2 (1947).
3. R.I. Yanus *Magnitnaya defektozhopiya (Magnetic defectozcopy)*, OGIZ, Gostekhizdat, 1946.
4. N.I. Eremin *Magnitnaya porostkovaya defektoskopiya (Magnetic powder defectoscopy)*, Mashgiz, 1947.

VOL. 4 1957

THE MAGNETIC SURFACE EFFECT WHEN FLAT BODIES ARE MAGNETIZED IN A CURVED FIELD *

YU. D. SYCHEV

(Received 24 September 1956)

Problems connected with the surface effect when flat bodies are magnetized in a longitudinal field have been studied in detail, and the solution of the appropriate Maxwell's equations permits the distribution of all the magnitudes characterizing the intensity of the electromagnetic process to be found.

However, the surface effect in flat bodies, magnetized in a curved field, has been little studied, although it is a matter not only of theoretical but also of practical interest. This instance of the surface effect is found in a number of sets of apparatus, for example in apparatus for measuring losses in electrotechnical sheet iron in alternating current (1), in some apparatus for induction heating (2) and so on.

In this connexion let us examine an instance where a variable double-component (curved) field penetrates into the conducting semi-field.

Let the normal and tangent components of the double-component field on the surface of the medium change in accordance with the following laws :-

$$B_z = B_{mz} \cos \frac{\pi}{\tau} y \cos \omega t, \tag{1}$$

$$B_y = B_{my} \sin \frac{\pi}{\tau} y \cos (\omega t + \alpha). \tag{2}$$

The following differential equations of the field are correct for each of the components in the metal:-

$$\mu\gamma \frac{\partial B_z}{\partial t} = \frac{\partial^2 B_z}{\partial y^2} + \frac{\partial^2 B_z}{\partial z^2}, \tag{3}$$

$$\mu\gamma \frac{\partial B_y}{\partial t} = \frac{\partial^2 B_y}{\partial y^2} + \frac{\partial^2 B_y}{\partial z^2}. \tag{4}$$

By solving these equations, when the magnetic permeability and specific conductivity of the medium are constant, and also when

$$\left(\frac{\omega\gamma\mu\tau^2}{\pi^2}\right)^2 \gg 1, \tag{5}$$

we obtain the following expression for the normal and tangent components of induction in the body :-

$$B_z = B_{mz} exp\,(-kz) \cdot \cos \frac{\pi}{\tau} y \cos (\omega t - kz), \tag{6}$$

$$B_y = B_{my} exp\,(-kz) \cdot \sin \frac{\pi}{\tau} y \cos \left(\omega t - kz + \frac{\pi}{4}\right). \tag{7}$$

Here B_{mz} is the amplitude of the normal component of induction (latitudinal field); B_{my} is the amplitude of the tangential component of induction (longitudinal field); τ is the pole pitch :

$$k = \sqrt{(\pi\mu f\gamma)};\ \mu = \mu_0\mu_r;\ \mu_0 = 4\pi \cdot 10^{-9}\ \text{henry/cm}$$

is the magnetic permeability of the vacuum. The amplitude of the normal and tangent components of magnetic induction are mutually linked by the relation

$$B_{my} = B_{mz} \frac{\sqrt{2}\,\tau k}{\pi}. \tag{8}$$

By making use of expressions (6) and (7) for induction, we find the active power, liberated in a band of unit width ($x = 1$) on one pole pitch in the whole semi-field to be as follows :-

$$P = \frac{f\tau^2}{2\sqrt{2}} B_{mz} H_{my}. \tag{9}$$

By way of practical application of the solutions we have obtained let us use the method of approximate calculation of an apparatus for induction heating.

The apparatus consists of a magnetic circuit in the shape of the Russian letter Ш and alternating current winding. We shall employ the following symbols for the geometric dimensions of the apparatus :-

a = the width of the outside pole, l = the width of the central pole, p = the width of the gap, g = the depth of the gap, h = the width of the magnetic circuit, δy = the pole pitch in the direction

* *Fiz. metal. metalloved.* 4, No.2, 378-380, 1957 [Reprint Order No. POM 62].

of the length of the magnetic circuit. c = the distance from the magnetic circuit to the centre of the latitudinal cross-section of the winding in the direction δx, e = the height of the cross-section of the winding, δ = the air gap between the poles and the body.

The following assumptions have been made in calculating the apparatus :-

1. The real three-dimensional distribution of the field is replaced by an equivalent, sinusoidal one.

2. The field is assumed to be uniform and only two-dimensional throughout the whole width of the apparatus.

3. It is assumed that the thickness of the object is sufficient for the field to be completely uniform in the metal.

The geometrical dimensions of the apparatus, determining the m.m.f. of the winding (WI), being known, we find the amplitude of the voltage of the longitudinal field to be as follows :-

$$H_{my} = \frac{\pi}{\sqrt{2}\,\tau_y} WI. \tag{10}$$

Through the curve of magnetization of the material being tempered we determine B_{my} and the magnetic current Φ_T

$$\Phi_T = \frac{h}{\sqrt{2}\,k} B_{my}. \tag{11}$$

Making use of (11), let us find the amplitude of induction of the latitudinal field :-

$$B_{mz} = \frac{\pi}{\tau_y h} \Phi_T. \tag{12}$$

We shall find the active power, liberated in the heated body, by the formula :

$$P = \frac{f\tau_y^2 h}{\sqrt{2}} B_{mz} H_{my}. \tag{13}$$

The magnetic current, created by the winding of the apparatus, is equal to the sum of the magnetic current of the central pole ϕc and the magnetic current of leakage ϕp. Assuming an absence of phase displacement between the currents ϕc and ϕp, which should not occasion a large error in the approximate calculation, we find the magnetic current of the winding :-

$$\Phi_0 = \Phi_c + \Phi_p, \tag{14}$$

moreover

$$\phi c = 2\,\phi_T \tag{15}$$

and

$$\Phi_p = 2\sqrt{2}\mu_0 WIh\left(\frac{e}{3p} + \frac{g-e}{p}\right) + \frac{2\mu_0 h\tau_y H_{my}}{\pi^2} \ln\frac{\tau_y}{\delta}. \tag{16}$$

The electromotive force of the winding, considering it to be sinusoidal, is found by the formula

$$E = 4.44 f W \Phi_0. \tag{17}$$

In the case of a narrow apparatus, when the ratio is close to unity, it is essential to take into consideration the fields of the end windings. The application of theoretical considerations to these fields enables an approximate calculation to be made here, however, instead of the formulae (11), (13) and (16) the following formulae must now be used :-

$$\Phi_T = B_{my}\frac{h}{\sqrt{2}\,k}\left\{1 + \frac{\mu_2 k_1}{\mu_1 k_2}\cdot\left[\frac{2p}{\pi h}\ln\left(1 + \frac{2a}{p}\right) + 0.52\,\frac{p}{h}\right]\right\}, \tag{18}$$

$$P = \frac{f\tau_y^2 h}{\sqrt{2}} B_{mz} H_{my} + \sqrt{2}\, l\tau_x f B_{mz_A} H_{mx}\cdot\left(\frac{\tau_x - h}{4} + \frac{\tau_x}{4\pi}\sin\frac{h}{\tau_x}\pi\right), \tag{19}$$

$$\Phi_p = 2\sqrt{2}\mu_0 WIh\left(\frac{e}{3p} + \frac{g-e}{p}\right) + \frac{2\mu_0 h\tau_y H_{my}}{\pi^2}\ln\frac{\tau_y}{\delta} + \frac{2\mu_0 l H_{mx}\tau_x^2}{\pi^2(\tau_x - h)}\cos\frac{h}{2\tau_x}\pi\ln\frac{\tau_x}{h} \tag{20}$$

Here

$$k = \sqrt{\pi f\gamma\mu};\ k_1 = \sqrt{\pi f\gamma\mu_1}\ \text{и}\ k_2 = \sqrt{\pi f\gamma\mu_2}.$$

All the magnetic permeabilities are determined by the statistical curve of magnetization, moreover μ is determined by H_{my}, μ_1 by H_1 and μ_2 by H_2, where

$$H_1 = \frac{WI}{p},\quad H_2 = \frac{2WI}{\pi(p+a)}.$$

We shall find the amplitudes of voltage of the longitudinal field and the inductions of the latitudinal field of the frontal parts by the formulae

$$H_{mx} = \frac{\pi}{\sqrt{2}\tau_x}\left(c + \frac{d}{2}\right)H_1,$$

$$B_{mz_A} = \frac{\pi}{\tau_x l}\Phi_T.$$

We may observed that the experimental work has shown a satisfactory convergence of the calculated and empirically observed magnitudes.

The author is deeply grateful to N.M. Rodigin for a number of valuable pieces of advice and comments during the course of the work.

REFERENCES

1. A.D. Sokolov and R.I. Yanus *Fiz. metal. metalloved.* 1, No.1 (1955).
2. N.M. Rodigin and A.I. Alekseev *Novyi spozob podogreva metalla pered svarkoi (A new method of pre-heating metal before welding)*, Marhgiy, 1953.

VOL
4
195

THE MEASUREMENT OF CONTACT ANGLES OF IRON WETTING GRAPHITE BLOCK *

A. YA. KHRANOV and V.P. CHERNOBROVKIN

(Received 14 March 1956)

A method of measurement of contact angles of molten iron on graphite block is described. The effect of various factors (chemical composition, modification, method of treatment) on the contact angle of iron is shown. A conclusion is drawn about the relationship between this property of iron and its surface tension.

VOL. 4 1957

In the study of many phenomena occurring on the boundary it is necessary to take account of the change in the surface free energy on the interphase boundary.

The relationship between the surface free energies in a three phase system at equilibrium deduced by Laplace has the following form

$$\sigma_{s,l} = \sigma_{s,g} - \sigma_{l,g} \cdot \cos\theta$$

where $\sigma_{s,l}$ – is the specific surface free-energy of the solid on its boundary with liquid, $\sigma_{s,g}$ – is the specific surface free-energy of the solid on the boundary with its vapour or a neutral gas, $\sigma_{l,g}$ – is the specific surface free-energy of the liquid on the boundary with its vapour or a netural gas and θ the contact angle of wetting measured customarily into the liquid phase.

In the problems of crystallization of solutions and alloys the measurement of the interfacial tension $\sigma_{s,l}$, is of great interest. It is known from the crystallization theory [1] that the intensity of formation of the crystallization centres changes exponentially with the cube of the interfacial tension, and that the appearance of growing crystals depends on the interfacial tension on the boundary between the face of the growing crystal and the liquid.

It is impossible nowadays to determine $\sigma_{s,l}$ directly because of the imperfect experimental technique. This circumstance explains why the workers who study the form and the dimensions of crystals as affected by surface active additions [3-5] do not use $\sigma_{s,l}$, but the surface tension $\sigma_{l,g}$ assuming the existence of a parallelism between the two.

This assumption was verified indirectly in the case of some systems by Danilov and Kamenetskaya [2].

In order to confirm the behaviour of $\sigma_{s,l}$ and $\sigma_{l,g}$ for iron, experiments were carried out to determine $\sigma_{l,g}$ and the contact angle between iron and graphite. We have assumed that the contact angle θ when a drop of molten metal wets a solid basis in the atmosphere of an inert gas can be used as a measure of the interfacial tension $\sigma_{s,l}$. Actually, the lower the contact angle the lower the surface tension and the better the wetting of the solid. Hence, the measurement of the contact angles in a given system enables us to form a definite picture of the general change in $\sigma_{s,l}$ and to compare it with the imposed change in other factors.

EXPERIMENTAL METHOD

The measurement of the contact angles was carried out by the original method described by Levin [6]. This method is based essentially on fixing the picture of the metal drop contour on a screen through a series of lenses because of the light emitted by the metal itself at high temperatures. In connexion with the special features of the problem certain changes were made in the experimental apparatus. In order to simplify and speed up the fixing of the metal drop contour a photographic camera was used instead of a screen and a lens of a long focal length. In taking the photographs of the drop, high sensitivity film was used with 1/50 sec exposure. In these experiments iron samples taken during the surface tension measurements (carried out by the method of maximum bubble pressure) were used.

In order that the size of the drop did not influence the contact angle all specimens weighed 0.3 g and the drops were 3 mm in diameter.

The horizontal surface of the graphite block was polished on three finest grades of emery paper

* *Fiz. metal. metalloved.* 4, No. 2, 381-383, 1957 [Reprint Order No. POM 63].

and finished off on cloth. The temperature in the working part of the tube furnace was measured with the accuracy ± 5°C with a tungsten-nickel thermocouple connected to a potentiometer. The diagram of the apparatus is shown in Fig. 1.

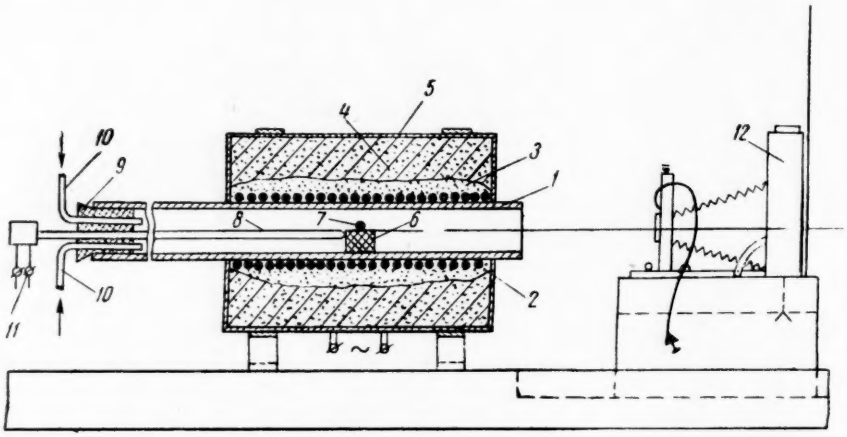

FIG. 1. Diagram of the apparatus for the measurement of the contact angles of iron.
1 – porcelain tube 1000 mm long, 40 mm in diameter, 2 – heating spiral, 3 – protective plaster, 4 – insulating filling, 5 – shell, 6 – graphite base, 7 – iron drop, 8 – tungsten-nickel thermocouple, 9 – rubber bung, 10 – tubes for introduction of argon, 11 – free ends of the thermocouple, 12 – camera.

EXPERIMENTAL PROCEDURE

Simultaneously with the switching of the heater 2, purified argon was let in through tubes 10 and continued to flow during the whole of the experiment. When the temperature of the working part of the furnace reached 1200°C the graphite base was introduced into it. After 2-3 min the hot base was withdrawn, the iron specimen put on it and the whole pushed back into the furnace so that it touched the end of the thermocouple 8. Next the contour of the iron specimen was focused on the ground glass of the camera. Further observation of the specimen was carried out through the camera, all changes in the specimen were clearly seen on the ground glass of the camera. As soon as the piece of iron began to melt, the ground glass was withdrawn and replaced by a cassette with the film and the iron drops were photographed.

The pictures of drops were enlarged approximately 10 times during printing. The contact angles were then determined by the graphical method described by Lewin [6].

This procedure was chosen for the following reasons: the measurement of the contact angle was carried out at temperatures very close to the melting point of iron and during the short period of time (the melting of the specimen and taking of the photograph lasted 25-30 sec) at these temperatures the chemical composition of the specimen studied practically did not change.

The experimental results obtained with iron of various chemical compositions are given in the Table.

The data given in the table show that the contact angles for common iron are about 104-108° which agrees with the results of other workers [6]. Graphite is not wetted by iron.

The contact angles of iron treated with manganese are 125-130° which is considerably more than the contact angles of the original irons.

The contact angles decrease from 115° to 90° when the sulphur content increases from 0.1 per cent to 0.5 per cent.

The comparison of the contact angles with the surface tensions measured earlier leads to the conclusion that there is a general regularity in the parallel change of $\sigma_{l,g}$ and θ or $\sigma_{l,g}$ and $\sigma_{s,l}$.

In conclusion it should be pointed out that the measurement of the contact angles of iron on graphite base can find wide application as a technological test in the works practice as it is possible to establish the principal relationship between θ and the form of the separating graphite.

VOL. 4 1957

TABLE 1. The values of contact angles between molten iron and graphite block

No. of melt	Contact angle (average from 3 measurements) at $T \sim T_m$	Surface tension $\sigma_{l,g}$ (erg/cm²)	Temperature of $\sigma_{l,g}$ measurement (°C)	Chemical composition (%) and treatment of the specimen	Remarks
44	108	850	1140	3. 5 C, 1. 14 Si 0. 57 Mn, 0. 03 S 0. 03 P	The values of $\sigma_{l,g}$ at $T \sim 1140$°C. were obtained by the extrapolation of $\sigma = f(T)$ curves for these two types of iron
80	104	760	1140	3. 3 C, 2. 0 Si, 1. 0 Mn, 0.053 S, 0.075 P	
95	127	1100	1300	3. 3 C, 2. 0 Si, 1. 0 Mn, 0.053 S, 0.075 P (iron treated with 0.3 per cent Mg)	2 min after Mg addition
95	130	1120	1300		4 min after Mg addition
95	125	1080	1300		8 min after Mg addition
79	115	700	1300	4. 0 C, 0. 2 Mn 0. 2 Si, 0. 03 P	Sulphur content 0. 1 per cent
79	112	800	1300		Sulphur content 0.17 per cent
79	110	640	1300		Sulphur content 0. 2 per cent
79	104	580	1300		Sulphur content 0.35 per cent
79	97	540	1300		Sulphur content 0.42 per cent
79	90	510	1300		Sulphur content 0. 5 per cent

OL.
4
957

REFERENCES

1. V.D. Kuznetsov *Kristally i kristallizatsiya (Crystals and crystallization)* GITTL, Moscow, 1954.
2. V.I. Danilov and D.S. Kamenetskaia *Problemy metallovedeniya i fiziki metallov, (Problems of metallography and physics of metals)* Metallurgizdat, 2, p.8, 1951.
3. N.S. Kreshchanovskii and R.P. Zaletaeva Liteinoe proizvodstvo, No. 3, 1953.
4. R.P. Zaletaeva, N.S. Kreshchanovskii and L.L. Kunin Liteinoe proizvodstvo, No, 2, 1951.
5. Y.A. Klyachko, L.L. Kunin *et al. Dokl Akad. Nauk SSSR.* 72, 927 (1950).
6. A.M. Levin Trudy *Dnepropetrovskogo metallurgichevskogo instituta, issue* 28, 1951.

INTERNAL FRICTION IN RECRYSTALLIZED ALLOYS OF ALUMINIUM AND MAGNESIUM*

A.V. GRIN'

(Received 4 January 1957)

The relationship between temperature and internal friction in recrystallized alpha solid solutions of magnesium in aluminium has been studied by low-frequency torsional vibrations. The magnesium content of the alloys was: 0.01; 0.05; 0.5; 1 and 2 per cent by weight.

All the alloys were heated at various temperatures at approximately the same rate in order to obtain the necessary grain size.

The measurements showed that for small concentrations of magnesium (0.01 and 0.05 per cent) there is only one maximum on the curve and that it occurs around 300°C and is related to the development of the viscous properties of the grain boundaries in the metals [1]. The dependence of this maximum on the grain size is similar to that reported by Kê [1].

In alloys containing 0.5 or 1 per cent magnesium, there is an additional maximum at about 380°C but at 2 per cent magnesium, this second maximum disappears. In this case the effect of the grain size on the internal friction is of a more complicated type.

A previous appearance of two maxima in recrystallized 99.998 per cent pure gold was explained as due to two different stages of crystallization [2], but our results show that the appearance of the second maximum directs the stress relaxation along the block boundaries of the mosaic structure. There are many references to the fact that the alloying of aluminium leads to a strong decrease in block size after deformation and also in the rate of growth of the blocks during the subsequent heating. When aluminium is alloyed with magnesium, a greater number of mosaic block boundaries can be obtained by recrystallization and these give a maximum on the internal friction curve.

With regard to the effect of the concentration of magnesium in the study of stress relaxation the following points are brought to notice: there is a lowering of the height of the maximum of internal friction along the grain boundaries; in an alloy containing 0.5 per cent magnesium, the decrease in the height of this maximum with increasing grain size, takes place more quickly than with 0.01 per cent magnesium; there is no second maximum when the magnesium content is increased to 2 per cent. These facts are explained sufficiently by Arkharov's theory of intercrystalline internal adsorption [3].

I wish to thank V.A. Pavlov for much valuable advice during his direction of this work.

REFERENCES

1. T.S. Kê *Phys. Rev. 71*, 533 (1947); *72*, 41 (1947).
2. D.R. Mash and L.D. Hall *J. Metals, N.Y.* 5, 937 (1953).
3. V.I. Arkharov *Trud. Inst. fiz. met. Urals. fil. Akad. Nauk SSSR* 8, 54 (1947).

* *Fiz. metal. metalloved.* 4, No. 2, 383-384, 1957 [Reprint Order No. POM 64].

70th BIRTHDAY OF V.D. KUZNETSOV

13th May 1957 was the seventieth birthday of the great Soviet scientist Vladimir Dmitrievich Kuznetsov.

Vladimir Dmitrievich Kuznetsov has devoted more than forty-five years to scientific, educational and social activity which has brought him deserved fame in the broad circles of the scientific and technical world.

V.D. Kuznetsov's works and teaching in the sphere of surface energy and hardness, plasticity and strength, crystallization and recrystallization, cutting, friction and wear of metals, and on many other subjects are widely known and deservedly give him the right to be considered one of the founders of the physics of solids in the U.S.S.R. V.D. Kuznetsov has published a multi-volume work *"Fizika tverdogo tela" (Physics of solids)* and also a number of monographs, teaching aids, and more than 150 scientific papers.

In 1928, on Kuznetsov's initiative, the Siberian Physicotechnical Institute of Scientific Research (SFTI) was formed in Tomsk. As director of SFTI Kuznetsov was able to place it in the ranks of the leading institutes of nation-wide importance. V.D. Kuznetsov carries on a great deal of scientific teaching work as head of the department of metal physics in the Tomsk State University. For many years Kuznetsov has played an active part in public life. During the second world war he was the initiator and one of the organizers of the Tomsk committee of scientists for aid to industry, transport and agriculture.

Over many years Kuznetsov has been a deputy of the Tomsk city soviet and president of the Tomsk district committee for the defence of peace. From 1947 to 1951 he was a deputy of the Supreme Soviet of the R.S.F.S.R.

The party, the Soviet government and the people value highly Kuznetsov's scientific and public activities and his services to his country: the title of honoured scientist has been bestowed on him, he has received a Stalin prize for the second volume of his monograph *"Fizika tverdogo tela"*, and has twice been awarded the order of Lenin.

In December 1946 Kuznetsov was elected corresponding member of the U.S.S.R. Academy of Sciences.

His seventieth anniversary finds Kuznetsov full of creative powers and daring new ideas.

The editorial staff of Physics of Metals and Metallography join the whole scientific world in wishing him many years of life, health and further successes in this scientific work.

VOL. 4 1957

PRINTED IN GREAT BRITAIN BY
BILLING AND SONS LIMITED, GUILDFORD AND LONDON